Mutation analysis of GABAergic neuroinhibitory genes in childhood genetic generalised epilepsies.

Hunt-Jones, Charlotte Amy

Mutation analysis of GABAergic neuroinhibitory genes in childhood genetic generalised epilepsies

Charlotte Amy Hunt-Jones

Submitted to Swansea University in fulfilment of the requirements for Degree of Doctor of Philosophy

Swansea University

2015

ProQuest LLC.
789 East Eisenhower Parkway
P.O. Box 1346
Ann Arbor, MI 48106 – 1346

Declaration

This work has not previously been accepted in substance for any degree and is not being concurrently submitted in candidature for any degree.

Signed . ..... (Candidate)

Date .....06/07/15.....

Statement 1
This thesis is the result of my own investigations, except where otherwise stated. Where correction services have been used, the extent and nature of the corrections is clearly marked in a footnote(s).
Other sources are acknowledged by footnotes giving explicit references. A bibliography is appended.

Signed .... (Candidate)

Date .....06/07/15.....

Statement 2
I hereby give consent for my thesis, if accepted, to be available for photocopying and for inter-library loan, and for the title and summary to be made available to outside organisations.

Signed .... (Candidate)

Date .....06/07/15.....

Acknowledgments

I would like to thank my supervisors Dr Rhys Thomas, Dr Seo-kyung Chung, Dr Owain Howell and Professor Mark Rees for their support, guidance and advice over the last four years. I would also like to thank Dr Jeff Davies for the continuous support especially in the early stages of my PhD. I must acknowledge both the neuroscience and diabetes group of ILS1 for the practical and emotional support, it has been a privilege to work closely with all of you.

I would like to thank Wales Gene Park for the funding provided for my research, without which this thesis would not have been possible. A special thank you must go to Professor Sam Berkovic (University of Melbourne), Dr Kate Everett (St George's Medical School, London) and Dr Peter Bergin (University of Auckland) for providing the samples for the study.

I am indebted to my ever supportive parents and family, for their guidance and advice always. Finally, I give my love and thanks to my husband Rhys for his unconditional support, advice and patience.

Summary

Epilepsy affects over 450,000 people in the UK and there are over 50 epilepsy phenotypes; genetic generalised epilepsy (GGE) account for up to 30% of seizure types. It is established that GGE and other neurological disorders are, in some cases, caused by channelopathies within post-synaptic inhibitory neurotransmitter systems such as GABA (epilepsy) and Glycine (hyperekplexia). GABA is the primary inhibitory neurotransmitter in the brain and is synthesised from glutamate by GAD65 and 67, and is released from the pre-synaptic nerve terminal into the synaptic cleft, where it binds to post-synaptic GABA receptors and initiate neuroinhibition. This inhibition is removed by post-synaptic GABA transporters (GAT1 and GAT3) that uptake GABA back into the cell for re-packaging in presynaptic vesicles or breakdown by transamination. Abnormalities in this system have been linked to diseases including anxiety, psychosis, Parkinsons's Disease and epilepsy. GABAergic animal models have demonstrated a tendency to seizure, including GABA transporter and enzyme models in relation to epilepsy.

Given the above, the aim of this study was to identify GGE causing variants in four GABAergic genes. GGE patient samples (n=707) were recruited from 3 global centres and screened for variations in GAT1, GAT3, GAD65, GAD67 using high-throughput LightScanner analysis and bi-directional Sanger sequencing. Control population studies (n=480) were carried out and analysis of online databases to determine the frequency of variants. Twenty novel or very rare variants were identified in 48 patient samples representing a detection rate of 6.8%, where a clustering of phenotypes included a predisposition towards absence seizures. The biological consequences of these variants were predicted using three online predictive programmes, multiple phylogenetic alignments and 3D structural modelling. Mutation expression constructs were prepared and expression levels were validated by immunocytochemistry. Functional characterisation of these variants will hopefully improve genetic diagnosis in GGE and determine causality of GABAergic absence seizures.

Abbreviations

°C	Degrees centigrade
µl	microlitre
µM	Micromole
A	Adenine
ADHD	Attention deficit hyperactivity disorder
AED	Anti-epileptic drug
ALDH	Aldehyde dehydrogenase
Asn	Asparagine
ATP	Adenosine triphospahte
BOLD	Blood oxygenation level-dependant
bp	Base pair
BSA	Bovine Serum Albumin
C	Cytosine
CACN	Voltage dependant calcium channel
CAE	Childhood absence epilepsy
cAMP	Cyclic adenosine monophosphate
CASR	Calcium sensing receptor
cDNA	Complementary DNA
CHRN	Cholinergic receptor
CLCN	Chloride channel
CMV	Cytomegalovirus
CNS	Central nervous system
CO_2	Carbon dioxide
C-terminal	Carboxyl-terminal
dbSNP	Single Nucleotide Polymorphism Database
DMEM	Dulbecco's Modified Eagle Medium
DMSO	Dimethyl sulfoxide
DNA	Deoxyribonucleic acid
DPBS	Dulbecco's Phosphate Buffer Saline
dsDNA	Double standed DNA
EDTA	Ethylenediaminetetraacetic acid
EEG	Electroencephalogram
EFHC	E-F hand domain (C-terminal)
ELP	Elongator acetyltransferase
EPSP	Excitatory post-synaptic potentials
EtOH	Ethanol
FBS	Fetal Calf Serum
fMRI	Functional magnetic resonance imaging
FRET	Fluorescence resonance energy transfer
G	Guanine

GABA	Gamma-Aminobutyric acid
GABARAP	GABA receptor associated protein
GABAT	GABA transaminase
GABR	GABA A receptor
GAD	Glutamic acid decarboxylase
GAERS	Genetic Absence Epilepsy Rat from Strasbourg
GAT	GABA transporter
GGE	Genetic generalised epilepsy
GHBDH	Gamma-hydroxybutyrate dehydrogenase
GlyR	Glycine receptor
GlyT	Glycine transporter
GRIN	Glutamate receptor
GTCS	Generalised tonic-clonic seizures
GTP	Guanosine triphosphate
HEK	Human embryonic kidney
HIV	Human immunodeficiency virus
HRM	High resolution melting
IBE	International Bureau for Epilepsy
IgG	Immunoglobulin G
ILAE	International League Against Epilepsy
IPSP	Inhibitory post-synaptic potentials
JAE	Juvenile absence epilepsy
JME	Juvenile myoclonic epilepsy
KCN	Voltage gated potassium channel,
kDa	Kilodalton
LGI1	Leucine-rich glioma-inactivated 1
MAF	Mean allelic frequency
MASS1	Monogenic audiogenic seizure-susceptible 1
MBD	Methyl-CpG-binding domain
ME	Malic enzyme
mV	Millivolt
NAD	Nicotinamide adenine dinucleotide
NADH	Nicotinamide adenine dinucleotide plus Hydrogen
NCBI	National centre for biotechnology information
NET	Norepinephrine transporter
ng	Nanograms
NMDA	N-methyl-D-aspartate
N-terminal	Amino-terminal
NTP	Nucleoside triphosphate
OCD	Obsessive compulsive disorder
ORF	Open reading frame
PBS	Phosphate buffered saline
PC12	Pheochromocytoma cells
PCDH	Protocadherin

PCR	Polymerase chain reaction
PDB	Protein data bank
PKA	Protein kinase A
PLL	Poly-L-Lysine
PLP	Pyridoxal phosphate
pmol	Picomole
PolyPhen	Polymorphism phenotyping
PRRT	Prolein rich repeat protein
REM	Rapid eye movement
RNA	Ribonucleic acid
rpm	Revolutions per minute
RT-PCR	Real-time polymerase chain reaction
SCN	Voltage-gated sodium channel
SDS	Sodium dodecyl sulphate
SIFT	Sorting Tolerant From Intolerant
SLC	Solute carrier family
SNP	Single nucleotide polymorphism
SSA	Succinic semialdehyde
SSADH	Succinic semialdehyde dehydrogenase
SSADHD	Succinic semialdehyde dehydrogenase deficiency
SWD	Spike wave discharge
T	Thymine
TB	Tuberculosis
TBC1D	TBC1 domain family
Tm	Melting temperature
TM	Transmembrane
TRN	Thalamic reticular nucleus
UCL	University College London
UTR	Untranslated region
UV	Ultraviolet
V	Volts
WAG/Rjj	Wistar Albino Glaxo from Rijswijk
WERN	Wales epilepsy research network
WT	Wild-type

Table of content

Chapter One

Introduction

1.1 Epilepsy

Epilepsy is a neurological disorder that affects adults and children from every major population in the world; over 450,000 people in the United Kingdom and 50 million people worldwide. The highest incidence of epilepsy occurs in young children and the elderly, with approximately 3% of all living people under the age of 80 receiving a diagnosis (Hesdorffer et al., 2011). The prevalence of epilepsy is 25% higher in the most socially deprived areas of the United Kingdom (Purcell et al., 2002) and the cost of epilepsy management and treatment in the UK is estimated as £268 million (Joint Epilepsy Council, 2011) per annum. The misdiagnosis of epilepsy, which can occur in 20-30% of patients, contributes an additional cost of £130-£190 million a year (Stokes et al., 2004).

Epilepsy is characterised by the onset of spontaneous convulsive and non-convulsive seizures, which are synchronous momentary electrical discharges that occur in the brain, resulting in too much excitation or too little inhibition (Treiman, 2001). The official terms for epilepsy and seizures as agreed by the International League Against Epilepsy (ILAE) and International Bureau for Epilepsy (IBE) are as follows (Fisher et al., 2005):

"Epilepsy is a disorder of the brain characterized by an enduring predisposition to generate epileptic seizures and by the neurobiological, cognitive, psychological and social consequence of the condition".

"An epileptic seizure is a transient occurrence of signs and/or symptoms due to abnormal excessive or synchronous neuronal activity in the brain."

1.1.1 Causes of Epilepsy

Epilepsies are divided according to their aetiology. Three main groups were recognised by ILAE: Idiopathic, Symptomatic and Cryptogenic (1989). However, recent modifications to disease classifications have occurred as recommended by ILAE (2011) and the current aetiology stratifiers are i) Genetic, ii) Structural/Metabolic and iii) Unknown (Berg and Scheffer, 2011). Epilepsies that are considered i) genetic are understood to be the direct result of a known or presumed genetic defect where seizures are the core symptoms of the disorder. ii) Structural/metabolic epilepsies occur due to a distinct structural or metabolic condition or disease affecting the CNS; this can include trauma, stroke, tumours and/or infection. iii) Unknown epilepsies are those remaining cases where there is no known cause. These may have an unidentified fundamental genetic source or they may be the consequence of an unrecognised structural or metabolic disorder. Epilepsy is often multifactoral and even if a major cause is identified, there can often be additional contributing factors (Berg and Scheffer, 2011). Comorbidities occur in epilepsy including cognitive problems such as learning difficulties, psychiatric issues such as depression and physical problems such as chronic fatigue.

There is a large variation in epilepsy cause depending on age groups and environment (Figure 1.1). For example genetic epilepsy is more common in early life whereas epilepsy as a consequence of structural/metabolic deficits are more common in later life. Epilepsy caused by infectious and post-infectious diseases such as TB and HIV is more common in certain parts of the world than others, although meningitis is an epilepsy-causing infection that is common worldwide (Marks et al., 1992). Several single-gene disorders that cause epilepsy are associated with variable and complex syndromic phenotypes. These include disorders such as tuberous sclerosis, neuronal migration disorders such as double cortex syndrome, Rett syndrome and the spectrum of epileptic encephalopathies (Dravet Syndrome, Lennox Gastou, Otahara syndrome). With improved patient classification and phenotyping combined with the rapid development of genetic analysis technologies, more single-gene disorder epilepsies will be identified (Merwick et al., 2012).

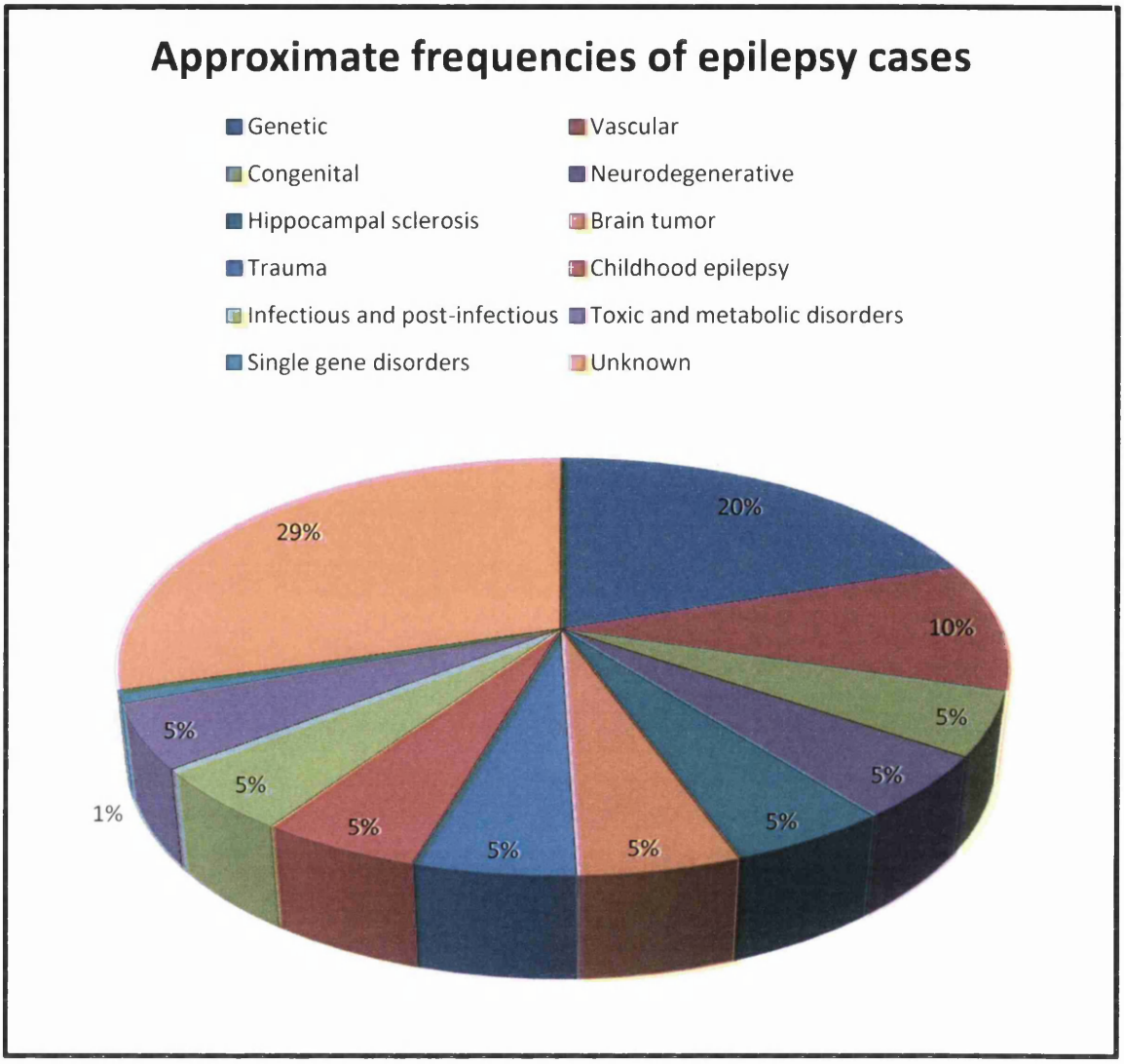

Figure 1.1 Approximate frequencies of epilepsy cases. Whilst approximately 70% of epilepsies fit into a causal category, the cause of up to 30% of epilepsies still remains unknown (Shorvon, 2009).

1.1.2. Epileptic syndromes and seizure types

Epileptic syndromes are categorised according to seizure type, age of onset, electroencephalogram (EEG) results and neuroimaging, amongst other features (Crompton and Berkovic, 2009). Table 1.1 shows the different categories of epilepsy syndromes, demonstrating their aetiology and anatomical origins according to ILAE criteria (1981, 1989, Berg et al., 2010). The ILAE classification scheme is based on clinical semiology (1981, Berg et al., 2010). According to this scheme, there are three

main seizure types; focal (previously called partial), generalised and unknown seizures. The ILAE, however, recognise that further improvements in classification, for example with seizures of an unknown type, can be made by means of magnetic resonance imaging, whilst some epilepsies of structural/metabolic category are neither truly structural nor metabolic. These include some epilepsies with an autoimmune, inflammatory, neurochemical, synaptic or degenerative pathologies (Uttam et al., 2013).

Focal seizures arise in one hemisphere of the brain's cerebral cortex at a specific site termed the epileptic focus. Symptoms of focal seizures vary, dependent on the location of the epileptic focus, and patients may or may not experience impairment of consciousness or awareness (Berg et al., 2010).

Generalised seizures occur in large areas of the cerebral cortex, involve both hemispheres simultaneously, and do not present a focal cerebral onset (Berg and Scheffer, 2011). There are six recognised types of generalised seizure (Figure 1.2); Tonic, Clonic, Tonic-clonic, Myoclonic, Atonic and Absence seizures. Tonic seizures involve tonic muscle contractions and changes in consciousness. These contractions cause movement of the neck, arms and legs, with pronation of the forearm and flexing of the wrists and feet; the patient may also cry out. Tonic seizures occur in all ages and may last less than 20 seconds (Lance, 1963). Clonic seizures are most frequently seen in children and neonates. This seizure is characterised by violent flexor movement and rhythmic spasms (Rosso et al., 2003). Tonic-clonic seizures are characterised initially by massive violent tonic muscle contractions, followed by a second clonic phase of jerking movements (Hsieh et al., 2008). Myoclonic seizures are sudden and brief involuntary movements caused by muscle contractions or inhibitions due to cortical discharges. These can occur as a single episode or they can be repetitive, with changes in the severity of the attack. The seizures tend to occur during the first few hours of awakening or whilst falling asleep; the patient will recover immediately from the seizure (Fahn et al., 1986). Seizures are very brief, lasting only a few seconds. Although they may involve the whole body, there is much less movement in comparison with other generalised seizures (Leppik, 2003). Atonic seizures involve a sudden loss of postural tone which can range from a slight loss (such as a jaw drop), to more severe loss of posture (whereby the whole body would drop to the ground), causing the seizure to adopt the name 'drop attack'. If there is loss of consciousness,

Focal			Generalised			Unknown	
Genetic	**Structural**	**Unknown**	**Genetic**	**Structural**	**Unknown**	**Focal and Generalised**	**Without unequivocal focal or generalised features**
Benign childhood	Chronic progressive	Temporal lobe	Benign myoclonic in infants	West syndrome	Early myoclonic encephalopathy	Neonatal seizures	
Childhood with occipital paroxysms	Syndromes with specific modes of precipitation	Frontal lobe	Childhood absence	Lennox-Gastaut syndrome	Early infantile epileptic encephalopathy with suppressed burst	Severe myoclonic in infancy	
Primary reading	Temporal lobe	Parietal lobe	Juvenile myoclonic	With myoclonic astatic seizures	Others	With continuous spike waves during slow wave sleep	
Epilepsy-aphasia syndromes	Frontal lobe	Occipital lobe	Generalised Tonic-clonic seizures on awakening	With mycolonic absences	Due to specific neurological disorder	Landau-Kleffner syndromes	
Migrating focal seizures of infancy	Parietal lobe	Unlocalised	Syndromes with specific modes of precipitation			Other	
	Occipital lobe		Others				
	Unlocalised						

Table 1.1 Epilieptic syndromes. Epilepsy syndromes are divided according to their localisation into focal, generalised and unknown. These categories are subdivided into genetic, structural and unknown. Adapted from ILAE classification (1981, 1989, Berg et al., 2010, Zarrelli et al., 1999).

it is very brief (Hsieh et al., 2008, Pazzaglia et al., 1985)

Absence seizures occur in numerous syndromes such as childhood absence epilepsy (CAE) and juvenile myoclonic epilepsy (JME), and are one of the most common types of seizures identified in patients with genetic generalised epilepsy (GGE) (Helbig et al., 2008). My work is concerned with the genetic aetiology of absence seizures. I will therefore consider these in more detail along with the syndromes they occur in.

There are three subtypes of absence seizure: typical, atypical and absences with special features (Figure 1.2). Typical absence seizures are the only neurological absences to occur almost exclusively in GGE. Absence seizures are characterised by recurrent non-convulsive episodes with brief loss of awareness and responsiveness (Jones et al., 2011). This can include brief staring episodes, behavioural arrest, and can sometimes result in facial myoclonus, blinking and automatisms (Sullivan and Dlugos, 2004). Patients are often unaware that an attack has occurred as it ends as abruptly as it started, with most seizures lasting less than 10 seconds. However, the seizures can take place hundreds of times in one day and they can often occur in clusters, especially when the individual is tired or drifting in and out of sleep. Seizures can also be brought on by fatigue, relaxation, photic stimulation and hyperventilation (Shorvon, 2009); the latter is used to provoke seizures to aid diagnosis and treatment (Panayiotopoulos, 1999).

Typical absence seizures occur due to abnormal electrical activity in the thalamo-cortical network, with little or no involvement of other brain regions. Many seizure types that occur in the thalamus have a genetic cause (Slaght et al., 2002). EEG results of a patient suffering with absence seizures would consist of a symmetrical 2.5-4 Hz 'spike and slow' wave complexes that occur without lateralising or localising features. The background EEG rhythm would ordinarily be normal for those cases presenting with absence seizures (Holmes et al., 2004, Cordelli et al., 2013).

Atypical absence seizures are far less common than typical absences, but have a more severe phenotype, they can occur at any age, and are associated with severe neurological impairment (Farwell et al., 1985). It is believed that, as with typical absence seizures, the thalamo-cortical network plays a key role in atypical absence

seizure generation but may also involve other brain regions. Velazquez et al (2007) suggest that the spread of a seizure from the thalamo-cortical network to other regions could be due to weakened inhibition leading to seizure recruitment in originally unaffected brain areas (Velazquez et al., 2007). EEG results show activation in the thalamus and deactivation in the medial frontal and posterior cingulate cortices as well as significant thalamic connections during generalised spike and wave discharges. (Carney et al., 2010, Zhang et al., 2014).

Absence seizures with special features such as absences with eyelid myoclonia involve typical childhood absences with jerking of the eyelid immediately after closing, rolling of the eyes and, on occasion, subtle loss of awareness (Jeavons, 1977). Seizures can be triggered by hyperventilation, photic stimulation and almost invariably by eye closure in the presence of light. Absence seizures with eyelid myoclonus are often missed by the medical practitioner and can be misdiagnosed as autonomic tics (Covanis, 2005). The average age of onset of absence seizures with eyelid myoclonia is 6 years and there is a female preponderance. Joshi and Patrick (2007) identified that 77% of patients with absence seizures and eyelid myoclonia had low IQ and were four times more likely to experience difficulties with school compared to their peers (Joshi and Patrick, 2007).

As previously mentioned absence seizures are the most predominant seizure type in GGE patients. As GGE accounts for a large percentage of all epilepsies the phenotype and subgroups will be discussed in more detail.

1.2 Genetic generalised epilepsy (GGE)

There are over 50 epilepsy phenotypes, and GGEs account for up to 30% of all epilepsies (Jallon et al., 2001). These genetic epilepsies are characterised by generalised spike waves on EEG that typically arise from normal background activity. Patients suffering with GGE may experience seizures including absences, myoclonic jerks and tonic-clonic seizures that arise in both hemispheres of the brain and show no

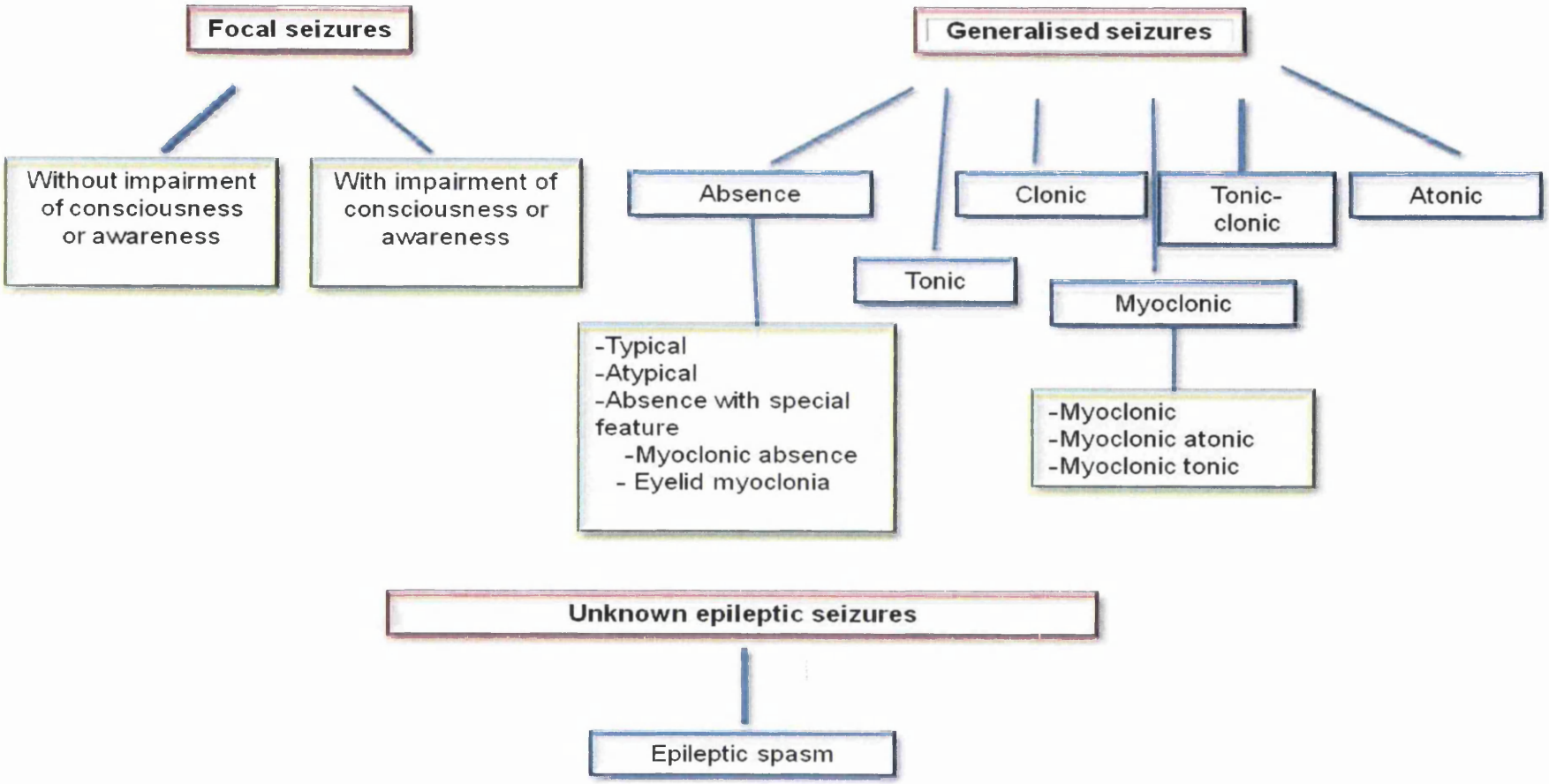

Figure 1.2 Major seizure classification. The three seizure classes are shown in red boxes and different seizure types within the classes shown in blue boxes. Sub groups are shown in a green box. Adapted from The International League Against Epilepsy (ILAE) 1981, 1989 and Berg et al, 2010.

identifiable macroscopic or microscopic structural brain abnormality (1989) (Woermann et al., 1998).

Two of the more common GGEs are childhood absence epilepsy (CAE) and juvenile myoclonic epilepsy (JME), followed by juvenile absence epilepsy (JAE) and myoclonic absence epilepsy (MAE).

1.2.1 Childhood Absence Epilepsy (CAE)

CAE affects otherwise neurologically normal children between the ages of 4 and 10 years, with incidence peaking between 5 and 7 years of age. CAE involves brief absence seizures that occur numerous times a day, end abruptly and are more common in females (Pal et al., 2006). Early onset CAE is uncommon, occurs in children under the age of four and affects more males than females (Asadi-Pooya et al., 2012). Early onset childhood epilepsy is believed to share some common biological and possibly genetic determinants as typical CAE, however they may have additional seizure types, movement disorders and neurodevelopmental delay. For example, generalised tonic-clonic seizures (GTCS) have been reported in 30-60% of patients with CAE: A study by Asadi-Pooya and colleagues, (2012) found that 56% of early onset CAE patients had GTCS, whilst febrile convulsions are reported in 25% of early onset CAE compared to 10% of CAE. There is an almost equal occurrence of myoclonic seizures in both typical and early-onset CAE (Asadi-Pooya et al., 2012).

1.2.2 Juvenile Myoclonic Epilepsy (JME)

JME is characterised by teenage onset of myoclonic jerks. There are differences amongst myoclonic jerks experienced by those diagnosed with JME; some experience only upper limb jerking and others experience leg and head movement. GTCS and absences are also common in JME. Seizures usually occur after waking and are related to sleep deprivation, stress and illness (Genton and Gelisse, 2001; Clement and Wallace, 1988). This is taken into account when treating patients with JME as they are advised to avoid precipitants such as sleep deprivation and excessive alcohol. The age of onset of

JME depends on the individual and can present itself between the ages of 8 and 36 years; peaking between the ages of 12 and 18 (Sullivan and Dlugos, 2004). Many individuals experience childhood absence epilepsy or juvenile absence epilepsy before evolving to JME, though some experience absence seizures following their first myoclonic episode at puberty (Thomas et al., 2013, Delgado-Escueta and Enrile-Bacsal, 1984).

1.2.3 Juvenile absence epilepsy (JAE)

Juvenile absence epilepsy (JAE) is a GGE that occurs between the ages of 8 and 16 and peaks at puberty (1989). Patients have severe absence seizures albeit at a lower frequency than that of typical CAE patients, but with a higher frequency of tonic-clonic seizures (Wolf and Inoue, 1984). Seizures tend to occur in clusters in the hour following waking, or as one daily seizure lasting 4-20 seconds. The normal trigger for a seizure in a patient with JAE is, as with CAE, sleep deprivation as well as hyperventilation (Trinka et al., 2004). Patients with JAE can demonstrate normal neurodevelopmental and physical characteristics, and is predominantly identified in females (Christensen et al., 2005).

1.2.4 Myoclonic absence epilepsy (MAE)

MAE is a rare epilepsy syndrome with male predominance, occurring between the ages of 5 months and 13 years. MAE is characterised by absence seizures that can manifest with rhythmic bilateral myoclonic jerks with varied consciousness impairment. The seizures tend to last between 10 and 60 seconds and occur numerous times throughout the day. Two-thirds of patients with MAE also experience tonic-clonic seizures (Engel, 2001).

Developing childhood absence epilepsy can be life changing. Diagnosis and prognosis with the aid of genetic testing can significantly improve epilepsy management and quality of life.

Table 1.2 Genes identified in generalised epilepsy

Generalized epilepsies; febrile seizures, absence seizures		
Gene symbol	**Gene name**	**Score**
ALDH7A1	Aldehyde dehydrogenase 7 family, member A1	2
CACNA1A	Voltage dependant calcium channel, alpha 1A subunit	3
CACNA1H	Voltage dependant calcium channel, alpha 1H subunit	3
CACNB4	Voltage dependant calcium channel, beta 4 subunit	3
CASR	Calcium sensing receptor	2
CHRNA2	Cholinergic receptor, alpha 2 (Nicotinic)	3
CHRNA4	Cholinergic receptor, alpha 4 (Nicotinic)	3
CHRNB2	Cholinergic receptor, beta 2 (Nicotinic)	3
CLCN2	Chloride channel 2	2
EFHC1	E-F hand domain (C-terminal) containing 1	3
ELP4	Elongator acetyltransferase complex subunit 4	1
GABRA1	GABA A receptor, alpha 1	3
GABRB3	GABA A receptor, beta 3	3
GABRD	GABA A receptor, delta	3
GABRG2	GABA A receptor, gamma 2	3
GRIN2A	Glutamate receptor, N-methyl; D aspartate	3
GRIN2B	Glutamate receptor, ionotropic, N-methyl D-aspartate 2B	3
KCNA1	Voltage gated potassium channel, shaker-related subfamily, member 1	3
KCNMA1	Potassium large conductance calcium-activated channel, subfamily M, alpha member 1	3
KCNQ2	Voltage-gated potassium channel, KQT-like subfamily, member 2	3
KCNQ3	Voltage-gated potassium voltage-gated channel, KQT-like subfamily, member 3	3
KCNT1	Potassium channel subfamily T, member 1	3
MBD5	Methyl-CpG-binding domain protein 5	2
ME2	Malic enzyme 2, NAD(+)-dependent, mitochondrial	1
PCDH19	Protocadherin 19	2
PRRT2	Prolein rich repeat protein type 2	2
SCN1A	Voltage-gated sodium channel, voltage-gated, type I, alpha subunit	4
SCN1B	Voltage-gated sodium channel, type I, beta subunit	3
SCN2A	Voltage-gated sodium channel, type II, alpha subunit	4
SCN9A	Voltage-gated sodium channel, type IX, alpha subunit	3
SLC2A1	Solute carrier family 2 (facilitated glucose transporter), member 1	4
TBC1D24	TBC1 domain family, member 24	3

Table 1.2 Genes identified in generalised epilepsy. The most relevant genes identified in generalised seizures have been scored from 1 to 4 based on the level and depth of evidence: 1 represents genes that were identified from linkage studies, however no mutation have been identified in the gene nor has any functional work been carried out; 2 would suggest that mutations in the gene have been identified, however, no validation had been carried out by means of function or population studies; 3 if mutations had been identified which had supporting functional results; and 4 for genes with extensive supporting functional work for the causality of mutations and the gene associated with large unrelated cohorts and robust population study results.

1.3 Epilepsy associated genes

The identification of causal epilepsy genes has impact on diagnosis & prognosis, assist with treatment & management, and is informative in the risk of the epilepsy occurring in offspring. Numerous genes and mutations have been identified in relation to generalised epilepsies (Table 1.2) (Lemke et al., 2012, Garofalo et al., 2012), however, the number of cases with a definitive disease-associated genetic signature are only a very small proportion of the epilepsy population. Although the genes listed in table 1.2 are the primary genes associated with generalised epilepsy, there are additional genes, identified in syndromic disorders, where epilepsy plays a substantial role in the patient phenotype (Lemke et al., 2012, Garofalo et al., 2012).

Mutations in ion channel genes and neurotransmitter receptors have been discovered in genetic epilepsies, although mutations where epilepsy is the primary morbidity feature may also be linked to genes important for cortical development, cell metabolism and mitochondrial function (Deng et al., 2013). Linkage analysis in multiplex families, candidate gene analysis in cohorts and findings in animal models of epilepsy have confirmed that channelopathies are an important cause of GGE. Channelopathies have been instrumental in providing the molecular insights into epileptogenesis.

1.3.1 Sodium Channels

Sodium channel dysfunction is recognised as being extremely important in the aetiology of GGEs and have long been a target for anti-epileptic drugs. The sodium channel is made up of a pore-forming α-subunit and regulatory β-subunits; nine genes are known to encode α-subunits and four genes encode β-subunits (Scheffer and Berkovic, 2003). Numerous epilepsy syndromes have been associated with mutations in the sodium channel *SCN1A;* the majority of mutations (over 100) interestingly occur in patients suffering with Dravet syndrome. Sodium channelopathies due to mutations in *SCN1B* and *SCN2A* have also been linked to generalised epilepsy with febrile seizures–plus (GEFS+) and benign familial neonatal infantile spasm (Mulley et al., 2005).

1.3.2 Potassium Channels

There are three structural families of approximately 100 potassium channel genes identified in the human genome that are primarily expressed in the brain. Potassium channels are required for stabilising the resting membrane potential of cells and regulating neuronal excitability by repolarising action potentials or producing M currents to mediate hyperpolarisation; therefore a loss of voltage-gated potassium channel function can result in increased excitation (Jentsch, 2000, D'Adamo et al., 2013).

1.3.3 Chloride Ion Channels

Chloride channel mutations had been shown to cause impairment of chloride efflux resulting in an increase in intracellular chloride. This in turn lowers the transmembrane gradient for chloride and causes a decrease in GABA mediated inhibition. Mutations in the chloride channel gene *CLCN1* are identified in association with GGE and mutations in *CLCN2* are associated with four GGEs: CAE, JAE, JME and epilepsy with grand mal seizures on awakening (Haug et al., 2003; Chen et al., 2013).

1.3.4 Calcium channels

Mutations in voltage gated calcium channels in HEK293 cells cause a slowing of inactivation, causing a shift of inactivation potential toward depolarisation, which are electrophysiological features characteristic of absence seizures (Khosravani et al., 2004). Numerous animal models show that the consequences of calcium channel mutations can include symptoms of idiopathic generalised epilepsy; especially absences with ataxia, which is a rare phenotype (Escayg et al., 2000).

1.3.5 Neurotransmitter receptors and transporters

Ligand-gated ion channels have been widely researched and mutations have been identified in GABA receptors and neuronal nicotinic acetylcholine receptors in relation

to epilepsy. Mutations in both $GABA_A$ and $GABA_B$ receptors have been associated with the childhood epilepsies JME and CAE. Studies of the R43Q mutation, identified in *GABRG2,* demonstrates the slowing of receptor deactivation and an increase in the rate of desensitisation, resulting in CAE. This resulted in a build up of desensitised receptors, and therefore excessive excitation occurs (Bowser et al., 2002). Mutations in the major CAE causal gene of GLUT1 (*SLC2A1*) were identified by Suls et al. (2009) in 12% of early onset CAE cases, which is now a gene used to aid in CAE diagnosis and allow genetic counselling (Suls et al., 2009).

Nicotinic acetylcholine receptors in neurons are expressed in abundance at synapses. They are involved in numerous neurotransmitter systems and in both excitatory and inhibitory systems; it is therefore unsurprising that mutations have been identified in both *CHRNA4* and *CHRNB2* having functional affects on the alpha and beta subunits of this protein respectively (Scheffer and Berkovic, 2003).

The identification of these ion channel genes has significantly improved successful epilepsy magangement and treatment as well as other diseases. Numerous epilepsy drugs are available and patient symptoms along with genetic testing has allowed for accurate drug selection and protein targetting.

1.4 Epilepsy treatments

Over the past 30 years, there has been rapid development in anti-epileptic drugs (AEDs). However, 30% of epilepsy patients do not achieve successful seizure control from current seizure treatment including AEDs, surgery or vagus nerve stimulation (Perucca et al., 2007). The main AEDs dispensed are presented in table 1.3, along with their primary mechanism of action and the type of epilepsy treated.

1.4.1 Antiepileptic drugs and genetic generalised epilepsy

Most genetic generalised epilepsies respond well to AEDs, but treatment is often lifelong. Valproate, lamotrigine, ethosuximide, topiramate and levetiracetam are the most common AEDs for children used today (Beydoun and D'Souza, 2012). Valproate

has been the medication of choice for JME patients for decades and is considered the first-line of treatment for these patients (Nicolson and Marson, 2010). Absence seizures and GTCS are the primary GGE seizure type treated by valproate, but if valproate is ineffective or poorly tolerated, then lamotrigine may be offered. Valproate is not generally recommended for women as it can lead to the development of polycystic ovary syndrome, but how valproate may be causal is unclear. Lamotrigine blocks the conductance of sodium channels to prevent excitation and therefore seizure; the actions of valproate are not fully understood at this time although it is known that it has an effect on GABA and glutamine activity as well as calcium and potassium conductance (Sullivan and Dlugos, 2004).

JME can also be treated with the synaptic vesicle protein binding AED levetiracetam, which acts to prevent myoclonic seizures as well as generalised tonic-clonic seizures. This drug is beneficial for epilepsy patients as it does not cause the usual sedative affects that other AEDs can, however, it can cause irritability and weight gain (Sullivan and Dlugos, 2004). The AED topiramate works in numerous ways including enhancing GABA activity, blocking sodium channel conductance and blocking glutamate receptors. The drug is used in the treatment of generalised tonic-clonic seizures and can be used as a monotherapy or as an adjunctive therapy with lamotrigine. As with JME, CAE is also treatable with valproate and is again a first line treatment along with the calcium channel inhibitor ethosuximide and lamotrigine (Sullivan and Dlugos, 2004). Ethosuximide suppresses the spike and wave activity associated with lapses in consciousness (Goldenberg, 2010).

Tiagabine is generally used in conjunction with other AEDs and is used when other lines of treatment have failed. Tiagabine is used to treat primary generalised seizures by selectively inhibiting the GABA transporter, GAT1. This increases the GABA levels, especially in the hippocampus and thalamus. Interestingly, tiagabine also has unwanted proepileptic effects, which involve desensitisation of $GABA_A$ receptors and increased synchronisation. This was seen to occur most frequently in the thalamocortical circuit resulting in absence seizures and myoclonic jerks (Walker, 2002, Angehagen et al., 2003). GABA receptors have been extensively studied in a number of epilepsies, implicating the wider GABAergic system to disease onset. This will be discussed and analysed further in the following section.

Drug	Major putatative mechanism of action	Treated epilepsy
Carbamazepine	Block sodium channel conductance	First line partial and generalised tonic-clonic seizures, excluding absence and myoclonus
Clobazam	Enhance GABA actions	Second line for partial and generalised tonic-clonic seizures
Clonazepam	Enhance GABA actions	Second line for partial and generalised tonic-clonic seizures including absence and myoclonus
Ethosuximide	Inhibit T-type calcium channels	Generalised absence seizures only
Gabapentin	Binds to voltage-dependant calcium channel	Adjunctive for partial or secondary generalised epilepsy
Lacosamide	Enhances slow inactivation of sodium channel	Adjunctive for partial-onset seizure and/or secondary generalised epilepsy
Lamotrigine	Block sodium channel conductance	First line or adjunctive in partial and generalised epilepsy
Levetiracetam	Binds to synaptic vesicle protein SV2A	First line/adjunctive in partial-onset seizures and IGE
Oxcarbazepine	Block sodium channel conductance	Partial and secondary generalised epilepsy
Perampanel	Blocks AMPA receptors	Partial epilepsy
Phenolbarbital	Enhances GABA and inhibits Glutamate	Partial or secondary generalised epilepsy
Phenytoin	Block sodium channel conductance	Partial and primary and secondary generalised seizures excluding absences and myoclonus
Pregabalin	Binds to voltage-dependant calcium channel	Econd line partial seizures with or without generalised epilepsy
Primidone	Pro drug of pheolbarbitual	Partial or secondary generalised epilepsy
Retigabine	Activates potassium channels	Partial onset seizures with or without secondary generalised epilepsy
Tiagabine	Inhibits GABA re-uptake	Adjunctive for partial or secondary generalised epilepsy.
Topiramate	Primarily blocks sodium channel conductance	Adjunctive/monotherapy in partial and secondarial generalised epilepsy
Valproate	Not fully understood	All forms of epilepsy at any stage
Vigabatrin	Inhibit GABAT	First line in infantile spasm and adjunctive in partial epilepsy
Zonisamide	Primarily inhibits sodium and T-type calcium current	Refractory partial epilepsy

Table 1.3 Primary drugs involved in the treatment of epilepsy. The above 20 drugs are considered first or second line treatments for a variety of epilepsy types.

1.5 The GABAergic system

Gamma-aminobutyric acid (GABA) is the primary inhibitory neurotransmitter in the mammalian brain, whilst glutamate is the principal excitatory neurotransmitter. GABA is present in almost all prokaryotic and eukaryotic organisms, identified not only in the central nervous system where it is believed to be present in 60-70% of all synapses, but also in the immune system (Nagga et al., 1999). It is also present in many organs throughout the body such as the testes, uterus, ovaries, pancreas, pituitary, gastrointestinal tract and adrenal medulla (Gladkevich et al., 2006). A change in level of either GABA or glutamate has great affect on an organism, increased levels of glutamate (or decreased GABA levels) can cause seizures, increased GABA levels (or decreased glutamate levels) can cause drowsiness, sleep deprivation, nervousness, anxiety and instability amongst other symptoms (Rimmer and Richens, 1984).

1.5.1 GABA formation

The formation of GABA occurs in the central nervous system of vertebrates from glutamate. This process is catalysed by the enzyme glutamic acid decarboxylase (GAD) and involves the swift α-decarboxylation of L-glutamic acid in the brain (Figure 1.3). The mitochondrial aminotransferase, GABA-transaminase (GABAT), is responsible for the transamination of GABA, causing the removal of an amino group and adding it to α-ketoglutarate. This process reloads glutamate and produces succinic semialdehyde (Kim et al., 2009). Succinic semialdehyde dehydrogenase (SSADH) catalyses succinic semialdehyde oxidation into succinic acid which in turn is utilised in the Krebs cycle; the final aerobic oxidation pathway (Figure 1.4). It must be noted however that there is an absence of GAD in astrocytes, and glutamate cannot therefore be converted to GABA in these cells. In astrocytes, glutamate is synthesised into glutamine for transfer to axon terminals by transporters, where it is converted back into glutamate by glutaminase and the cycle is repeated (Schousboe et al., 1993). The delicate balance between the glutaminergic excitation and GABAergic inhibition is crucially conserved via this pathway (Pearl et al., 2009).

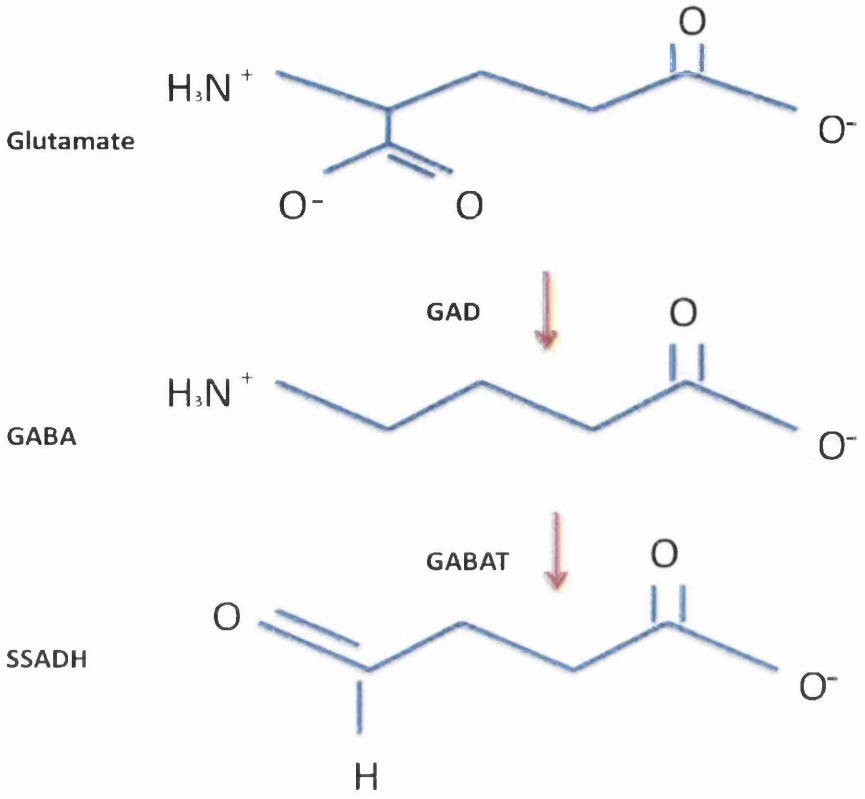

Figure 1.3 Glutamate molecule conversion. GABA is formed by the α-decarboxylation of Glutamate by GAD. GABAT removes an amino group from GABA to form SSADH.

1.5.2 GABA activity

The regulated expression of GABA receptors at the post-synaptic cell surface and the controlled release and re-uptake of GABA are vital to uphold the equilibrium between neural excitation and inhibition. Upon stimulation, there is a slight increase in membrane potential of a neuron from -70mV. If this potential reaches the threshold of approximately -55mV, further depolarisation occurs causing opening of voltage-gated sodium channels and a sodium ion influx; this triggers an all or nothing action potential. As the voltage of the cell increases to approximately 40mV, the sodium channels close and voltage gated potassium channels open. The opening of potassium channels causes efflux of positively charged potassium from the cell as they are repelled by the positive charge in the cell and a decrease in membrane potential is therefore seen which results in a negatively charged cell in relation to its microenvironment once more. Potassium channels remain open until the voltage reaches, at least, resting membrane potential. This is followed by a refractory period where the voltage is stabilised to approximately

-70mV once more, in this time another action potential cannot be fired (Stuart et al., 1997). This nerve impulse is propagated along axons due to sodium ions entering the cell and depolarising neighbouring regions of the axonal membrane as they move laterally along the axon. In a wave like fashion, the action potential is transmitted from the input source to the axons synapse (the pre-synapse) at the target dendrite (the post-synapse) (Bean, 2007).

Neurotransmitters such as GABA are packaged into vesicles by the proteins encoded by the *SLC17* and *SLC18* genes (Chen et al., 2004). Depolarisation of the pre-synaptic cleft causes calcium channels to open and there is an increase in intracellular calcium. This allows the fusion of the GABA filled vesicles with the pre-synaptic membrane causing GABA to be exocytosed from the pre-synapse into the synaptic cleft, where it binds and activates $GABA_A$ and $GABA_B$ receptors of the post-synapse that mediate chloride influx across the post-synaptic membrane. GABA acts as an agonist ligand if bound to phase-active $GABA_A$ receptors and if bound to G-coupled $GABA_B$ receptors stimulates tonic inhibitory influences (Mao et al., 2010, Madsen et al., 2010). GABA is removed rapidly from the post-synapse and taken up by glial processes and the pre-synaptic nerve terminal, where it is catabolised by GABAT (Treiman, 2001). This rapid removal is carried out by GABA transporters (GATs) and occurs in order to regulate synaptic transmission and reduce GABA spill-over to neighbouring synapses (Borden, 1996, Velisek et al., 2011), preventing disproportionate tonic activation of synaptic and extra synaptic GABA receptors (Figure 1.3) (Semyanov et al., 2004).

1.5.3 GABA receptors

Speedy inhibitory neurotransmission in the brain is primarily due to GABA's actions on GABA receptor type A ($GABA_A$). A member of the Cys-loop ligand gated ion channel superfamily, the receptors are heteropentametric GABA-gated chloride channels, typically composed of two α-subunits, two β-subunits and a third subunit. Nineteen mammalian subtypes of $GABA_A$ have been cloned including α 1-6, β 1-3, γ 1-3, δ, ε, π, and θ (Olsen and Sieghart, 2009). Binding of GABA ions to the $GABA_A$ receptor's two GABA binding sites causes the opening of chloride channels and an influx of negatively charged chloride ions, decreasing the membrane potential. This causes a decrease in

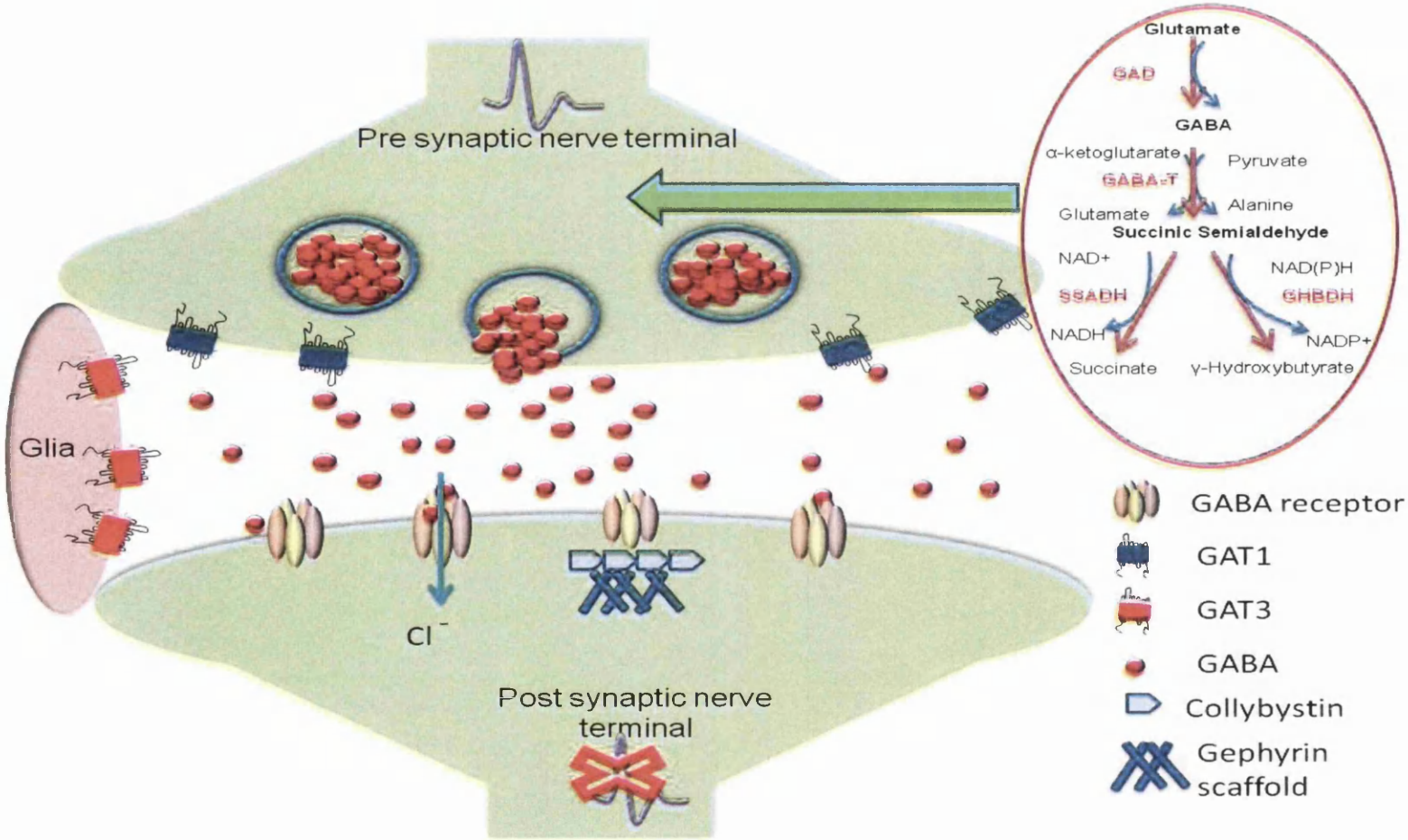

Figure 1.4 GABA activity at a nerve terminal. Electrical impulse causes vesicular GABA to be released from the nerve terminal (pre-synapse) into the synaptic cleft where it binds to post synaptic GABA receptors to cause inhibition of the post-synapse. GABA is rapidly cleared from the synaptic cleft by GABA transporters (GAT1/ 3) of the pre-synaptic nerve terminal and glial processes, whereby it undergoes processes described in section 1.2.1.

overall voltage of the cell and prevents it reaching the threshold for depolarisation and therefore reduces the chance of propagating the action potential in the post-synaptic nerve terminal (Bean, 2007).

$GABA_A$ receptors are expressed in abundance in neurons along their entire axis, hence any changes in their activity and expression level affect brain function immensely (Luscher et al., 2011). Although every neuron contains $GABA_A$ receptors, the expressed subtypes change dependant on the stages of development of the different neurons. Other members of this superfamily include nicotinic acetylcholine receptors, glycine receptors and 5-HT3 receptors. All named receptors have four transmembrane domains, an extracellular N-terminal domain and an extended cytoplasmic loop mediating interactions with trafficking and signalling factors (Figure 1.4) (Luscher et al., 2011).

Gephyrin is a multifunctional protein that is involved in the clustering of $GABA_A$ receptors in the synaptic membrane; the two associate via the $GABA_A$ receptor-associated protein (GABARAP) (O'Sullivan et al., 2005). The guanine nucleotide exchange factor and gephyrin-associated protein, Collybistin, translocates gephyrin from the cytoplasm to the submembranous regions. The N-terminal domain of collybistin regulates collybistin as well as gephyrin cluster size (Kins et al., 2000). It is believed that $GABA_A$ receptors are trafficked to the cell membrane by palmitoylation where gephyrin controls the cell surface dynamics of the receptor (Jacob et al., 2005).

Mutations in the $GABA_A$ receptor have been identified in four subunits ($\alpha 1$, $\beta 3$, δ and $\gamma 2$) that are associated with the childhood epilepsy syndromes, JME (Cossette et al., 2002) and CAE (Table 1.2) (Wallace et al., 2001; Tanaka et al., 2008). Mouse models show that the deletion of the $\alpha 1$ subunit gene shows no epileptic phenotype that may demonstrate a compensatory mechanism of additional inhibitory systems, and as with other diseases, the loss of a receptor could be less dangerous than a receptor with a mutant subunit (Noebels, 2003, Kralic et al., 2002). Mutations in the $\beta 3$ subunit have however been linked to a susceptibility to seizure (Tanaka et al., 2008) and variants in the subunit are also believed to cause insomnia (Buhr et al., 2002). Patients with a missense mutations in the GABA receptor δ subunit have demonstrated a susceptibility to generalised epilepsy with febrile seizure plus and JME (Dibbens et al., 2004). The $\gamma 2$

subunit also been linked with CAE and numerous epileptic encephalopathies and seizures, including absences, myoclonic jerks and tonic-clonic seizures; these phenotypes were due to missense mutations, including one *de novo* mutation (Wallace et al., 2001; Carvill et al., 2003)

Unlike the $GABA_A$ receptor, GABA receptor type B ($GABA_B$), contain only two subunits, GABA-$_{B1}$ and GABA-$_{B2}$. There is a third GABA receptor, $GABA_C$, which, as with the $GABA_A$ receptor, forms a ligand gated chloride channel, however this channel is primarily expressed in the retina (Euler and Wassle, 1998) and will not be considered further in this thesis. Heterodimerisation of the two subunits of $GABA_B$ are required for optimal function and cell surface expression to occur, whereby subunits combined primarily by a coiled coil motif between the two carboxyl termini (Figure 1.5) (Bowery et al., 2002). In some brain regions such as the striatum, however, GABA-$_{B1}$ is functionally expressed without GABA-$_{B2}$, suggesting that another protein could be replacing GABA-$_{B2}$ trafficking GABA-$_{B1}$ to the cell surface. GABA-$_{B1}$ is the subunit capable of agonist binding, whereas GABA-$_{B2}$ is responsible for G-protein coupling (Duthey et al., 2002).

Activation of $GABA_B$ by GABA causes a decrease in L-glutamate release in the pre-synapse by causing the release of heterotrimeric GTP-binding proteins $G_{\beta\gamma}$ and $G_{\alpha i}/G_{\alpha o}$. $G_{\beta\gamma}$ diffuses locally to open potassium channels and close calcium channels, causing lowered calcium conductance and increased potassium conductance; deactivating the molecular machinery of vesicle fusion (Malcangio and Bowery, 1996). $G_{\alpha i}/G_{\alpha o}$ is also involved in post-synaptic inhibition, by firstly inhibiting adenylyl cyclise activity, which, prevents the conversion of ATP into cAMP. Under normal circumstances cAMP would activate PKA, which, would then activate targets such as the glutamate receptor, NMDA.

Mouse studies of deleted neuronal $GABA_B$ show an epileptic phenotype with clonic and rare absence seizures, with a reduction in pre and post synaptic $GABA_B$ responses (Schuler et al., 2001). Disruption in GABA receptor function has been linked to numerous diseases including anxiety (Shekhar et al., 1990) and mood disorders (Brambilla et al., 2003).

Figure 1.5 $GABA_A$ receptor

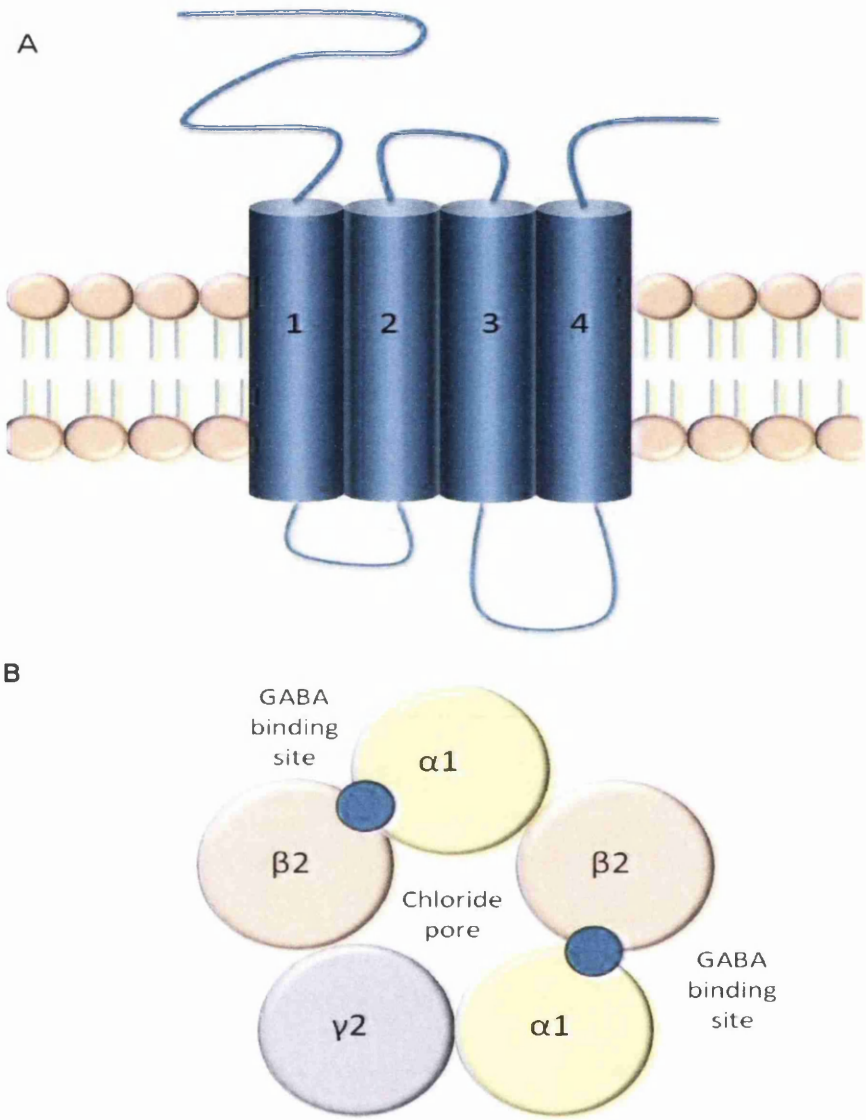

Figure 1.5 $GABA_A$ receptor. A. The membrane bound $GABA_A$ receptor comprises of four transmembrane domains, with both the N and C terminals lying extracellularly. **B.** The $GABA_A$ receptor comprises of two α-subunits (yellow), two β-subunits (pink) and a γ-subunit (purple). The receptor has must have two GABA molecules bound for successful activation (Dark blue circles).

Mutations in the glycinergic inhibitory system, which, includes the post-synaptic glycine receptor gene GlyR as well as the pre-synaptic membrane transporter gene GlyT2, have been identified as the principle cause of hyperekplexia (Rees et al., 2006). It is therefore possible that other members of the GABAergic system such as GABA transporters could be involved with the GABA receptors in being the primary cause of disease.

Figure 1.6 $GABA_B$ receptor heterodimer

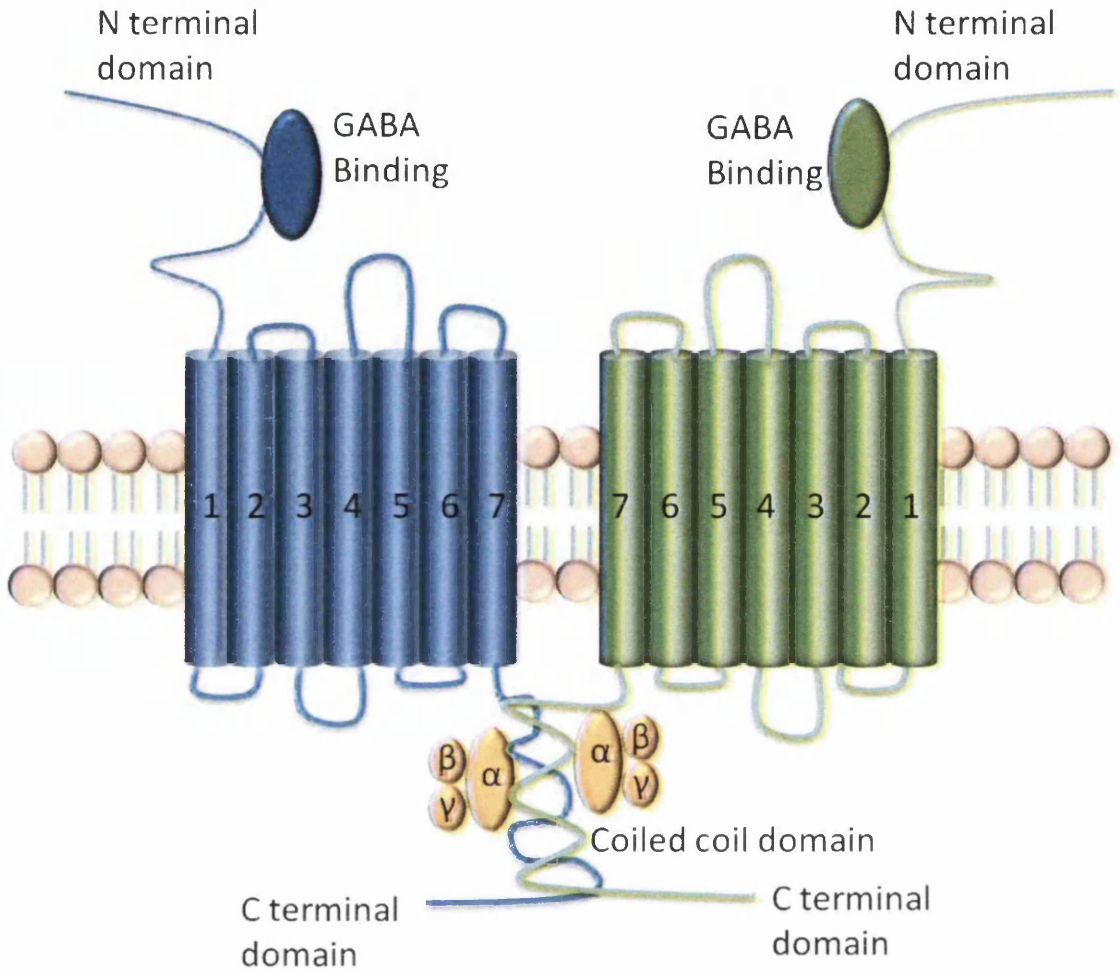

Figure 1.6 $GABA_B$ receptor. Heterodimerisation of two $GABA_B$ subunits occurs via a C-terminal coiled coil motif. Binding of GABA to subunit 1 causes activation of the receptor and G protein coupled inhibition via subunit 2.

1.5.4 GABA Transporters

Four subtypes of GABA transporters (GATs) have been cloned in rodents; GAT subtype 1 (GAT1) (Guastella et al., 1990), betaine/GABA transporter subtype 1 (Yamauchi et al., 1992), GAT subtype 2 (GAT2) and GAT subtype 3 (GAT3) (Borden et al., 1992). Rat brain GAT1 was the first to be cloned in 1990 from purified protein (Guastella et al., 1990). These four subtypes can be distinguished by their pharmacological properties and tissue distribution (Hirunsatit et al., 2009). GAT1 and GAT3 are the most extensively expressed GATs in the human brain. GAT1 is primarily localised at GABAergic axons and nerve terminals and is expressed in abundance in the

cerebral cortex (Conti et al., 2004), hippocampus and striatum. GAT3 is exclusively localised to astroglia and is abundantly expressed in the glomerular layer of the olfactory bulb, thalamic paraventricular nucleus and the inner nucleus of the retina (Jin et al., 2011).

The neurotransmitter transporter family SLC6 commands the translocation of solutes across cell plasma membranes by coupling solute transport with the cotransport of sodium and chloride down their electrochemical gradients (Chen et al., 2004). GAT1 and GAT3 both function with the stochiometry of a GABA molecule, two sodium ions and one chloride ion; Chloride is required for transport but may not undergo net translocation (Yu et al., 1998).

The solute carrier family 6 member 1 (*SLC6A1*) gene, encodes for the Na^+Cl^- GABA transporter GAT1, which, was initially identified by Lam et al (1993). Using *in situ* hybridisation mapping, *SCL6A1* has been mapped to chromosome 3p24-p25 (Huang et al., 1995). Initially identified in 1993, *SLC6A1* contained 15 exons and was approximately 25 kb in length (Lam et al., 1993). The March 2006 genome build however, identified that there are in fact 16 exons in *SLC6A1* spanning 46.5kb; in addition there are two main transcripts (Hirunsatit et al., 2007). The first transcript comprises of all 16 exons whilst the second is coded by only 14 exons; exons 3-16 (Hirunsatit et al., 2009). *SLC6A1* encodes a protein of 599 amino acids and this single polypeptide has a molecular weight of 67kDa (Guastella et al., 1990).

The GABA transporter, GAT3, is encoded by solute carrier family 6, member 11 (*SLC6A11*) gene. *SLC6A11*, mapped to chromosome 3p25.3 by Borden et al (1992), has been shown to have 632 amino acids and demonstrates 52% homology to GAT1 at this level (Minelli et al., 1996; Chen et al., 2004). Fewer studies have been carried out independently examining GAT3 in the brain.

The SLC6A transporter family penetrates at least one phospholipid bilayer of the plasma membrane and all of the peptide sequence is embedded in the membrane. It has been shown that approximately 50% of the protein is on the plasma membrane at basal state and the remainder of the protein is found intracellularly in the vesicle (Deken et al., 2003). SLC6A comprise of 12 putative transmembrane α-helices and due to the

lacking of a signal peptide, it is believed that the N and C-termini both face the cytoplasm. As these regions contain phosphorylation sites working in conformity, it is thought that both, especially the N-terminal, may be responsible for the regulation of transportation (Bennett and Kanner, 1997). Mutagenesis studies relating to the GAT1 N-terminus support this and suggest that intracellular transport domains regulate substrate transport; the mechanism however is uncertain (Bennett et al., 2000). The functional roles of the C- terminal tail of SLC6A1 transporters include transporter trafficking, stability and degradation (de Juan-Sanz et al., 2013).

As demonstrated in Figure 1.7 the large extracellular loop between transmembrane domains 3 and 4 contains the three preserved N-glycosylation sites Asn176, Asn181 and Asn184. It has been demonstrated that N-glycosylation is most importantly a post-translational modification in eukaryotic cells and can result in the manipulation of physicochemical and biological properties of the protein including protein folding, stability, targeting and ligand binding (Bismuth et al., 1997). Importantly it has been suggested that the transport activity and surface expression of neurotransmitter transport is regulated by N-glycosylation. Via site-directed mutagenesis, Bennett and Kanner (1997) found that the removal of either one or two of the N-glycosylation sites had little effect on GABA uptake activity, yet the removal of all three sites caused a reduction in GABA uptake activity (Bennett and Kanner, 1997).

Residues in close proximity to or in the first and sixth transmembrane domain of GAT1 have been mapped as the ion binding sites (Hansra et al., 2004). There is a break in the helical structure of TM1 and TM6, which, expose main-chain carbonyl oxygen and nitrogen atoms, which, binds hydrogen and can therefore organize ions. Mutations have suggested that substrate binding occurs in the third and eighth transmembrane domain as well as in extracellular loops of the protein (Bismuth et al., 1997, Tamura et al., 1995). It is believed that the V-shape created by TM4 and TM5, and TM9 and TM10, hold TM3 and TM8 in place like pincers. Transmembrane domains 2, 4, 5, 7, 9, 10, 11

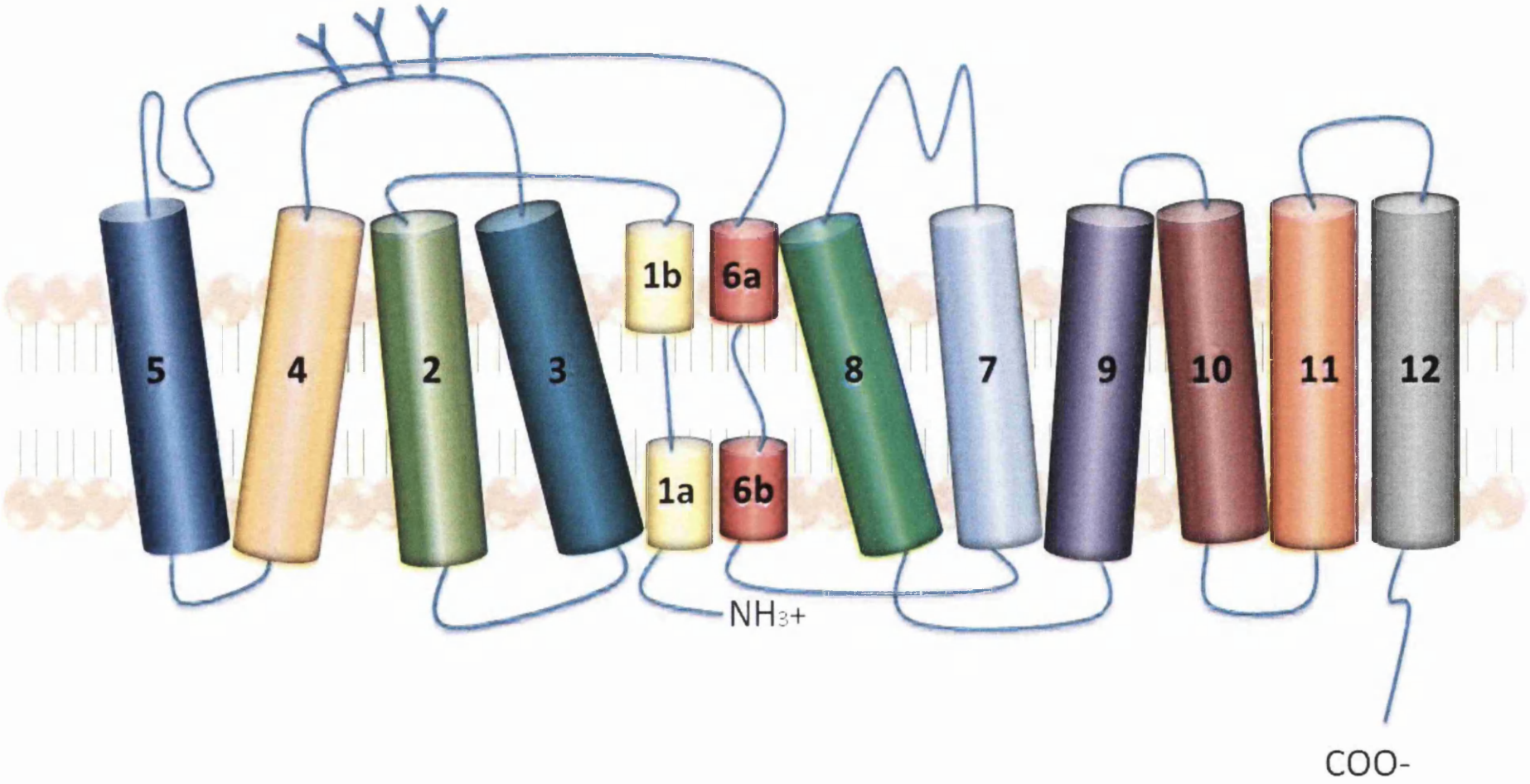

Figure 1.7 A topological model of the 12 transmembrane domains of a GABA transporter. Three N-glycosylation sites can be seen on the large extracellular loop between transmembrane domain 3 and 4. Adapted from (Bennett and Kanner, 1997).

and 12 are believed to contain highly conserved residues, which, emphasises their importance (Yamashita et al., 2005).

The identification of novel naturally occurring mutations as well as the formation of transgenic animals has linked the *SLC6A* family and the GABAergic system to numerous diseases. There is substantial evidence associating human disorders such as anxiety disorders (Tasan et al., 2011), diabetes (Chattopadhyay et al., 2011), Huntington's disease (Sherif and Ahmed, 1995) & epilepsy (Luscher et al., 2011) with altered GABAergic transmission.

GABA receptors have been extensively explored and many mutations in their genes have been found in epilepsy cases (Macdonald, 2001). None have yet been identified in GABA transporters however. Conversely, *Gat1* knockout mice show that an increase in GABA levels resulting from GAT1 deficiency, can induce post and pre-synaptic changes in GABAergic synapses causing epileptogenesis (Velisek et al., 2011, Conti et al., 2004). *Gat1* knockout mice have also been found to display the phenotype of attention deficit/hyperactivity disorder, identifying *Gat1* as a possible gene for drug therapy (Yang et al., 2013). Additional *Gat1* knock-out mice have also displayed signs of motor disorders, constant tremors, mild anxiety and nervousness (Chiu et al., 2005).

To date, no *Gat3* knockout animal model studies have been published. However, in an animal model for depression, a significant decrease in GAT3 levels was identified demonstrating a link with neurological disease (Zink et al., 2009). Other transporters relating to GABA, such as glutamate transporters have been published due to their association with seizures in early infancy (Demarque et al., 2004), and mutations in Na^+/Cl^- glycine transporter GlyT2 can results in human startle disease; these give reason to believe that mutations in the GATs could result in epilepsy (Rees et al., 2006).

One missense mutation and one duplication in *GAT1* have been identified and suspected to be linked with disorders in humans. The missense mutation was identified by exome sequencing of autism spectrum disorders, and involves the conversion of alanine to valine at protein position 228 (Sanders et al., 2012). The duplication, which, is 21bp in length alters promoter activity and is believed to be useful in predicting clinical responses to pharmacological modulators such as tiagabine and GAT1 inhibitors; this

variant was only identified in African-Americans and not in other populations (Hirunsatit et al., 2009). A missense mutation has also been identified in *GAT3* at protein position 524 that has been linked with anti-epileptic drug pharmacoresistance, increasing the risk of seizure by 1.5 fold in the epileptic brain (Kim et al., 2011).

1.5.5 Glutamate Decarboxylase (GAD)

The biosynthetic enzyme for GABA, GAD, presents itself in the two isoforms GAD65 and GAD67 which are primarily localised in the GABAergic neurons in the brain. GAD has been identified outside of the nervous system in tissues such as the pancreas, ovaries and testes (Taniguchi et al., 1977; Erdo et al., 1982; Bu et al., 1992). These isoforms are named after their approximate molecular mass of 65 and 67 kDa respectively (Battaglioli et al., 2003). Both GAD65 and GAD67 have 16 coding exons, however GAD67 has an additional non-coding exon (Bu and Tobin, 1994). GAD65 and GAD67 are encoded by two genes that have been identified on separate chromosomes, GAD65 on chromosomes 10 at 10p11.23 and GAD67 on chromosome 2 at 2q31. GAD67 cDNA encodes 594 amino acids and GAD65 cDNA encodes 585 amino acids (Bu et al, 1992)

The GAD monomers comprise of an N-terminus, C-terminus and pyridoxal-5'-phosphate (PLP) binding domain. The PLP binding site comprises of nine α-helices that encase nine stranded β-sheets and the C-terminal domain contains three α-helices and four anti-parallel β-sheets. The N-terminal's two parallel α-helices form the functional dimer by packing against the N-terminal and PLP binding of a neighbouring monomer. N-terminus truncated crystal structures demonstrate that each of the GAD67 active sites are enclosed by a catalytic loop which is contributed in *trans* by the additional monomer. This however is not the case with GAD65, this region is incorrectly formed leaving the active sites exposed (Fenalti et al., 2007).

Derived from a common precursor, GAD65 and GAD67 demonstrate 65% homology at protein level, demonstrating prevalent homology in their mid-regions and C-terminus. However, in the N terminal regions, which, is 90-100 amino acids in length, the isoforms demonstrate only 22% homology (Kanaani et al., 2010, Bu et al., 1992). All known phosphorylation sites of GAD65 and GAD67 have been identified in the N-terminal domain, as have the palmitoylation sites (Bao et al., 1995). The GAD65 N-

terminal contains three trafficking signals that are responsible for the targeting of the enzyme to the pre-synaptic nerve terminals, Golgi membranes and post-Golgi trafficking to cytosolic vesicles (Kanaani et al., 2002, Namchuk et al., 1997).

Both GAD65 and GAD67 are synthesised as soluble and hydrophilic though GAD65 undergoes N-terminal modifications causing hydrophobic post-translational changes; GAD67 however does not and remains hydrophilic. Hydrophobic GAD65 is targeted to the cytosilic membrane of the Endoplasmic Reticulum and Golgi, where palmitoylation causes its trafficking to the trans-Golgi network and cytosolic vesicles in non-neuronal cells. In neurons however, GAD65 is targeted selectively to axons and pre-synaptic clusters, which, facilitates rapid filling of synaptic vesicles for intense firing of GABAergic neurons (Kanaani et al., 2008). Kanaani et al. (1999) demonstrated in mice that GAD67 remains membrane-anchored and targets pre-synaptic clusters in the absence of GAD65 (Kanaani et al., 1999).

GAD activity, as with many enzymes, is altered by phosphorylation; this can be an increase or decrease in activity depending on whether GAD is soluble or membrane bound (Namchuk et al., 1997). Phosphorylation of GAD65 by protein kinase C activates the enzyme, but phosphorylation of GAD67 mediated by protein kinase A causes inhibition of activity (Buddhala et al., 2008). The majority of GAD remains inactive in the brain and is regulated by the co-factor PLP (Miller et al., 1977). GAD is active when it contains the bound PLP (holoenzyme) and only then will it convert glutamate into GABA. In the majority of cases the PLP will stay attached during this process but in a small percentage of reactions, if glutamate is decarboxylased, GAD will cause an additional reaction whereby SSADH and pyridoxamine-P (PMP) are produced and PLP will readily dissociate from GAD leaving inactive apoGAD. HaloGad can however reform and create a cycle of activation and inactivation by binding with free PLP (Porter and Martin, 1984).

Battaglioli et al (2003) found that haloGAD$_{67}$ activity was 72% of GAD67 activity compared to 6.7% of haloGAD$_{65}$. One reason could be that haloGAD$_{65}$ is converted to apoGAD approximately 15 times faster than haloGAD$_{67}$. Also the activation of apoGAD$_{65}$ is strongly associated with and affected by inorganic phosphate and NTPs such as ATP, while GAD67 is fundamentally unaffected by these factors. However,

apoGAD_{65} can be activated by PLP 10 times faster than GAD67 (Battaglioli et al., 2003). This may support work by Buddhala et al (2012) that claims 90% of GABA is due to the expression of GAD67, whilst GAD65 is activated to reinforce GABA for high frequency GABAergic neurotransmission at the synapse (Buddhala et al., 2012).

Animal models demonstrate that *Gad65* knockout mice appear normal at birth, there is no change in the GABA concentration in the brain and the changes in animal behaviour are anxiety phenotypes and the more severe susceptibility to fatal seizures (Asada et al., 1996). A conflicting mouse study indicates that GAD65 caused the majority of increased GABA synthesis during a seizure in the cortex (Patel et al., 2006). In *Gad67* knockout mice, the mice had a severe cleft palate which resulted in neonatal death the morning after birth and a 90% decrease in the GABA content in the brain, though no structural brain defects (Asada et al., 1997).

One disease associated mutation has been identified in *GAD65* and two in *GAD67*; as well as two disease causing mutations. The *GAD65* regulatory mutation is believed to associate *GAD65* and obesity whilst the two disease associated mutations in *GAD67* cause familial association between the gene and schizophrenia (Boutin et al., 2003; Straub et al., 2007, Du et al., 2008). Cerebral palsy and Complex I deficiency are the two diseases believed to be caused by mutations identified in *GAD67* at protein positions 12 and 330 (Lynex et al., 2004; Calvo et al., 2010).

1.5.6 GABA Transaminase (GABAT)

As stated in section 1.5.1, the enzyme GABA transaminase (GABAT; 4-aminobutyrate transaminase) catabolises GABA into glutamic acid and succinic acid. GABAT is present, not only in the human brain, but throughout the body and especially in the liver. It is localised in the inner matrix of mitochondria and is the primary enzyme for eliminating GABA. The PLP dependant transamination of GABA occurs by firstly recruiting two ketoglutarate, formed by the GABA shunt, as nitrogen acceptors which regenerates glutamate by their removal from GABA; a process which also produces succinic semialdehyde (SSA) (Medina-Kauwe et al., 1999).

Mouse models have demonstrated that inhibition of between 55% and 85% of GABAT action resulted in a 5- to 10-fold increase in GABA, which had an anticonvulsant affect on a variety of rodents and photosensitive baboons. This discovery has allowed for great advances in anticonvulsant therapy (Meldrum and Horton, 1978). Vigabatrin, is used to inhibit the actions of GABAT by decreasing its activity, increasing the GABA levels in the brain and therefore inhibiting synaptic transmission. GABA levels are increased in the cytoplasm but this increase is not always transferred to GABA levels in the vesicles or vesicular GABA release. Vigabatrin increased GABA levels was found to be not only due to blockage of GABAT but also due to reversal of GABA transporters, which occurred spontaneously and continuously (Wu et al., 2001).

Mutations in the GABAT gene (*ABAT*, chromosome 16p13.3) have been discovered in patients that suffered with GABAT deficiency. These patients experienced severe psychomotor retardation, hypotonia, hyperreflexia, and seizures; patients died before the age of two (Jaeken et al., 1984). In socially isolated mice, reducing GABAT level caused a decrease in anxiety and aggression.

1.5.7 Succinic semialdehyde dehydrogenase (SSADH)

Succinic semialdehyde dehydrogenase (SSADH) is the enzyme responsible for the oxidation of SSA into succinic acid in the mitochondrial matrix. This carbon skeleton form of GABA then enters the tricarboxylic acid cycle (Krebs cycle) and eventually reloads glutamate in the form of α-ketoglutarate (as described in section 1.5.1) (Kim et al., 2009). SSADH knock-out mice initially experience a milder absence seizure, which in time leads to lethal tonic-clonic seizures. This is believed to be due to a rapid increase in GABA in the synapse but also due to a downregulation of the $GABA_A$ receptor subunits in the cerebral cortex of the mice (Gupta et al., 2004).

One disease that is associated with SSADH pathology is Succinic semialdehyde dehydrogenase deficiency (SSADHD). SSADHD is a rare inherited metabolic disorder with a range of mild and extremely severe phenotypes resulting from insufficient GABA degradation by SSADH (Akaboshi et al., 2003). Patients in one study revealed symptoms such as behavioral disturbances (42% of patients), and 13% experienced

episodes of psychosis (Gibson et al., 2003). However, the most common symptoms are seizures (especially absences and myoclonic seizures) but patients also experience delays in development, hypotonia, myopathy, and ocular abnormalities. Neonatal problems can also occur and can cause prematurity, respiratory difficulties, and hypoglycaemia (Gordon, 2004).

Numerous mutations have been identified in the SSADH gene, *ALDH5A1* (chromosome 6p22) including point mutations, deletions and insertions. In one study, 36 of 37 missense mutations identified caused a reduction in SSADH to 5% its normal level. To date however, treating patients with SSADHD is very difficult due to the wide variation in phenotypes (Akaboshi et al., 2003).

1.6 GABAergic neurons and the thalamo-cortical network

GABAergic neurons are interneurons that are involved in regulating information processing and oscillations are also hugely important to normal functioning of the cerebrum. GABAergic neurons are born in the medial and caudal ganglionic eminences of the ventral telencephalon, from where they migrate tangentially to their desired cortical region before then moving radially through the cortical plate to their correct laminar location. GABAergic neurons migrate to locations that are highly populated with excitatory neurons (mainly glutamatergic) that are birth-date matched (Sahara et al., 2012). Although GABA is the primary inhibitory neurotransmitter in mature neurons, GABA has an excitatory role in immature neurons. In immature neurons, GABA causes the efflux of chloride ions due to an increased intracellular chloride concentration compared to extracellularly, causing an increase in membrane potential and cell depolarisation (Hori and Hoshino, 2012).

The thalamus is located between the cerebral cortex and the midbrain and plays a pivotal role in relaying information to and from the cerebral cortex. It has many functions including controlling motor function, receiving auditory and visual sensory inputs, and controlling awake and sleep states of consciousness. The dorsal thalamus contains two types of neurones: relay neurons that project to areas outside the thalamus, which are excitatory and local circuit neurons, which do not leave the thalamus and are

GABAergic (Arcelli et al., 1997). The thalamus and the pyramidal cells of the cortex are connected by excitatory (primarily glutamatergic) connections, whilst GABAergic neurons are positioned throughout the thalamus and form an almost continuous layer along the lateral, rostral and ventral part of the thalamus (Thalamic reticular nucleus (TRN)) (Steriade et al., 1987).

The cerebral cortex forms the outer layer of the brain and receives and processes inputs from various regions of the brain. The cerebral cortex maintains general cognitive function such as sensation, intelligence, personality and motor function. Across most cortical regions in the adult forebrain one in five inter-neurons are GABAergic. GABAergic interneurons function to influence the response of pyramidal cells to incoming signals, prevent excessive excitement, process cortical receptive fields and manage the timing and synchrony of population rhythms expressed as cortical oscillations (Rossignol, 2011).

The inter-connections between the cortex and thalamus, the thalamo-cortical network, not only generates normal synchronous oscillations (7 to 15Hz), which include sleep spindles, but also the spike-wave discharges (SWD) observed in absence seizures (2.5 to 4Hz) (Crunelli and Leresche, 2002). More recent blood oxygenation level-dependant (BOLD) signal studies have reported the involvement of the frontotemporal network in SWD generation as well as consistently reported increments in BOLD signal in the thalamus (Lee et al., 2014). Cortical fMRI signal has been shown to increase many seconds before thalamic signal emphasising the neocortex as the site of ictogenesis. Animal models of absences show focal bilateral cortical changes, believed to cause seizures. It has also been reported that SWD are strongly related to the default mode network of the brain (wakeful rest state) (Bai et al., 2010).

Spindle waves are generated by bursts of action potentials in the GABAergic cells of the TRN and thalamo-cortical neurons. These action potentials are caused by cortical discharges which hyperpolarise thalamo-cortical cells by activating chloride conductance via $GABA_A$ receptors resulting in temporal summation of inhibitory post-synaptic potentials (IPSP) (Ushimaru et al., 2012). Recovery from hyperpolarisation causes a low-threshold calcium spike followed by bursts of action potentials. This induces sodium action potentials, which once again excite the TRN cells initiating the

next cycle. The pacemaker of the rhythm of sleep spindles is the TRN, and its continuous firing in this way causes excitatory post-synaptic potentials (EPSP) of cortical pyramidal neurons forming EEG spindles. Neurons of the TRN are inhibitory and cause both feedback and feed forward inhibition to thalamo-cortical neurons (Kostopoulos, 2000, Bazhenov et al., 1999, Stroh et al., 2013).

Absence seizures usually emerge in periods of restful wake, the transition to and from sleep and in light non-REM sleep. An increase in burst firing of thalamo-cortical and TRN neurons by $GABA_A$ receptors blockade was found by Kim et al. in ferrets (1997). This resulted in a decrease in calcium spike duration and therefore ESPS. It has been identified that fast activating IPSP by $GABA_A$ receptors can be produced upon stimulation of TRN. In pathological circumstances, $GABA_B$ receptors are activated, causing slow activating IPSP and changing oscillation frequency from 7-15 Hz to 3-4Hz (Kim et al., 1997, Blumenfeld, 2003).

It has been suggested that an increase in cortical synaptic transmission causes increased firing of thalamic GABA neurons and therefore a large-scale increase in TRN GABA. Increased GABA release causes hyperpolarisation of most TC neurons resulting in little neuronal firing. Astrocytic GAT1 malfunction resulting in high GABA levels also causes activation of $GABA_A$ receptors, maintaining the hyperpolarisation stage, which is modulated by $GABA_B$ receptors, causing absence seizures (Crunelli et al., 2010, Pirttimaki et al., 2013).

GAT1 and GAT3 are the primary GABA transporters identified in the brain and are present predominantly in astrocytic cells of rat and human thalamus. Pirttimaki et al (2013) identified a lack of astrocytic GAT1 transporter current in the well established genetic animal model of absence seizures, the genetic absence epilepsy rats from Starsbourgh (GAERS) compared to a non-epileptic control strain (NEC) (Pirttimaki et al., 2013). This would suggest that mechanisms such as glial transport, would be affected by the dysfunctional transporter consequently interfering with astrocyte-neuron signalling. This was proven in the study by a slower outward current decay time as well as decreased amplitude. The frequency of this slow outward current in the thalamo-cortical neurons was restored by the introduction of the GABA transaminase inhibitor vigabatrin, which typically exacerbates absence seizures (Pirttimaki et al., 2013). This

could suggest that GABA uptake mechanisms from astrocytic cells may contribute to absence seizure generation.

GABA receptors and the GABAergic system are identified as a primary cause of epilepsy; however numerous neurological diseases have been associated with the system.

1.7 Hypothesis

GABAergic pathway genes have the mutational capacity to cause Genetic Generalised Epilepsy by compromising inhibitory neurotransmission.

1.8 Aims and objectives

1. Identify genetic variations in GABAergic genes, *GAT1, GAT3, GAD65* and *GAD67* in 707 individuals with genetic generalised epilepsy.
2. Utilise *in silico* methods to predict the consequences of identified variants with particular focus on bioinformatics and molecular modelling.
3. Prepare the mutation expression-constructs for suspected deleterious variants to begin functional characterisation.
4. *in vitro* expression validation of the mutation constructs in preparation for functional validation assays.

1.9 Justification for research

1. Epilepsy affects approximately 3% of the population as an expression of lifetime prevalence. 40% of patients will not reach seizure-freedom upon medication.
2. Epilepsy causality is heterogeneous but 60% will have a simple or complex genetic basis. Gene discovery in epilepsy remains a research priority.
3. The GABAergic system is already linked to genetic generalised epilepsy with numerous reports of GABA receptors mutations.

4. Knock-out animal models of *GAT1* show signs of epileptogenesis. No animal models for *GAT3* have been created to date but the transporter shares significant homology and biological synergy with *GAT1*. Mutations in other neurotransmitter transporters (DAT, GLUT1) cause epilepsy.
5. GAD65 and GAD67 synthesises GABA in the brain. Animal models of GAD65 knock-outs show a susceptibility to seizure and is significantly homologous to GAD67.
6. Anti-epileptic drugs vigabatrin (GABAT) and tiagabine (GAT1) directly targets the GABAergic pathway to increase GABAergic tone in epilepsy patients. On occasion, drugs can mimic the effects of acquired or inherited gene mutations in the target system. Tiagabine can inadvertently increase the number of absence seizures by hyperpolarising thalamo-cortical neurones.
7. No GGE mutations have been identified in any of the four GABA synthetic and transporter genes investigated in this study in relation to epilepsy.
8. Glycine, the other inhibitory neurotransmitter system, works in tandem with GABAergic action. Mutations in the inhibitory glycine receptor (*GLRA1, GLRB*) and transporter genes (*SLC6A5*) cause neuromotor disorder hyperekplexia and so demonstrating cognate implications for GABA transporters.
9. Identifying a cause for certain epilepsies will be vital for current patients their families and future patients with the same mutations. The data identified could be used to diagnose patients and help treat patients with current drugs and future interventional research.

1.10 Experimental approach

To fulfil the aims and objectives of this study the following experimental approaches were carried out. Each point will be addressed and discussed in greater in detail in Chapter Two - *Materials and Methods.*

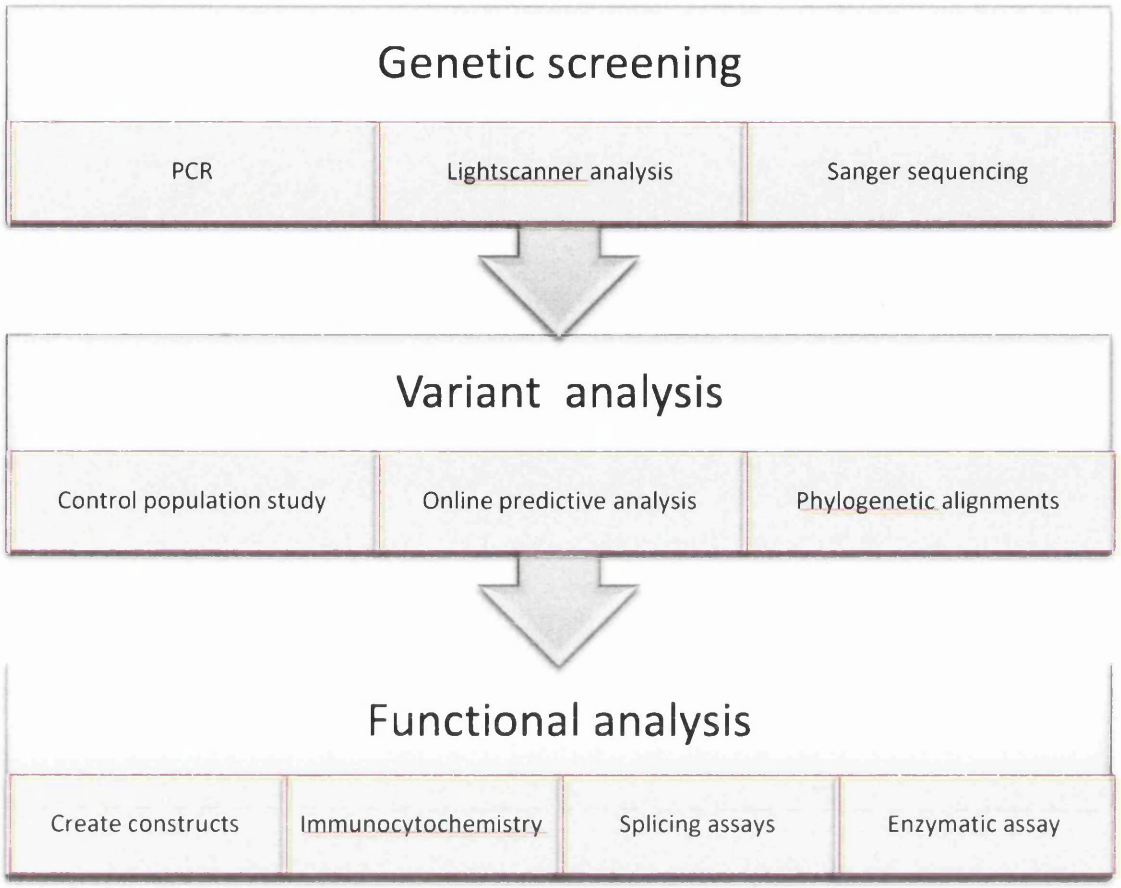

Figure 1.9. General workflow. Proposed research workflow for this study ranging from genetic screening and variant analysis to functional analysis.

A genetic study in human disorders begins with well phenotyped and ethically reputable assembly of patient samples. Prior to this study, the neurology team at Swansea had collected over 700 GGE samples by combining cohorts from the Wales Epilepsy Research Network (WERN), the Epilepsy Research Centre, University of Melbourne (Berkovic, Scheffer), the Neurology Unit at Auckland District Healthboard (Bergin), and the UCL historical cohort now hosted by St. George's Medical College, London (Everett, Gardner).

With the samples secured, the next stage genetically analysed GAT1, GAT3, GAD65 and GAD67 by working out the genomic structure, exon/intron boundaries, the ATG initiation site, the STOP codon, SNP maps and the respective 5' and 3' untranslated regions. To amplify and analyse the coding region and splice site regions of the genes, Polymerase Chain Reaction (PCR) was carried out on the GGE

patient samples. Optimised PCR products were tested using heteroduplex Lightscanner™ technology to ensure high-throughput variant detection.

Samples which deviated from normalised melt profiles were isolated and purified before being outsourced for bi-directional Sanger sequencing. Sequencing results returned to Swansea were analysed using Mutation Surveyor™ analysis software with comparison to wild-type sequences. Any gene variants discovered by sequencing were scrutinised using on-line and *in silico* methods including PDB molecular modelling. In addition, the population frequencies were assessed for suspected damaging non-synonymous variants in a panel of commercially sourced controls using the Lightscanner™ protocols.

To investigate the pathogenic potential of non-synonymous variants, expression constructs were be prepared from C-terminally DDK tagged wild-type vectors for GAT1, GAT3, GAD65, and GAD67. Mutations were introduced to wild-type vectors using site-directed mutagenesis (Origene, Cat.PS100001), with successful clones being mini- and maxi-prepped (Qiagen) after transformation into *E.coli* bacteria (One Shot TOP10 Chemically competent *E.coli,* Life technologies, Cat.C404006). Sequence validated mutation constructs were used to investigate the expression level of each mutant using HEK293 cells which were visualised using confocal microscopy and semi-quantitative approaches.

The mutation constructs were also used in further functional analysis (for future use after this thesis) which will incorporate an enzymatic assay for GAD65 and GAD67, biotinylation of cell-surface proteins GAT1 and GAT3, splice-site assays of exon skipping candidate mutations, and mass spectrometry quantification of GABA transporter and GAD activity. Lastly, these constructs will also be used in collaborative project in and around the creation of model systems and in-depth electrophysiology.

Chapter Two

Materials and Methods

Aseptic techniques were practised at all times and equipment sterilised prior to use by autoclaving. Disposable gloves and lab coats were worn in order to prevent contamination of samples and for personal safety. All designated lab work surfaces, pipettes and equipment were cleaned and sprayed with 70% ethanol to ensure a sterile environment. Standard operating procedures were accessed and adopted to ensure best-practice and uniform approaches relative to each technique in this chapter.

2.1 Patient samples and ethical approval

Four hundred and eighty five genetic generalised epilepsy patient DNA samples were ascertained from Australia, New Zealand and the Wales Epilepsy Research Network (WERN). A further one hundred and eighty seven DNA samples from childhood absence seizure patients were then recruited from University College London based on initial preliminary data and represented a replication cohort (Table 2.1). Samples were not linked to known epilepsy genes and had not previously gone through screening projects involving *SLC6A1 (GAT1), SLC6A11 (GAT3), GAD2 (GAD65)* and *GAD1 (GAD67)* genes.

Table 2.1 Sample Ascertainment and Origin

	Origin of samples	Epilepsy type	Sample number
Cohort 1	Melbourne, Australia	GGE	400
Cohort 2	Auckland, New Zealand	GGE	59
Cohort 3	Wales (WERN)	GGE	59
Cohort 4	UCL, London	CAE	189

Inclusion criteria included a secure diagnosis of genetic generalised epilepsy or childhood absence epilepsy as declared by a neurologist with a speciality in epileptology and the electro-clinical signatures that reflect the diagnosis. Ethical approval for the sample archiving and genetic analysis was approved under the WERN epilepsy Biobank IRAS framework (Wales REC study # 12/WA/0150).

2.2 Mutation detection by candidate gene analysis

This section outlines the procedures adopted for the screening and mutation analysis of genomic DNA from epilepsy cases.

Polymerase chain reaction (PCR) has become one of the most widely used and integral techniques in molecular biology and medical genetics. In essence, PCR accumulates small sections of DNA by exponentially amplifying target sequence to enable visualisation, sequencing, cloning and further manipulation of the DNA (Higuchi and Ochman, 1989). The last twenty years has witnessed extensive development in the PCR technique concept that facilitated more advanced molecular approaches such as quantification of DNA and RNA levels, Sanger sequencing and the detection/cloning of mutations and polymorphisms. PCR is now an automated process carried out using high-throughput approaches enabling simultaneous analysis of hundreds or thousands of samples.

Mimicking the basic components of naturally occurring replication machinery from within the cell, short fragments of DNA are amplified in a PCR reaction mixture. This reaction mixture typically contains a buffer to maintain optimum pH and ionic concentrations, deoxynucleotides as the building blocks of DNA, primers complementary to target sequence that will be amplified and a DNA polymerase enzyme to catalyse the reaction amplification. LC green fluorescent dye was also added for visualisation of double stranded DNA as a result of increased temperature to enable light-scanner mutation analysis.

DNA is amplified exponentially with a linear phase in which DNA concentration is directly proportional to the cycle number. There would be a point therefore, where one of the constituents of the reaction is exhausted and amplification will cease. PCR is an extremely sensitive technique and can be very easily confounded by contamination, leading to false-positive results. To avoid contamination, aseptic techniques were adopted such as the use of designated, regularly cleaned PCR pipettes and lab work surfaces, sterile filter tips, and centrifuge tubes. This is also in combination with good laboratory practice positioning of PCR consumables, discarding tips to avoid cross contamination and a consistent action of methodology.

2.2.1 PCR Primer design

PCR primers were designed using gene sequence information from publicly available databases such as NCBI (http://www.ncbi.nlm.nih.gov/) and Primer 3 (http://frodo.wi.mit.edu/primer3). Oligonucleotide primers were typically designed within intronic regions of genes and flanking the desired exonic target, avoiding SNPs and repeat structures as outlined on dbSNP. Primers were designed to be approximately 20 nucleotides in length with an annealing temperature of approximately 60°C. To prevent secondary structure formation, self-complimentary sequences and non-specific binding were avoided using BLAST2.2.14 (NCBI) software. Custom designed primer sets were manufactured by Eurofins MWG Operon. Primer sequences, their corresponding anneal temperatures and fragment sizes were calculated and shown in tables 2.2, 2.3, 2.4 and 2.5.

2.2.2 Polymerase chain reaction

Each PCR Lightscanner reactions contained a master mix of 1.5µl sterile water, 0.25µM forward and reverse strand primer (Eurofins MWG Operon), 5µl Type-it Multiplex PCR Mastermix (2x) (Qiagen, Cat. 206143) and 1µl LC Green Dye (Idaho technology, Aquascience Cat.BCHM-ASY-0006). 8µl of master mix per sample was aliquoted into a sterile 96 well Lightscanner plate; 10ng of DNA was then added as well as 15µl of mineral oil to each sample reaction to prevent sample evaporation. Negative controls were also carried out for all PCR reactions, by replacing the DNA with sterile water. All exons screened were optimised using their specific primers between 55°C and 70°C. On occasions where unclear or multiple bands were witnessed via gel electrophoresis, DMSO or $MgCl_2$ (percentages used range from 1% to 10% DMSO/$MgCl_2$) were added in order to improve optimisation.

The reaction mixture was cycled 40 times through three temperature stages after an initial denaturation stage at 94°C for three minutes, which, denatures the DNA strands by breaking the hydrogen bonds between matched base pairs. The temperature cycles include a second denaturation stage at 94°C for 30 seconds; an annealing step for one

Table 2.2 *SLC6A1 (GAT1)* PCR primer sequences

Exon	Forward Primer Sequence (5'-3')	Reverse Primer Sequence (3'-5')	Amplicon Length(bp)	Annealing temperature (˚C)
1	GTGACATCGCACGTCCATC	ACAGTTGCCCCAGAAAAATG	371	63
2	GCGGGTCTTGAAAGT	TGGTGGATGGATATGTGA	300	63
3	TGCCTGTCTCCGAGATCAATA	GTGTGGCTTCTGCTGGATG	247	63
4	GTGCACTGGGACCACTCAT	TGACTGTAGCCCCTTTATCCA	296	63
5	GGTGTCAGCACAGTTCTAGGG	CTCTATCCAGTGCCCTCCTG	298	60
6	GTGTACAGGAGGAGGGGTCA	GGCAACAAACCTGGTCTACAG	278	63
7	CACTGTAGACCAGGTTTGTTGC	ATGAGTGTGGGATGTGGACTC	286	63
8	CCTTTCCTGACCCTGATCTTC	GGTAATGGTGATGATGGCAAA	390	63
9	AAGGGGCTGAAAACACTCACT	AGGAGTCTGGGGATGGAGAG	300	63
10	GGACTCTCCTGAGGTCACAAA	CAGGAAAGGTGGGATACAACA	381	63
11	AGAGTCCATGTGGTCTGTGAA	GACTCAAGAAAGGAATGAATGG	246	63
12	AAAGTGGTAGAACCAGGCTTTG	TTTCTCCCTGGACCTGAGTC	249	63
13	AAGACCTTGGGCCTCTGTAAG	CCCAGCTAGACTGTGAGCTTC	391	63
14	TAGAGAGCAGGAGAGGGAAGC	CCTCAGACATCAAGTGGTGGT	273	63

Table 2.2 Primer sequences for *GAT1* exons. Forward and reverse primer sequences for the 14 coding *GAT1* exons and their annealing temperatures(˚C). The fragment sizes from forward (5' to 3') to reverse primer (3' to 5') were also calculated.

Table 2.3 *SLC6A11 (GAT3)* PCR primer sequences

Exon	Forward Primer Sequence (5'-3')	Reverse Primer Sequence (3'-5')	Amplicon Length(bp)	Annealing temperature (˚C)
1	CCTCCTGAAAAGCCAGCTC	CCCTTCTCCTCACTATCACCT	352	60
2	TTCTTGAGCCAAGTATGAATCG	CAAAAGAAAGGAAGGAATTTGAG	300	63
3	CCCAGGGAATGTCAACT	AAGGGCATGAACAAACC	289	63
4	GACGCATGTTTACCTGGAGTG	GCAAGACCAACTGAGCAGAAC	286	63
5	CCTGCTCCTCTGCAGTACTA	CCCTGTTACTCTCTAGGTCAT	288	63
6	CATTGTGCTGAGTGAAGTAAC	GAATCTCAGTGGCCAGTGGCA	292	63
7	TTTCAGAGACCAGGGCTACC	GGTGGGCAGACAAACATAAACTA	267	63
8	CTCGGGTGGAGAACGTTTGA	CCGAGGAGGAAGATCGCA	287	63
9	GGCATCAGAATAGCACCAAAC	GGGTAAGTGTAGAGCCCACCT	496	63
10	CTCGTCTGCATTAATGGGTGT	CAGCTGGTCACTTTTAGAGCTG	343	63
11	CAGAGCAGAGAGAGGGACCTT	AGAACCAGAGCCAACCAGAGT	289	63
12	AGGCTGGAGAAAGCAAACACT	GGTAGATGGGTGGGTAGATGG	246	63
13	CTCAGACCCCTCATGGCCTA	GCACCATGCAGATGAGGAAA	318	63
14	GTGTGCTTGGGAGAGGC	TGGCCACCTTAAAATTAACTTGT	376	63

Table 2.3 Primer sequences for *GAT3* exons. Forward and reverse primer sequences for the 14 coding *GAT3* exons and their annealing temperatures(˚C). The fragment sizes from forward (5' to 3') to reverse primer (3' to 5') were also calculated.

Table 2.4 *GAD2 (GAD65)* PCR primer sequences

Exon	Forward Primer Sequence (5'-3')	Reverse Primer Sequence (3'-5')	Amplicon Length(bp)	Annealing temperature(˚C)
1	GTCTCCAGCTCGGATACACAC	TCCTTCGTCTTCTCCGTAGTT	358	58
2	ACCCCGGACTGATTGATTTT	TCCAAGCAGTCTTCTCACCTC	222	63
3	AGTCTTCTCACCTCCGCATC	CGCATTTCTCGCTTTTATCTG	429	58
4	CATTCATTCCCTTCACCTTTG	GAGCTTTATTATTTTCGATGAGACA	443	63
5	GAGAGGCATTTATTTTCACTGG	GATTACATGGAAGATGTATCAGGAC	333	58
6	TTGTAAATGTATGTTTTGAAAAAGGA	AAGCAGAGGCATAGGCTAGATT	319	63
7	CCAAGGAGGACTCAGGTCAG	CCCAAGGTGTCTTCCAGAAA	330	63
8	AGCCAGTGGAATGGATCTTGT	CCGTGGTCCTCTCCTATTTTC	235	63
9	CGGCCACTTACGTTGTAAAGA	CATTAAACCTGGGAGATTGAGG	245	63
10	TCCATTGCTTTGAATCAGCTT	GCACGGTGTGTACTGTGTGAG	375	63
11	CCAGAAGGAGGTGGTCAACTT	CACTCAGTATTCCAAAAGTTCCTG	291	63
12	TCAATCTGGAGTCTGAGAAACAA	CACCCTGCAGACAGGAATCTA	342	63
13	AATTTCCTAAATTTTCTCTTCTCTCTTG	AAAGCAAATCTTGGGTAAGGAA	301	63
14	CGCACTCTTAGCCTGCTTAAT	CAGTGATGAGGGTTGGAATTG	212	63
15	TCGATTTGAAATGTTCTTGGA	GCCACAGGCATATGTCATAAA	246	60
16	CTTGCTGTTGGGTTCTTTGAC	TTGTCTAACCTAGAGAAGTGGAACAG	290	58

Table 2.4 Primer sequences for *GAD2* exons. Forward and reverse primer sequences for the 16 coding *GAD2* exons and their annealing temperatures(˚C). The fragment sizes from forward (5' to 3') to reverse primer (3' to 5') were also calculated.

Table 2.5 *GAD1 (GAD67)* PCR primer sequences

Exon	Forward Primer Sequence (5'-3')	Reverse Primer Sequence (3'-5')	Amplicon Length(bp)	Annealing temperature(˚C)
1	CACAGCTCTCGCTTCTCTTTG	CATTTATTTCCCAGCCTCCAT	295	60
2	CAAGAAAACCATTGTCCTCCA	CTGGCTGTCCTGGCTGTAAT	284	58
3	GCAGTTTGCAGCACTCTCTCT	ATTCCCCCAAAGTCACAAAAG	351	63
4	CAGGTGAAAACCATTCATTGC	GGCTGTGTTTTTCTTCCAACA	381	62
5	TGCCTTCAAGATAGGTTGAGAA	GCAACAAGCCATAGTCATACATC	208	62
6	CTAAACCAATCCTCTGTGTTCCT	ATCCCAAACCTTGAGAAGAGG	233	60
7	TTCCTGACCTCCCTTGTCTCT	CACTATCCATGAGAAAGCATCC	249	60
8	ACTGGTCCTCTTCACCTCAGA	CAGCTTGGCACAATGTACTGA	296	60
9	CAAGCTGCTAATGGTCTGTTG	TGGCACAATGAAGATAGGACA	420	63
10	CTTCTTCCTGTGAAAATCAGCA	ACATGGACTGGCCTGAGTTAT	222	60
11	GTGTGGGCTGAACTTTTCTGA	CCTGCTGAACTGAAGCAAACT	339	60
12	AGAACAGTTGCGTCTTTCCAA	AGACCCCACGTGTGTCTTTTT	212	60
13	AAAAGGGCATCAGAACAAGTG	ATATCTTTGCCCCTCTTTTGC	382	60
14	CCCATAGACAGGGACAGCATA	TGTGTACCTGGTCCATGATGA	221	58
15	CTCCCTGGTGTGGAAGTAACA	CCACTAGAAAGGCACATTGGA	330	60
16	TGTTAAAAAGAGAGGGTGTTCAT	GAGTGCCAGAGGGAAAAGG	287	63

Table 2.5 Primer sequences for *GAD1* exons. Forward and reverse primer sequences for the 16 coding *GAD1* exons and their annealing temperatures (˚C). The fragment sizes from forward (5' to 3') to reverse primer (3' to 5') were also calculated.

minute at a temperature specific to the primer set (typically 50°C - 65°C optimisation range) which allows primers to bind to the DNA template at a specific homologous location; and an extension stage at 72°C for one minute, the optimum temperature for the DNA polymerase enzyme to add nucleotides to the 3'-OH end of the newly forming DNA, thus producing new duplex molecules. This is the stage at which new DNA is synthesised (Figure 2.1) and the number of cycles can depend on the efficacy of the PCR reaction. Following the multiple cycle steps, a final ten minute extension stage at 72°C is needed before samples are held at 94°C for 30 seconds and 25°C for 30 seconds to form heteroduplexes; samples are retained at 4°C until removed for analysis.

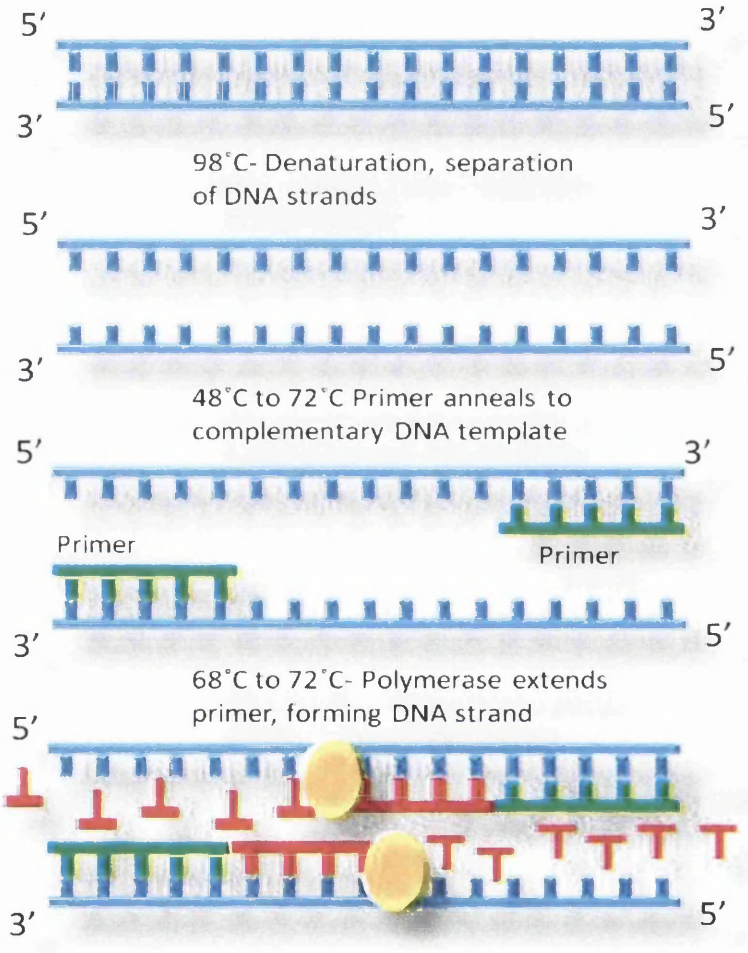

Figure 2.1 Polymerase chain reaction. The exponential amplification of DNA occurs by an initial denaturation of DNA, an annealing stage which allows the binding of specific primers and an extension phase where the primer is extended by polymerase to form a new duplex molecule. This cycle is repeated 39 times create large amounts of desired DNA product.

Amplification of exons was not always possible, even following the use of DMSO and $MgCl_2$ to create the ionic conditions or help resolve complex annealing structures. For example, this was the case with the GC rich exon 1 of GAT3, where alternative amplification approaches were needed. In this case a Q5® Hot Start High Fidelity DNA polymerase protocol (NEB, Cat M0493L) was used to successfully amplify the exon. A PCR master mix for the exon consisted of 0.2µM of both forward and reverse primer, 200µM of each deoxynucleotide triphosphate (Promega, Cat U1330), 2µl Q5 Reaction Buffer (5x), 2µl Q5 High GC Enhancer (5x) (NEB, Cat B9027S, 1µl LCGreen dye (Idaho technology, Aquascience Cat.BCHM-ASY-0006), 1µl DMSO (Sigma, Cat D2650) and 0.1µl Q5 hot start high-fidelity DNA polymerase; 10ng of DNA was added to the mastermix. The reaction mix was cycled 40 times following an initial 30 second denaturation stage at 98°C. The cycle included a second denaturing stage of 10 seconds at 98°C, an annealing step at 63°C for 45 seconds, followed by an initial extension stage at 72°C for 20 seconds. Following the 40 cycles, a final extension stage at 72°C for 2 minutes followed by two 30 second holding stages at 98°C and then 25°C.

2.2.3 Lightscanner™ analysis

Lightscanner analysis is a high-throughput method using high-resolution melting analysis of post-PCR products. Upon completion of PCR cycles the plated samples were centrifuged for one minute at 2500g and placed into the Lightscanner on a platform-stage. The Lightscanner heated the plates with PCR products causing separation of the double stranded DNA (dsDNA) and the release of LC Green dye, an intercalating dye that binds to dsDNA causing high fluorescence. Therefore, upon melting, the dye cannot bind as strongly and will fluoresce at a lower level (Figure 2.2). The level of fluorescence is detected for each well and the presence of genetic variance will generate differences in melt-curve properties. Sequence factors affecting melt differences include GC-content, product length and whether a variant genotype is homozygous or heterozygous. The platform is sensitive enough to detect Single-Nucleotide Polymorphisms (SNPs) and was used as an initial screening process where deviations in

melt profiles would be Sanger sequenced to confirm or reject the presence of sequence variation.

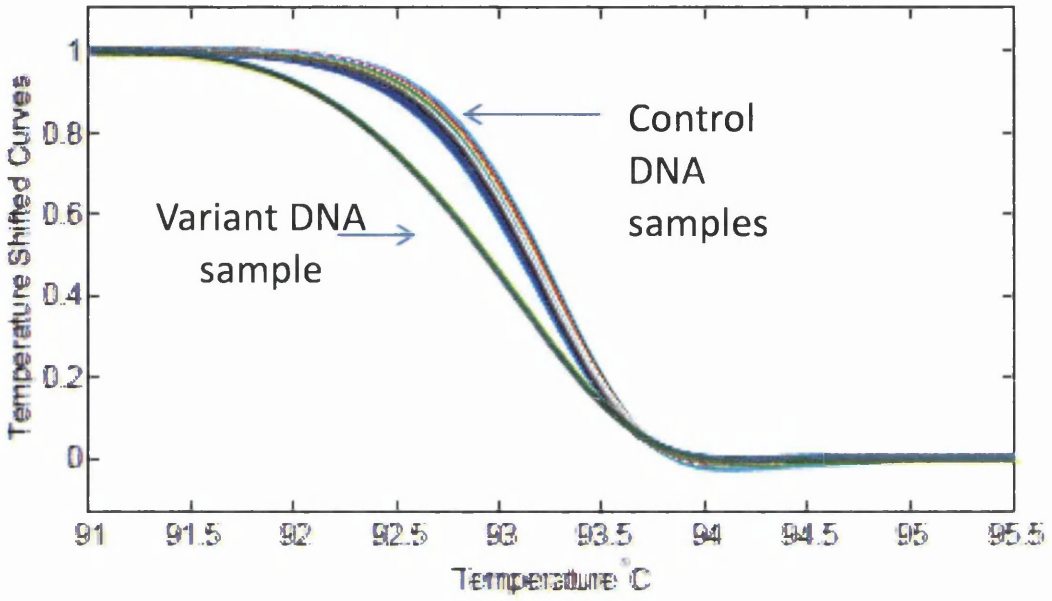

Figure 2.2 Lightscanner melt profile. Patient DNA, which contained a novel variant, was highlighted in dark green. As the Lightscanner heats the DNA of each patient in 96 well form, variant DNA melts at a different rate to the control DNA samples (indicated by arrows).

2.2.4 PCR product purification

Prior to Sanger sequencing, all samples were purified using a QIAquick PCR purification kit (Qiagen, Cat.28106), to remove any unwanted PCR mix that may inhibit downstream applications. Briefly, 50µl of Buffer PB was added to each sample (5x volumes of Buffer PB to 1x volume of PCR product, excluding mineral oil) and transferred into a QIAquick spin column and collection tube. Solutions were centrifuged at 17,000g for one minute allowing DNA to bind to the spin-column membrane and removal of flow-through eluate. 750µl of Buffer PE was added to wash the DNA, and centrifuged for one minute at 17,000g with any flow-through discarded. Samples were then centrifuged again at 17,000g with no added buffer in order to completely remove the wash solution and QIAquick spin columns were placed in clean 1.5µl collection tubes. Clean PCR products were eluted by adding 30µl of sterile water to the spin-

column membrane for one minute, before a final minute centrifuge at 17,000g. The spin column was then discarded leaving purified DNA remaining in the collection tube.

2.2.5 Agarose gel electrophoresis

To determine the success of the PCR purification, samples were visualised on agarose gels. Agarose gel electrophoresis determines the size and presence of the PCR amplicon and can detect any generalised contamination that may compromise the reliability of sequencing results. If contamination was detected or the amplicon was the incorrect size, then the sample would be PCR repeated under re-optimised conditions. Generally, the percentage of agarose used in gels is dependent on the size of the amplicons, however the DNA fragments in this study typically ranged between 200bp and 500bp in length and consequently 1.5% agarose gels were used.

1.5% agarose gels were created by adding 1.5g Ultra pure agarose (Invtrogen, Cat. 16500500) to 100ml 0.5 x TBE (Tris/borate/EDTA) buffer; TBE contains a mix of 108g tris-base (Sigma Cat.154563), 55g boric acid (Fisher scientific, Cat.B3F00/60) and 40ml EDTA (Fisher scientific, Cat.10011123) in one litre of sterile water. The agarose and TBE solution was heated to boiling point in a microwave before cooling and stirring to approximately 60°C. A 1:10,000 dilution of Sybr safe DNA gel stain (Invitrogen, Cat.533102) was added and poured into a plastic mould held in a casket with a toothcomb inserted. The gel was left to solidify at room temperature before being placed in a horizontal electrophoresis tank and covered with 0.5% TBE. The comb was removed to reveal loading wells; 5µl PCR product and 1µl of 6x loading dye (NEB, Cat.B70215) were mixed and loaded into the gel. One hundred base pair DNA ladder (NEB, Cat.N3231L) was added to the first well, which, was made up of 1µl 6x loading dye, 0.25µl 100bp ladder and 3.75µl sterile water. Depending on the size of the gel, the conditions of the electrophoresis equipment were set between 80-120V, for between 35-60 minutes, until the dye band reached approximately three quarters of the gel. The recommended voltage to be used, as described by Life technologies, is 4-10V/cm (distance between anode and cathode) (https://www.lifetechnologies.com).

Gel images were captured using the Trans UV BIO-RAD Gel Doc via Quantity One (version 4.6.3) analysis software. If clear DNA bands of the correct size were observed, then samples were quantified using a NanoDrop™ spectrophotometer 8000 (Thermo Scientific, version 2.2.0), so that DNA could be standardised to 5ng/µl. The DNA and 1.5pmol/µl of exon-specific forward primers were sent for Sanger sequencing using a sequencing provider centre and ABI 3730 XL sequencing machines (Eurofins).

2.2.6 Gene-variant identification, validation and analysis

Sequencing files were visualised in chromatograph form by using Chromas software (Technelysium Pty Ltd). SNPs and variants were identified using Mutation Surveyor software (version 3.10, SoftGenetics, State College, PA) on sequences obtained by comparison to a wild-type reference sequence obtainable in GeneBank Sequence Database (http://www.ncbi.nlm.nih.gov/genbank/). The detection of a variant was further checked using NCBI dbSNP for SNP status i.e. common, rare and novel; synonymous or non-synonymous.

For the purpose of this study rare SNPs were defined by the 'Common-disease common-variant' hypothesis as polymorphisms with a frequency ≥1% (Gorlov et al., 2008). Any variants identified that were in the public domain with a frequency greater than 1% were excluded from the study but noted along with any synonymous SNPs for further scrutiny for expression effects or splicing abnormalities. If a novel or rare variant was identified using a forward primer this was validated by sequencing in the antisense direction from stock samples to control for positional errors using 96-well plates. Following bi-directional sequencing confirmation, a population study would be used to further assess the presence or absence of the rare/novel variation in the unaffected population (section 2.2.8).

2.2.7 Bioinformatic Predictions

All variants underwent bioinformatic predictive analysis to assess putative pathological effects. This was carried out using three prediction webtools; 'Sorting Tolerant From

Intolerant' (SIFT) (http://sift.jcvi.org/), Polymorphism phenotyping (PolyPhen) (http://genetics.bwh.harvard.edu/pph2/) and Align GVGD (http://agvgd.iarc.fr/agvgd_input.php); all three tools predicted whether an amino acid substitution affects normal protein function.

SIFT calculated the degree of amino acid conservation in sequence alignments with closely related sequences using a PSI-BLAST algorithm (Ng and Henikoff, 2001). In a study by Kumar et al. (2009), SIFT was proven to be 69% accurate in correctly identifying pathogenic mutations (Kumar et al., 2009). A SIFT score ranges between 0 and 1 with position specific scoring matrices and if predicted to be less than 0.05 then a variant would be considered deleterious and probably pathogenic. A SIFT score of more than or equal to 0.05 would suggest that the effect of the amino acid change was tolerated by the protein and considered benign. However, no one-prediction tool is accurate and is prone to type-2 false negative outcomes.

PolyPhen predicts whether any structural changes have occurred to the protein as a result of an amino acid change. This prediction was based on multiple phylogenic and structural information regarding the new amino acid substitution (Ramensky et al., 2002). PolyPhen gave a result by calculating the probability of false-positive and true-positive rates (Bergman et al., 2012).

Align GVGD, which was an extension on the Grantham Difference (the assessment of alignment with the physicochemical characteristics of the amino acid) and used conservation and alignment scores to calculate amino acid effects on protein, taking into account composition, polarity and volume of amino acid substitutions. Align GVGD scores that placed variants in group C0 are considered probably benign, groups C15, C25 and C35 are possibly pathogenic and C45, C55 and C65 are probably pathogenic. (McGee et al,. 2010)

2.2.8 Population studies

Population studies involved 480 commercially available control DNA samples with no previous disease history (Sigma-Aldrich, Dorset, UK). Lightscanner PCR was carried

out with the patient DNA sample carrying the suspected novel variant in the 96th well of the Lightscanner plate as a positive melt-curve control, and control DNA in the remaining 95 wells. Post-PCR samples were centrifuged for one minute at 2500g and placed in the Lightscanner. From the melt-curve profiles it is apparent if the control population DNA has some samples that follow the positivecontrol profile or remain typically wild-type. Some population control samples created novel melt-curves due to the presence of common SNPs. Typically, all melt-curve samples that did not have wild-type melt-profiles were Sanger sequenced. In the event where a control sample contains the target variant, but at a low proportion (<1%) of the population, it remained a pathogenic candidate since rare SNPs can be epileptogenic. One further interpretation consideration is that we are dealing with childhood epilepsies with subtle features and consenting adults providing DNA for control status may have forgotten their childhood illness and not declared a history.

2.2.8 Structural homology modelling

To date, homology modelling involving the recognition and comparison of known 3D structure homologs is the most successful *in silico* method for predicting protein structure. There are limited protein folds in nature and homologous sequences adopt similar protein structures along biophysical rules and possibilities. Each variant and wild-type sequence was uploaded on to Phyre2 server (sbg.bio.ic.ac.uk/phyre2) which uses a library of known protein structures from the 'Structural Classification of Proteins Database' to create a variant sequence model which is enhanced with current data from the 'Protein Data Bank' (PDB). This server compared the sequences uploaded with numerous proteins that had previously determined experimental structures. On identification of a homolog, the two sequences were aligned and the 3D protein models were created (Kelley and Sternberg, 2009).

The visualisation and analysis of the molecular structure of variants identified in this study were carried out using the UCSF Chimera package. Chimera is developed by the Resource for Biocomputing, Visualization, and Informatics at the University of California, San Francisco (supported by NIGMS P41-GM103311). The software enabled the direct comparison of wild-type structure with variant structure by aligning

them to each other. Any changes in structure due to sequence variants were visible for analysis at an amino acid side chain level and at a protein structure level (Pettersen et al., 2004).

2.3 Preparation of Gene-Specific Mutation Constructs

All gene-variants that were linked with putative pathogenic properties were introduced into gene-specific construct to enable cellular function experiments. Figure 2.3 illustrates the workflow pipeline to achieve mutagenesis on a relatively large scale.

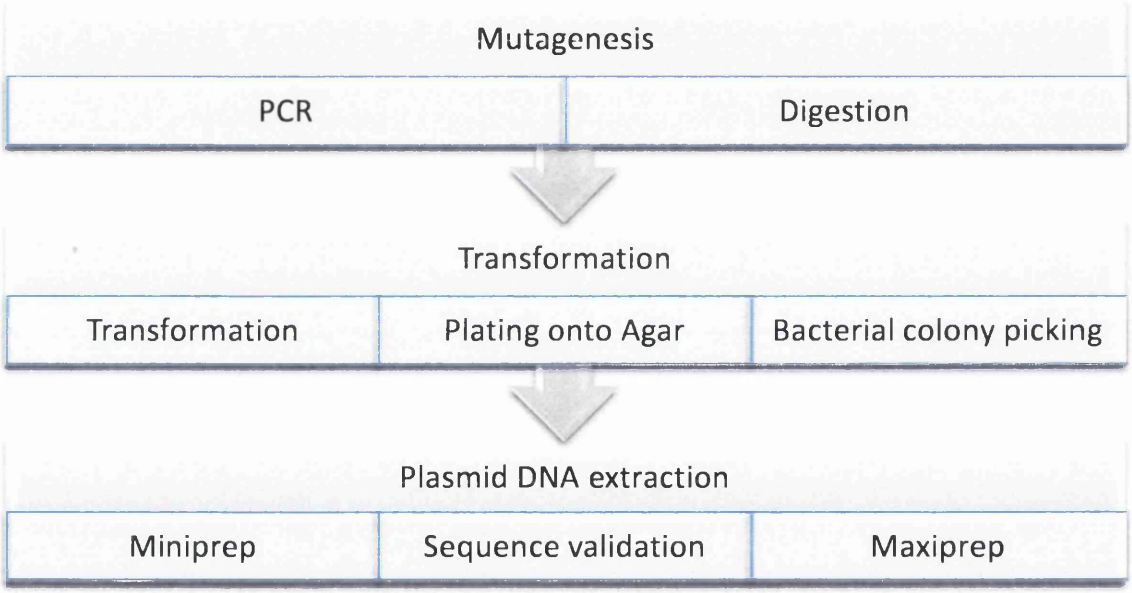

Figure 2.3 Flow diagram of construct preparation process. Creating constructs for functional analysis follows the systematic approach of mutagenesis, transformation and plasmid DNA extraction. These steps can be sub-divided and Mutagenesis involves PCR and digestion steps, the transformation stage following the incorporation of the bacterial cells by the plasmid DNA also involves plating the constructs onto agar and bacterial colony picking. Plasmid DNA extraction is sub-divided into Miniprep, and larger scale Maxiprep stages with sequence validation at each step.

2.3.1 Mutagenesis

The wild-type constructs were externally-sourced for all four GABAergic genes and were C-terminal Myc and DDK-tagged pCMV6-Entry destination vectors that had been

genetically-engineered to contain the open reading frame (ORF) of the corresponding gene with an expression tag (Origene, Cat.PS100001). The 4.9kb Kanamycin resistant vector contained the human cytomegalovirus (CMV) promoter, which, enhances the expression of the cloned inserts, a Kosak sequence (GCCGCCGCGATCGC) situated prior to the insert to encourage translation of the gene and a C-terminal DDK tag sequence (GATTACAAGGATGACGACGATAAG) (Figure 2.4). A DDK antibody was used for visualisation (as described in section 2.4). The wild-type vectors were modified and the novel gene-variants and rare SNPs were inserted individually and amplified by mutagenesis.

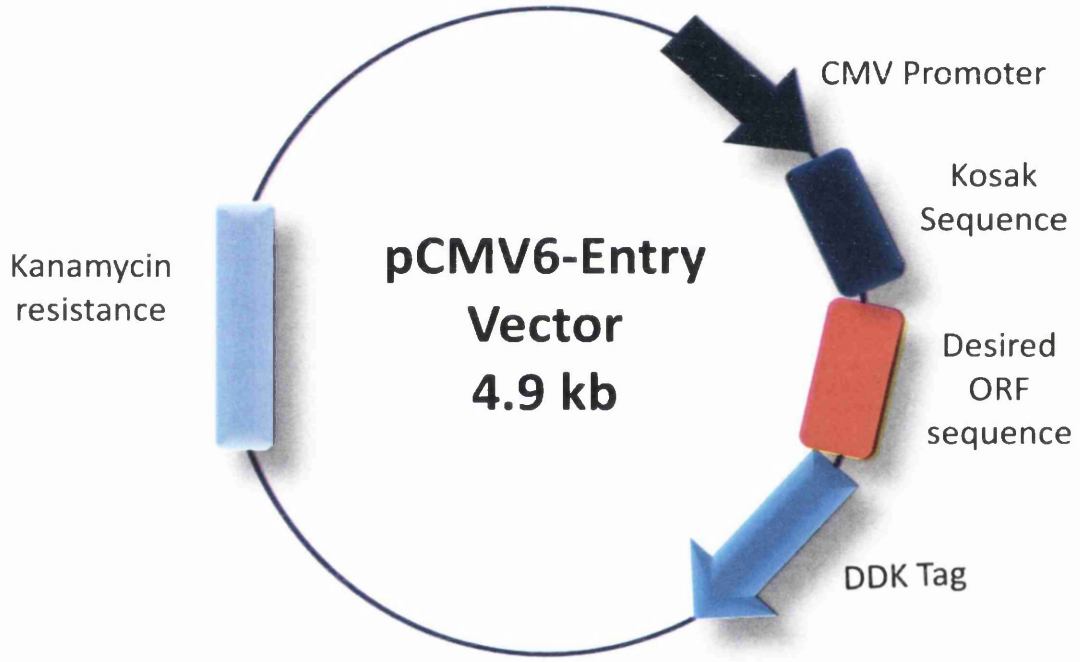

Figure 2.4 Vector map of pCMV6-Entry Vector (C-terminal Myc and DDK tagged). The pCMV6-entry vector contains a Cytomegalovirus (CMV) promoter, a Kosak sequence, the desired open reading frame sequence (red triangle), Myc/DDK flag and a Kanamycin resistance sequence.

2.3.2 Primer design

Mutagenic oligonucleotide primers were designed individually as outlined by Stratagene Site directed mutagenesis protocol, with forward and reverse primers containing the desired variant nucleotide. To ensure successful annealing, primers were optimally designed to be between 25 and 45 base pairs in length, have a melting

Table 2.6 GAT1 and GAT3 mutagenesis primers

GAT1					
Variant	**Forward Primer**	**Reverse Primer**	**Length (bp)**	**GC Content (%)**	**Tm (˚C)**
1	CTTCTCCAACTACAGCGTGGTCAACACTACCAAC	GTTGGTAGTGTTGACCACGCTGTAGTTGGAGAAG	34	50	79
2	TGAGTACCCCAGGATCCTCCGCAACCG	CGGTTGCGGAGGATCCTGGGGTACTCA	27	63	79
3	CCGGGTACATGGCCTACGTGTTCCTCACCTTAAAG	CTTTAAGGTGAGGAACACGTAGGCCATGTACCCGG	35	54	81
GAT3					
1	CACAGGTGATTGAGGCCTATCTGAATGTGTACTAC	GTAGTACACATTCAGATAGGCCTCAATCACCTGTG	35	46	78
2	TGGGCCATTTTTTACCTGAGCAAGTGCTTCACTACT	AGTAGTGAAGCACTTGCTCAGGTAAAAAATGGCCCA	36	44	78
3	CTACAGGAAAGGTTGTATACTTGACTGCGACATTCCC	GGGAATGTCGCAGTCAAGTATACAACCTTTCCTGTAG	37	46	79
4	CCCGGCTCTCCAACCCCCAGGTC	GACCTGGGGGTTGGAGAGCCGGG	23	74	78
5	GAGGGGTTACCGGCAGGAGCTGCTCATC	GATGAGCAGCTCCTGCCGGTAACCCCTC	28	64	80
6	CCAGCACAGATCTGAAAATGTGGGGCAAGCTTGGG	CCCAAGCTTGCCCCACATTTTCAGATCTGTGCTGG	35	54	81

Table 2.6 Mutagenesis primers of GAT1 and GAT3 variants. Forward and reverse mutagenesis primers designed for the generation of three GAT1 and six GAT3 variants identified. To calculate the Tm (˚C) of the primers, the length (bp) and GC content (%) were identified.

Table 2.7 GAD65 and GAD67 mutagenesis primers

GAD65					
Variant	**Forward Primer**	**Reverse Primer**	**Length (bp)**	**GC Content (%)**	**Tm (°C)**
1	CGGAAACAAACTGTTCGCCCTGCTCTACGG	CCGTAGAGCAGGGCGAACAGTTTGTTTCCG	30	57	79
2	GCTGCCGGCGTGTAATGGAGAAAGGCC	GGCCTTTCTCCATTACACGCCGGCAGC	27	63	79
3	GGGAATTGGCAGACCAACAACAAAATTTGGAGG	CCTCCAAATTTTGTTGTTGGTCTGCCAATTCCC	33	45	76
4	TTGGCTGGCCAGAGGGCTCTGGCGATG	CATCGCCAGAGCCCTCTGGCCAGCCAA	27	67	80
5	GAATGAGTCGCCTCTTGAAGGTGGCTCCAG	CTGGAGCCACCTTCAAGAGGCGACTCATTC	30	57	79
6	GACATTGACTTCCTGACTGAAGAAATAGAACGCC	GGCGTTCTATTTCTTCAGTCAGGAAGTCAATGTC	34	44	77
GAD67					
1	GATGCCCGCTTCGGGCGCACAGAGAC	GTCTCTGTGCGCCCGAAGCGGGCATC	26	70	80
2	GATGCCCGCTTCTGGCGCACAGAGAC	GTCTCTGTGCGCCAGAAGCGGGCATC	26	65	78
3	GACATACTCCTCAACTTTGTCCGCAAGACATTTG	CAAATGTCTTGCGGACAAAGTTGAGGAGTATGTC	34	44	77

Table 2.7 *GAD65* and *GAD67* Mutagenesis primers. Mutagenesis primers were created for all *GAD65* and *GAD67* missense variants identified in this study. To do this the length (bp) and GC content (%) were identified which enabled the calculation of the Tm (°C)

temperature (Tm) of ≥78°C, and %GC content of ≥40%. The following formula was used to calculate the Tm of the primers for which %GC was a whole number:

Tm: 81.5 + 0.41(%GC) - 675/N -% mismatch

So that no secondary structures were formed, primers were screened using OligoCalc: Oligonucleotide Properties Calculator, (www.basic.northwestern.edu/biotools/OligoCalc.html).The mutagenesis primers designed to introduce the missense and nonsense variants of this study are shown in Tables 2.6 and 2.7.

A different approach was adopted for the deletion variant identified in this study. This deletion occurs in the final exon of GAT1 causing a frameshift and addition of 16 amino acids running into the 5'UTR owing to the elimination of the obligatory stop codon. A mutagenesis primer had to initially be created (megaprimer) which would span the desired region of the gene from the deletion and to include the additional amino acids created by the frameshift; this primer ended with a sequence that would bind to that of the vector. The forward primer caused the deletion of the desired nucleotide from control DNA which resulted in a frameshift and consequently the removal of the stop codon. The reverse primer bound to the previously intronic sequence that was now a part of the protein due to the frameshift (as shown in table 2.8).

GAT1 deletion variant	Primer Sequence	Amplicon Length (bp)	Annealing temperature (°C)
Forward primer	CGGGCAGCTCCACCGCAAGGAGGCCTACATC	103	70
Reverse primer	TGCTCGAGCGGCCGCGTACGCGTGCCAGGTCGG GGGGTGAGAGT		

Table 2.8 Primer sequences of the GAT1 deletion to create megaprimer. The forward and reverse primer sequences for the identified deletion in GAT1 include the changes needed to mutate GAT1 wild type sequence into the desired variant by PCR. Highlighted in red in the reverse primer is the sequence that binds to the DNA and in blue is the sequence corresponding to the vector sequence. The primers created a fragment (megaprimer) at the optimal annealing temperature of 70°C, which was 103 base pairs in length.

2.3.3 Mutagenesis PCR in Gene Constructs

In 0.2ml tubes on ice, 2µl of the Wild-type expression construct template (at 25ng/µl) was added to 25µl *Pfu* Ultra Hotstart DNA Polymerase (Stratagene), 1.25µl (at 100ng/µl) of both sense and antisense primer, and 20.5µl of sterile water. These were briefly centrifuged before being placed on the thermocycler (MJ Research). On the thermocycler the samples were held at 95°C for one minute before 18 cycles of denaturation at 95°C for one minute, annealing stage at 55°C for one minute and an extension stage at 68°C for two minutes/kb. Incubation periods were approximately 4-6 hours depending on the size of the plasmid. In this study the vectors were on average 4.9 kb in length, and therefore the extension stage was 10 minutes long.

To degrade the parental wild-type DNA, 1µl of the restriction enzyme *DpnI* (NEB, Cat.R01765) was added to each sample upon completion of the PCR programme and incubated for one hour at 37°C, leaving only the desired mutant copy remaining. Following the incubation period, samples were visualised on a 1% agarose gel at 85Mv for an hour. As the parental wild-type would have been degraded by the enzyme, the presence of a clear band at the correct size would indicate successful amplification of a variant construct.

For the deletion variant an initial PCR was carried out before mutagenesis using 1µl of forward and reverse primer in a 0.2 µl PCR tube along with 0.5µl sterile water, 25µl of Type-it™ Multiplex PCR Mastermix 2x (Qiagen Cat:206343) and 100ng of control genomic DNA. The genomic DNA used was previously sequenced to ensure that there were no exonic or intronic SNPs in the sequence for amplification. The PCR programme carried out on this sample involved an initial denaturing period of 95°C for five minutes followed by 34 cycles of a denaturing step at 95°C for 30 seconds, annealing stage at 70°C for 90 seconds, and an extension stage at 72°C for 45 seconds. The programme ended with a final extension phase of 68°C for 15 minutes.

Following PCR, samples underwent electrophoresis on a 3% agarose gel for 60 minutes at 80v with a 100bp ladder (3% gels were suitable for fragments from 10bp to 200bp in length). The megaprimer was then extracted from the gel by being placed

on a UV plate in a dark room, which illuminated the DNA product for removal by cutting out with a scalpel. Using a QIA Quick gel extraction kit (Qiagen, Cat.28704) the DNA was extracted and purified from the agarose gel. Samples were weighed and a buffer was added to dissolve the gel. The sample and buffer solution was incubated for 10 minutes at 50°C. Isopropanol was added for precipitation and the mix transferred to a filter, which, was washed with two separate buffers. DNA was then eluted in 50 µl of water.

300-500ng of megaprimer was used in mutagenesis PCR. The PCR programme carried out involved an initial denaturing stage of 95°C for one minute followed by only five cycles of denaturation at 95°C for one minute, annealing for one minute at 52°C and an extension stage at 68°C for two minutes per kb. This was followed by 13 cycles of an ordinary mutagenesis programme as described above. The number of cycles are kept low to ensure that no unwanted variants appear and the initial five cycles are used to increase the yield of product as the megaprimer has trouble priming to the template (Datta, 1995).

2.3.4 Transformation of Wild Type and Mutant Vectors

Throughout the preparation stages of ampicillin-resistant constructs, a 1:1,000 dilution of ampicillin (Sigma, Cat.A5354) was required in LB Broth/LB Agar. However, Kanamycin-resistant constructs required a 1:2,000 dilution of kanamycin (Invitrogen, Cat. 15240062). Before beginning transformation the LB Broth and LB Agar were prepared. In a glass bottle 20g of LB Broth (Sigma, Cat.L2897) was added to one litre of deionised water and sterilised in a bench top autoclave for approximately 45 minutes. To prepare LB Agar (Sigma, Cat.L3022), a magnetic flea and 35g of LB Agar was added to one litre of water and sterilised in a bench top autoclave for approximately 45 minutes. Following this the LB Agar was allowed to cool to approximately 50°C before adding the required antibiotic. Once the antibiotic was added the LB agar was mixed with a magnetic stirrer. In a bacterial hood 20-30ml of LB Agar was added to petri dishes by pouring and allowed to cool until solidified. Dishes were then sealed with parafilm and stored at 4°C until needed.

One vial of *E.coli* bacteria (One Shot TOP10 Chemically competent *E.coli,* Life technologies, Cat.C404006) per construct was placed on crushed ice. Once thawed, 50µg of plasmid DNA was added to each of the vials, mixed by gentle tapping and placed on ice for 20 minutes. The vials were then transferred to a heat-block preset at 42°C for exactly 30 seconds before returning to ice for two minutes, causing incorporation of the bacterial cells into the plasmid DNA. After two minutes, 250µl of pre-warmed LB Broth was added to the bacteria and incubated for one hour at 37°C, whilst shaking at 750rpm. After 30 minutes, LB Agar plates were pre-warmed to 37°C. Following the incubation period, 100µl of the bacteria-containing broth was transferred to the pre-warmed plates in three dilutions respectively with broth; 1:0, 1:1 and 1:3. These dilutions differ for wild-type to 1:10 and 1:100. Plates were incubated for 16-18 hours at 37°C to allow the growth of bacterial colonies prior to selection.

Following the incubation period, plates were sealed with parafilm and stored at 4°C for approximately six hours. Six labelled falcon tubes per construct were prepared in a bacterial hood and into each tube 3ml of pre-warmed LB Broth and the corresponding antibiotic was added. Bacterial colonies were picked (using a pipette tip) and dropped directly into the LB Broth/antibiotic mix. Six bacterial colonies per construct, were incubated at 37°C for 16 hours, rotating at 225rpm to allow bacterial growth.

A derivation in the protocol was adopted for the deletion variation and ten colonies were selected and visualised on a 1.5% Agarose gel and five samples were selected for Miniprep dependant on the size of the bands. If the sample had been successfully transformed the product would have been 50bp larger than the wild type/not transformed and is a cost effective way to select for the variant sequence before investing in large Maxiprep cultivations.

2.3.5 Plasmid DNA extraction

To extract the plasmid DNA from the Miniprep bacteria, a QuickLyse Miniprep Kit (Qiagen, Cat.27406) was used to purify a small volume of

plasmid for validation by Sanger sequencing (Eurofins). Upon sequence verification of successful mutagenesis and colony selection, the remaining Miniprep was used to seed larger volumes of LB Broth with antibiotics and purified using a HiSpeed Plasmid Maxi Kit (Qiagen, Cat.12663). Both these processes involved the selective denaturation of chromosomal bacterial DNA without affecting the covalent links of the plasmid DNA; this could only occur at a pH of 12.0-12.5 (Birnboim and Doly, 1979). Cell walls were weakened by a lysozyme and completely lysed by a combination of sodium dodecyl sulphate (SDS) and sodium hydroxide (NaOH) (Kado and Liu, 1981). NaOH along with glucose maintained the desired alkaline pH value (Birnboim and Doly, 1979).

To extract plasmids from the post incubation Miniprep, 2ml of starter culture was centrifuged for one minute at 17,000g to pellet the bacteria (all centrifuge steps were one minute at 17,000g). Ice-cold complete lysis solution was added to the pelleted bacterial cells and mixed using a pipette to re-suspend before a three minute incubation at room temperature. After the incubation period, the lysate was transferred by decanting to a spin column and centrifuged. The spin column was washed with buffer QLW and centrifuged with the flow-through discarded. An additional centrifuge step was carried out to dry the QuickLyse spin column. The QuickLyse spin column was transferred into a clean 1.5ml collection tube. DNA was eluted by pipetting 50µl of warmed water directly onto the centre of the QuickLyse spin column to solubilise the vector plasmids and pulled through with centrifugation generating an eluate suspension.

Samples were then quantified using a NanoDrop™ and sent for Sanger sequencing at concentrations ranging from 5-10ng/ul to ensure clean products, the presence of the desired variant and make sure no additional nucleotide variants had emerged into the plasmid sequence. One sample from the Sanger sequencing results of the six bacterial colonies was selected for Maxiprep cultivation.

Maxipreps were established by adding 200ml of autoclaved LB Broth with antibiotic (see previous dilutions) to autoclaved conical flasks. Five hundred micro litres of the successful Miniprep colony was then added with the tops of the flasks loosely-covered using foil and secured with tape before incubation at 37°C in an Innova 4230

refrigerated incubator shaker (New Brunswick, USA) at 225 rpm, for approximately 16 hours. Following the incubation period, the bacterial cells were then harvested by being centrifuged at 6000g for 15 minutes at 4°C.

Bacterial cell-pellets were re-suspended using 10ml Buffer P1. 10ml Buffer P2 was then added, mixed and incubated at room temperature for five minutes. A chilled 10ml Buffer P3 was added, mixed and incubated at room temperature for 10 minutes in the barrel of QIAfilter cartridge. Using a plunger, the cell lysate was filtered into a HiSpeed tip and the lysate was allowed to enter the resin by gravity flow. Following a wash with 60ml Buffer QC, DNA was eluted with Buffer 15ml QF and precipitated with 10.5ml isopropanol at room temperature for five minutes. The DNA/isopropanol mix was then filtered and 2ml of 70% ethanol was added before the solution filtered. Air was forced through the filter twice to ensure no ethanol remained. DNA was re-suspended in 750µl of sterile water and the DNA quantified using the NanoDrop™ system. Sanger sequencing was used to ensure a successful Maxiprep cultivation, which, included sequence coverage for both the vector and ORF insert.

2.4 Immunocytochemistry

Once the wild-type and mutagenesis constructs were created and sequence verified there was a requirement to ensure all constructs in cell-lines were functioning and expressing. Immunocytochemistry in HEK293 was carried out on all mutation and wild-type constructs followed by visualisation of expression via high-resolution confocal microscopy. All cell culture work was carried out in laminar flow hoods under sterile conditions.

Immunocytochemistry is a popular technique that visualises the expression and localisation of proteins within a cell. Consequently, this was used to check the expression validity of the GABAergic mutations and wild-type constructs but also may show large variations in expression and or localisation when compared. A primary antibody is added to the cells which recognises and binds to a specific antigen, a secondary antibody raised in the same species is then introduced (Figure

2.5). The secondary antibody will typically be labelled with a fluorescent probe, which, once bound, will allow detection of the target epitope by high-resolution confocal microscopy.

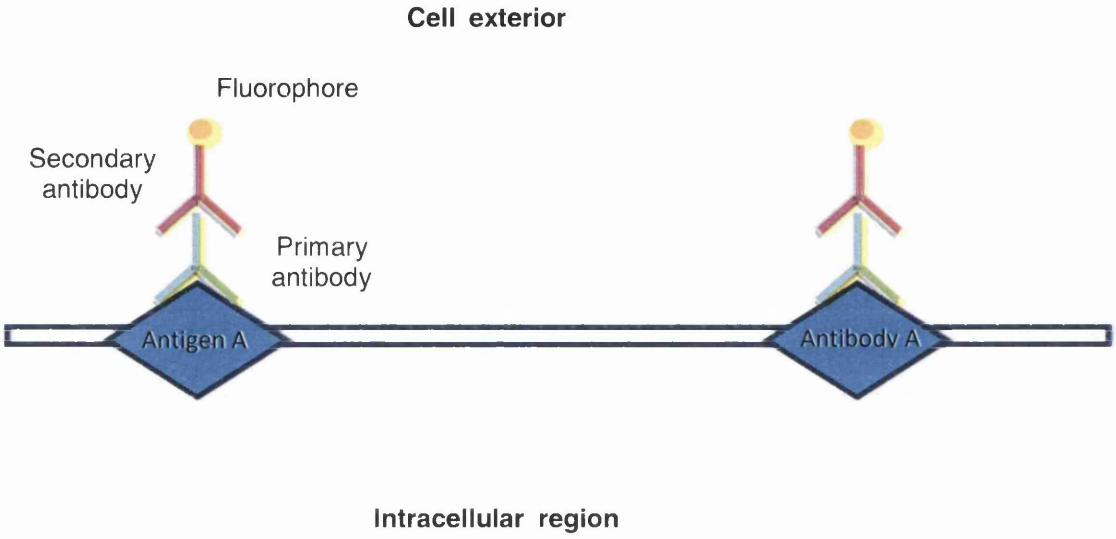

Figure 2.5 Antibody binding to target antigen. The primary antibody, as shown in green, recognises antigen A and binds. The secondary antibody (highlighted in red) recognises the primary antibody. Once bound, antigen A can be detected due to the fluorescent probe contained in the secondary antibody (yellow circle).

2.4.1 Culturing the HEK293 Cell Line

HEK293 cells are human embryonic kidney cell-line that are characteristically used as an expression or targeting validation platform for recombinant proteins. HEK293 cell-lines were created by transformation of normal HEK cells with human adenovirus type-5 to form the permanently transformed cell-line HEK293 (Graham et al., 1977). In comparison to native neuronal cell-lines, HEK293 had dissimilar architecture and the sub-cellular organisation differed but they are widely used due to its dependable reconstitution of numerous neuronal proteins and they also demonstrated similar complexities topographically and biochemically as could be observed in the central nervous system (Thomas and Smart, 2005).

The culture of HEK293 cells is the first process of immunocytochemistry and occurred in 75cm^2 culture flasks with 15 ml of Dulbecco's Modified Eagle Medium

(DMEM) (Life technologies, Cat.41966-029) (supplemented with 10% Fetal Calf Serum (FBS) and 1% Penicillin/Streptomycin (PenStrep)). In a sterile incubator at 37°C and 5% CO_2, healthy, viable cells adhered to the base of the flask to form a cell lawn. To sustain the health of cells, when they reached 80% confluencey they were passaged which involved firstly removing the old media by aspiration. The cell lawn was then rinsed with 5ml pre-warmed Dulbecco's Phosphate Buffer Saline (DPBS) (Life technologies, Cat10010-015) before being treated with 1.5ml 0.25% pre-warmed Trypsin-EDTA (Life technologies, Cat.25300-054) causing detachment of cells from the flask base. Following removal of any excess Trypsin-EDTA, the flask was placed back in the incubator in the same conditions as previously stated for two minutes.

10ml of pre-warmed media was added to the flask following the incubation to terminate the actions of Trypsin-EDTA. This solution was placed over the cell lawn and repeatedly mixed to ensure the efficient dispersing of any clumps of cells to form a single-cell suspension. Sub-culturing requires a 1:10 dilution of cells and so 1ml of cells were removed and added to a new flask with 15ml of pre-warmed fresh media. The remaining 9ml of cells were discarded and added to bleach unless proceeding to section 2.4.2, where cells were placed in a falcon tube. The new flask was then incubated at the optimal conditions until ready for its next passage as indicated by close daily observations.

2.4.2 Coating cells onto coverslips

Cells were seeded onto pre-treated glass coverslips when being imaged using Confocal Microscopy. Coverslips were autoclaved and thoroughly dried before being transferred to a 12-well plate, rinsed with sterile tissue culture-grade water three times and treated with 10µg/ml poly-L-Lysine (PLL) (Sigma, Cat.P4707) which enabled cell adherence; coverslips were incubated at room temperature for one hour. After the incubation period, the PLL was removed from the coverslips by pipetting and they were allowed to air dry for approximately 30 minutes. Once dry, coverslips were rinsed three times with sterile tissue culture-grade water and again allowed to air dry at room temperature; coverslips were now ready for seeding.

1ml of pre-warmed media was added to each well with a PLL treated coverslip. Cells previously placed in a falcon tube (section 2.4.1) were quantified using Scepter™ cell counter (Millipore) and a standardised 8 x 10^4 cells/ml was added to each well. The plate was then covered and incubated at 37°C with 5% CO_2 for 24 hours to allow cells to adhere to the glass coverslips.

2.4.3 Transfection of gene constructs into cultured cells

Constructs previously created were transfected into cultured cells via Magnetofection™. Magnetofection™ involves combining magnetic nanoparticles to the gene vectors by salt-induced colloidal aggregation and electrostatic interaction, causing a remarkable increase in the uptake of the vector and high transfection efficiency. The biodegradable iron oxide magnetic nanoparticles were coated with cationic molecules, which were drawn to and endocyted by cells via magnetic fields (Mykhaylyk et al., 2007, Buerli et al., 2007).

To carry out this stage of the study on a 12-well plate with glass coverslips, two separate transfection mixtures were made. The first contained 15µl Opti-MEM reduced serum medium (Life technologies, Cat.31985-062) and 0.5µg of DNA construct; the second contained 15µl Opti-MEM and 1µl Lipofectamine™ 2000 reagent (Invitrogen, Cat.11668). Mixtures were incubated at room temperature for 5 minutes before being combined and 1µl of CombiMag (OzBiosciences, Cat.CM20200) 1:10 solution added. The mixture was again incubated at room temperature for 15 minutes. 30µl of transfection mixture was added to the media of the HEK293 cells coverslips and circulated around the well by swirling. The 12 well plate was placed on a magnetic plate and incubated at 37°C with 5% CO_2 for 25 minutes. After the incubation period, the media was removed and replaced with fresh pre-warmed media for 24 hours to allow *in vitro* expression of the constructs before any further analysis.

2.4.4 Intracellular staining

Coverslips that had undergone transfection were removed from the incubator and media was removed before they were rinsed twice with 1x PBS solution (Sigma: P-4417). Cells were fixed using 4% paraformaldehyde (Sigma, Cat.P-6148) and incubated at room temperature for 10 minutes. Paraformaldehyde was removed by aspiration and cells were rinsed with PBS solution to remove any excess before being quenched twice with 50mM NH_4Cl (Sigma, Cat.254134) for 10 minutes at room temperature to stop any chemical or enzymatic reactions. Following removal of NH_4Cl by aspiration and rinsing with PBS solution, the cells were permeabilised at room temperature in Fetal Bovine Serum (FBS) (Sigma, Cat.F6178) / Bovine Serum Albumin (BSA)(Sigma, Cat.A9647-50G)/Triton X-100 solution (Sigma, Cat.T8787) (*10ml of FBS/BSA (as stated below) + 10µl Triton X-100 (0.1% v/v)* for 15 minutes. The solution was then removed, the cells rinsed twice in PBS solution and washed in FBS/BSA solution for one minute.

The mouse monoclonal (IgG2a) primary antibody Anti-DDK tag (Origene, Cat:TA50011) was diluted at 1:1000 dilution in FBS/BSA solution *(45ml PBS, 5ml FBS (10% v/v), 0.25g BSA (0.5% w/v))*. The antibody recognises the overexpression of the D epitope tag (DYKDDDDK), which would be fused to the amino or caboxyl terminal of the transfected target protein in the HEK293 cells. The antibody solution was added by pipetting into a humidifying chamber and the coverslips were inverted on to the solution to be incubated at room temperature with a mild rotation (25rpm) for two hours. Following the incubation period, cells were removed from the humidifying chamber and washed for five minutes with mild rotation once with FBS/BSA and twice with PBS.

Alexa488 goat anti-mouse IgG (H+L) (Invitrogen) was the secondary antibody used in this study for all missense and deletion variants. The secondary antibody came labelled with photostable green-fluorescence Alexa488 dye that reacts with IgG heavy chains and immunoglobulin light chains from mouse; the antibody had been adsorbed against human IgG and serum to minimise any cross reactivity. Diluted at 1:200 in FBS/BSA solution, 30µl of antibody/FBS/BSA solution was transferred by

pipetting into the humidifying chamber with the coverslips placed on top. The cells were incubated at room temperature for 30 minutes with mild rotation and were protected from light due to its light sensitivity, before the final five minute wash with FBS/BSA and two five minute washes with PBS. Coverslips were left to dry at room temperature and then mounted using Prolong gold onto clean glass slides.

2.4.5 Confocal Microscopy and analysis of transfected HEK293 cell lines

High-resolution images of transfected HEK293 cells were created using the Carl Zeiss LSM 710 confocal microscope. Cells were initially imaged at 20x magnification to demonstrate and ensure cell confluence, even distribution and transfection efficiency. Following this, cells of interest were selected and imaged at the higher magnification, 63x. To ensure consistency, reliability and fair testing, the following criteria were outlined and adhered to throughout analysis:

1. Wild-type images of transfected proteins were firstly captured to determine normal expression levels and select the optimal parameters.
2. Variant images were created and analysed, blind to the gene-variants, using the parameters as set out by the wild-type standardisation.
3. Only HEK293 cells showing high expression of the transfected DDK-tagged GABAergic gene variants were selected for analysis.

Chapter Three

Mutation analysis of GAT1 and GAT3 in relation to Epilepsy

We know from previous work that there are genetic, pharmacological, neuroanatomical and animal studies that implicate the GABAergic system with epileptogenesis and seizure predisposition. Prior to this study no causative mutations had been identified in the GABA transporter genes SLC6A1 and SLC6A11 (known from this point as proteins GAT1 and GAT3) in relation to epilepsy. This was intriguing as other neurological disorders were linked to cognate receptor/transporter systems, which seemed plausible for genetic forms of epilepsy.

A targeted, hypothesis-led candidate gene approach was adopted to allow efficient and systematic screening in 485 patient samples with clinically confirmed genetic generalised epilepsy (GGE; Melbourne). To validate and replicate the relevance of the data obtained from the preliminary GGE results, an additional 187 childhood absence seizure (CAE; UCL) and 35 juvenile myoclonic epilepsy (JME; WERN) patient samples were recruited and screened. Control population studies were carried out on 480 commercially available samples (Sigma) to assess population frequencies of potentially pathogenic gene variants.

The outcome of this chapter demonstrates the discovery of synonymous, novel non-synonymous missense/nonsense, splice site and intragenic variants identified in the GAT1 and GAT3 transporters. From the catalogue of variants with a mean allelic frequency (MAF) of less than 0.01 (1%), the result of *in silico* analysis is presented and considered to assess causative potential.

3.1 Mutation analysis of GAT1

Thirty-three variants were identified in GAT1 coding sequence and flanking intronic regions in 107 patient samples (Table 3.1), which, consisted of 3 non-synonymous, 1 splice site, 1 base pair frameshift deletion, 11 synonymous, and 17 intronic variants.

Exon	Nucleotide change	Type of Mutation	Amino acid change	Sample frequency (n=707)	Reference	MAF
1	5'UTR-57 G>A	Intronic		1	Novel	
	c.6 G>A	Synonymous	p.A2A	1	rs6343	0.0018
2	c.246 C>T	Synonymous	p.F82F	1	Novel	
	IVS1-81 C>A	Intronic		1	Novel	
	IVS1-26 G>A	Intronic		1	rs41308232	0.0009
	c.312 G>A	Synonymous	p.L104L	2	Novel	
3	IVS3+46 G>C	Intronic		4	Novel	
	IVS3+1 G>A	Donor Splice Site		1	Novel	
4	IVS4+54 C>T	Intronic		18	Novel	
	c.535 A>G	Non-synonymous	p.M179V	2	rs34299874	0.0119
5	c.651 G>T	Synonymous	p.T217T	25	rs6344	0.0496
6	c.801 C>T	Synonymous	p.G267G	2	rs150519659	0
	c.780 G>A	Synonymous	p.T260T	1	rs6344	0.0496
	IVS6+72 G>A	Intronic		1	Novel	
	IVS5-3 C>T	Intronic		1	Novel	
7	IVS7+21 G>T	Intronic		1	rs35736058	0.0115
8	IVS7-41 G>A	Intronic		1	Novel	
	c.1002 A>G	Synonymous	p.A334A	1	rs35513423	0.006
	IVS7-90 C>T	Intronic		1	Novel	
	c.960 C>T	Synonymous	p.S320S	1	rs35972647	0.0096
9	IVS8-51 G>A	Intronic		1	Novel	
	IVS8-64 G>A	Intronic		1	Novel	
10	c.1243 C>A	Non-synonymous	p.L415I	7	rs112095333	0.0014
	IVS9-23 G>T	Intronic		5	rs150889270	0.0032
	IVS9-36 G>A	Intronic		1	Novel	
	IVS10+43 G>T	Intronic		2	Novel	
11	c.1335 T>C	Synonymous	p.Y445Y	2	Novel	
12	IVS12+23 C>T	Intronic		4	rs200922468	0.0009
	c.1527 G>A	Synonymous	p.A509A	2	rs34969656	0.0009
13	c.1663 A>G	Non-synonymous	p.M555V	1	rs139846326	0
	IVS13+16 C>G	Intronic		13	rs35957531	0.0707
14	c.1713 C>T	Synonymous	p.V571V	1	Novel	
	c.1780 Deletion A	Deletion	p.S594A FS 22X	1	Novel	

Table 3.1 The GAT1 *all*-variants table. Variant table of all variants identified via *GAT1* screening of genetic generalised epilepsy patients. The frequency the variant occurs amongst samples is highlighted as well as the mean allelic frequency of any variants previously identified.

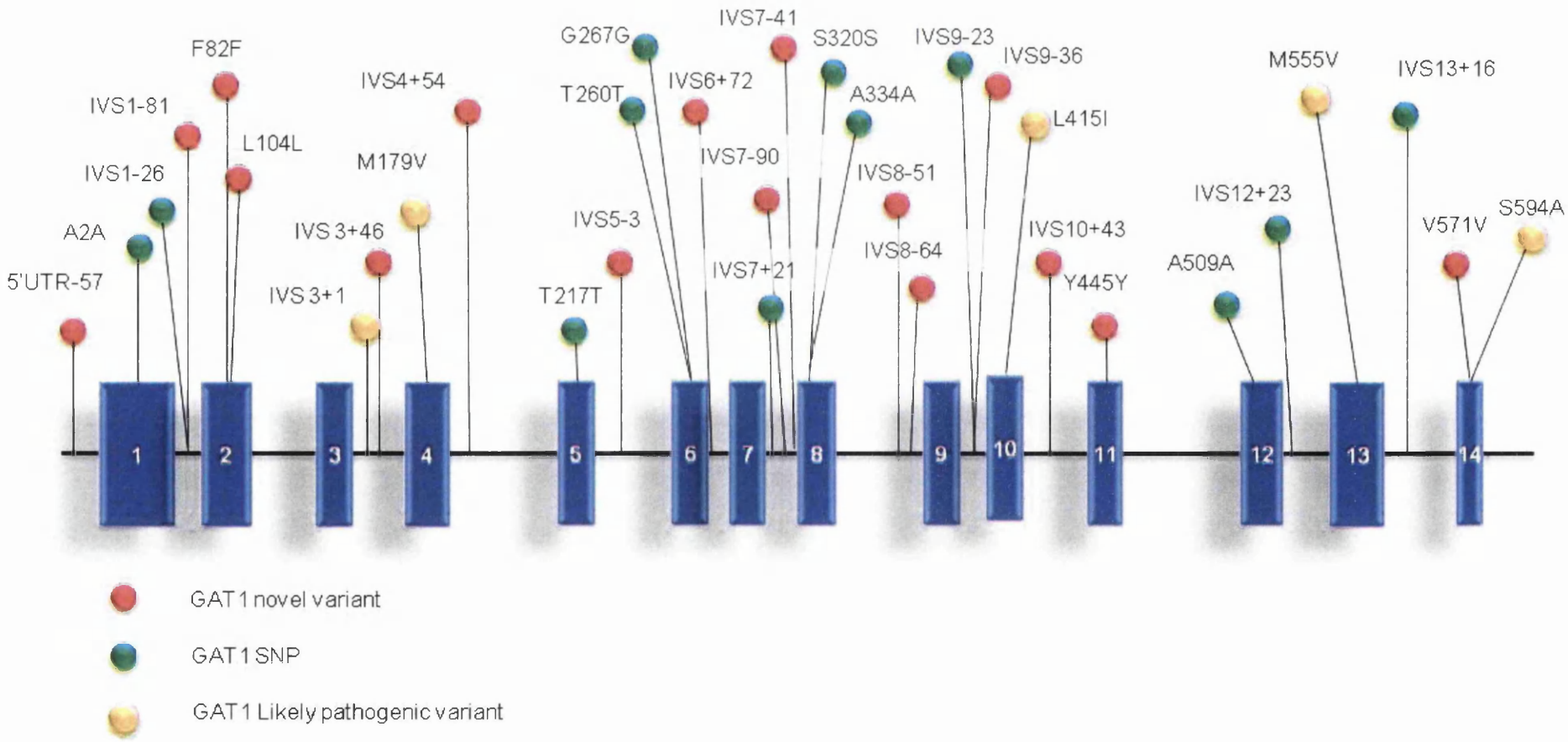

Figure 3.1 Genetic location of *GAT1* variants identified in 707 epilepsy patient samples; Schematic exon diagram demonstrating the genomic structure and location of identified polymorphisms in the GAT1 gene. Exons 1-14 are demonstrated as blue numbered boxes and the non-coding intronic regions by the connecting black lines. The novel mutations are symbolised by the red circles and were identified in the corresponding exons as indicated; previously identified variants are shown as green circles. Non-coding exons are not highlighted in this schematic.

Gene	Exon	Variant	Nucleotide change	Genbank reference (Mean Allelic Frequency)	Case frequency (Allelic frequency)	Control population frequency (Allelic frequency)	Sift consequence (Score)	Grantham class (Score)	Polyphen result (Score)
GAT1 (*SLC6A1*)	3	N/A	IVS3+1 G>A	Novel	1/693 (0.0007)	0/480 (0)	N/A	N/A	N/A
	4	p.M179V	c.535 A>G	rs34299874 (0.0119)	2/691 (0.0014)	0/480 (0)	Tolerated (0.58)	C15 (20.52)	Benign (0.001)
	10	p.L415I	c.1243 C>A	rs112095333 (0.0014)	7/631 (0.0055)	3/480 (0.003)	Tolerated (0.21)	C0 (4.86)	Benign (0.002)
	13	p.M555V	c.1663 A>G	rs139846326 (0)	1/679 (0.0007)	0/480 (0)	Tolerated (0.32)	C15 (20.52)	Benign (0.051)
	14	p.S594A fs22X	c.1780delA	Novel	1/701 (0.0007)	0/480 (0)	N/A	N/A	N/A

Table 3.2 GAT1 novel variants and rare SNPs indentified in epilepsy patient samples. SLC6A1 variants identified in 707 epilepsy patient samples are shown. In addition the corresponding variant frequencies in patient samples, previously identified SNP frequencies, control population frequencies and the predicted consequences (using three prediction tools) of variants on the protein have been included.

These variants are mapped onto genomic positions and their novelty status indicated (Figure 3.1). From this compendium of gene-variations, the most likely pathogenic variants were selected for further analysis which included the splice variant, deletion variant and three non-synonymous variants (Table 3.2).

Of the five variants identified as potentially pathogenic in GAT1 3 were heterozygous missense variants; 1) p.M179V (c.535A>G), 2) p.L415I (c.1243C>A) and 3) p.M555V (c.1663A>G); 1 was a heterozygous frameshift variant 4) p.S594A-fs22X; and there was 1 heterozygous splice site variant 5) IVS3 +1 G>A (Table 3.2, Figure 3.1 and Figure 3.2). The damaging status case for each variant is presented in table 3.2, taking into account bioinformatics databases and control frequency datasets; Structure/function data is presented in Chapter Five.

3.1.1 Missense Variant p.M179V

The missense variant p.M179V, is an amino acid change from methionine to valine at residue 179 with a single nucleotide change from adenine to guanine at position 535 in exon 4 of GAT1 (Figure 3.2). GAT1$^{p.M179V}$ was not identified in the 480 unaffected control population study (Figure 3.3) but was identified twice from 691 patient samples. This missense variant is listed as a polymorphism on dbSNP in a control sample of n=2,393 with a mean allelic frequency of 0.024 but this frequency was not supported by our data and analysis.

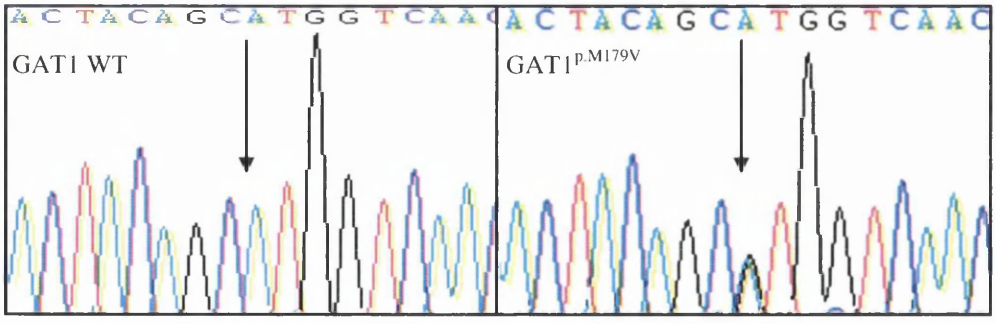

Figure 3.2 Sequence chromatogram of variant GAT1$^{p.M179V}$ identified in epilepsy patient samples and the corresponding wild type sequence. The variant is identified by an arrow in the right hand column of the figure and the corresponding wild-type sequence in the left hand column. The double peak indicates the heterozygous c.535 A>G nucleotide change in the coding sequence.

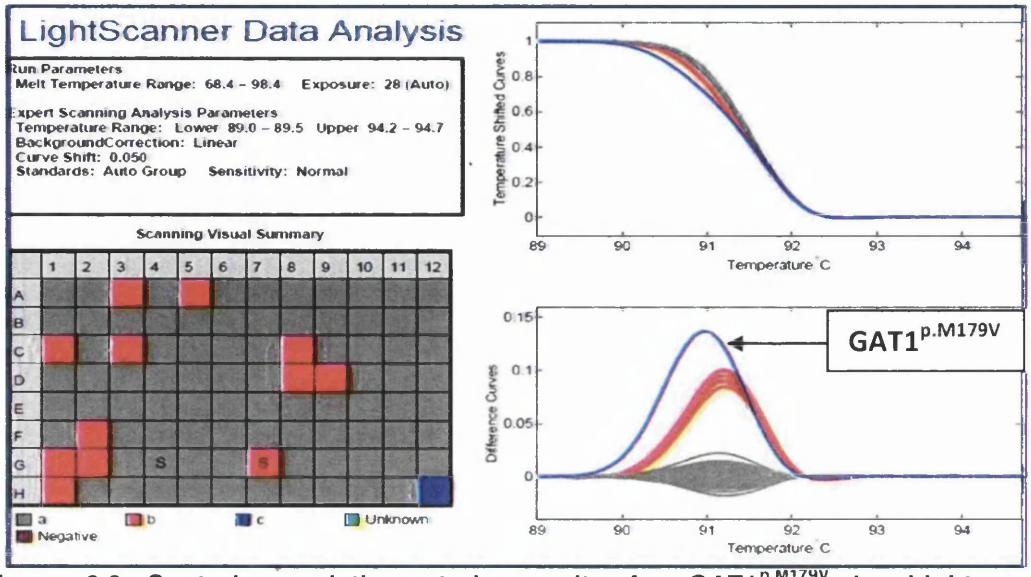

Figure 3.3 Control population study results for GAT1$^{p.M179V}$ by Lightscanner technology. p.M179V (positive control) melts at a rate that is different to the other 95 control samples. A further 12 samples (shown in red) also melt at a different rate to the other controls, but they do not contain the variant M179V, and instead contain a common SNP.

	GAT1$^{p.M179V}$
GAT1 variant	FSNYSVVNTT
H.sapien	FSNYSMVNTT
P.troglodytes	FSNYSMVNTT
M.mulatta	FSNYSMVNTT
B.taurus	FSNYSALNTT
C.lupus	FSNYSIVNTT
G.gallus	FSNYTLANTT
R.norvegicus	FSNYSLVNTT
M.musculus	FSNYSLVNTT

Figure 3.4 Multiple phylogenetic alignments of the *GAT1*$^{p.M179V}$. *GAT1* variants were aligned against their respective wild-type sequence alignments and their species homologs. The mutated amino acid valine in this instance, was highlighted in red and its corresponding residue highlighted in green for different species and wild-type to indicate the level of evolutionary conservation.

Multiple species alignments show that the amino acid substitution is highly-conserved residue in primates but diverges in mammalian lines indicating a degree of tolerance (Figure 3.4). This is supported by the mutation prediction software using

conservation analysis (Table 3.2) that predicts GAT1$^{p.M179V}$ would be benign (PolyPhen and Grantham) and would be tolerated by the protein (SIFT). Therefore, GAT1$^{p.M147V}$ is regarded as a rare SNP that in theory is tolerated and benign, however, the functional properties and consequences of this SNP require investigation due to conflicting population and *in silico* evidence.

3.1.2 Missense Variant p.L415I

p.L415I, is a heterozygous c.1243 C>A gene variant in exon 10 of SLC6A1 causing a non-synonymous amino acid change from leucine to isoleucine at residue 415 of GAT1 (Figure 3.1, Figure 3.5). Seven of 631 patient samples were confirmed to present GAT1$^{p.L415I}$ as were three samples of the directly analysed 480 control population (Table 3.2; Figure 3.6). In dbSNP, this variant has a mean allelic frequency of 0.003 from 2,752 control samples.

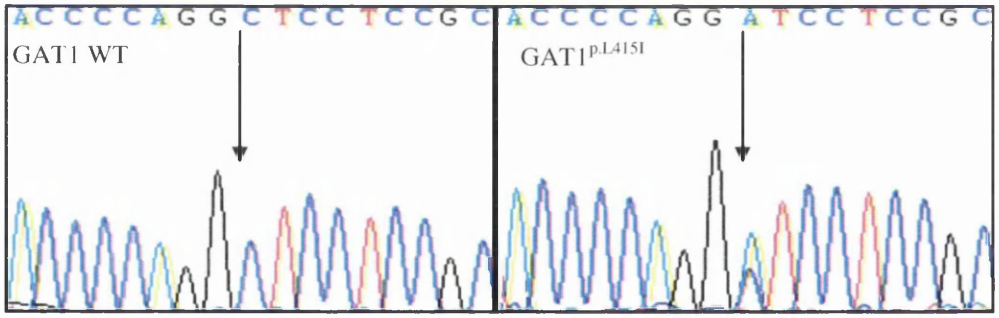

Figure 3.5 Sequencing trace of the *GAT1*$^{p.L415I}$ compared to the *GAT1* wild-type. The heterozygous c.1243 C>A nucleotide change causes an amino acid change from leucine to isoleucine. The double peak of the variant is indicated by an arrow and differs in comparison to the wild-type.

The GAT1$^{p.L415I}$ amino acid change has no effect on protein conservation, structure and composition according to all three predictive software tools, SIFT, Grantham and PolyPhen (Table 3.2). However, multiple species alignment analysis (Figure 3.8) demonstrates that the Leucine at position 415 of GAT1 is highly conserved across mammalian species, which highlights the importance of the residue and the equally preserved flanking amino acids.

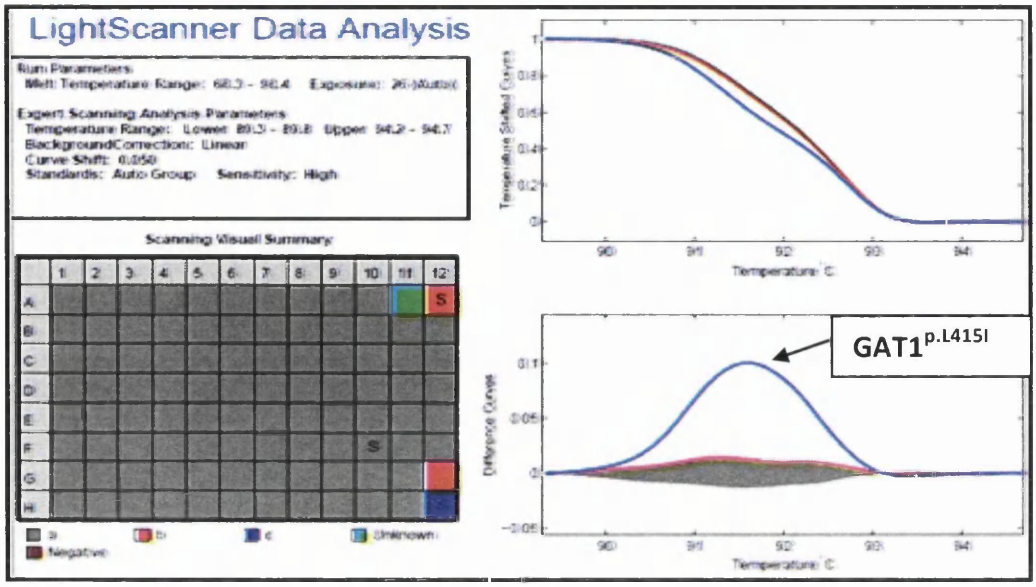

Figure 3.6 Lightscanner profile of the GAT1$^{p.L415I}$ variant population study. Of the 96 samples that underwent Lightscanner HRM analysis, the variant can be clearly identified as having a deviated melt profile from the 95 healthy control samples.

	GAT1$^{p.L415I}$
GAT1 variant	DEYPR**I**LRNRR
H.sapien	DEYPR**L**LRNRR
P.troglodytes	DEYPR**L**LRNRR
M.mulatta	DEYPR**L**LRNRR
B.taurus	DEYPR**L**LRNRR
C.lupus	DEYPR**L**LRNRR
G.gallus	DEFPK**L**LRNRR
R.norvegicus	DEYPR**L**LRNRR
M.musculus	DEYPR**L**LRNRR

Figure 3.7 p.L415I multiple species phylogenetic alignments. p.L415I was aligned against the GAT1 wild-type sequence and its putative mammalian homologs. Isoleucine was highlighted in red, and its corresponding residue highlighted in green for different species and wild-type to specify the level of evolutionary conservation.

Collectively GAT1$^{p.L415I}$ is a rare population SNP in a highly conserved region of the protein and has a higher allele frequency in epilepsy cases. It therefore warrants further investigation on the effect of GAT1 patho-biology.

3.1.3 Missense Variant GAT1 p.M555V

The final missense variant identified in GAT1 was p.M555V, a heterozygous c.1663 A>G nucleotide change in exon 13 causing a methionine to valine substitution (Figure 3.1 and Figure 3.8). GAT1$^{p.M555V}$ was identified in one patient sample of 679, but was not identified in the 480 unaffected control population study and has a mean allelic frequency of zero in 2,276 control samples in dbSNP. (Table 3.2 and Figure 3.9).

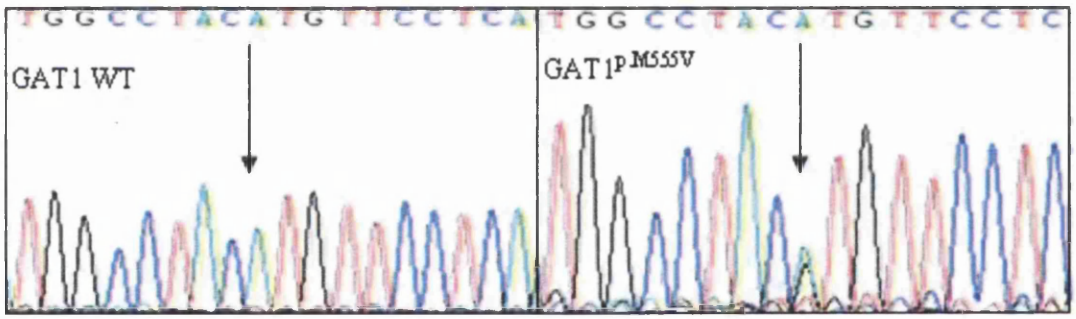

Figure 3.8 GAT1$^{p.M555V}$ sequence chromatogram compared to wild-type. The heterozygous variant can be identified by the double peak beneath the arrow and reflects a c.1663 A>G nucleotide change compared to wild-type.

The predicted consequences of GAT1$^{p.M555V}$ is identical to GAT1$^{p.M179V}$ where tolerated effects were predicted with SIFT, benign structural changes were predicted by PolyPhen and a possibly damaging result was predicted by the Grantham score when considering the effect of the amino acid on composition and polarity (Table 3.1). Phylogenetic alignment demonstrates that methionine at position 555 of GAT1 is a highly conserved residue in a region of highly conserved amino acids, indicating a selective evolutionary pressure to not mutate this site and region (Figure 3.10).

Triage of GAT1$^{p.M555V}$ into functional studies was decided via the novelty of the genotype, some indication of damaging effects by *in silico* methods and the highly conserved nature of the amino acid substitution.

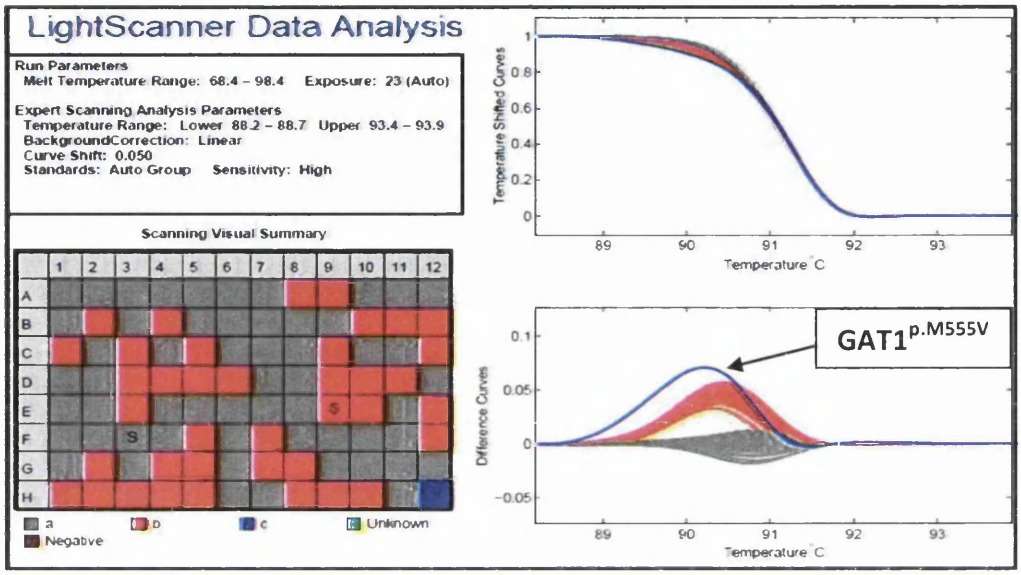

Figure 3.9 Lightscanner data analysis profiles of a control population study. GAT1$^{p.M555V}$ was identified in one patient. As shown above p.M555V has a different melt profile to the 95 control samples and has been highlighted in blue. The results of all 5 lightscanner population studies (n=475) indicates that M555V is not present in the healthy control population.

	GAT1$^{p.M555V}$
***GAT1* variant**	GYMAY**V**FLTLK
H.sapien	GYMAY**M**FLTLK
P.troglodytes	GYMAY**M**FLTLK
M.mulatta	GYMAY**M**FLTLK
B.taurus	GYMAY**M**FLTLK
C.lupus	GYMAY**M**FLTLK
G.gallus	GYMAY**M**FLTLK
R.norvegicus	GYMAY**M**FLTLK
M.musculus	GYMAY**M**FLTLK

Figure 3.10 Multiple species phylogenetic alignments of GAT1$^{p.M555V}$ Wild-type GAT1 and GAT1$^{p.M555V}$ were aligned with homologous species with position 555 highlighted in green and the GAT1$^{p.M555V}$ variant sequence in red.

3.1.4 A 1bp deletion causing a frameshift c.1760delA / p.S594Afs22X

This frameshift variant occurs in the final exon (exon 14) of the GAT1 gene and is a heterozygous one base-pair deletion of adenine at the first position of the serine amino acid at position 594 of the polypeptide (Figure 3.1 and figure 3.11). GAT1$^{p.S594Afs22X}$ causes a change in the open reading frame starting with a substitution of serine to alanine and a 22 amino acid nonsense message thereafter. In wild-type GAT1 the serine is six amino acids away from the constitutional stop codon, however, the deletion abolishes this stop codon but reaches a new stop codon 22 amino acids from the deletion. This action results in an additional 17 amino acids being added to GAT1$^{p.S594Afs22X}$ in the C-terminus of the polypeptide creating a potentially pathogenic outcome and a possible dominant-negative effect in GAT1 dimerisation (Figure 3.12). The additional amino acid stretch does not correspond to any known functional domain or known proteins sequences.

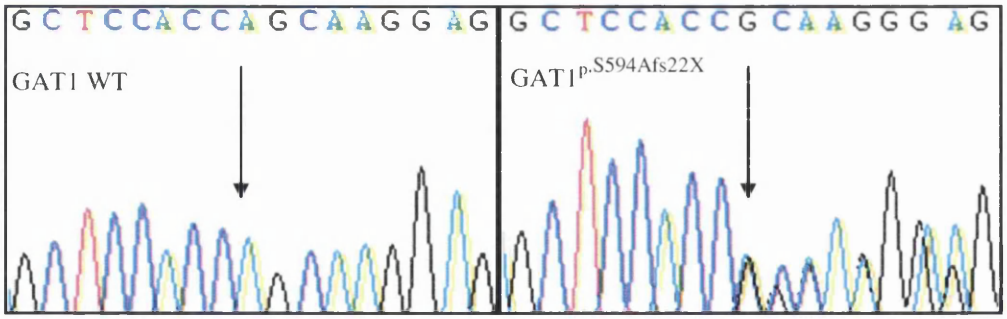

Figure 3.11 Sequence chromatogram for *GAT1* wild-type and GAT1$^{p.S594Afs22X}$. Compared to wild-type it can be seen that a 1bp deletion at nucleotide position 1780 (as indicated by arrows) causes a nucleotide frameshift immediately after the deletion.

GAT1$^{p.S594Afs22X}$ was identified in one patient sample out of 701 and not found in the 480 unaffected control population study nor on online databases (Figure 3.13). Predictive analysis could not be carried out for such a variant, however, the very nature of the frameshift does indicate a likely pathogenic outcome and triage through to functional studies

Wild-type protein sequence	D-S-T- S-K-E-A-Y-I- STOP
GAT1$^{p.S594Afs22X}$	D-S-T- A-R-R-P-T-S-R-V-G-A-T-H-R-P-D-T-L-T-P-R-P-G- STOP

Figure 3.12 GAT1 wild-type protein sequence aligned with GAT1$^{p.S594Afs22X}$. Following Serine at amino acid position 594, the wild-type sequence has five amino acids before the stop codon. C.1760delA causes a protein change from serine to alanine as well as a frame shift resulting in 21 amino acids before the next stop codon.

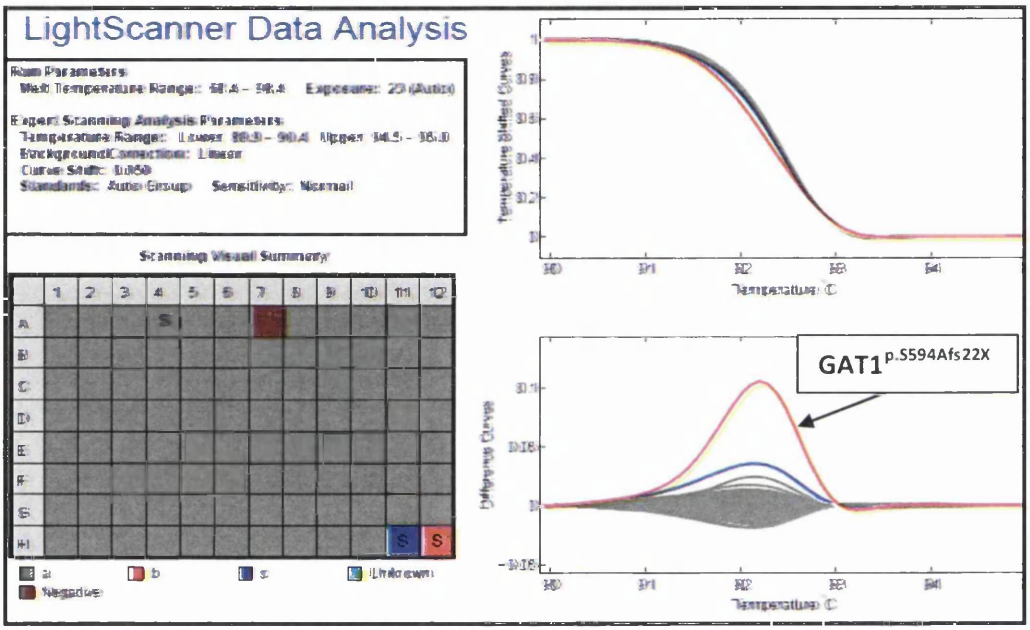

Figure 3.13 Profiles of lightscanner population study results for *GAT1*c.1780delA . The patient DNA was placed in the 96th well of the PCR plate as a positive control and the resultant melt profile has been highlighted in red. Control DNA samples failed to replicate the mutation melt profile and excluding GAT1$^{p.S594Afs22X}$ from the control population.

3.1.5 A Donor Splice site Variant: GAT1 IVS3+1 G>A

One novel heterozygous donor-splice site variant was identified in the beginning of intron 3 of the GAT1 gene (Figure 3.1 and 3.14). GAT1$^{IVS3+1G>A}$ was present in one patient sample from 693 (0.001) and was absent from 480 population controls and online databases such as dbSNP (Table 3.1 and Figure 3.15).

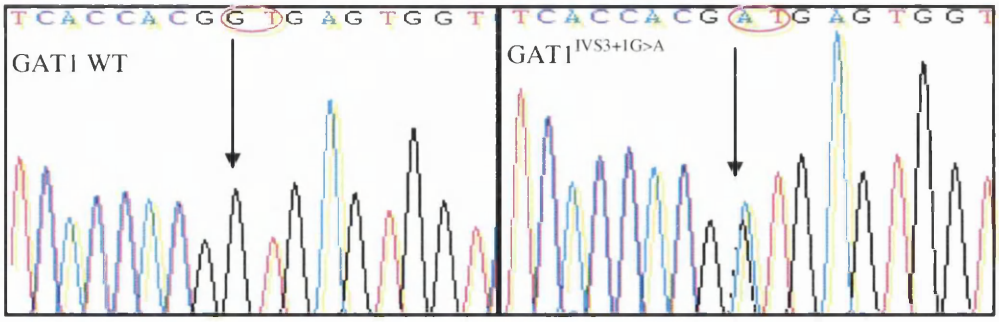

Figure 3.14 Sanger Sequencing profiles of GAT1 wild-type and GAT1$^{IVS3+1G>A}$. The arrows indicate the heterozygous G>A donor splice site (GT) in GAT1 exon 3. The exon GT boundary site has been circled in red.

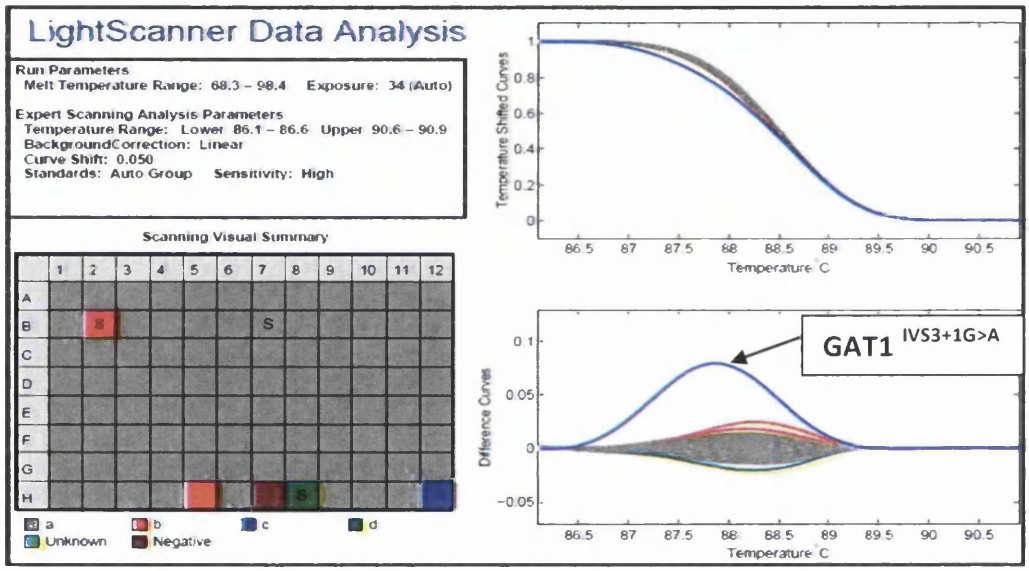

Figure 3.15 Lightscanner data analysis profiles of a population study for the GAT1$^{IVS3+1G>A}$ variant. The melt profiles of 95 control samples and the GAT1$^{IVS3+1G>A}$ case are shown. The trace clearly indicates that there is a difference in melt profiles between the variant and the control samples. This would suggest that the control samples do not have the variant sequence and the variant is, therefore, novel and not in the healthy population.

GAT1$^{IVS3+1G>A}$ is not in the coding region so predictive analysis and phylogenetic alignment is not possible. However, the substitution of the +1 donor splice site is found in hundreds of genetic disorders and is very likely to cause exon skipping or intron retention with cryptic stop codons (Figure 3.16).

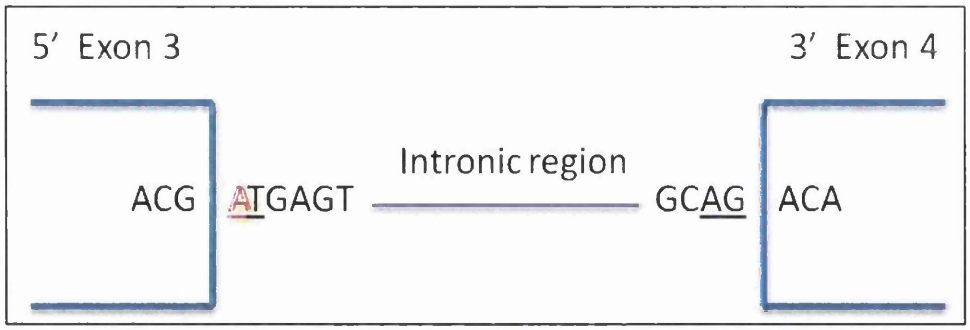

Figure 3.16 Splicing dynamics of GAT1 exon 3 and exon 4. The splice variant is shown in red resulting in elimination of the consensus 'GT' site. This could possibly result in exon skipping or intron retention.

3.2 Mutation analysis of GAT3

Twenty-nine variants were identified in GAT3 coding sequence and flanking intronic regions in 202 patient samples: ten intronic variants, 13 synonymous and six non-synonymous variants were identified in total. These variants are mapped onto their gene positions and their novelty status is indicated (Table 3.3). Six heterozygous missense variants (3 novel, 3 rare) were identified in the GAT3 gene that are most promising as pathogenic (Table 3.4).

3.2.1 Missense Variant GAT3 p.H142Y

The first variant identified in the *SLC6A11* (GAT3) sequence was a cytosine to thymine nucleotide substitution at position 426 (c.426C>T) of exon three. This causes the amino acid conversion of histidine to tyrosine at residue 142 of GAT3 (p.H142Y) (Figure 3.17 and figure 3.18). $GAT3^{p.H142Y}$ was identified in one patient sample from 697 cases, however, it was also identified in two of 480 control samples (Figure 3.19). $GAT3^{p.H142Y}$ is listed as a polymorphism in dbSNP in a control sample of n=2,276 but with an unknown frequency (Table 3.4).

Exon	Nucleotide change	Variation Classification	Amino acid change	Sample frequency (n=707)	Reference	MAF
3	c.426 C>T	Non-synonymous	p.H142Y	1	rs144440521	No
	c.498 C>T	Synonymous	p.L166L	6	rs61746357	0.0037
	c.480 C>G	Non-synonymous	p.N160K	1	rs374893074	No
5	c.645 T>C	Synonymous	p.S215S	29	rs2304725	0.3356
	c.750 A>T	Synonymous	p.T250T	1	Novel	
6	c.883 G>A	Non-synonymous	p.D295N	1	Novel	
	c.766 G>T	Non-synonymous	p.V256L	1	rs138109295	No
7	c.987 C>T	Synonymous	p.N329N	8	rs41308275	0.0083
	IVS6-11 C>CT	Intronic		1	Novel	
	IVS7+56 C>T	Intronic		1	Novel	
	c.912 G>A	Synonymous	p.T304T	1	rs371390454	No
8	IVS8+30 C>CT	Intronic		1	Novel	
	IVS8+42 G>GA	Intronic		1	Novel	
9	c.1170 T>C	Synonymous	p.P390P	33	rs2272395	No
	c.1143 G>A	Synonymous	p.A381A	11	rs2272394	0.0445
	IVS9+62 G>GA	Intronic		2	Novel	
10	IVS10+22 G>GA	Intronic		5	rs41295968	0.0023
	c.1307 G>A	Non-synonymous	p.R436Q	1	rs202136147	0.0005
	IVS10+16 C>T	Intronic		1	rs201196996	No
11	c.1461 C>T	Synonymous	p.I487I	3	rs78605794	0.0179
	c.1464 C>T	Synonymous	p.G488G	1	rs149598471	0.0009
	IVS11+32 G>GC	Intronic		1	Novel	
12	IVS11-7 C>T	Intronic		37	rs2272399	0.3352
	c.1572 C>T	Synonymous	p.C524C	9	rs2272400	0.0441
13	c.1737 A>G	Synonymous	p.T579T	31	rs2245532	0.3531
	c.1728 G>T	Synonymous	p.T576T	4	rs145331331	0.0028
	c.1692 C>T	Synonymous	p.C564C	6	rs138805066	No
	IVS13+28 G>GA	Intronic		3	rs149195347	0.0023
14	c.1791 C>T	Non-synonymous	p.R597W	1	rs142712079	0.0023

Table 3.3 The *GAT3 all*-variants table. Variant table of all variants identified via GAT3 screening of genetic generalised epilepsy patients. The frequency the variant occurs amongst samples in highlighted as well as the mean allelic frequency of any variants previously identified.

Gene	Exon	Variant	Nucleotide change	Genbank reference (Mean Allelic Frequency)	Case frequency (Allelic frequency)	Control population frequency (Allelic frequency)	Sift consequence (Score)	Grantham class (Score)	Polyphen result (Score)
GAT-3 (*SLC6A11*)	3	p.H142Y	c.426 C>T	rs144440521 (N.D)	1/697 (0.0007)	2/480 (0.002)	Tolerated (1)	C65 (83.33)	Benign (0)
	3	p.N160K	c.480 C>G	rs374893074 (0.0037)	1/697 (0.0007)	0/480 (0)	Tolerated (0.25)	C65 (93.88)	Possibly damaging (0.815)
	6	p.V256L	c.766 G>T	rs138109295 (N.D)	1/700 (0.0007)	0/480 (0)	Damaging (0.02)	C25 (30.92)	Benign (0.053)
	6	p.D295N	c.883 G>A	Novel	1/700 (0.0007)	0/480 (0)	Tolerated (0.12)	C15 (23.01)	Probably damaging (1)
	10	p.R436Q	c.1307 G>A	rs202136147 (0.0005)	1/688 (0.0007)	2/480 (0.002)	Damaging(0)	C35 (42.81)	Probably damaging (1)
	14	p.R597W	c.1791 C>T	rs142712079 (0.0023)	1/691 (0.0007)	0/480 (0)	Tolerated (0.08)	C65 (101.29)	Benign (0.031)

Table 3.4 GAT3 novel variants and rare SNPs indentified in epilepsy patient samples. SLC6A11 variants identified in 707 epilepsy patient samples are shown. In addition the corresponding variant frequencies in patient samples, previously identified SNP frequencies, control population frequencies and the predicted consequences (using three prediction tools) of variants on the protein have been included.(N.D =no data)

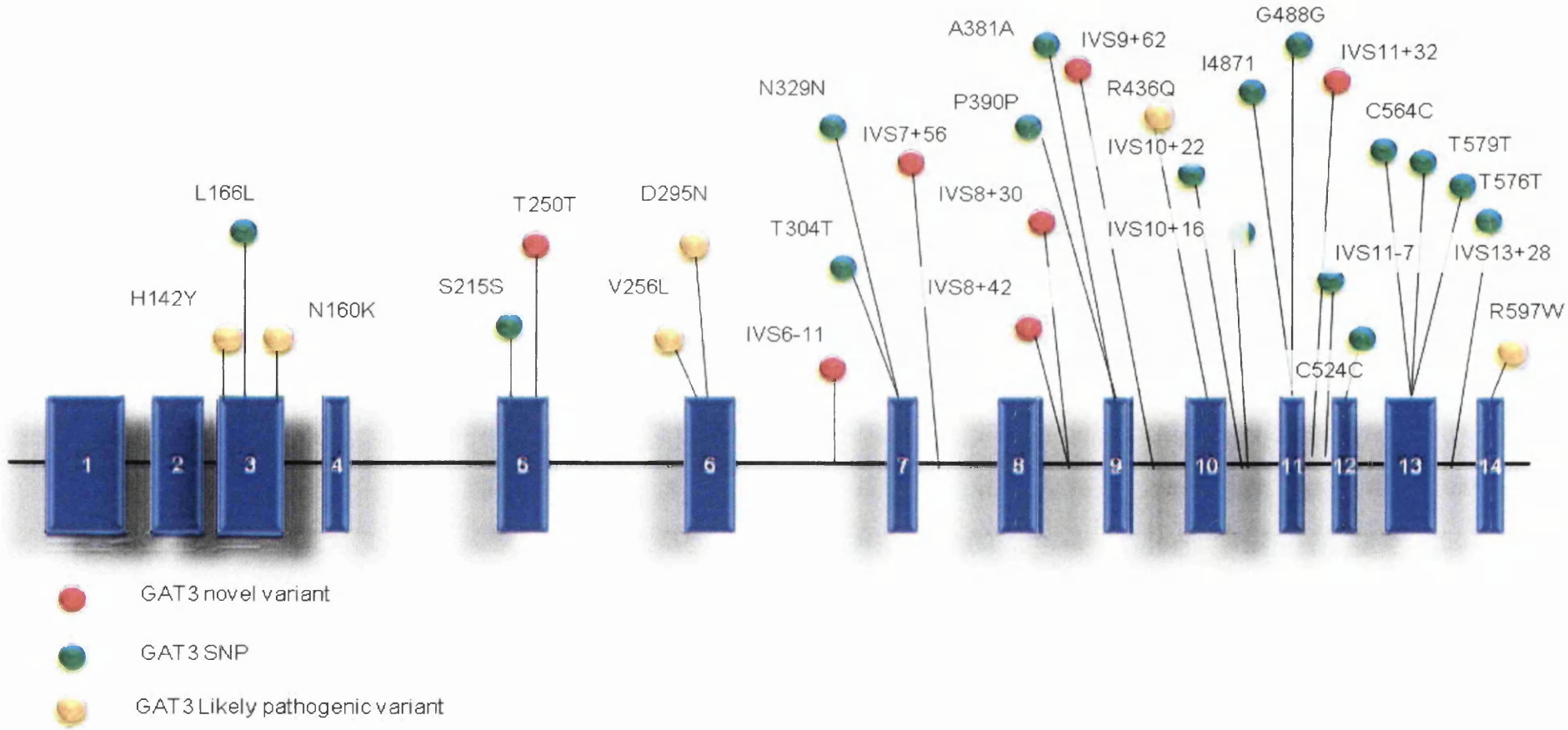

Figure 3.17 Genetic location of GAT3 variants identified in 707 epilepsy patient samples; Schematic exon diagram of the genomic structure and location of identified polymorphisms in the *GAT3* gene. Exons 1-14 are demonstrated as blue numbered boxes and the non-coding intronic regions by the connecting black lines. The novel mutations are symbolised by the red circles and were identified in the corresponding exons as indicated; SNPs are shown as green circles.

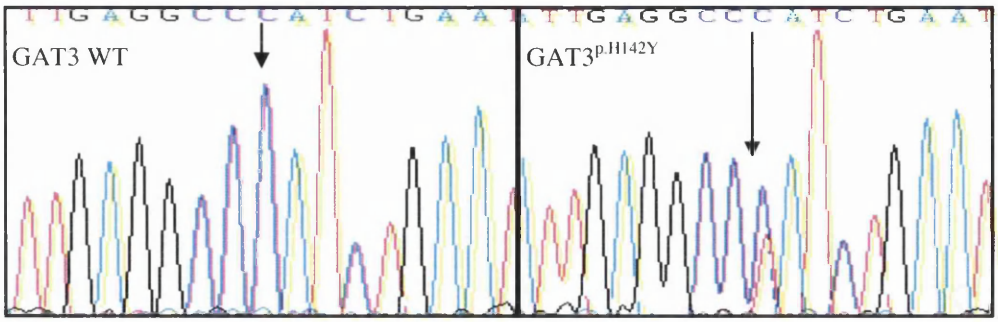

Figure 3.18 Sequence chromatogram of the GAT3$^{p.H142Y}$ identified in epilepsy patient samples and the corresponding wild-type sequence. The heterozygous variant is denoted in the right hand column of this figure by a double peak and shown by arrows. The corresponding wild-type sequence is shown in the left hand column and the substituted nucleotide indicated by an arrow.

GAT3$^{p.H142Y}$ was assigned to Grantham class C65, suggesting pathogenic consequences to the protein by means of composition and polarity. Benign effects were predicted from conservational analysis, and the structural changes of the variant are believed to be tolerated (SIFT & Polyphen) (Table 3.4). Multiple species alignment analysis of GAT3$^{p.H142Y}$ shows the variant and its surrounding amino acids are highly conserved residues (Figure 3.20).

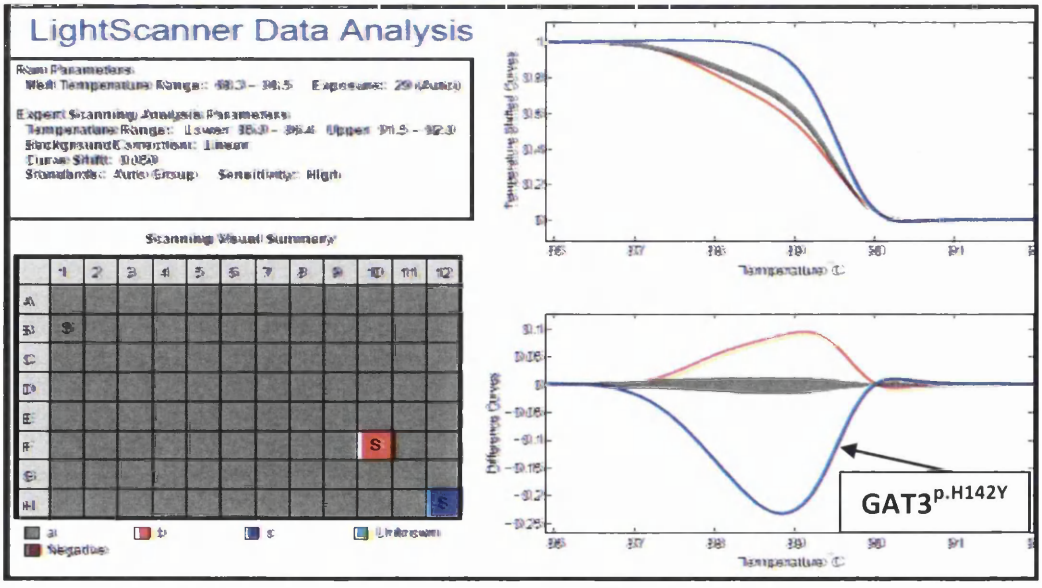

Figure 3.19 Population study results of GAT3$^{p.H142Y}$. The above lightscanner profile shows the melting temperature range for GAT3 exon 3. The patient sample containing variant GAT3$^{p.H142Y}$ melts at a different rate to the control samples, suggesting that the variant is not present in the control population.

	GAT3$^{p.H142Y}$
GAT3 variant	QVIEAYLNVYY
H.sapien	QVIEAHLNVYY
P.troglodytes	QVIEAHLNVYY
M.mulatta	QVIEAHLNVYY
B.taurus	QVIEAHLNVYY
C.lupus	QVIEAHLNVYY
G.gallus	QVIEAHLNVYY
R.norvegicus	QVIEAHLNVYY
M.musculus	QVIEAHLNVYY

Figure 3.20 Multiple phylogenetic alignments of GAT3$^{p.H142Y}$. GAT3$^{p.H142Y}$ was aligned against the wild-type GAT3 sequence and its putative homologs. The mutated amino acid was highlighted in red and its corresponding residue highlighted in green for different species and wild-type to indicate the level of evolutionary conservation. It can be noted that p.H142Y occurs in a highly conserved residue of the protein.

In summary, GAT3$^{p.H142Y}$ is a rare SNP as observed from dbSNP and control population studies, however, Grantham class results and phylogenetic alignments suggest functional analysis is required to assess any pathogenic effects.

3.2.2 Missense Variant GAT3 p.N160K

GAT3$^{p.N160K}$, is an amino acid substitution from asparagine to lysine at residue 160 due to a nucleotide change in exon three at nucleotide position 480 reflecting a cytosine to guanine change (c.480C>G) (Figure 3.17 and figure 3.21). This variant has been identified on online databases such as dbSNP with a mean allelic frequency of 0.0037, however, the variant which was identified in one patient sample out of 697, was not found in a control study of 480 unaffected participants (Figure 3.22).

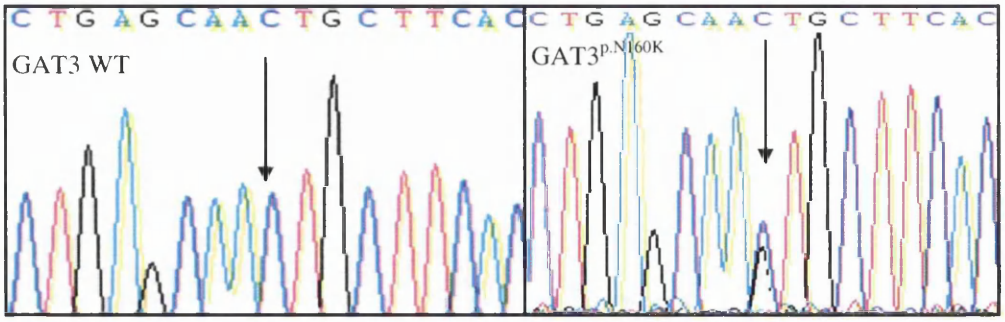

Figure 3.21 GAT3 wild-type and GAT3$^{p.N160K}$ sequence chromatogram. The nucleotide change from cytosine to guanine at position 480 of the coding sequence creating the variant GAT3$^{p.N160k}$, is indicated by arrows. The heterozygous variant causes a double peak on the sequencing trace as indicated.

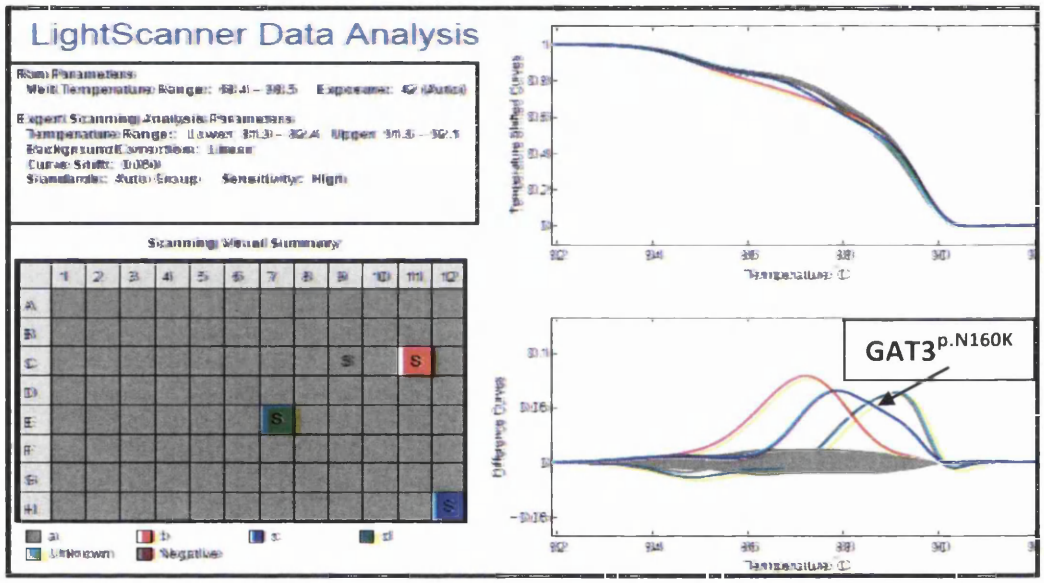

Figure 3.22 Lightscanner data analysis of GAT3$^{p.N160K}$ population study. The patient sample which possesses GAT3$^{p.N160K}$ (Shown in blue), melts at a different rate to the control population. However, as there are two samples that also have melt profiles deviating from the average (shown in red and green). They were also sequenced to ensure a lack of p.N160K. The sequencing results indicated that GAT3$^{p.N160K}$ was not present in these samples.

According to SIFT conservation analysis, GAT3$^{p.N160K}$ is tolerated by the protein, however, the structural, composition and polarity changes caused by the amino acid change is predicted to be damaging and possibly damaging by Grantham and PolyPhen respectively (Table 3.4). Multiple species alignment analysis showed a highly conserved pattern, supporting Grantham and Polyphen results.

Collectively, GAT3$^{p.N160K}$ is a damaging and very rare SNP that is highly conserved in phylogenetic analysis. The decision was taken on this evidence base to proceed to functional analysis and preparation of mutation constructs (Chapter Five).

	GAT3$^{p.N160K}$
GAT3 variant	IFYLSKCFTTE
H.sapien	IFYLSNCFTTE
P.troglodytes	IFYLSNCFTTE
M.mulatta	IFYLSNCFTTE
B.taurus	IFYLSNCFATE
C.lupus	IFYLSNCFTTE
G.gallus	IFYLFNCFTTE
R.norvegicus	IFYLSNCFTTE
M.musculus	IFYLSNCFTTE

Figure 3.23 Multiple phylogenetic alignments of GAT3$^{p.N160K}$. GAT3 variants were aligned against the respective wild-type sequence and their putative homologs. The affected residue is highlighted in green for all species and the variant residue is in red. It can be noted that GAT3$^{p.N160K}$ occurs in a highly conserved residue throughout various species.

3.2.3 Missense Variant GAT3 p.V256L

GAT3$^{p.V256L}$ is a heterozygous guanine to thymine nucleotide change in exon 6 of GAT3, at position 766 of the coding sequence (c.766C>T) (Figure 3.17). It causes an amino acid change from valine to leucine at residue 256 (p.V256L). (Figure 3.24). GAT3$^{p.V256L}$ was identified in one patient sample out of the 700 cases, was absent from the control population of 480 and was present with an unknown mean allelic frequency on dbSNP (Figure 3.25).

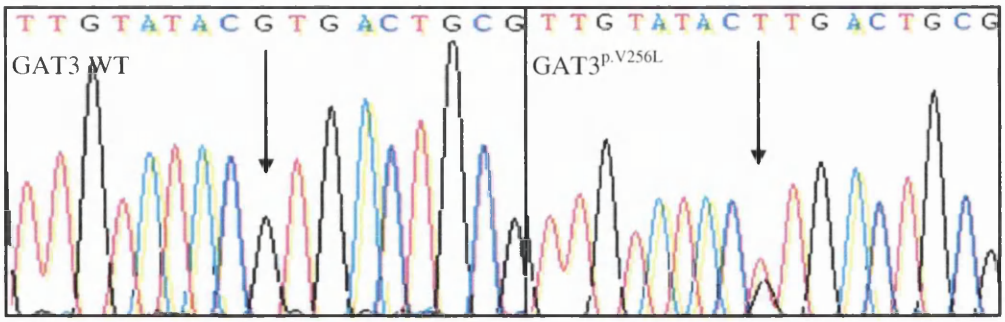

Figure 3.24 Sequence chromatogram of GAT3$^{p.V256L}$. The disparity in sequencing traces between wild-type and variant GAT3$^{p.V256L}$ is clearly indicated by arrows. The peak representing guanine at position 766 become suppressed in the variant trace and appears along with an additional thymine trace representing heterozygosity.

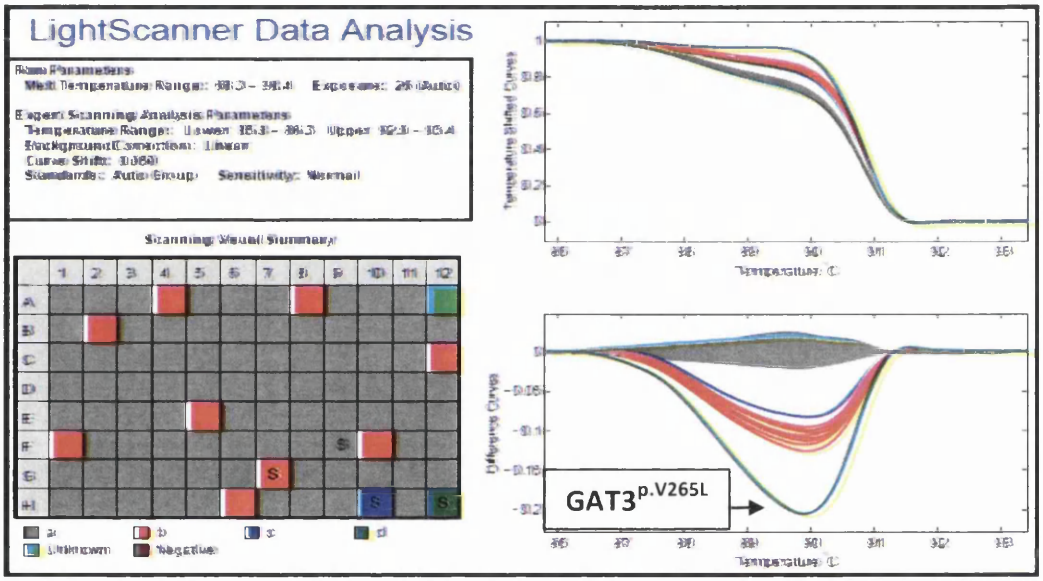

Figure 3.25 Lightscanner population study of GAT3$^{p.V256L}$. The presence or absence of GAT3 variants in a control population was assessed using Lightscanner technology. The lightscanner results show variation in melt profiles on DNA samples and can therefore be indicative of changes in DNA sequence. It can be seen above that GAT3$^{p.V256L}$ has a different melt profile to the control population, which, suggests that none of the control samples contain the variant sequence.

GAT3$^{p.V256L}$ was predicted to have a benign effect on the protein by the Polyphen software, but paradoxically was predicted possibly damaging and damaging by SIFT and Grantham respectfully. Alignment analysis demonstrated that the amino acid change is highly conserved and is placed within a conserved region reflecting an important functional preservation through the evolutionary process (Figure 3.26).

Considering all the data, this conserved novel SNP is not confirmed on population databases and is predicted to be damaging giving us reason to investigate the pathological consequences.

	GAT3$^{p.V256L}$
GAT3 variant	GKVVY**L**TATFP
H.sapien	GKVVY**V**TATFP
P.troglodytes	GKVVY**V**TATFP
M.mulatta	GKVVY**V**TATFP
B.taurus	GKVVY**V**TATFP
C.lupus	GKVVY**V**TATFP
G.gallus	GKVVY**V**TATFP
R.norvegicus	GKVVY**V**TATFP
M.musculus	GKVVY**V**TATFP

Figure 3.26 Multiple phylogenetic alignments of the GAT3$^{p.V256L}$. The variant sequence was aligned against the GAT3 wild-type sequence and their putative homologs. The affected residue is highlighted in green for all species and the variant residue is in red. It can be noted that GAT3$^{p.V256L}$ occurs in a highly conserved but also in a highly conserved region of the protein.

3.2.4 Missense Variant GAT3 p.D295N

GAT3$^{p.D295N}$ involves a heterozygous nucleotide change in GAT3 exon six from guanine to adenine at position 883 of the coding sequence (c.883G>A), which creates an amino acid change from aspartic acid to asparagine at position 295 of the polypedtide (p.D295N) (Figure 3.17 and figure 3.27). GAT3$^{p.D295N}$ was identified in one patient sample out of 700 cases and was absent from both the 480 unaffected control population and online databases such as dbSNP (Figure 3.28).

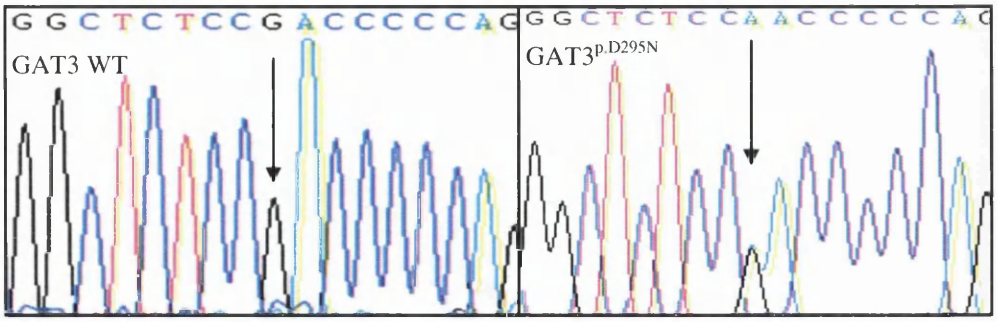

Figure 3.27 GAT3 wild-type sequencing chromatogram compared to GAT3$^{p.D295N}$. Differences in sequencing traces can be seen between wild-type and variant sequences at the variant position (see arrows). Although almost identical in size and shape it is perceptible that an adenine peak occurs at the same position as the indicated guanine, suggesting a heterozygous variant.

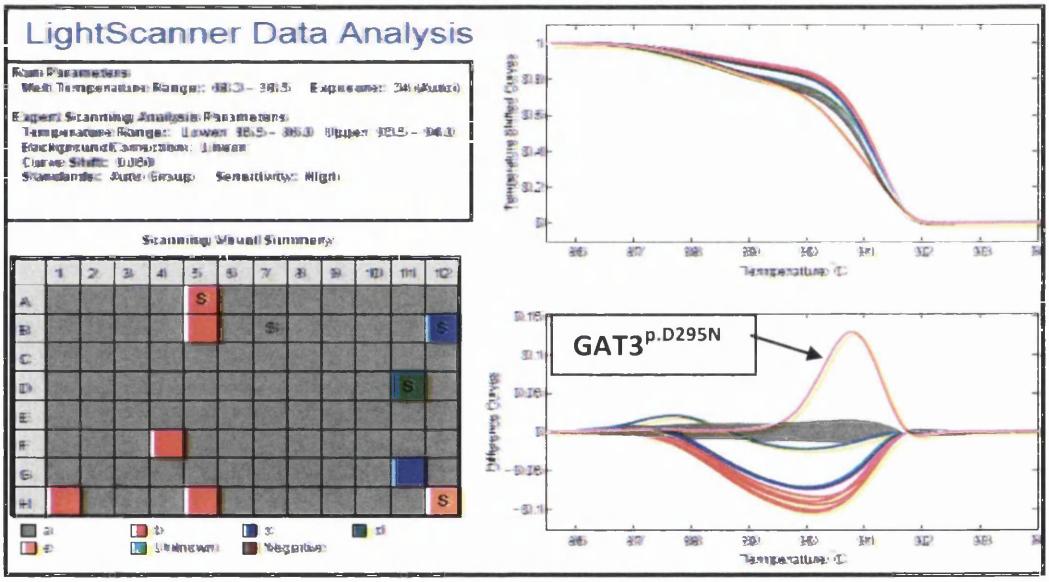

Figure 3.28 Lightscanner data analysis of GAT3$^{p.D295N}$ population study. The lightscanner profiles show that the variant sample (shown in orange) melts at a different rate to the 95 healthy control samples. GAT3$^{p.D295N}$ is not present in the healthy population.

GAT3$^{p.D295N}$ was predicted to have tolerated consequences by SIFT and Grantham, however, PolyPhen predicted damaging structural changes to the protein. Multiple species alignment analysis showed that GAT3$^{p.D295N}$ occurred in a highly conserved residue and region of the protein (Figure 3.29).

In summary, enough evidence was gathered from population analysis and predictive tools to justify further structure / function analysis of GAT3$^{p.D295N}$.

	GAT3$^{p.D295N}$
GAT3 variant	LSRLS**N**PQVWV
H.sapien	LSRLS**D**PQVWV
P.troglodytes	LSRLS**D**PQVWV
M.mulatta	LSRLS**D**PQVWV
B.taurus	LSRLS**D**PQVWV
C.lupus	LSRLS**D**PQVWV
G.gallus	LSRLS**D**PQVWV
R.norvegicus	LSRLS**D**PQVWV
M.musculus	LSRLS**D**PQVWV

Figure 3.29 Phylogenetic alignments of GAT3$^{p.D295N}$. GAT3$^{p.D295N}$ protein sequence was aligned against GAT3 wild-type sequence and their putative homologs. The affected residue is highlighted in green for all species and the variant residue is in red. GAT3$^{p.D295N}$ as demonstrated occurs in a highly conserved residue and is also surrounded by conserved residues suggesting a highly conserved region of the protein.

3.2.5 Missense Variant GAT3 p.R436Q

The missense variant p.R436Q is an amino acid change from arginine to glutamine at residue 436 as a result of heterozygous c.1307G>A variant in GAT3 exon ten (Figure 3.17 and figure 3.30). The variant was recognised in one patient sample of 688 cases but also identified in two of the 480 control samples (Figure 3.31) and on online databases with a low mean allelic frequency of 0.0005.

SIFT analysis predicted GAT3$^{p.R436Q}$ as damaging which was supported by the PolyPhen and Grantham results which also gave a probably damaging outcome. Phylogenetic alignment analysis also revealed a highly conserved target residue/adjacent regions, suggesting consequences on the protein (Figure 3.32).

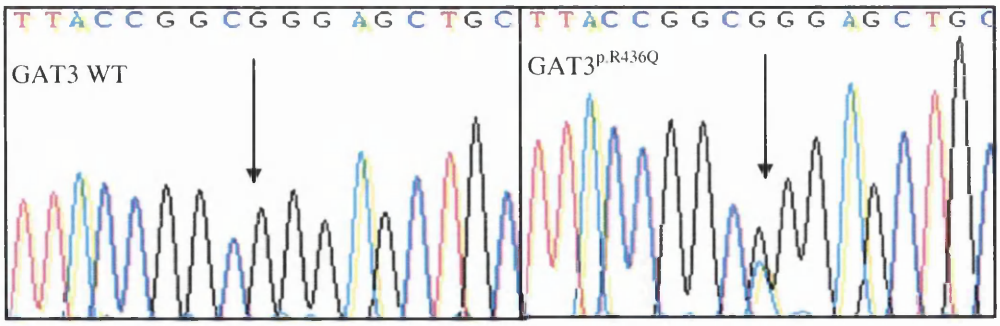

Figure 3.30 GAT3 wild-type compared to GAT3$^{p.R436Q}$ chromatogram. A double peak representing a heterozygous variant is noted when comparing GAT3 wild-type and GAT3$^{p.R436Q}$ sequencing traces. This double peak suggests a nucleotide change from guanine to adenine resulting in an amino acid change from arginine to glutamine.

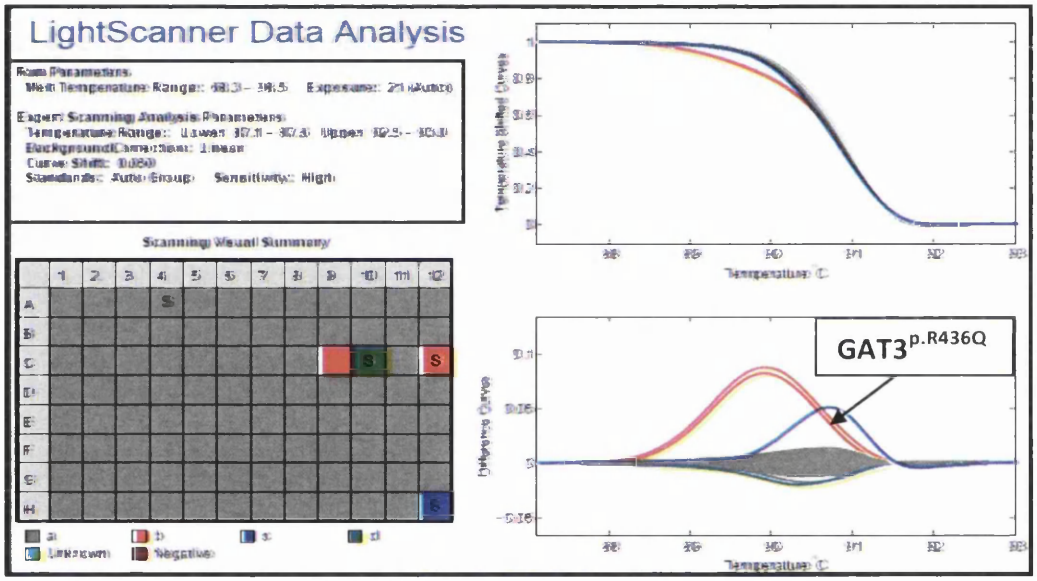

Figure 3.31 Population study results for GAT3$^{p.R436Q}$ via Lightscanner analysis. A Lightscanner population study was carried out for GAT3$^{p.R436Q}$ to determine whether the variant was present in the healthy population. As the patient sample containing the variant (blue trace) melts at a different rate to the average control samples we can determine that the variant, in this case, is not present in the population. The two red traces shown were sequenced and they did not contain the variant, instead they showed another SNP. However, there are 5 population studies (n=480) in total and p.R436Q was identified in 2 control samples.

	GAT3$^{p.R436Q}$
GAT3 variant	RRGYRQELLIL
H.sapien	RRGYRRELLIL
P.troglodytes	RRGYRRELLIL
M.mulatta	RRGYRRELLIL
B.taurus	RRGYRRELLIL
C.lupus	RRGYRRELLIL
G.gallus	RRGYRRELLIL
R.norvegicus	RRGYRRELLIL
M.musculus	RRGYRRELLIL

Figure 3.32 Phylogenetic alignments of GAT3$^{p.R436Q}$. GAT3$^{p.R436Q}$ protein sequence was aligned against GAT3 wild-type protein sequence as well as their putative homologs. The residue in question is highlighted in green for all species and the variant residue in red. GAT3$^{p.R436Q}$ occurs in a highly conserved residue as well as highly conserved region of the protein.

Consequently, GAT3$^{p.R436Q}$ is a rare-variant SNP that is highly conserved, and predicted to have damaging consequences; thereby, justifying further analysis.

3.2.6 Missense Variant GAT3 p.R597W

The variant p.R597W was an amino acid change identified in exon 14 of *SLC6A11* (Figure 3.17). GAT3$^{p.R597W}$ is a heterozygous c.1791C>T nucleotide change which results in an arginine to tryptophan amino acid substitution at position p.597 of the polypeptide. (Figure 3.33). The variant was identified in one case out of 691 patient samples and was also identified in dbSNP with a rare allelic frequency of 0.0023 out of 2,276 samples. Conflictingly, none of the 480 control population samples have the variant (Figure 3.34).

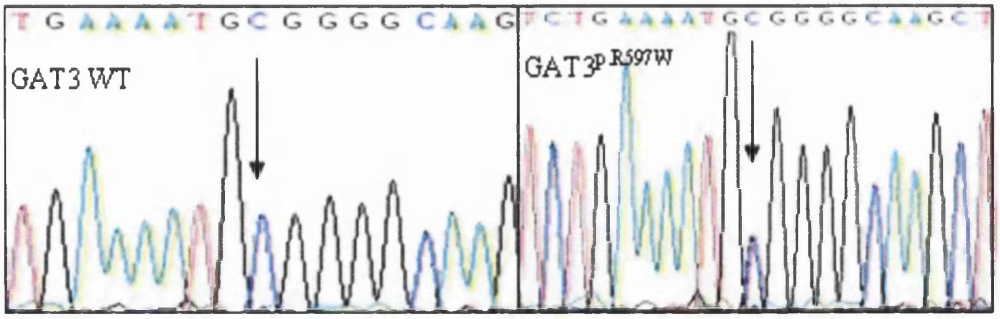

Figure 3.33 Sequence chromatogram of the GAT3$^{p.R597W}$ and its corresponding wild-type. GAT3$^{p.R597W}$ sequencing trace was compared to wild-type and a variant was identified at amino acid position 597 (arrows). The variant is a nucleotide change from cytosine to thymine and is visible by double peaks as indicated.

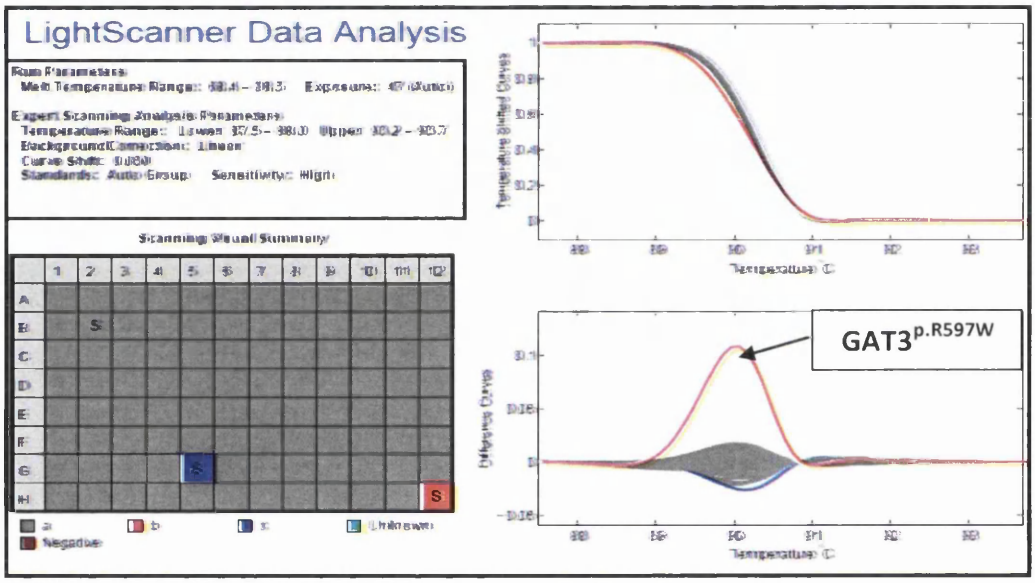

Figure 3.34 GAT3 variant p.R597W, population study result. It is clear from the lightscanner traces above that the patient sample containing GAT3$^{p.R597W}$ melts at a different rate to the 95 control samples. This would indicate that they do not contain the variant sequence that causes such deviation from the average melt curve.

Predictive conservation analysis by SIFT and PolyPhen suggest that GAT3$^{p.R597W}$ has benign effects on the protein, however, a Grantham class of C65 suggests that there would be pathogenic consequences (Table 3.4). Phylogenetic analysis of multiple species reveals a highly conserved amino acid and surrounding sequence suggesting that GAT3$^{p.R597W}$ is likely to have pathogenic consequences on protein function (Figure 3.35).

	GAT3$^{p.R597W}$
GAT3 variant	TDLKMWGKLGV
H.sapien	TDLKMRGKLGV
P.troglodytes	TDLKMRGKLGV
M.mulatta	TDLKMRGKLGV
B.taurus	ADLKMRGMLGA
C.lupus	ADLKMRGKLGA
G.gallus	SDLKMRGKLGG
R.norvegicus	ADLKMRGKLGA
M.musculus	ADLKMRGKLGA

Figure 3.35 Multiple phylogenetic alignments of GAT3$^{p.R597W}$. The protein sequence of GAT3$^{p.R597W}$ was aligned against GAT3 wild-type protein sequence as well as its putative homologs. The residue in question is highlighted in green for all species and the variant residue in red. It appears that GAT3$^{p.R597W}$ occurs in a decidedly conserved residue.

From the convergent evidence it was decided to take GAT3$^{p.R597W}$ forward to further structure / function studies as a result of *in silico* prediction, population frequency and phylogenetic alignments.

3.3 Summary of mutation analysis of GAT1 and GAT3 genes

The genetic screening of GAT1 and GAT3 in GGE patients saw the heterozygous identification of one novel missense variant, one novel splice variant and a novel deletion variant which had the potential to be directly pathogenic. A further eight rare SNPs were also identified in these samples with unknown general population frequencies or frequencies of less than 1% but affecting conserved regions of the protein and some *in silico* evidence for damaging effects. All 11 gene variants identified were heterozygous variants that corresponded to epilepsy phenotypes with a component of absence seizures.

Chapter five will contain further analysis of the 11 variants including protein context and topology, 3D structural modelling analysis and the expression validation of gene specific mutation constructs that were created for transfection and causality research. Chapter 6 will contain details of the scheduled purpose of the constructs to determine

the pathological consequences of these variants. The next chapter (4) will focus on the results from the screening of the GAD65 and GAD67 proteins that constitute a bio-synthetic component of the GABAergic system.

Chapter Four

Mutation analysis of GAD65 and GAD67 in Genetic Generalised Epilepsy

Prior to this study, no mutations had been identified in the GABAergic genes *GAD2* and *GAD1* (known from this point as proteins GAD65 and GAD67 respectively), in relation to epilepsy. The genes encode for biosynthetic GABA enzymes maintaining levels of GABA in pre-synaptic terminals and were selected for candidate gene analysis in 485 clinically-confirmed genetic generalised epilepsy (GGE; Melbourne) patient samples. Results obtained from this preliminary data led to the recruitment and analysis of an additional 187 absence seizure (CAE; UCL) and 35 juvenile myoclonic epilepsy patient samples (JME; WERN). Control population studies were carried out on 480 commercially-available samples (Sigma) to assess the population frequencies of gene variants in addition to accessing bioinformatics sources.

This chapter outlines the identification of genetic variants identified in the GABAergic enzymes GAD65 and GAD67. Synonymous, novel non-synonymous missense, and intragenic variants were identified in the GABAergic enzymes GAD65 and GAD67. As described for the GABA transporters in chapter three, this analysis will involve the assessment of sequencing data, evaluation of unaffected control population data and any previously identified online data, the investigation of the predictive consequences of the variants including multiple species alignments, and the appraisal of the variant positioning within the protein at a 2D level.

4.1 Mutation analysis of GAD65

Twenty-six variants were identified in the coding region and flanking intronic regions of GAD65 in 149 patient samples (Table 4.1), which consisted of 8 non-synonymous, 6 synonymous, and 12 intronic variants. These variants are mapped onto genomic positions and their novelty status indicated (Figure 4.1). From these gene variations, six non-synonymous gene variants were selected as most likely pathogenic variants and targeted for further analysis (Table 4.2).

Exon	Nucleotide change	Type of Mutation	Amino acid change	Sample Frequency (n=707)	Reference	MAF
1	IVS1+8 G>A	Intronic		19	rs2839671	0.253
	IVS1+11 G>A	Intronic		2	Novel	
2	IVS2+11 A>T	Intronic		1	Novel	
	c.134 G>T	Non-synonymous	p.C45F	1	rs142982041	No
	IVS2+17 C>T	Intronic		1	Novel	
3	IVS3+79 G>A	Intronic		13	rs41304609	0.043
	IVS3+110 A>G	Intronic		10	rs8190597	0.199
	IVS2-19 G>T	Intronic		1	rs112021218	0.028
4	c.304 G>A	Non-synonymous	p.D102N	1	rs139888003	No
	c.358 C>A	Non-synonymous	p.P153Q	16	rs2839672	0.004
	IVS4+14 G>A	Intronic		3	Novel	
6	c.695 G>A	Non-synonymous	p.G232E	6	rs2839673	0.006
	c.705 C>T	Synonymous	p.G235G	4	rs55789936	0.002
	c.612 G>A	Non-synonymous	p.M204I	2	rs61735922	0.001
7	c.807 G>A	Non-synonymous	p.A269T	6	rs52834041	0.001
	IVS7+50 G>A	Intronic		1	Novel	
	c.789 G>A	Synonymous	p.K263K	1	Novel	
	IVS7+43 A>G	Intronic		1	rs202139948	No
8	IVS8+8 C>T	Intronic		18	rs2839677	0.057
9	IVS8-20 A>G	Intronic		6	rs8190708	0.003
10	c.1017 C>T	Synonymous	p.T339T	15	rs1805397	0.010
	c.978 G>C	Synonymous	p.G326G	17	rs2839678	No
11	c.1107 G>A	Synonymous	p.G369G	1	rs8190729	0.006
12	c.1218 T>G	Synonymous	p.A406A	1	Novel	
15	c.1580 C>T	Non-synonymous	p.S527L	1	rs149742560	0.001
16	c.1725 T>C	Non-synonymous	p.I575T	1	rs145419731	No

Table 4.1 The GAD65 *all*-variants table. Variant table of all variants identified via GAD65 in GGE patients via genetic screening. The gene variant frequency and the mean allelic frequency are presented.

Gene	Exon	Variant	Nucleotide change	Genbank reference (Mean Allelic Frequency)	Case frequency (Allelic Frequency)	Control population frequency (Allelic Frequency)	SIFT consequence (Score)	Grantham class (Score)	Polyphen result (Score)
GAD65 (GAD2)	2	p.C45F	c.134G>T	rs142982041 (0)	1/674 (0.0007)	0/480 (0)	Damaging (0)	C65 (204.39)	Probably damaging (0.999)
	4	p.D102N	c.304G>A	rs139888003 (0)	1/664 (0.0008)	0/480 (0)	Tolerated (1)	C15 (23.01)	Benign (0)
	4	p.P153Q	c.358C>A	rs2839672 (0.008)	16/664 (0.012)	2/480 (0.002)	Tolerated (0.11)	C65 (75.14)	Probably damaging (0.991)
	6	p.G232E	c.695G>A	rs2839673 (0.014)	6/683 (0.0044)	1/480 (0.001)	Tolerated (0.17)	C65 (97.85)	Benign (0.046)
	15	p.S527L	c.1580C>T	rs149742560 (0.003)	1/681 (0.0007)	1/480 (0.001)	Tolerated (0.31)	C65 (144.08)	Benign (0.004)
	16	p.I575T	c.1725T>C	rs145419731 (0.001)	1/697 (0.0007)	0/480 (0)	Damaging (0.01)	C65 (89.28)	Possibly damaging (0.763)

Table 4.2 GAD65 missense variants identified in epilepsy patient samples. The position and nucleotide/amino acid changes of all novel/rare variants identified in our patient samples for *GAD2* were shown. The frequency of the variants in the patient samples as well as previously identified SNPs and control populations were shown. Predicted consequences of the variants were predicted via SIFT, PolyPhen and Grantham software.

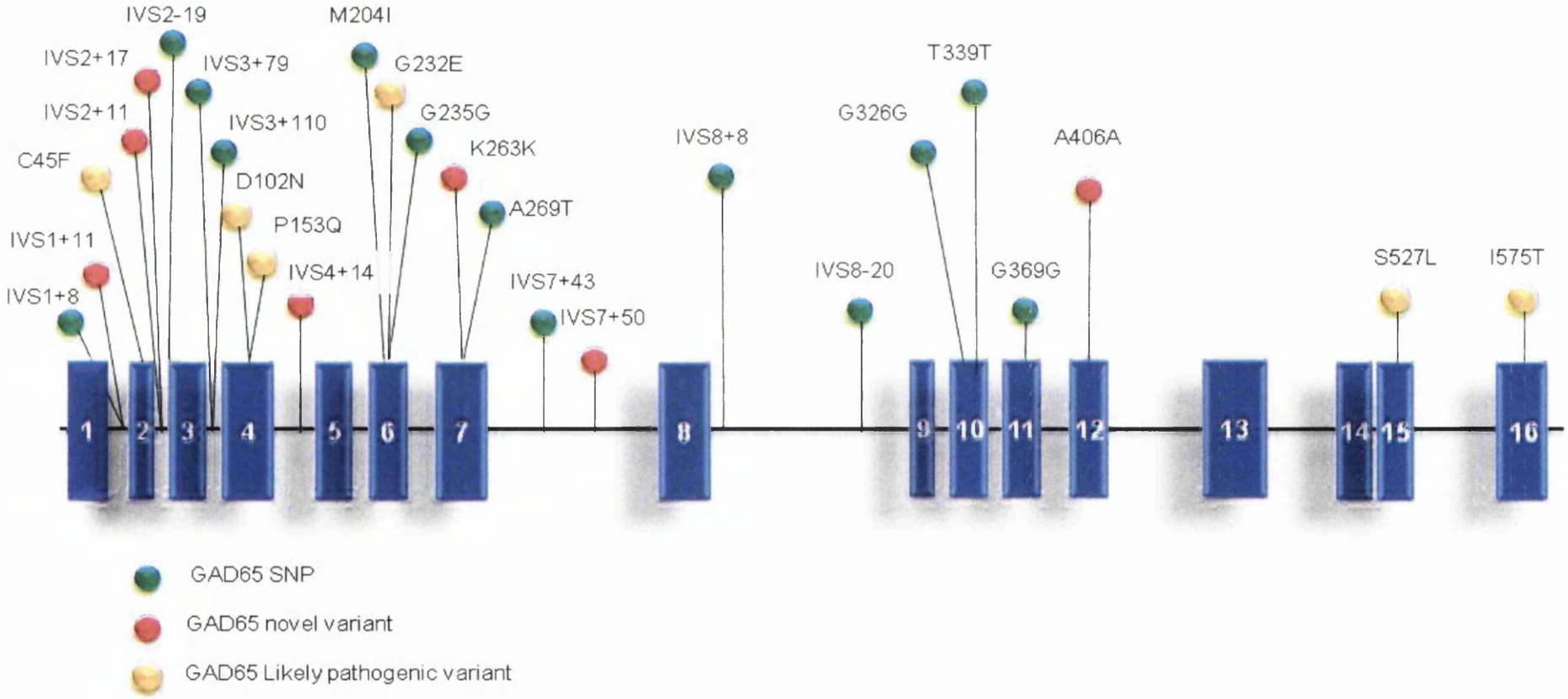

Figure 4.1 *GAD65* variants identified in 707 epilepsy patient samples; Schematic exon diagram demonstrating the genomic structure and location of identified novel variants and rare polymorphisms in the GAD65 gene. Exons 1-16 are demonstrated as blue numbered boxes and the non-coding intronic regions by the connecting black lines. The very rare polymorphisms (occurring in less than 1% of the population) are shown as green rectangles.

The six heterozygous GAD65 variants identified as potentially pathogenic were: 1) p.C45F (c.134G>T), 2) p.D102N (c.304G>A), 3) p.P153Q (c.358C>A), 4) p.G232E (c.695G>A), 5) p.S527L (c.1580C>T) and 6) p.I575T (c.1725T>C). The damaging status case for each variant is presented in table 4.2 taking into account bioinformatics databases and control frequency datasets; structure/function data is presented in Chapter Five.

Population study and predictive analysis was also carried out for the non-synonymous variants p.M204I and A269T. Due to the high population study frequencies of the variants and limited causal effects calculated by predictive tools, these variants were not considered any further in this thesis.

4.1.1 Missense Variant p.C45F

The first variant identified in *GAD2* was GAD65$^{p.C45F}$. A guanine to thymine nucleotide change at position 134 of the coding sequence resulted in a cysteine to phenylalanine amino acid substitution at position 45 of the polypeptide (Figure 4.2). This variant was identified in exon two of one patient sample of the 674 cases successfully screened. It was not found in the 485 unaffected control samples and was registered online with a frequency of zero out of 2176 individuals screened according to SNP databases (Figure 4.1 and Figure 4.3).

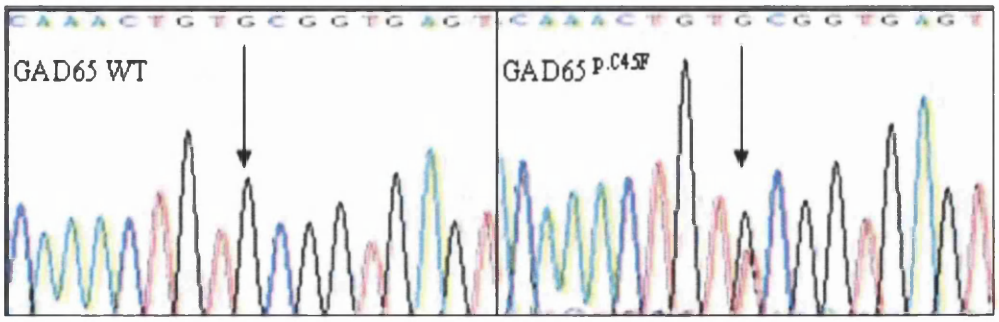

Figure 4.2 Sequence chromatogram of the GAD65 variant GAD65$^{p.C45F}$ and the corresponding wild type sequence. GAD65$^{p.C45F}$ is a heterozygous variant, as illustrated from the double peaks on the right hand column sequencing trace. The variant was demonstrated by means of an arrow, as were the corresponding wild-type sequences in the left hand column of the figure.

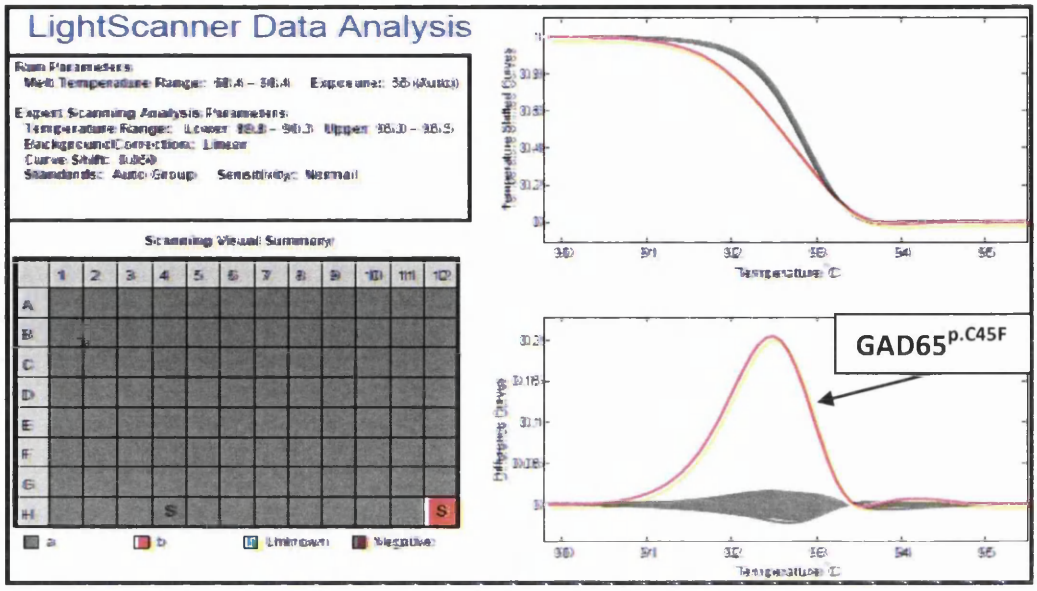

Figure 4.3 GAD65$^{p.C45F}$ lightscanner control population study results; The sample harbouring GAD65$^{p.C45F}$ was placed in well H12 and is shown in red on the trace. GAD65$^{p.C45F}$ does not have the same melt profile as any of the control samples, suggesting that it is not present in the healthy population as a common non-pathogenic SNP.

Predictive tools suggested that GAD65$^{p.C45F}$ will have damaging effects on the protein. Species alignment analysis also suggested that the amino acid change would be damaging to the protein as the variant affects a conserved residue in a conserved region of the protein (Figure 4.4).

	GAD65$^{p.C45F}$
GAD65 variant	IGNKL**F**ALLYG
H.sapien	IGNKL**C**ALLYG
P.troglodytes	IGNKL**C**ALLYG
M.mulatta	IGNKL**C**ALLYG
B.taurus	IGNKL**C**ALLYG
C.lupus	IGNKL**C**ALLYG
G.gallus	FLSAL**R**VVAQG
R.norvegicus	IGNKL**C**ALLYG
M.musculus	IGNKL**C**ALLYG

Figure 4.4 Phylogenetic alignment of the GAD65 missense variant, p.C45F. The variant was aligned against the GAD65 wild-type and the corresponding homologs in various phylogenetic species. The mutated amino acid was highlighted in red and the related wild-type and phylogenetic amino acids were highlighted in green.

Predictive analysis, population study results and species alignments all give collective evidence to believe that GAD65$^{p.C45F}$ will have pathogenic effects on the protein. This supports the triage of this variant for *in silico* and functional analysis.

4.1.2 Missense Variant p.D102N

Two variants were identified in exon 4 of *GAD2*, the first being p.D102N (Figure 4.1). GAD65$^{p.D102N}$, is a guanine to adenine nucleotide change at position 304 consequentially leading to an amino acid change from aspartic acid to asparagine at residue 102 of the polypeptide (Figure 4.5). The variant was identified in one patient sample of 664 screened and was not identified in the 480 unaffected control population and was registered on online databases with a frequency of zero out of 2275 samples (Figure 4.6).

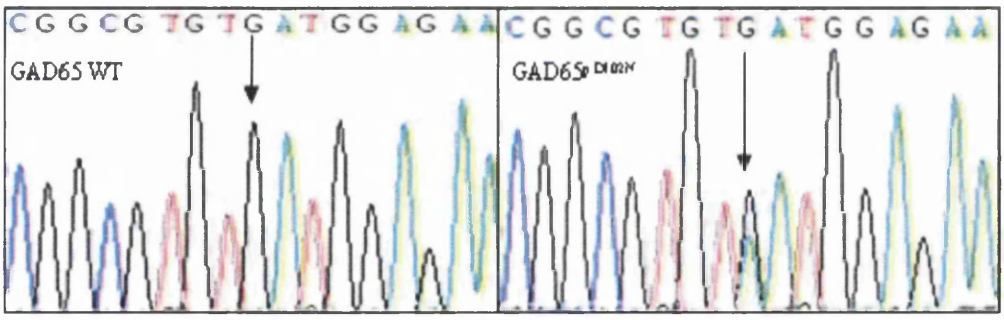

Figure 4.5 Sequence chromatogram of GAD65$^{p.D102N}$ and the corresponding wild type sequence. The heterozygosity of GAD65$^{p.D102N}$ was identified by the double peak as highlighted by an arrow in the right hand column. The sequencing trace shows the nucleotide change from guanine to adenine at position 304.

The predicted consequences of SIFT and PolyPhen suggest that the amino acid change would not affect normal protein function nor would it have a damaging effect on the structure of the protein. The Grantham score predicted a possibly pathogenic score, suggesting damaging changes in polarity and composition. Species alignments show that the variant occurred in a very conserved residue and region of the protein (Figure 4.7).

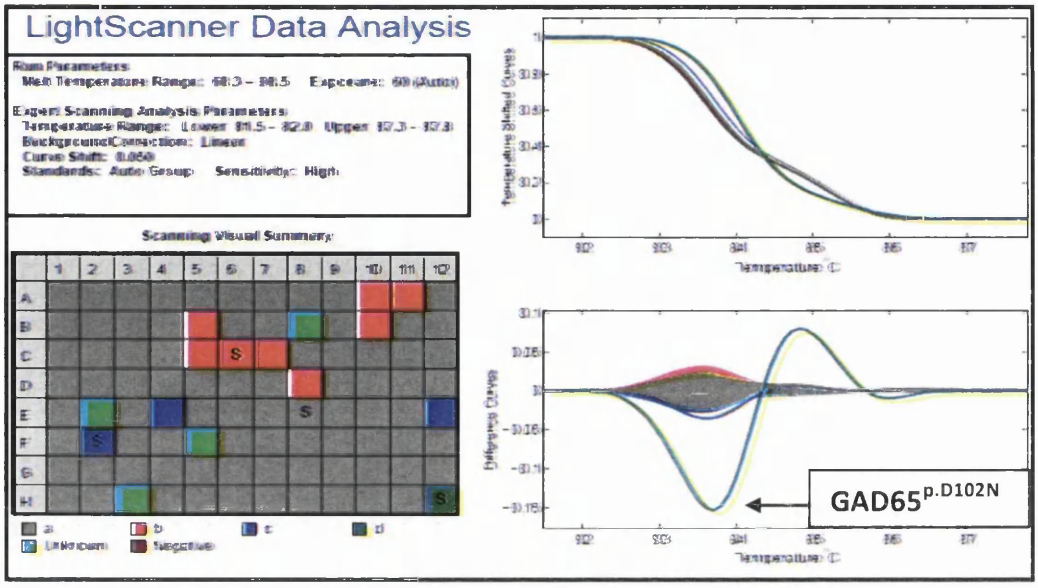

Figure 4.6 GAD65$^{p.D102N}$ lightscanner population study traces. The patient sample containing GAD65$^{p.D102N}$ was place in the 96th well of a lightscanner plate, with 95 control patient samples occupying the remaining plate for analysis via Lightscanner technology. DNA melting rates were recorded and compared. The patient sample produces a unique melt rate profile suggesting the variant is not present in the healthy control population.

	GAD65$^{p.D102N}$
GAD65 variant	LLPAC**N**GERPT
H.sapien	LLPAC**D**GERPT
P.troglodytes	LLPAC**D**GERPT
M.mulatta	LLPAC**D**GERPT
B.taurus	LLPAC**D**GERPT
C.lupus	LLPAC**D**GERPT
G.gallus	LLPAC**D**GEAAT
R.norvegicus	LLPAC**E**GERPT
M.musculus	LLPAC**D**GERPT

Figure 4.7 Multiple species alignment of the GAD65$^{p.D102N}$. The amino acid substitution producing the variant GAD65$^{p.D102N}$ was aligned against the GAD65 wild-type and the corresponding homologs in various phylogenetic species. The mutated amino acid was highlighted in red and the related wild-type and phylogenetic amino acids were highlighted in green.

Multiple species analysis as well as study/online population frequency data give reason to further analyse GAD65$^{p.D102N}$ by means of *in silico* and functional analysis to determine its effect on GAD65 pathobiology.

4.1.3 Missense Variant GAD65$^{p.P153Q}$

The variant p.P153Q is a cytosine to adenine nucleotide change at position 358 resulting in a proline to glutamine amino acid substitution at residue 153 of the polypeptide (Figure 4.8). Interestingly, this variant was identified in 16 patient samples of 664 at an allelic frequency of 0.012. However, the variant was also identified in two samples from the control population study of 480 at a lower allelic frequency (0.002) and on online databases at a frequency of 0.008 out of 3121 samples (Figure 4.9).

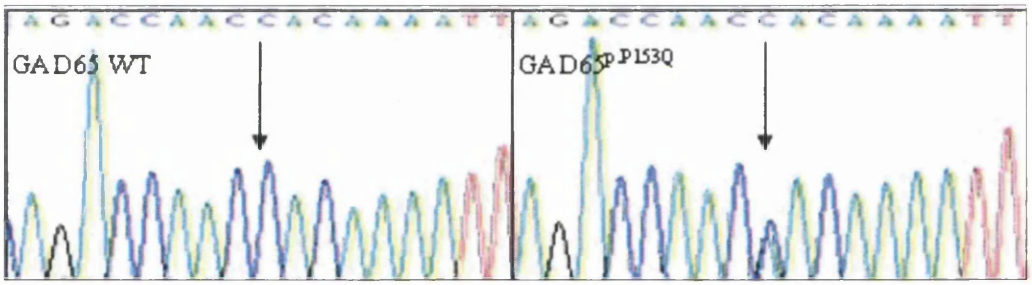

Figure 4.8 Sequence chromatogram of the GAD65 variant p.P153Q and the corresponding wild type sequence. GAD65$^{p.P153Q}$ was identified by the double peak as highlighted by an arrow in the right hand column, representing heterozygosity. The sequencing trace shows the nucleotide change from cytosine to adenine at position 358.

Predictive variant analysis via SIFT suggested that the variant would be tolerated by the protein and normal protein function would be unaffected. Grantham and PolyPhen results, however, suggest that the structural changes caused by the variant would probably have damaging consequences. This was supported by the species alignment analysis which showed the variant to be a highly conserved residue (Figure 4.10).

Despite the presence of p.P153Q in the normal population, the over representation in epilepsy patient samples is justification for further structure/function analysis. The

loss of a proline is typically highly significant for protein structures and p.P153Q may represent a significant risk factor variant rather than have driver mutation status.

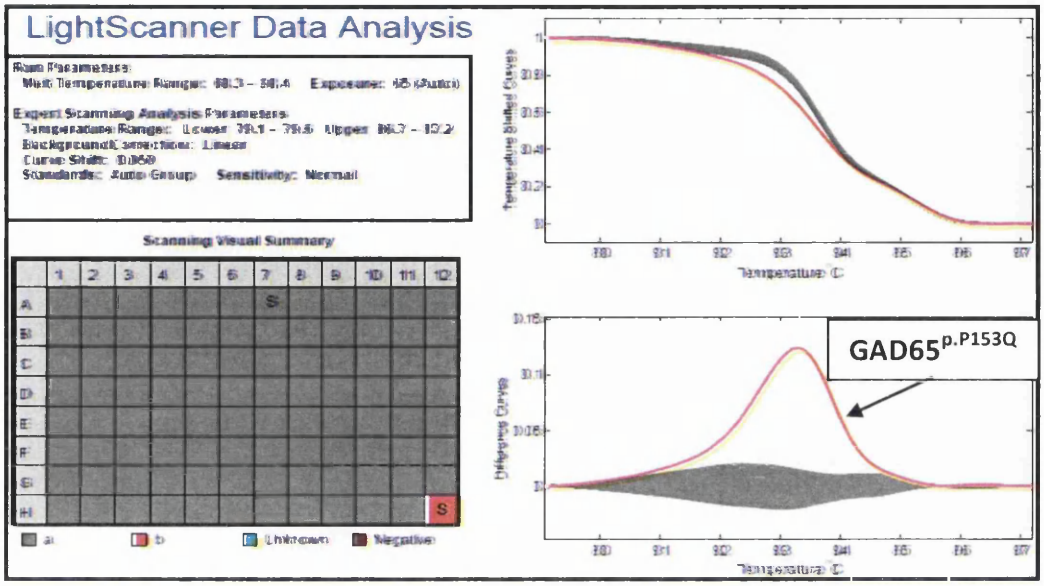

Figure 4.9 Lightscanner population study results for GAD65$^{p.P153Q}$. 480 control samples were analysed using lightscanner technology for the population study of each variant. The melt profile of the patient sample containing GAD65$^{p.P153Q}$ differs from its respective 95 control samples as shown. This indicates that the control samples do not possess the change in sequence that is causing the variant sample to melt at such a rate.

	GAD65$^{p.P153Q}$
GAD65 variant	ELADQQQNLEE
H.sapien	ELADQPQNLEE
P.troglodytes	ELADQPQNLEE
M.mulatta	ELADQPQNLEE
B.taurus	ELADQPQNLEE
C.lupus	ELADQPQNLEE
G.gallus	ELAEQPQTLEE
R.norvegicus	ELADQPQNLEE
M.musculus	ELADQPQNLEE

Figure 4.10 Multiple species alignment of the GAD65 missense variant, p.P153Q. GAD65 wild-type and GAD65$^{p.P153Q}$ amino acid sequences were aligned against corresponding homologs in various phylogenetic species. The mutated amino acid was highlighted in red and the related wild-type and phylogenetic amino acids were highlighted in green.

4.1.4 Missense Variant GAD65$^{p.G232E}$

p.G232E was identified in six out of 683 patient samples. A guanine to adenine nucleotide change at position 695 in exon six results in an amino acid change from glycine to glutamic acid at residue 232 of the polypeptide (Figure 4.11). The variant was not identified in the 480 unaffected control samples and was identified on online databases with a frequency of 0.014 out of 3134 participants (Figure 4.12).

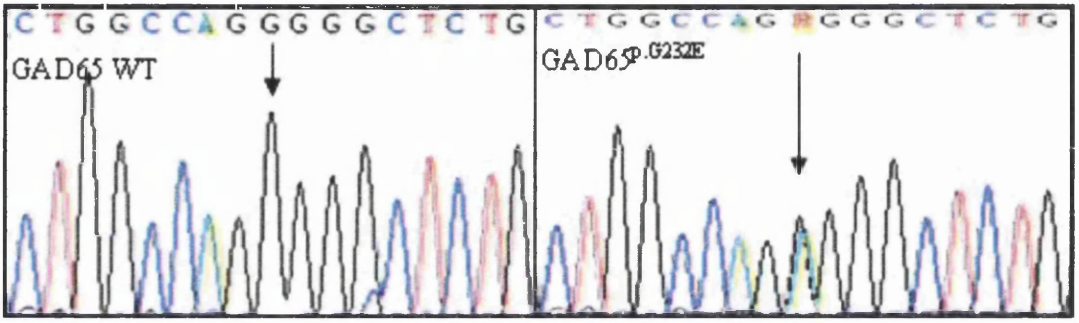

Figure 4.11 Sequence chromatogram of the GAD65 variant p.G232E and the corresponding wild type sequence. The heterozygous variant GAD65$^{p.G232E}$ was identified in the right hand column of the figure, identified by double peaks in sequencing (highlighted by an arrow). The sequencing trace shows the nucleotide change from guanine to adenine at position 695.

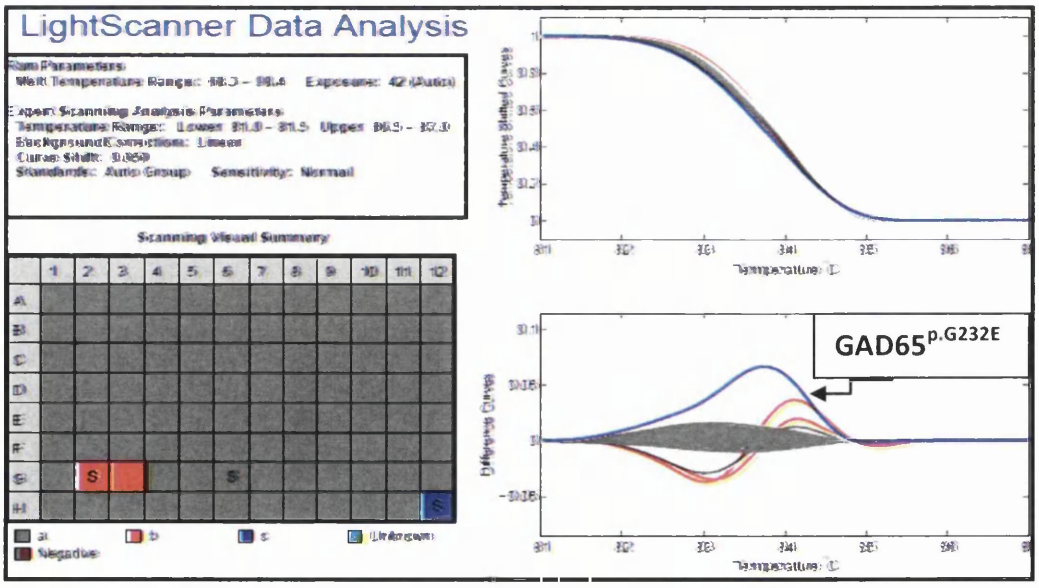

Figure 4.12 GAD65$^{p.G232E}$ lightscanner data analysis profile. The melt profile of the patient sample containing the variant GAD65$^{p.G232E}$ shows deviation from the average, This deviation is not portrayed by any of the control patient samples which leads us to trust that GAD65$^{p.G232E}$ is not present in the healthy control population.

The normal function of the protein was predicted to be unchanged by SIFT and Polyphen. However, with a Grantham class result of 65 the variant was predicted to probably have damaging effects, a result supported by alignment analysis which showed the amino acid change occurred in a highly conserved residue (Figure 4.13).

Collectively, these results confirm that GAD65$^{p.G232E}$ should be taken forward for further analysis to determine the pathogenic effects of the amino acid change on protein function.

	GAD65$^{p.G232E}$
GAD65 variant	IIGWPEGSGDG
H.sapien	IIGWPGGSGDG
P.troglodytes	IIGWPGGSGDG
M.mulatta	IIGWPGGSGDG
B.taurus	IIGWPGGSGDG
C.lupus	IIGWPGGSGDG
G.gallus	MVGWPGGCGDG
R.norvegicus	IIGWPGGSGDG
M.musculus	IIGWPGGSGDG

Figure 4.13 Phylogenetic alignment of the GAD65$^{p.G232E}$. p.G232E amino acid sequence was aligned against its corresponding wild-type and homologs in various phylogenetic species. The mutated amino acid was highlighted in red and the related wild-type and phylogenetic amino acids were highlighted in green. It can be seen that the variant occurs in a highly conserved amino acid residue.

4.1.5 Missense Variant GAD65$^{p.S527L}$

A nucleotide change from cytosine to thymine at position 1580 in exon 15 of GAD65 results in a serine to leucine amino acid substitution at amino acid position 527 of the polypeptide (Figure 4.14). GAD65$^{p.S527L}$ was identified in one patient sample out of 681 and one unaffected control sample of 681, but at a mean allelic frequency of lower than 1% (frequency 0.001). (Table 4.1 and Figure 4.15). The variant was also identified on online databases at a frequency of 0.003 out of 2275 participants.

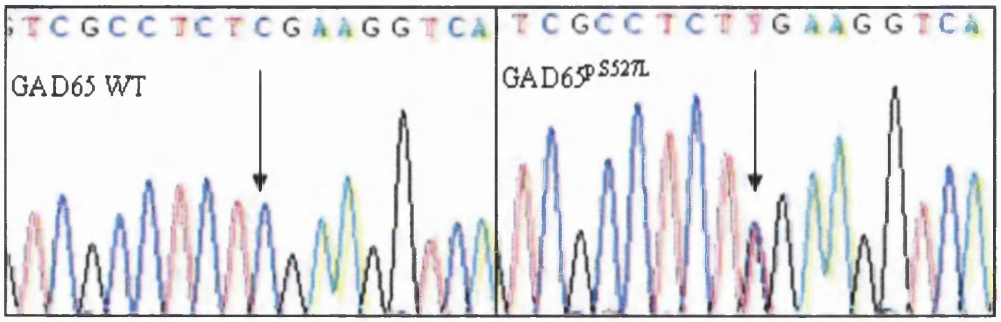

Figure 4.14 Sequence chromatogram of the GAD65$^{p.S527L}$ and the corresponding wild type sequence. p.S527L, a heterozygous variant, was identified in the right hand column of the figure by double peaks in the sequencing trace (indicated by an arrow). The sequencing trace shows the nucleotide change from cytosine to thymine at position 1580.

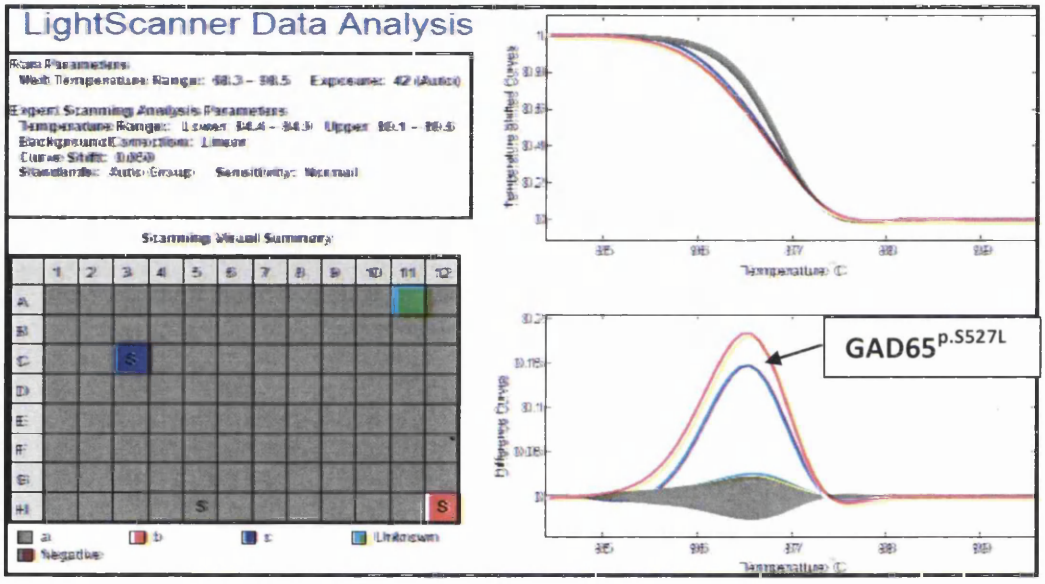

Figure 4.15 Population study of GAD65 variant, p.S527L. As seen in the above results, one control sample produced a similar melt profile to GAD65$^{p.S527L}$; although it has been highlighted by lightscanner technology in a different colour. This sample was Sanger sequenced which confirmed the control sample did contain GAD65$^{p.S527L}$.

The effects of GAD65$^{p.S527L}$ on the protein were predicted to be tolerated and benign by SIFT and Polyphen, however, a severe pathogenic effect was predicted by the Grantham score. The amino acid change occurs in a highly conserved residue by multiple species alignment analysis (Figure 4.16).

Triage of GAD65$^{p.S527L}$ into functional studies was approved via some indication of damaging effects by *in silico* methods and the highly conserved nature of the amino acid substitution and the GAD65 region.

	GAD65$^{p.S527L}$
GAD65 variant	RMSRL**L**KVAPV
H.sapien	RMSRL**S**KVAPV
P.troglodytes	RMSRL**S**KVAPV
M.mulatta	RMSRL**S**KVAPV
B.taurus	RLSRL**S**KVAPM
C.lupus	RMNRL**S**KVAPV
G.gallus	RMSRL**M**KVAPV
R.norvegicus	RMSRL**S**KVAPV
M.musculus	RMSRL**S**KVAPV

Figure 4.16 Multiple species phylogenetic alignment of the GAD65 missense variant, p.S527L. GAD65$^{p.S527L}$ amino acid sequence was aligned against its corresponding wild-type and homologs in various phylogenetic species. The mutated amino acid was highlighted in red and the related wild-type and phylogenetic amino acids were highlighted in green. The variant occurs in a highly conserved amino acid residue.

4.1.6 Missense Variant GAD65$^{p.I575T}$

A nucleotide change from thymine to cytosine at position 1725, causing an amino acid substitution from isoleucine to threonine at residue 575 of the polypeptide, was identified in exon 16 of GAD65 (Figure 4.17). This variant was identified in one patient sample out of 697 but was identified on online databases at a frequency of 0.001 out of 2937 and not identified in 480 unaffected control samples (Table 4.1 and Figure 4.18).

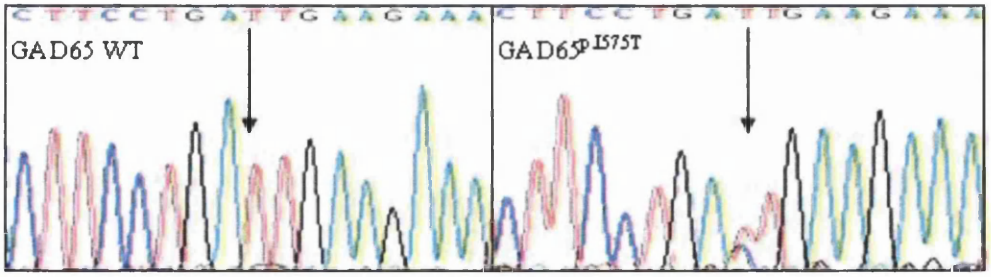

Figure 4.17 Sequence chromatogram of GAD65$^{p.I575T}$ and the corresponding wild type sequence. The heterozygous variant GAD65$^{p.I575T}$, was identified in the right hand column of the figure by double peaks in the sequencing trace (indicated by an arrow). The sequencing trace shows the nucleotide change from thymine to cytosine at amino acid position 1725.

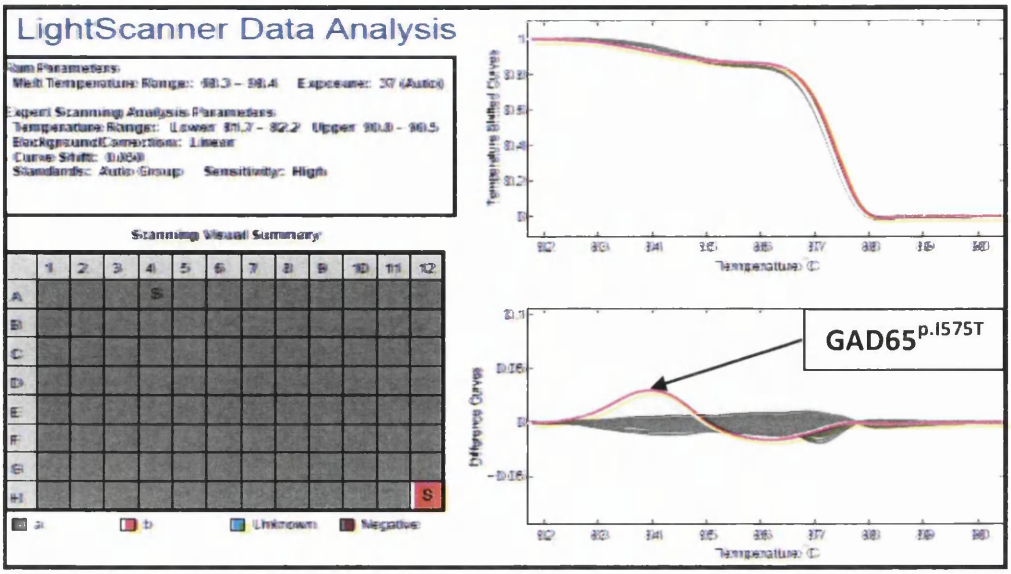

Figure 4.18 Lightscanner data analysis results for GAD65$^{p.I575T}$. Melt profiles of 480 healthy control samples were compared to a patient sample, which contained the GAD65$^{p.I575T}$. The variant sample melts at a different rate to the control population indicating a lack of presence.

Predictive analysis of the variant suggested that the amino acid change would affect normal protein function and cause damaging affects to the protein. These results along with highly conserved multiple species alignment analysis supports the functional analysis of the p.I575T variant (Figure 4.19).

	GAD65$^{p.I575T}$
GAD65 variant	DIDFL**T**EEIER
H.sapien	DIDFL**I**EEIER
P.troglodytes	DIDFL**I**EEIER
M.mulatta	DIDFL**I**EEIER
B.taurus	DIDFL**I**EEIER
C.lupus	DIDFL**I**EEIER
G.gallus	DIDFL**I**DEIER
R.norvegicus	DIDFL**I**EEIER
M.musculus	DIDFL**I**EEIER

Figure 4.19 Multiple species phylogenetic alignment of the GAD65 missense variant, p.I575T. The amino acid sequence of GAD65$^{p.I575T}$ was aligned against its corresponding homolog sequences in various phylogenetic species as well as its corresponding wild-type sequence. The mutated amino acid was highlighted in red and the related wild-type and phylogenetic amino acids were highlighted in green. The variant occurs in a highly conserved amino acid residues.

4.2 Mutation analysis of GAD67

Gene sequencing of the coding region and flanking intronic regions of GAD67 identified twenty-one variants in 111 patient samples (Table 4.3), which consisted of 5 non-synonymous, 6 synonymous, and 10 intronic variants. These variants are mapped onto genomic positions and their novelty status indicated (Figure 4.20). The most likely pathogenic variants were selected for further analysis which, for GAD67, comprised of three non-synonymous gene variants (Table 4.4).

Exon	Nucleotide change	Type of Mutation	Predicted consequences	Sample frequency	Reference	MAF
2	c.111 T>C	Synonymous	H37H	47	rs769404	0.364
3	c.265 C>T	Non-synonymous	R89W	1	rs150841255	No
	c.265 C>G	Non-synonymous	R89G	1	Novel	
4	c.380 A>T	Non-synonymous	Y127F	2	rs141004978	No
6	c.862 A>C	Non-synonymous	I228L	2	rs45566933	0.000
	c.750 T>C	Synonymous	P250P	1	rs369505970	No
	c.693 G>A	Synonymous	K231K	1	Novel	
9	IVS8-39 C>CT	Intronic		33	rs701492	0.274
	IVS9+4 T>TG	Intronic		1	rs139531653	0.001
	IVS9+12 G>GA	Intronic		5	rs701491	0.016
	IVS8-33 T>TC	Intronic		1	rs41311313	0.003
11	IVS11+102 T>TC	Intronic		1	Novel	
	IVS11+6 G>GA	Intronic		1	Novel	
13	IVS12-41 A>AT	Intronic		1	Novel	
	IVS13+29	Intronic		1	Novel	
14	c.1473 T>C	Synonymous	Y491Y	1	rs146199288	no
	c.1450C>T	Synonymous	L484L	2	rs769392	0.0376
15	c.1595 G>A	Non-synonymous	R532Q	3	rs769402	0.048
	IVS14-49 C>CT	Intronic		1	Novel	
16	IVS16+70 A>AG	Intronic		4	rs769406	0.019
	c.1644 G>A	Synonymous	E548E	1	Novel	

Table 4.3 The GAD67 *all*-variants table. Variant table of all variants identified via GAD67 in GGE patients via genetic screening. The frequency the variant occurs amongst samples is highlighted as well as the mean allelic frequency of any variants previously identified.

Gene	Exon	Variant	Nucleotide change	Genbank reference (Frequency)	Case frequency (Allelic frequency)	Control population frequency (Allelic frequency)	Sift consequence (Score)	Grantham class (Score)	Polyphen result (Score)
GAD67 (*GAD1*)	3	p.R89G	c.265 C>G	None	1/704 (0.0007)	0/480 (0)	Tolerated (0.21)	C65 (125.13)	Benign (0)
	3	p.R89W	c.265 C>T	rs150841255(0.001)	1/704 (0.0007)	0/480 (0)	Damaging (0.03)	C65 (101.29)	Probably damaging (0.958)
	4	p.Y127F	c.380 A>T	rs141004978(0.001)	2/696 (0.0014)	4/480 (0.004)	Damaging (0)	C15(21.61)	Possibly damaging (0.462)

Table 4.4 Missense variants identified in GAD67 in epilepsy patient samples. The position and nucleotide/amino acid changes of all novel/rare variants identified in our patient samples for *GAD1*. The frequency of the variants in the patient samples as well as previously identified SNPs and control populations are shown. SIFT, PolyPhen and Grantham software predictive tools calculate the effects of the amino acid changes on the protein.

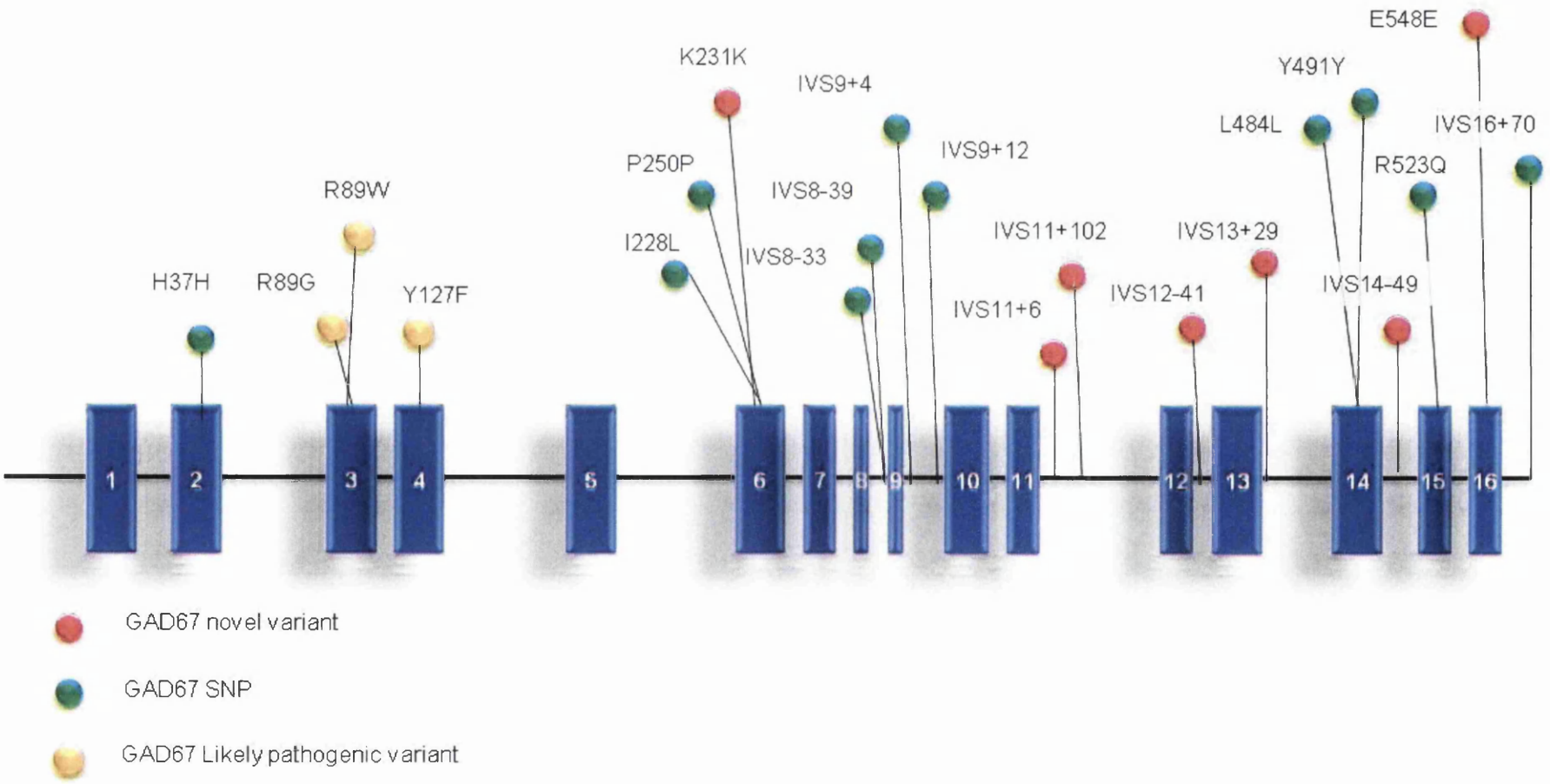

Figure 4.20 *GAD67* variants identified in 707 epilepsy patient samples; Schematic exon diagram demonstrating the genomic structure and location of identified novel variants and rare polymorphisms in the GAD67 gene. Exons 1-16 are demonstrated as red numbered boxes and the non-coding intronic regions by the connecting black lines. The novel mutations are symbolised by the red circles and were identified in the corresponding exons as indicated; very rare polymorphisms are shown as green rectangles.

Three heterozygous variant were identified in the GAD67 gene, *GAD1*: 1) p.R89G (c.265C>G); 2) p.R89W (c.265C>T) and 3) p.Y127F (c.380A>T) (Table 4.2). The status of each variant in terms of the likelihood of damaging consequences is presented in table 4.2 taking into account bioinformatics databases and control frequency datasets; Structure/function data is presented in Chapter Five.

Control population studies and predictive analysis was carried out for variants I228L and R532Q. High control population frequencies and benign consequences calculated by predictive tools prevented further analysis of the variants in this thesis.

4.2.1 Missense Variant GAD67$^{p.R89G}$

The novel mutation p.R89G was identified in *GAD1*, and represents a cytosine to guanine nucleotide change at amino acid position 265, causing a change from arginine to glycine at residue 89 (Figure 4.21). This variant was identified in exon three of one patient sample out of 704 cases and was not found in the 480 unaffected control samples, nor recorded on online databases (Figure 4.20 and figure 4.22).

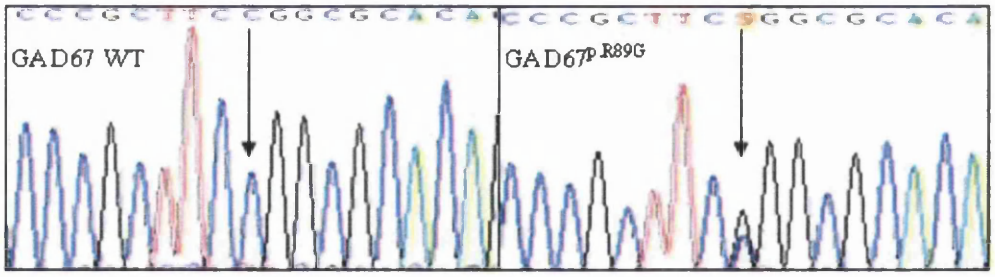

Figure 4.21 Sequence chromatogram of GAD67$^{p.R89G}$, and the corresponding wild type sequence. GAD67$^{p.R89G}$ chromatograms show a nucleotide change at position 265 which have been identified as heterozygous changes due to the double peak indicated by arrows. The same position on the wild-type sequence was also demonstrated by an arrow in the left hand column above.

GAD67$^{p.R89G}$ was predicted to have tolerated and benign consequences by SIFT and Polyphen. However, a high Grantham score suggests the variant will have damaging effects on the protein (Table 4.4). Phylogenic alignments support this as the amino-acid substitution affects a highly conserved residue, suggesting it is critical for correct protein function (Figure 4.23).

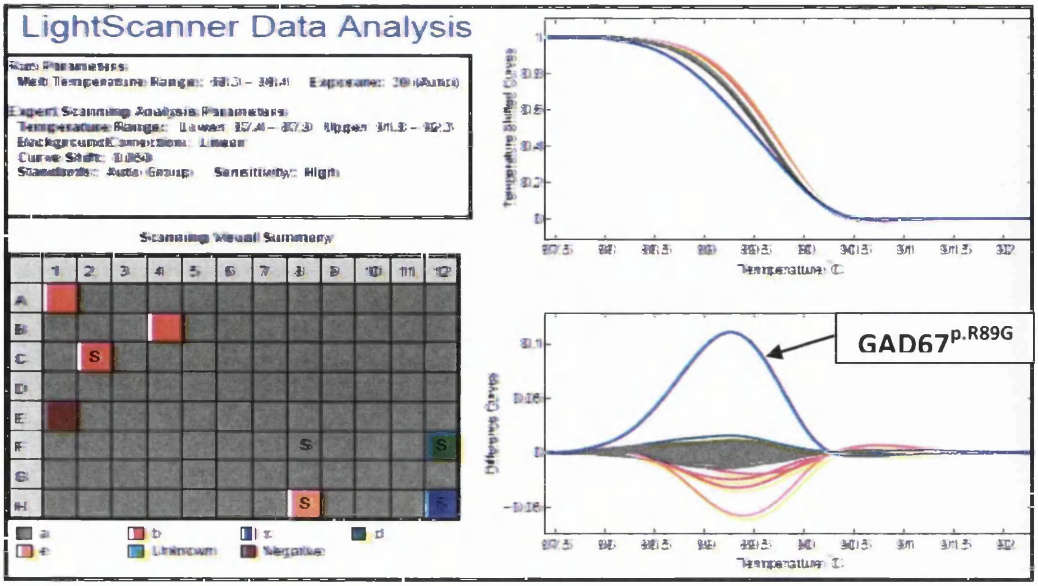

Figure 4.22 Lightscanner control population study results of GAD67$^{p.R89G}$. To determine whether GAD67$^{p.R89G}$ was present in the general population, lightscanner population studies were carried out on 480 control samples. The sample containing GAD67$^{p.R89G}$ melts at a different rate to the control samples and its profile is not closely resembled by any other sample; indicating that the variant is novel.

	GAD67$^{p.R89G}$
GAD67 variant	RDARF**G**RTETD
H.sapien	RDARF**R**RTETD
P.troglodytes	RDARF**R**RTETD
M.mulatta	RDARF**R**RTETD
B.taurus	KDGRF**R**RTETD
C.lupus	RDGRF**R**RTETD
G.gallus	REARF**R**RTETD
R.norvegicus	PGARF**R**RTETD
M.musculus	QGARF**R**RTETD

Figure 4.23 Multiple species phylogenetic alignment of the novel GAD67 missense variant, p.R89G. GAD67$^{p.R89G}$ amino acid sequence was aligned against its corresponding wild-type and homolog sequences in various phylogenetic species. The mutated amino acid was highlighted in red and the related wild-type and phylogenetic amino acids were highlighted in green.

In summary, GAD67$^{p.R89G}$ is a novel variant with damaging consequences according to population studies, species alignments and Grantham results. Functional analysis is required to assess any pathogenic effects.

4.2.2 Missense Variant GAD67$^{p.R89W}$

GAD67$^{p.R89W}$, an amino acid change from arginine to tryptophan, was also identified at amino acid position 89 but instead resulted from a different nucleotide change (cytosine to thymine) at position 265 of the coding sequence (Figure 4.24). GAD67$^{p.R89W}$ was identified in one patient sample out of 704, was not identified in any samples in the unaffected control population (n=480) but was identified on online databases with a rare frequency of 0.001 out of 2,914 (Table 4.2 and Figure 4.25).

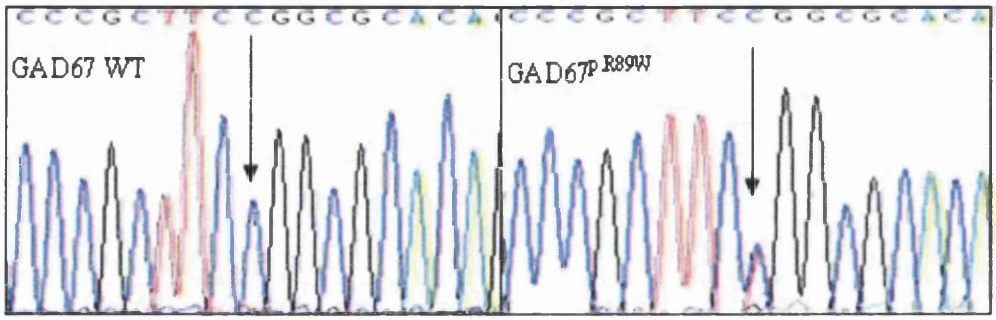

Figure 4.24 Sequence chromatogram of GAD67$^{p.R89W}$, and the corresponding wild type sequence. A heterozygous nucleotide change from cytosine to thymine can be noted by the double peak indicated with an arrow. The same position on the wild-type sequence was also demonstrated with an arrow in the left hand column above.

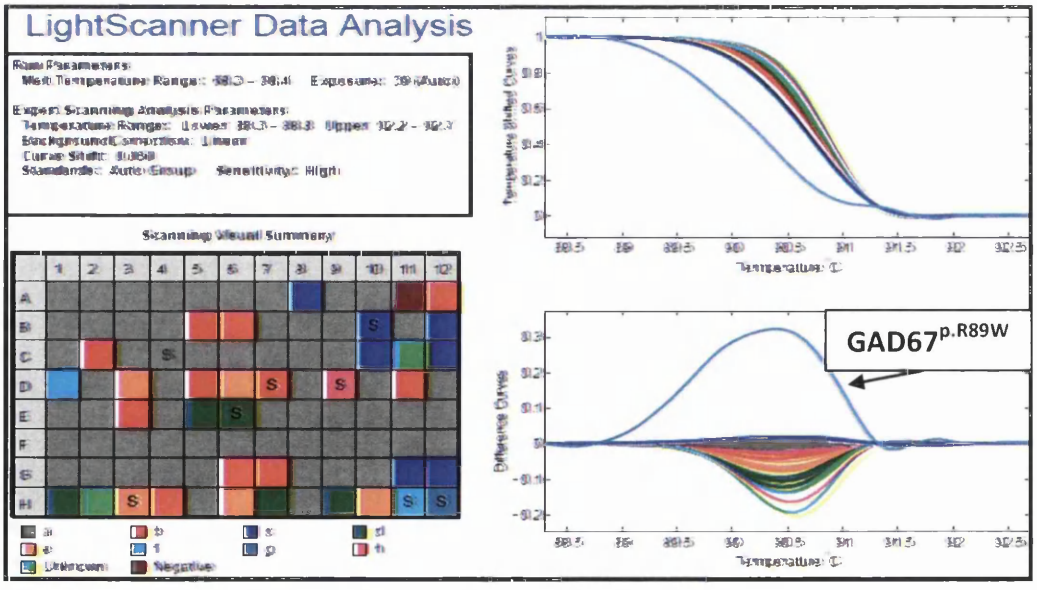

Figure 4.25 GAD67$^{p.R89W}$ Lightscanner population study results. Population study analysis using lightscanner technology shows that no control sample has a similar melt profile to p.R89W. This suggests that the variant is not present in the healthy control population.

Predictive analysis of this rare SNP suggested the variant would have damaging effects on normal protein function (Table 4.4). Independent species alignment supports the predictive analysis and suggests that the amino acid substitution affects a functionally critical residue (Figure 4.26).

In summary, GAD67$^{p.R89W}$ is a rare SNP as observed from dbSNP, however, predictive results and phylogenetic alignments suggest functional analysis is justified to assess any pathogenic effects.

	GAD67$^{p.R89W}$
GAD67 variant	RDARF**W**RTETD
H.sapien	RDARF**R**RTETD
P.troglodytes	RDARF**R**RTETD
M.mulatta	RDARF**R**RTETD
B.taurus	KDGRF**R**RTETD
C.lupus	RDGRF**R**RTETD
G.gallus	REARF**R**RTETD
R.norvegicus	PGARF**R**RTETD
M.musculus	QGARF**R**RTETD

Figure 4.26 Multiple species phylogenetic alignment of the GAD65 missense variant, p.R89W. The amino acid sequence of the variant p.R89W was aligned against its homolog sequences in various phylogenetic species as well as its corresponding wild-type sequence. The substituted amino acid is highlighted in red and the relevant wild-type and phylogenetic amino acids highlighted in green. It can be noted that the variant occurs in a highly conserved residue of the protein.

4.2.3 Missense Variant GAD67$^{p.Y127F}$

GAD67$^{p.Y127F}$, an adenine to thymine nucleotide change at position 380, resulted in a tyrosine to phenylalanine amino acid substitution at residue 127 in exon 4 (Figure 4.27). The variant was identified in two patient samples out of 696 GGE samples, but also four control samples out of 480 at a frequency of less than 1% (0.004); the variant was also identified on online databases with a frequency of 0.001 out 2,276 participants (Figure 4.20 and Figure 4.28).

Predictive analysis calculates that normal protein function will be affected by the variant, with damaging and possibly damaging results predicted. Alignment analysis shows the amino acid substitution occurs in a highly conserved residue, highlighting it as a critical residue for correct protein function (Figure 4.29).

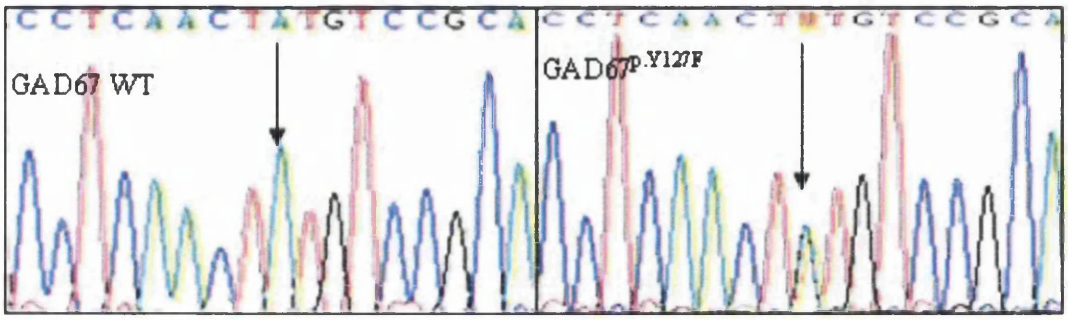

Figure 4.27 Sequence chromatogram of GAD67$^{p.Y127F}$, and the corresponding wild type sequence. The double peak of the right hand chromatogram shows the heterozygous nucleotide change from adenine to thymine constituting GAD67$^{p.Y127F}$. The position can also be identified on the GAD67 wild-type sequence.

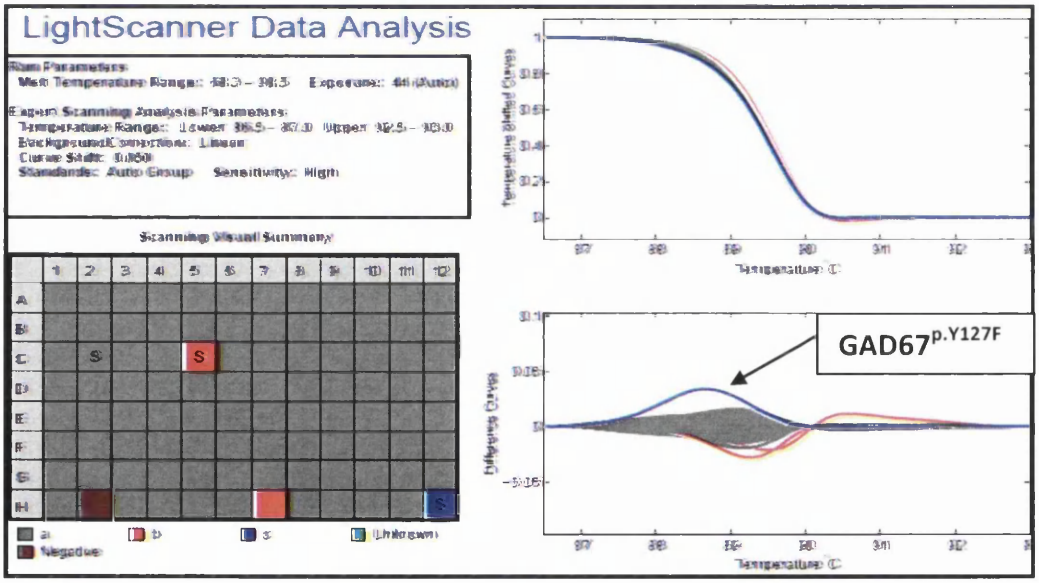

Figure 4.28 Example of population study results of GAD67$^{p.Y127F}$. This lightscanner profile shows the results of a population study carried out for GAD67$^{p.Y127F}$. The variant, patient sample was placed in well H12 and can be seen on the plate diagram in blue. This corresponds to the blue traces shown and a unique melt curve observed for GAD67$^{p.Y127F}$ indicates that it is not present in the control samples, suggesting it is not in the general unaffected population.

Online databases and population study analysis suggest that the rare variant will not have destructive effects on protein function. However, predictive analysis and multiple species alignments suggest the variant needs in *silico* and functional analysis to gather for evidence for pathogenicity.

	GAD67$^{p.Y127F}$
GAD67 variant	DILLN**F**VRKTF
H.sapien	DILLN**Y**VRKTF
P.troglodytes	DILLN**Y**VRKTF
M.mulatta	DILLN**Y**VRKTF
B.taurus	DILLN**Y**VRKTF
C.lupus	DILLN**Y**VRKTF
G.gallus	DILLN**Y**VRKTF
R.norvegicus	DILLN**Y**VRKTF
M.musculus	DILLN**Y**VRKTF

Figure 4.29 Phylogenetic alignments of the GAD67 missense variant, Y127F. The amino acid sequence containing GAD67$^{p.Y127F}$ was aligned against its corresponding homolog sequences in various phylogenetic species and corresponding wild-type sequence. The variant occurs in a highly conserved amino acid residue.

4.3 Summary of GAD65 and GAD67

The genetic screening of GAD65 and GAD67 in 707 GGE patient samples via lightscanner analysis has allowed for the identification of one novel missense variant and eight rare missense variants (occur in less than 1% of the general population). All are heterozygous variants that occur in highly conserved residues of the protein.

The outcome of this logistically challenging screening provides a rational to undertake *in silico* and *in vitro* functional analysis for each variant. Chapter Five will combine the gene variant outcomes from Chapter Three and Four and contain further analysis of GABA transporters and GAD65/GAD67 including protein context and topology, 3D structural modelling analysis and the expression validation of gene specific mutation constructs that were created for cellular transfection and functional research.

Chapter Five

Protein analysis of GGE GABAergic variants

Genetic screening of 707 GGE patient samples resulted in the identification of 20 novel or rare variants in GAT1, GAT3, GAD65 and GAD67. This included 18 heterozygous missense variants, a heterozygous 1bp deletion and a heterozygous splice-site variant. A rigorous process of bioinformatic analysis, population data and phyolgenetic alignment has lead to their selection for further analysis. The deletion and splice-site event have more direct pathogenic consequences discussed later and so we have focussed on the missense variants to determine the likelihood of pathogenicity of each genetic variants identified.

This chapter describes the protein context of the missense mutations including topology analysis, 3D molecular structure analysis and the preparation of mutation-expression constructs for cellular assays. This highlights that the GABAergic missense variants identified caused structural changes to their corresponding proteins. The creation of 18 mutation expression constructs proved successful and displayed functional intracellular expression of transgenes to validate their use in downstream molecular and cellular assays.

5.1 GAT1 Protein Context

Figure 5.1A and B represents the gene variants detailed in table 3.1 and mapped onto the protein domains and transmembrane topology of GAT1. They show that there are no amino acid substitutions within the transmembrane domains (TM domains) and they occur mainly in intracellular and extracellular linking domains and always in close proximity to TM domain boundaries. This may or may not confer a functional trend given the restricted numbers of gene variants .

A

```
  1 MATNGSKVADGQISTEVSEAPVANDKPKTLVVKVQKKAADLPDRDTWKGRFDFLMSCVGY
 61 AIGLGNVWRFPYLCGKNGGGAFLIPYFLTLIFAGVPLFLLECSLGQYTSIGGLGVWKLAP
121 MFKGVGLAAAVLSFWLNIYYIVIISWAIYYLYNSFTTTLPWKQCDNPWNTDRCFSNYSMV
181 NTTNMTSAVVEFWERNMHQMTDGLDKPGQIRWPLAITLAIAWILVYFCIWKGVGWTGKVV
241 YFSATYPYIMLIIFFRGVTLPGAKEGILFYITPNFRKLSDSEVWLDAATQIFFSYGLGL
301 GSLIALGSYNSFHNNVYRDSIIVCCINSCTSMFAGFVIFSIVGFMAHVTKRSIADVAASG
361 PGLAFLAYPEAVTQLPISPLWAILFFSMLLMLGIDSQFCTVEGFITALVDEYPRLLRNRR
421 ELFIAAVCIISYLIGLSNITQGGIYVFKLFDYYSASGMSLLFLVFFECVSISWFYGVNRF
481 YDNIQEMVGSRPCIWWKLCWSFFTPIIVAGVFIFSAVQMTPLTMGNYVFPKWGQGVGWLM
541 ALSSMVLIPGYMAYMFLTLKGSLKQRIQVMVQPSEDIVRPENGPEQPQAGSSTSKEAYI
```

B

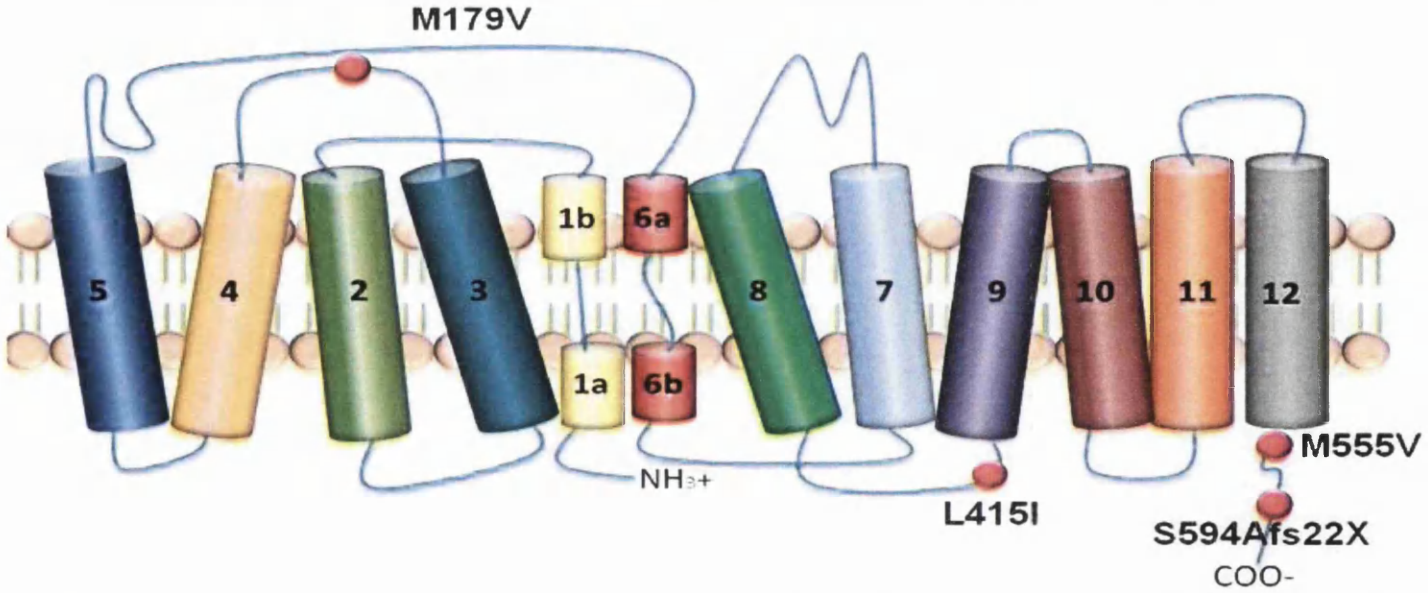

Figure 5.1 Transmembrane positions of GAT1 variants. A. The FASTA amino acid composition of the GAT1 polypeptide with a colour-coded representation of each transmembrane domain is highlighted. Blue triangles indicate the residues involved in co-ordinating sodium ions, empty rectangles encompass residues with side chain interaction with sodium, red triangles indicate GABA binding domains and green circles show residues involved in chloride binding. B. A topological representation of the 12 TM-spanning domains of GAT1 with the position of amino acid variants identified in GGE cases in this study.

GAT1$^{p.M179V}$ lies between two of the highly conserved N-glycosylation sites, Asn176 and Asn181 located on the extracellular loop between TM 3 and 4. If this variant affects one or more of the glycosylation sites, it could impact on properties of the protein such as protein folding, stability and GABA binding, thereby rendering the protein ineffective.

Independent conservation analysis of GAT1$^{p.L415I}$ shows a highly conserved amino acid residue is affected by this variant which resides in the intracellular loop between transmembrane domain eight and transmembrane domain nine (Figure 5.1). Transmembrane domain eight is a crucial part of the transporter as the transmembrane and corresponding extracellular loop contribute to successful GABA binding. Variants in this region could interfere with GABA binding resulting in the transporter being unable to activate and carry out its function.

GAT1$^{p.M555V}$ is close to the end of transmembrane domain 12 and leading into the final intracellular domain of GAT1 (Figure 5.1). This variant occurs in the region of the transporter that controls transporter trafficking, stability and degradation. Variants that would interfere with either of these processes could have detrimental effects on transporter activity either by preventing effective trafficking to the cell surface of being ineffective once reached. As with GAT1$^{p.M555V}$, GAT1$^{p.S594A}$ was identified following transmembrane twelve, in the C-terminal of the protein (Figure 5.1), this again could cause damaging effects to the transporter preventing it reaching its target, causing stability concerns and degradation queries.

GAT1$^{p.IVS3+1}$ occurs directly before exon three and transmembrane domain three, which could result in partial or complete loss of membrane domain. Transmembrane domain three is a crucial part of the protein and along with domains 1, 6 and 8 forms the inner ring of the central substrate binding site. A loss of this domain is likely to interfere with GABA binding possibly causing a loss of function.

5.2 GAT1 Structural Modelling

Structural models were created for wild-type and missense variants identified in this study from 'pdb' files obtained from Phyre2 and the Protein data bank, using

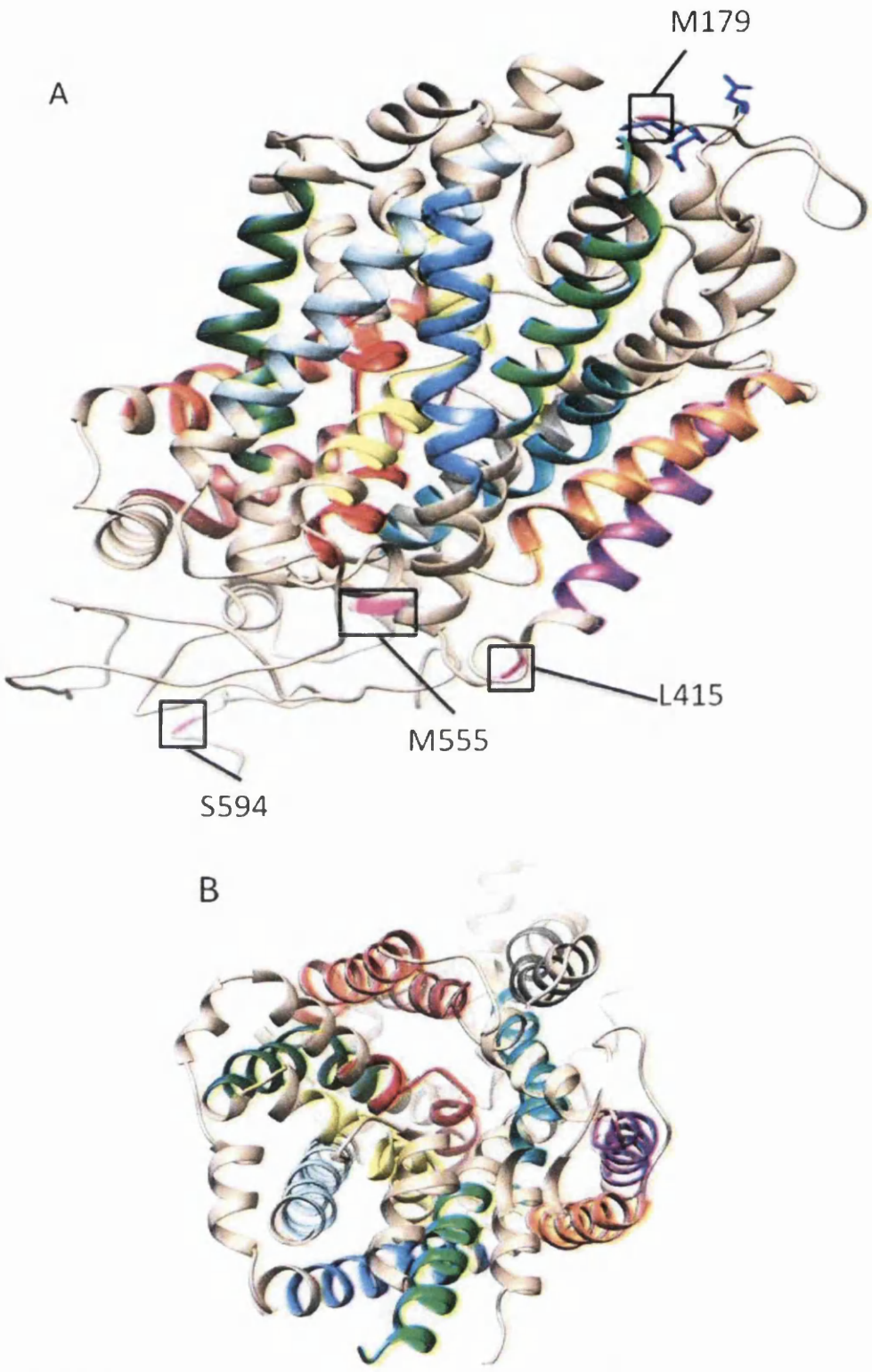

Figure 5.2 3D structural modelling of GAT1. A. Novel/rare missense variants identified in the study are highlighted in magenta and glycosylation site residues in blue. B. An aerial view of GAT1 with transmembrane domains highlighted as shown in figure 5.1, with the remaining sequence coloured in tan.

Chimera software (See section 2.2.8). Wild-type models of all four genes were created (Figures 5.2, 5.7, 5.15 and 5.23) with the positioning of the variants identified and transmembrane domains or enzymatic regions highlighted according to the 2D images (Figures 5.1, 5.16, 5.14 and 5.22). Aerial views showing the positioning of the transmembrane domains of the GABA transporters were also created (Figures 5.2 and 5.7).

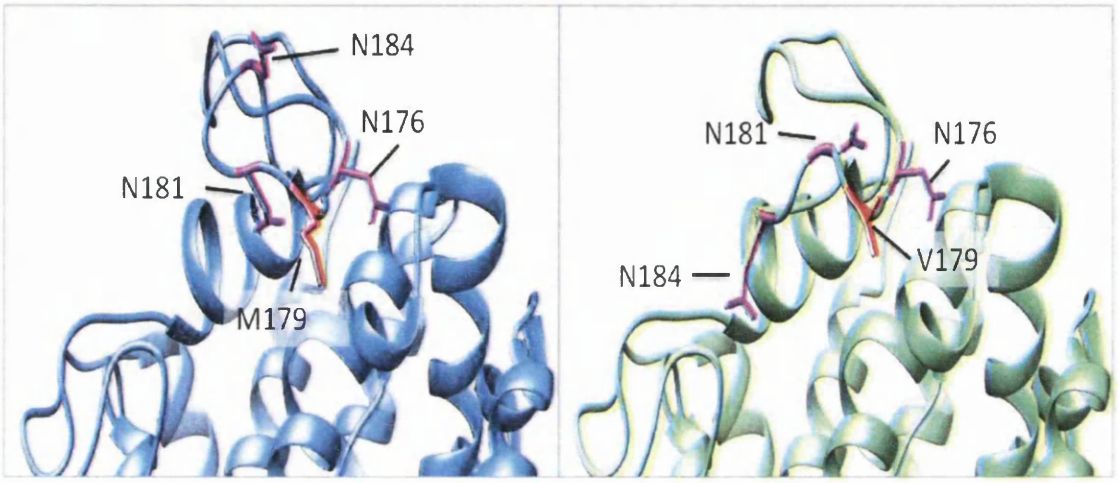

Figure 5.3 Homology modelling of GAT1 wild-type and GAT1$^{p.M179V}$. Wild-type modelling (blue) demonstrates the GAT1 positioning and side chain residue of methionine at position 179, as well as the glycosylation sites (purple) at amino acid positions 176, 181 and 184. The same can be seen on the variant sequence (green) which entails a change to valine at position amino acid 179. There is a clear change in positioning of the glycosylation sites following the variant amino acid compared to wild-type.

3D modelling images of GAT1$^{p.M179V}$ compared to wild-type show interesting results not only for residue 179 but also for the glycosylation sites in close proximity (Figure 5.3). In the conversion from methionine to valine the amino acid remains a nonpolar residue but the side chains differs in size and shape, which could affect interaction. The sequence change occurs amongst three glycosylation sites and is predicted to cause the deviation in positioning of the glycosylation site asparagine at positions 181 and 184, between wild-type and variant. Experiments involving the N-glycosylation sites of other neurotransmitter transporters have been carried out. Mutation of the glycosylation sites of GLYT2 found that the removal of one site gave similar transport activity assay results to the wild-type , whilst mutations of two and three of the glycosylation sites showed 74% and 58% of wild-type transport activity respectively (Martinez-Maza et al., 2001). Although mutations have not occurred in the glycosylation sites of the GAT1 transporter, two of the glycosylation

have deviated significantly from the wild-type position, possibly causing an inability to interact and lack of function.

Figure 5.4 shows the comparison of the 3D protein structure of GAT1 wild-type with the variant sequence of GAT1$^{p.L415I}$. The GAT1 wild-type structure contains leucine at amino acid position 415 whilst an amino acid change to isoleucine at this position causes the structural changes that modify the outward facing smaller nonpolar side chain residue to an inward facing nonpolar variant residue. 3D modelling of GAT1 including an amino acid change at position 555 from methionine to valine shows limited changes to the overall structure of the protein (Figure 5.5). However, changes between the hydrophobic nonpolar amino acid side chains can be noted as the variant residue does not reach as far in towards the pore of the membrane.

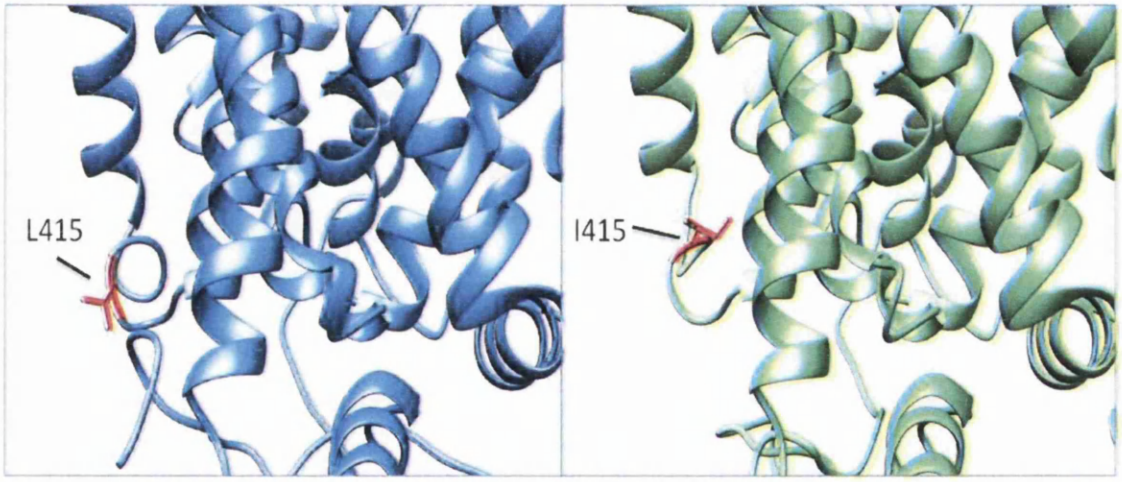

Figure 5.4 3D modelling of the wild-type GAT1 protein structure and GAT1$^{p.L415I}$. The GAT1 wild-type structure as shown in blue, contains leucine at amino acid position 415. An amino acid change to isoleucine at this position causes the structural changes shown in green and the change in amino acid side change shown in red compared to wild-type. The inward facing nonpolar variant residue replaced a outward facing smaller nonpolar residue.

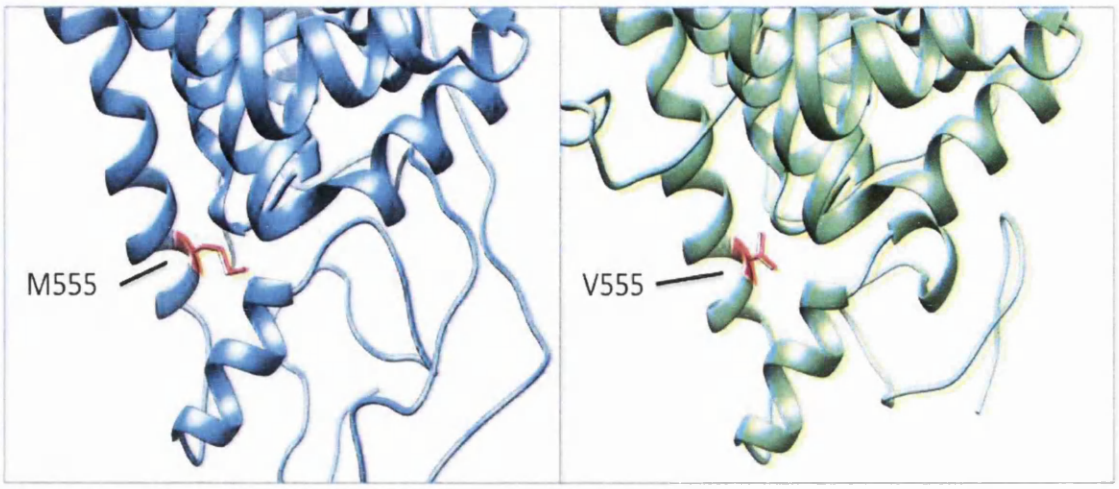

Figure 5.5 Structural homology modelling of GAT1 wild-type and variant sequence GAT1$^{p.M555V}$. A 3D model of the GAT1 protein sequence including an amino acid change at position 555 from methionine to valine (green structure) was created and compared to GAT1 wild-type (blue structure). Limited changes to the overall structure of the protein can be seen, however changes between the hydrophobic nonpolar amino acid side chains can be noted as the variant residue does not reach as far in towards the pore of the membrane.

5.3 GAT3 Protein Context

GAT3$^{p.H142Y}$ was localised to transmembrane domain three of the GAT3 protein (Figure 5.6). Transmembrane domain three along with domain eight is responsible for the binding of GABA to the transporter for its activation. If the binding of GABA were deterred due to a variant causing an inability to bind, the transporter will be unable to operate successfully. This in turn could not allow the reuptake of GABA from the synaptic space. The side chains of amino acid residues in this transmembrane domain are also responsible for the blockage of extracellular matter into the pore and any changes in amino acid could interfere with such processes.

Closely following GAT3$^{p.H142Y}$, GAT3$^{p.N160K}$ was identified on the extracellular loop between transmembrane domains three and four of GAT3; the variant precedes the three N-glycosylation sites, however is not believed to affect them (Figure 5.6 and figure 5.9). The variant does however occur between a highly conserved transmembrane domain four and a transmembrane domain which creates the GABA and sodium binding site an could therefore play a crucial role.

GAT3$^{p.V256L}$ was located to transmembrane domain 5 of the GAT3 (Figure 5.6). This domain along with transmembrane domain 4 acts as a pincer which holds in place

transmembrane domain 3 which is vitally important to maintain the structure of the pore acting as the central substrate binding site. The domain also contains a large amount of conserved residues which highlights the importance of the area as a whole. $GAT3^{p.D295N}$ was mapped following this domain in the extracellular loop between transmembrane domains five and six (Figure 5.6). Extracellular loops surrounding transmembrane domain six are highly important in the formation of the central substrate binding site. Side chains of the amino acids in this area are important to block extracellular matter from interfering with substrate binding. Variants in this area could therefore have negative effects on substrate binding, either from interference by other products or an ability for GABA and sodium binding.

$GAT3^{p.R436Q}$ presents itself on the intracellular loop connecting transmembrane domains eight and nine (Figure 5.6). Transmembrane domain eight and its surroundings are involved in creating the GABA binding site, whilst the role of transmembrane domain nine is to hold transmembrane domain eight in position along with the aid of transmembrane domain ten. Variants in this area could therefore have an impact on the binding site of GABA, interfering with GABA uptake from the synaptic space.

A

```
  1 MTAEKALPLGNGKAAEEARESEAPGGGCSSGGAAPARHPRVKRDKAVHERGHWNNKVEFV
 61 LSVAGEIIGLGNVWRFPYLCYKNGGGAFLIPYVVFFICCGIPVFFLETALGQFTSEGGIT
121 CWRKVCPLFEGIGYATQVIEAMLNVYSIIILAWAIFYLSNCFTTELPWATCGHEWNTENC
181 VEFQKLNVSNYSHVSLQNATSPVMEFWEHRVLAISDGIEHIGNLRWELALCLLAAWTICY
241 FCIWKGTKSTGKVVYVTATFPYIMLLILLRGVTLPGASEGIKFYLYPDLSRLSDPQVWV
301 DAGTQIFFSYAICLGCLTALGSYNNYNNNCYRDCIMLCCLNSGTSFVAGFAIFSVLGFMA
361 YEQGVPIAEVAESGPGLAFIAYPKAVTMMPLSPLWATLFFMMLIFLGIDSQFVCVESLVT
421 AVVDMYPKVFRRGYRRELLILALSVISYFLGLVMLTEGGMYIFQLFDSYAASGMCLLFVA
481 IFECICIGWVYGSNRFYDNIEDMIGYRPPSLIKWCWMIMTPGICAGIFIFFLIKYKPLKY
541 NNIYTYPAWGYGIGWLMALSSMLCIPLWICITVWKTEGTLPEKLQKLTTPSTDLKMRGKL
601 GVSPRMVTVNDCDAKLKSDGTIAAITEKETHF
```

B

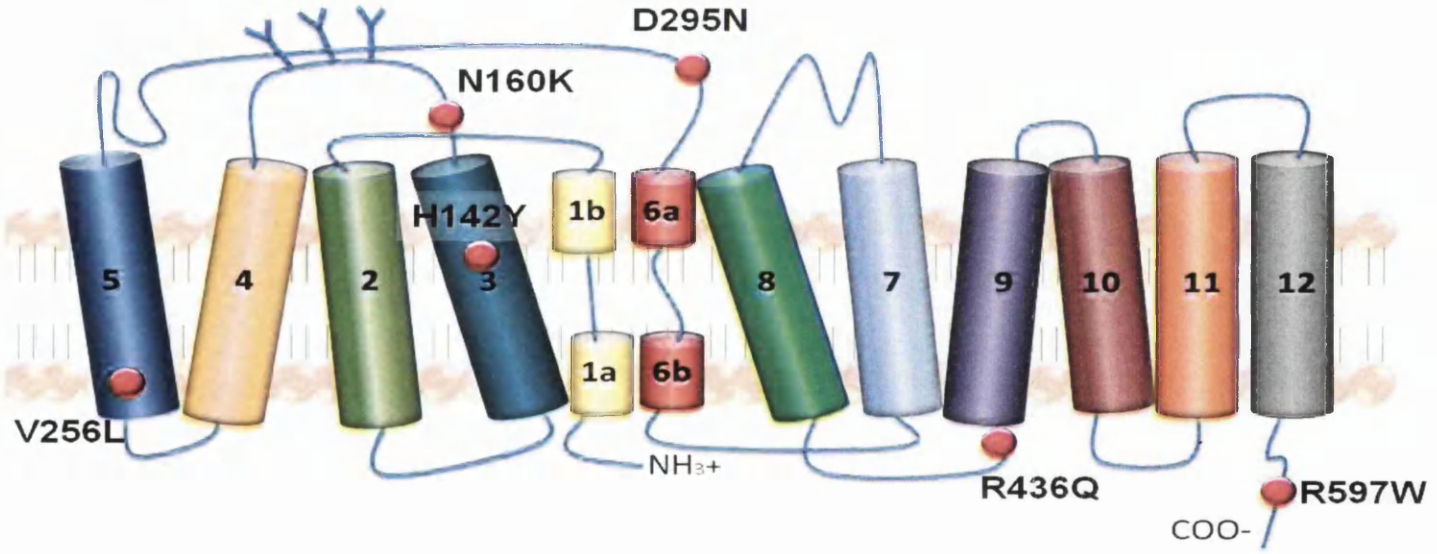

Figure 5.6 Transmembrane positions of GAT3 variants. A. FASTA amino acid composition of the GAT3 polypeptide with a colour-coded representation of each transmembrane domain is highlighted. Blue triangles indicate the residues involved in co-ordinating sodium ions, empty rectangles encompass residues with side chain interaction with sodium, red triangles indicate GABA binding domains and green circles show residues involved in chloride binding. B. A topological representation of the 12 TM-spanning domains of GAT1 with the position of amino acid variants identified in GGE cases in this study.

5.4 GAT3 Structural Modelling

The 3D structure of the GAT3 was modelled as in figure 5.7. The figure demonstrates the transmembrane domain location of the six missense variants identified, cross-referenced with figure 5.6. An amino acid change in GAT3 at position 142 from histidine to tyrosine compared to wild-type shows there is no significant change to the structure compared to wild-type (Figure 5.8). Both the positively charged wild-type residue and the larger uncharged variant residue are outward facing and located near the exterior of the protein.

The protein structure of the variant $GAT3^{p.N160K}$ appears relatively unchanged when compared to its wild-type equivalent. Both the variant and wild-type side chain residues which are present on the outer surface of the protein extend away from the protein pore (Figure 5.9). The uncharged residue is converted to a positively charged residue, and does not seem to alter the structure of glycosylation sites as with $GAT1^{p.M179V}$ (Figure 5.3).

GAT3 3D predictive modelling demonstrating the effects of a valine to leucine amino acid substitution at position 256, shows limited structural alterations compared to wild-type. Although similar in shape, the side chain residues of the wild-type and variant residues differ in residual mass and extension length (Figure 5.10). Limited modifications however can be seen to the protein structure and side chain features when considering the variant $GAT3^{p.D295N}$ (Figure 5.11). The variant does however cause a change in polarity of the residue from negatively charged to uncharged.

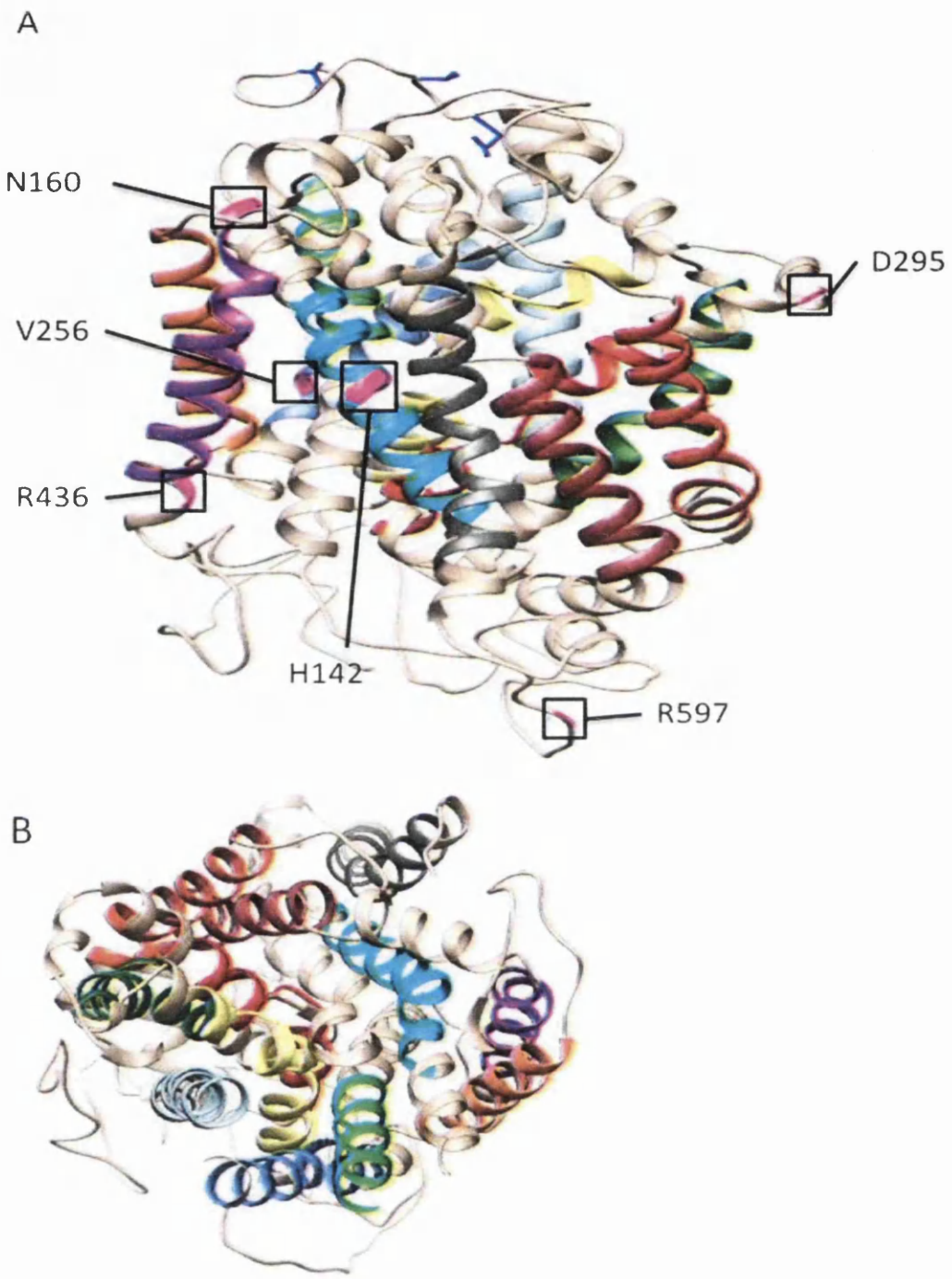

Figure 5.7 *In silico* modelling of GAT3 wild-type. A. 3D structural model of GAT3 with novel/rare variants identified in the study highlighted in magenta. Membrane domains are coloured according to the 2D structure (Figure 5.6) B. An aerial view of the 3D GAT3 structure.

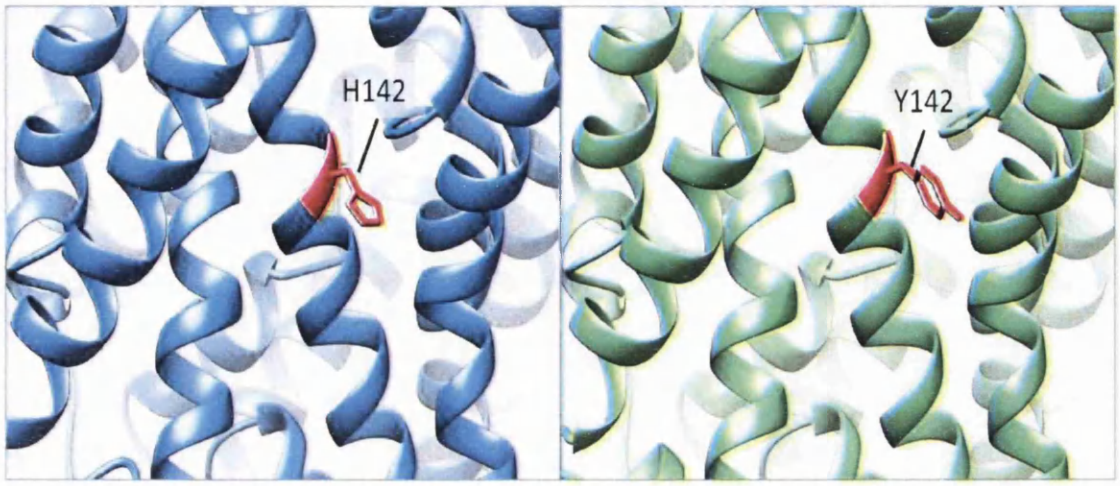

Figure 5.8 Predictive 3D structural modelling of GAT3$^{p.H142Y}$ and its corresponding wild-type. The variant amino acid structure compared to wild-type shows no significant change. Both the positively charged wild-type residue and the larger uncharged variant residue are outward facing and located near the exterior of the protein.

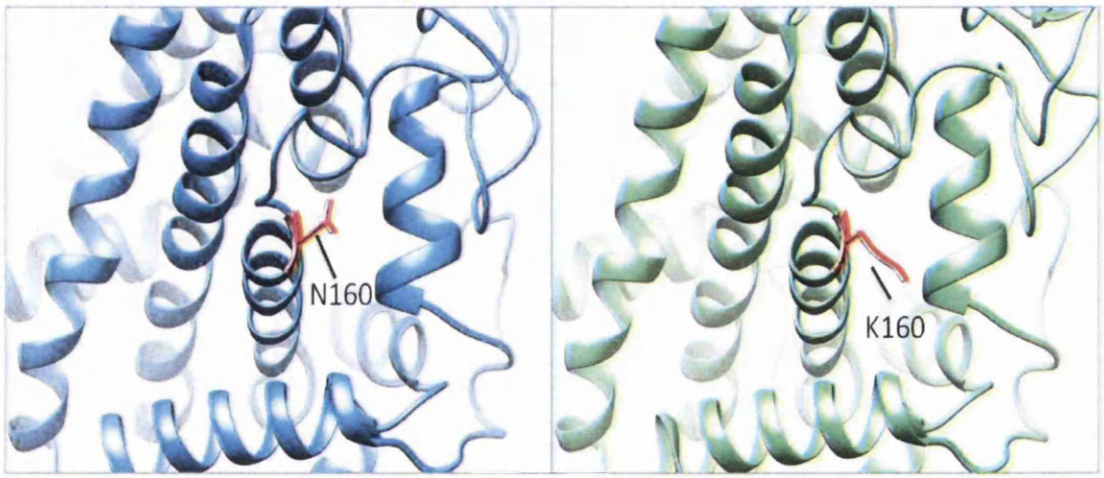

Figure 5.9 Homology modelling comparing the structures of *GAT3* wild-type and GAT3$^{p.N160K}$. Both the variant and wild-type residues which are present on the outer surface of the protein extend away from the protein pore. The change in amino acid modifies the residue from uncharged to being positively charged, and does not seem to alter the structure of glycosylation sites as with GAT1$^{p.M179V}$ (Figure 5.3).

Convincing results were obtained when analysing the structural modelling images of the variant GAT3$^{p.R436Q}$ compared to the GAT3 wild-type. The large positively charged arginine molecule that extends towards the central pore of the protein is converted to a negatively charged molecule, facing away from the pore towards the inside of the cell (Figure 5.12). Similar changes in side chain direction can be noted when studying structural predictions of GAT3$^{p.R597W}$ compared to wild-type. The

positively charged arginine is replaced with the larger nonpolar tryptophan. Figure 5.13 shows that whilst the wild-type variant faced toward the cell membrane, the variant residue sits facing extracellularly.

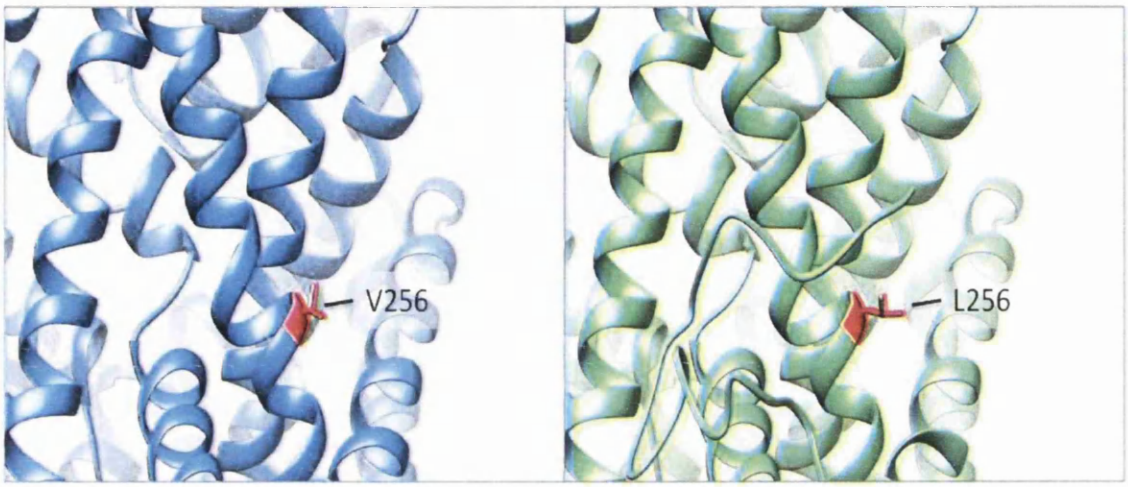

Figure 5.10 3D structural homology modelling comparing GAT3$^{p.V256L}$ to GAT3 wild-type. Predictive modelling shows that although at position 256 the amino acid change from valine to leucine does not alter the polarity of the residue (nonpolar) there is a slight increase in residue mass and extension length.

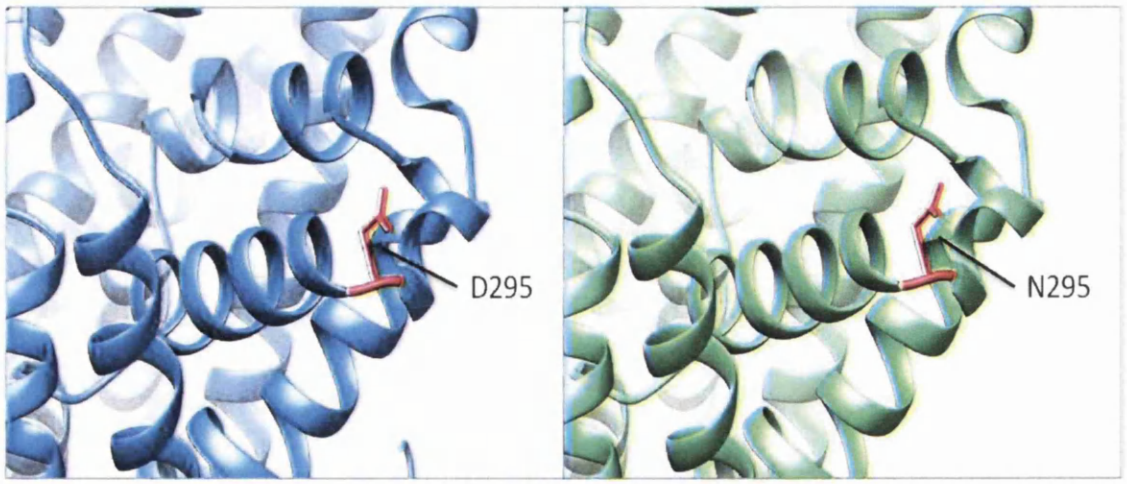

Figure 5.11 3D structural modelling of GAT3 wild-type and the variant GAT3$^{p.D295N}$. 3D predictive modelling of the variant was carried out and compared to wild-type sequence. Although there is only a slight alteration in the structure of the protein and its side chain, the variant residue is modified from negatively charged to uncharged.

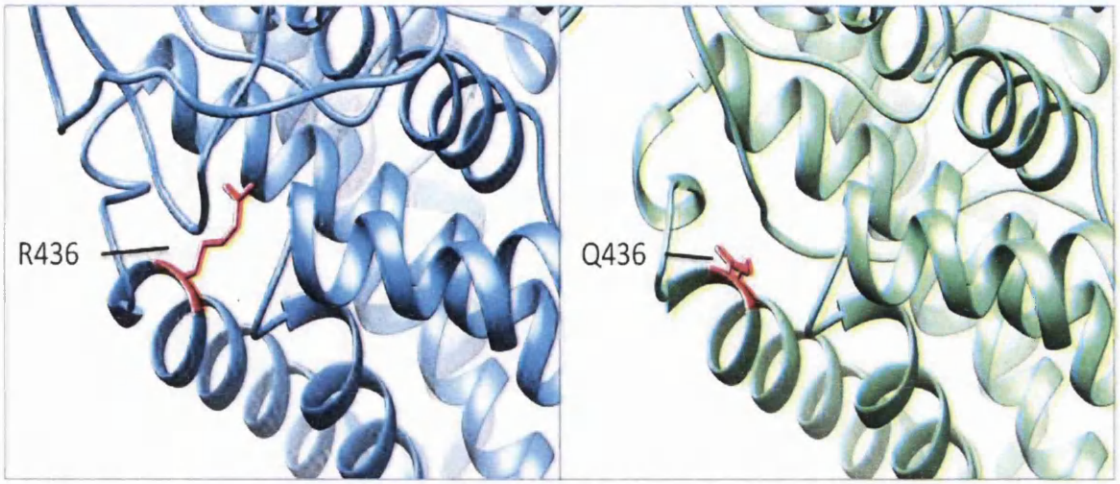

Figure 5.12 3D homology modelling of the variant GAT3$^{p.R436Q}$ and its corresponding wild-type model, GAT3. Predictive structural modelling of GAT3$^{p.R436Q}$ compared to the GAT3 wild-type showed convincing results as not only does the polarity of the residue change from positive to negative but there is also a change in positioning, from extending towards the central pore of the protein to facing intracellularly.

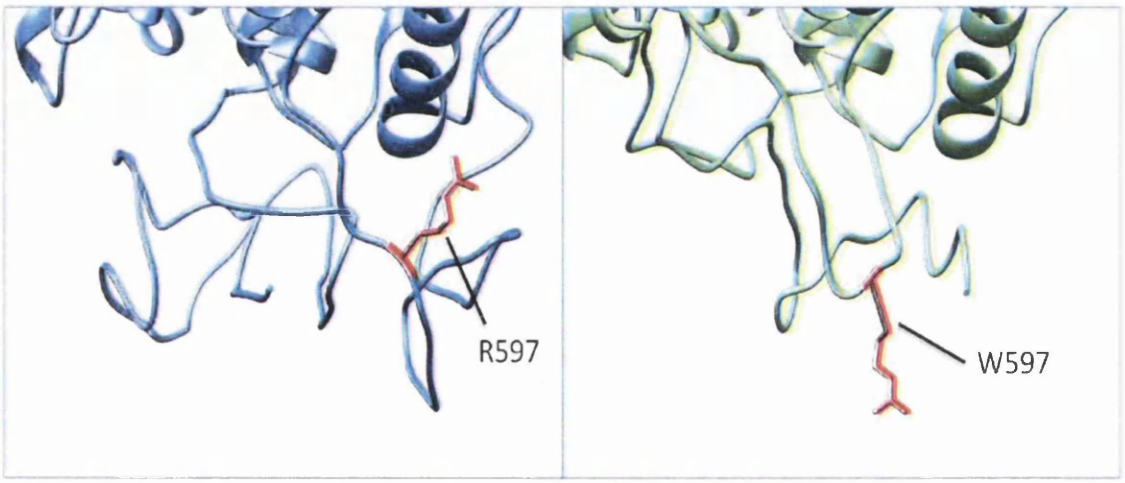

Figure 5.13 Structural homology modelling of GAT3 wild-type and the variant sequence GAT3$^{p.R597W}$. Predictive 3D modelling imaging shows the conversion of positively charged arginine to the larger nonpolar tryptophan. The image shows that whilst the wild-type variant faced toward the cell membrane, the variant residue sits facing extracellularly.

5.5 GAD65 Protein Context

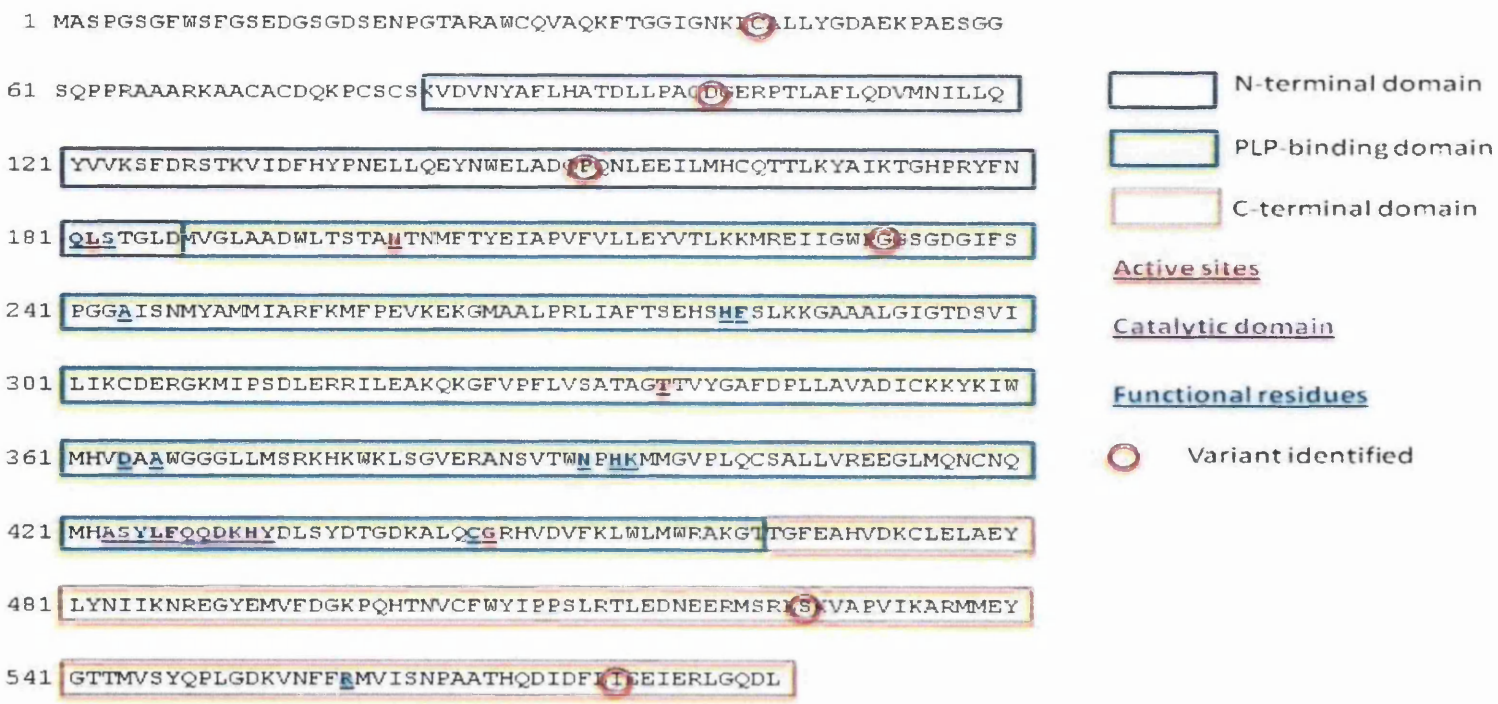

Figure 5.14 GAD65 variant mapping along with secondary structures. The three primary domains of the GAD65 monomer are N-terminal, blue rectangle; PLP-binding domain, green rectangle and C-terminal domain orange rectangle. The active sites have been underlined and highlighted in red, catalytic domain in purple and the functional domain in light blue. Residues affected by identified GAD65 variants are circled in red. This diagram is based on the N-terminal truncated crystal structure identified by Fenalti et al. (2007).

Crystal structures have identified three primary protein domains in GAD65 as indicated in figure 5.14. The structure demonstrates an N-terminal region from amino acid residue 84 to 187, a larger PLP binding domain from amino acid residue 188 to 465 and a C-terminal domain from residue 465 to the end of the protein at residue 585.

On a protein level, $GAD65^{p.C45F}$ was identified in the amino acid sequence in the N-terminal domain (Figure 5.14), however it resides in the region preceding the current crystal structure data as identified by Fenalti et al (2007). Palmytoylation is believed to occur in the N-terminal domain of GAD65 at amino acid positions 30 and 45 and primarily involves the covalent attachment of fatty acids to cysteine. The replacement of cysteine in this region with another amino acid could affect the level of palmytoylation and therefore the trafficking of the protein to the desired location within the terminal for the conversion of glutamate to GABA. The removal of cysteine could also affect the hydrophobicity of the protein and therefore its membrane association.

The N-terminal domain of GAD65 as well as containing palmytoylation sites, also contains trafficking signals which are potentially affected by the variant to prevent successful targeting to the nerve terminal and golgi membranes. The N-terminal domain is involved in the binding of two GAD65 proteins to create a functional dimer. If binding is affected by the amino acid change, it will be inactive. $GAD65^{p.D102N}$ and $GAD65^{p.P153Q}$ are both present in the N-terminal domain. These variants could affect protein trafficking, preventing successful targeting of the enzyme to the nerve terminal and golgi membranes. The creation of a functional dimer could also be affected, rendering the protein inactive (Figure 5.14).

Variant $GAD65^{p.G232E}$ is present on the PLP binding domain of the GAD2 protein (Figure 5.14). Mutations in this region could affect the successful binding of PLP and therefore prevent the activation of the enzyme. The creation of a functional enzyme monomer could also be affected as the N-terminal domain would normally pack against the N-terminal and PLP-binding domain of another monomer.

On a protein level, GAD65$^{p.S527L}$ and GAD65$^{p.S527L}$ have been mapped to the C-terminal domain (Figure 5.14). A variant at this position could affect substrate binding as the catalytic loop packs against the C-terminal domain, which further contributes to the dynamic role of the catalytic loop. The mobility of the enzyme could also be affected by the variants and is thought to occur in the C-terminal domain.

5.6 GAD65 Structural Modelling

GAD65 variants were identified and mapped throughout the protein as shown in figure 5.15. When comparing the variant protein GAD65$^{p.C45F}$ and the GAD65 wild-type protein via 3D structural modelling, there is a substantial change in the amino acid side chain structure from the uncharged cysteine to the larger nonpolar phenylanine (Figure 5.16). The variant however is preceding the identified truncated crystal structure so there is a decrease in the confidence level of the prediction, nevertheless there is a great difference in the protrusion and shape of the residual side chain.

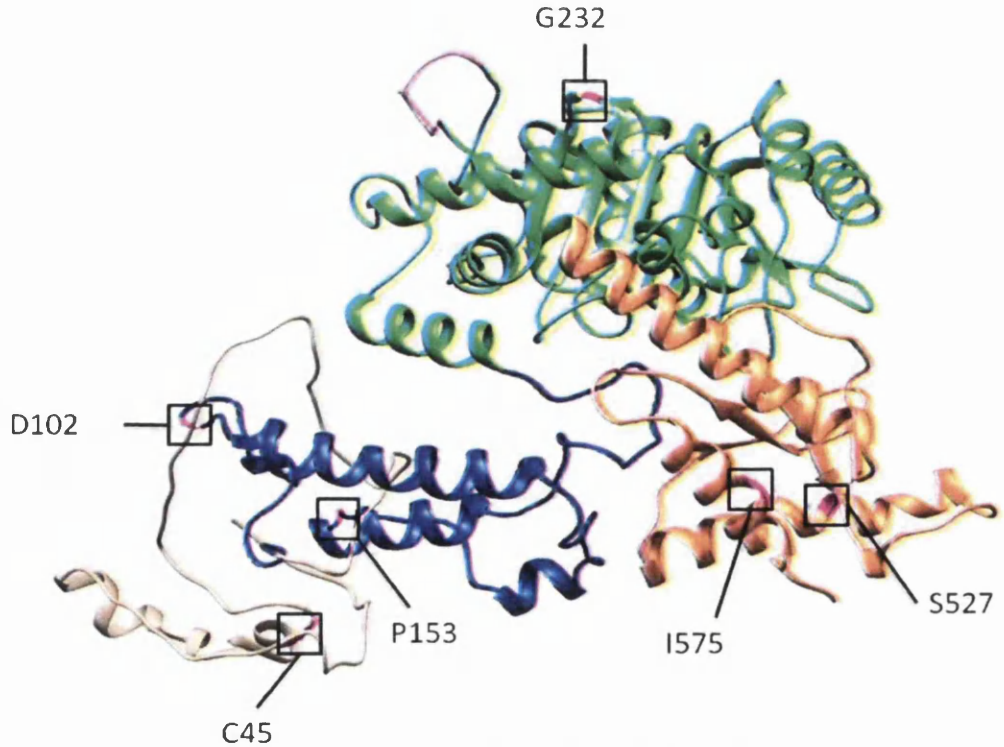

Figure 5.15 Structural modelling of GAD65 wild-type. GAD65 predictive model showing N-terminal tail in blue, PLP binding domain in green, C-terminal tail in orange and catalytic loop in purple. Also highlighted are the residues where variants have been identified in this study (magenta).

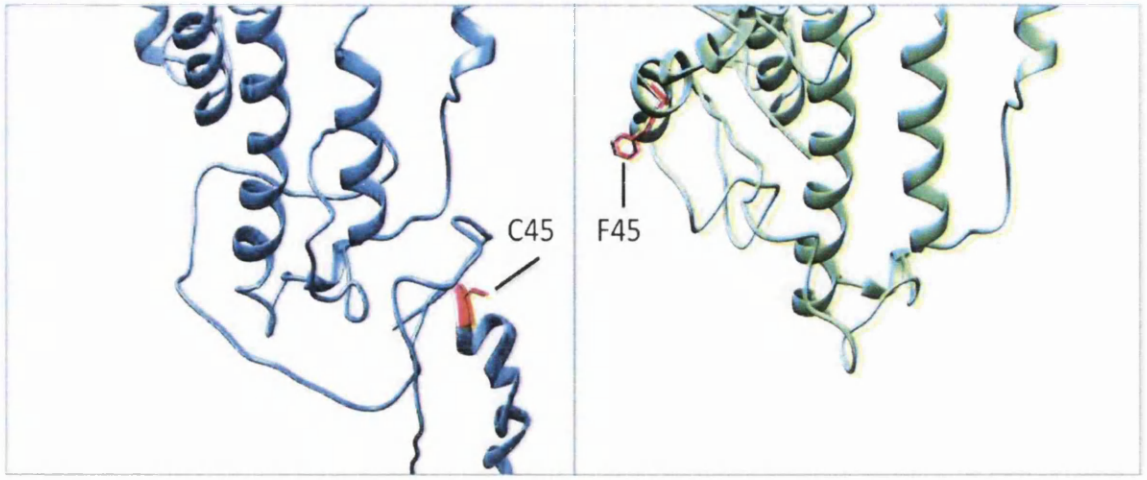

Figure 5.16 Homology modelling of GAD65 wild-type and variant sequence GAD65$^{p.C45F}$. Predictive 3D structural modelling shows that there is a substantial change in the amino acid side chain structure from the uncharged cysteine to the larger nonpolar phenylanine. Care must be taken however when assessing the affect of the variant on the structure of the protein as the variant occurs in the region preceding the previously identified truncated crystal structure.

The first variant occurring in the N-terminal domain of the protein is GAD65$^{p.D102N}$ which is an amino acid change from aspartic acid to asparagine at amino acid residue 102. 3D structural modelling of the variant protein compared to the GAD65 wild-type shows that the amino acid change at this position from a negative to uncharged amino acid causes the residue side chain to turn slightly away from the centre of the protein, but inward toward the cell (Figure 5.17).

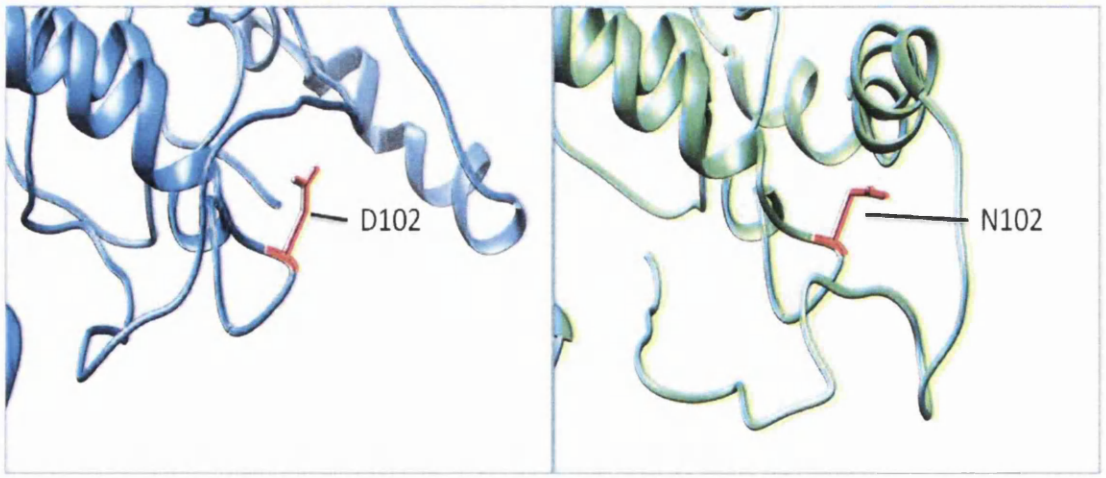

Figure 5.17 3D structural modelling of the variant p.D102N and its corresponding wild-type , GAD65. This N-terminal domain variant is the result of an amino acid change from aspartic acid to asparagines at amino acid residue 102. 3D modelling shows that the amino acid change at this position not only causes the residue side chain to protrude slightly outward but there is also a change in polarity from negative to uncharged.

3D predictive analysis demonstrates that an amino acid change from the cyclic amino acid proline to glutamine at amino acid position 153, causes limited changes to protein structure but substantial changes in residue side chain positioning can be observed when compared to wild-type. Under wild-type circumstances figure 5.18 shows that the normal forced bends of proline cause sudden changes in the direction of the chain. The figure also shows that the variant amino acid change at this position diminishes the rapid curvature of the side chain, changing the residue shape substantially. The nonpolar wild-type side chain of proline originally faced away from the enzyme whilst the negatively polar variant side chain extended toward the centre of the enzyme mass (Figure 5.18).

Comparison between the GAD65 wild-type and GAD65$^{p.G232E}$ protein structures in figure 5.19 shows that there is sizeable difference in the side chain makeup . The nonpolar wild-type residue glycine has no side chain residue opposing the negatively polar variant glutamic acid which has a side chain of relative large mass projecting away from the protein (Figure 5.19).

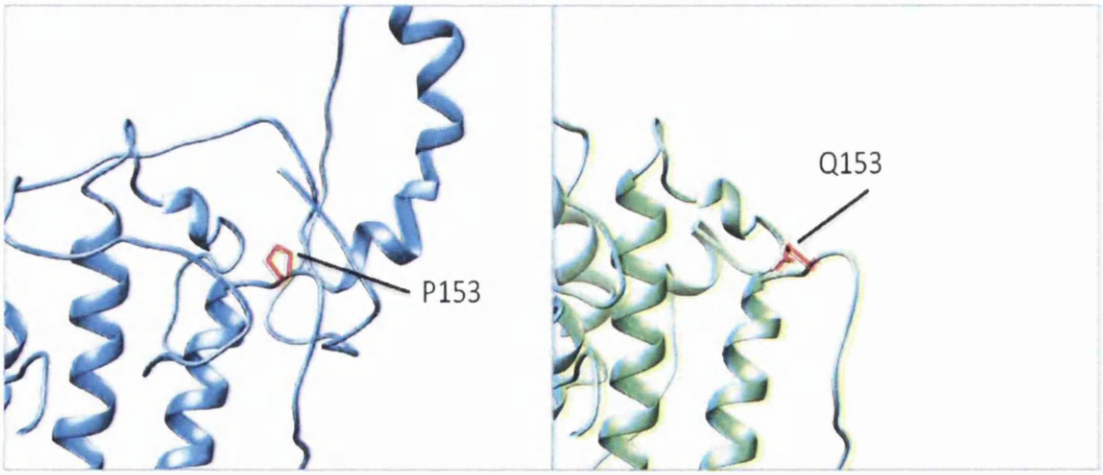

Figure 5.18 3D structural modelling of *GAD65* wild-type and the variant protein structure GAD65$^{p.P153Q}$. 3D predictive analysis demonstrates that an amino acid change from the cyclic amino acid proline to glutamine causes a change in residue side chain positioning. The normal forced bends of the proline causing abrupt changes in the direction of the chain due is diminished by the presence of glutamine, changing the residue shape substantially. The nonpolar wild-type side chain faced away from the enzyme, the negatively polar variant extended toward the centre of enzyme mass.

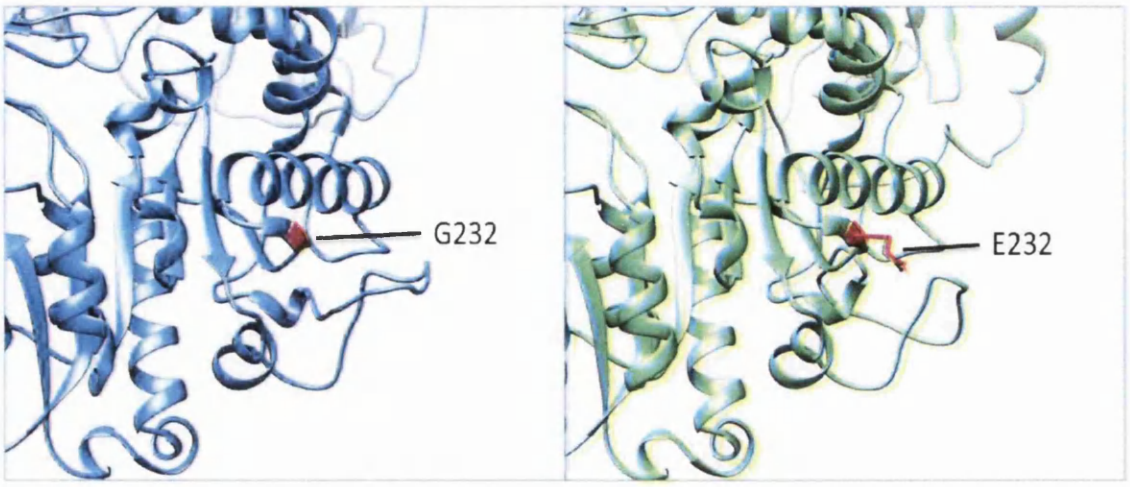

Figure 5.19 3D protein structure modelling of the variant GAD65$^{p.G232E}$ and its corresponding GAD65 wild-type sequence. There is a noticeable difference between GAD65 wild-type and GAD65$^{p.G232E}$ when considering 3D structural modelling. The nonpolar wild-type residue glycine has no side chain whereas the negatively polar variant glutamic acid has a side chain of relative large mass that projects away from the residue.

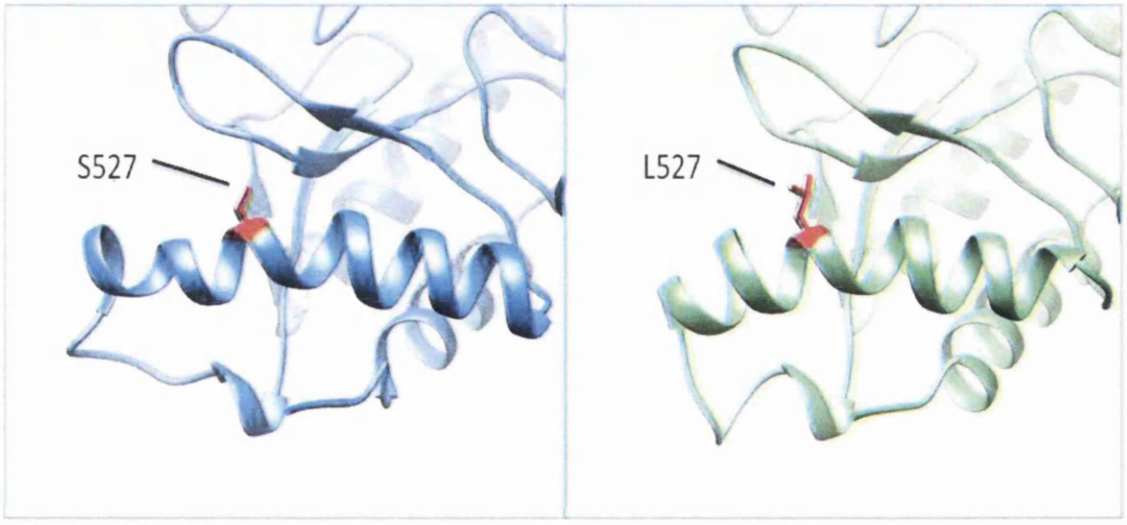

Figure 5.20 3D structural modelling of the predicted consequence of GAD65$^{p.S527L}$ compared to its GAD65 wild-type. Structural homology analysis suggested that there limited change to the protein structure of GAD65 when an amino acid change occurred at position 527 from serine to leucine. However the uncharged side chain of serine differs in mass, structural formula and polarity compared to its corresponding nonpolar variant.

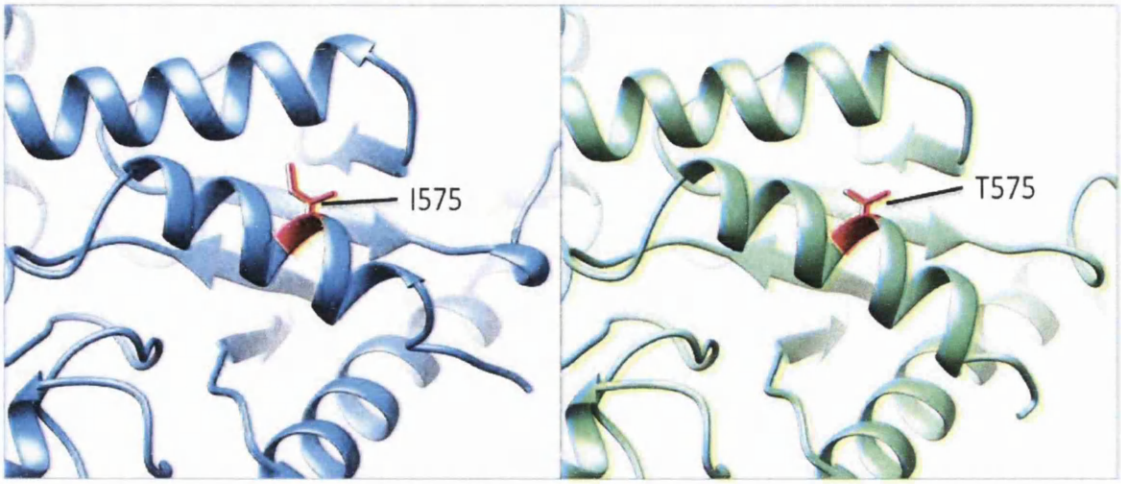

Figure 5.21 Predictive structural modelling of the GAD65 wild-type compared with the variant GAD65$^{p.I575T}$. The protein structure of GAD65 was created (blue) using chimera software and compared to the variant sequence containing an amino acid change at position 575 (green). 3D predictive analysis shows that the nonpolar wild-type residue extends further from the enzyme than the nonpolar, smaller in mass variant. Little knock on change can be seen affecting the overall protein structure.

3D Structural homology analysis suggested that there is a slight change in the protein structure of GAD65 wild-type when an amino acid change occurred at position 527 from serine to leucine (Figure 5.20). The uncharged side chain of serine differs not only in mass but also in structural formula and polarity compared to its corresponding nonpolar variant. These changes cause the variant residue to protrude and extend further away from the protein than in the wild-type protein. Similar results were obtained when examining the predictive 3D structural modelling of the variant GAD65$^{p.I575T}$ compared to the GAD65 wild-type protein. In this case the nonpolar wild-type side chain advances further from the enzyme than the smaller nonpolar variant side chain, with limited overall effect on the protein structure (Figure 5.21).

5.7 GAD67 Structural Modelling

Figure 5.22 GAD67 variant and secondary structure mapping. GAD67 variant residues are highlighted on the protein sequence at their corresponding amino acid with a red circle. The N-terminal domain is represented by a blue rectangle, the PLP-binding domain by a green rectangle and the C-terminal domain by an orange rectangle. The amino acids that create active sites have been highlighted in red and underlined, the catalytic domain in purple and the functional domain in light blue. This diagram is based on the crystal structure identified by Fenalti et al, (2007).

Crystal structures have also identified three primary protein domains in GAD67, the N-terminal, PLP binding and C-terminal domain, as indicated in figure 5.22. The protein regions differ slightly to those of the GAD65 protein with the N-terminal region spanning from amino acid residue 92 to 196, the larger PLP binding domain from amino acid residue 197 to 473 and a C-terminal domain from residue 474 to the end of the protein at residue 594.

$GAD67^{p.R89G}$ and $GAD67^{p.R89W}$ variants were identified in the N-terminal domain but in the amino acid sequence preceding the N-terminal truncated crystal structure described by Fenalti et al. (2007) (Figure 5.22). A variant in the N-terminal domain may affect the generation of a functional dimer which, in turn, could render the protein inactive. This is a possible outcome as the N-terminus of one monomer is packaged against the N-terminus and PLP binding domain of another monomer to create the functional dimer; a variant affecting the structure of this site could affect the successful binding of two monomers.

Figure 5.22 shows that the variant $GAD67^{p.Y127F}$ occurred in an α-helix of the N-terminal domain of the protein. The α-helix is packaged with the N-terminal domain and PLP site of another monomer to create the functional domain. A variant in the α-helix could affect the successful binding of the two monomers leaving them inactive (Figure 5.22).

5.8 GAD67 Structural Modelling

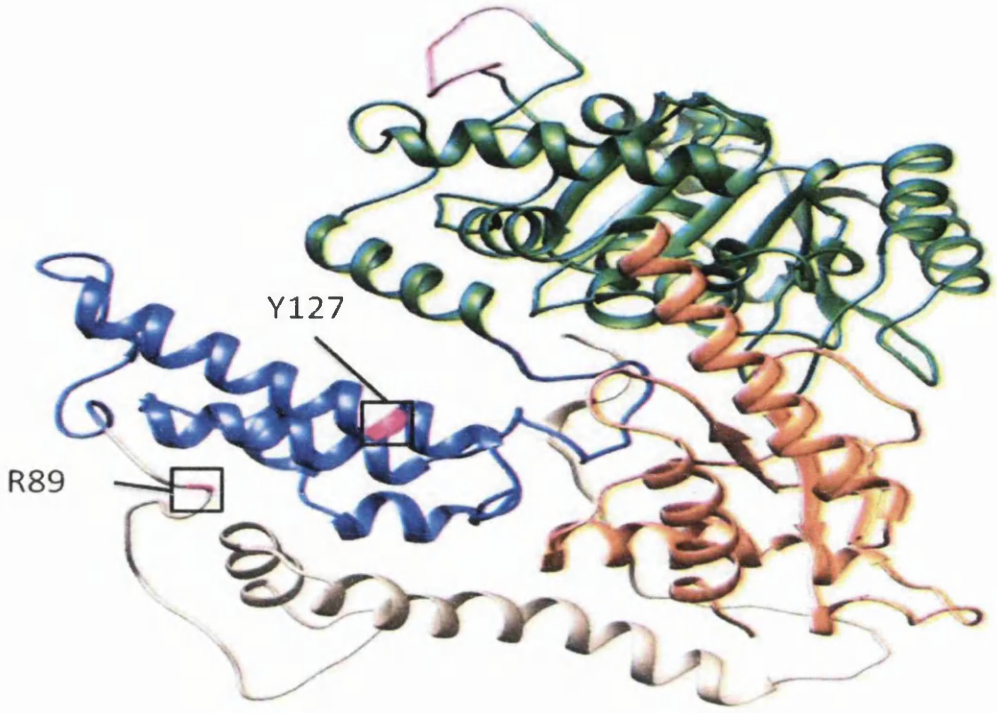

Figure 5.23 3D structural modelling of GAD67 wild-type. The 3D model shows all domains of the protein; N-terminus (blue), PLP binding (green), C- terminus (orange) and catalytic domain (purple). The variants identified in this study are highlighted in magenta.

Figure 5.23 highlighted that the variants identified in GAD67 in this study occurred in the N-terminal domain and the region preceding this. Both the variants GAD67$^{p.R89G}$ and GAD67$^{p.R89W}$ occur at the same amino acid position but 3D structural modelling predicts that the variants have different consequences. The positively charged polar arginine wild-type protrudes toward the centre of the enzyme, in the variant protein GAD67$^{p.R89G}$ this protrusion is replaced by the nonpolar amino acid glycine which has no side chain, possibly affecting interaction with other amino acids (Figure 5.24). When considering an amino acid substitution to tryptophan at this position, the inward facing arginine is replaced by a larger nonpolar heterocyclic residue which extends away from the enzyme mass. The amino acid side chain shows a distinct difference not only in mass but also in residue structure, direction and polarity to the wild-type (Figure 5.25).

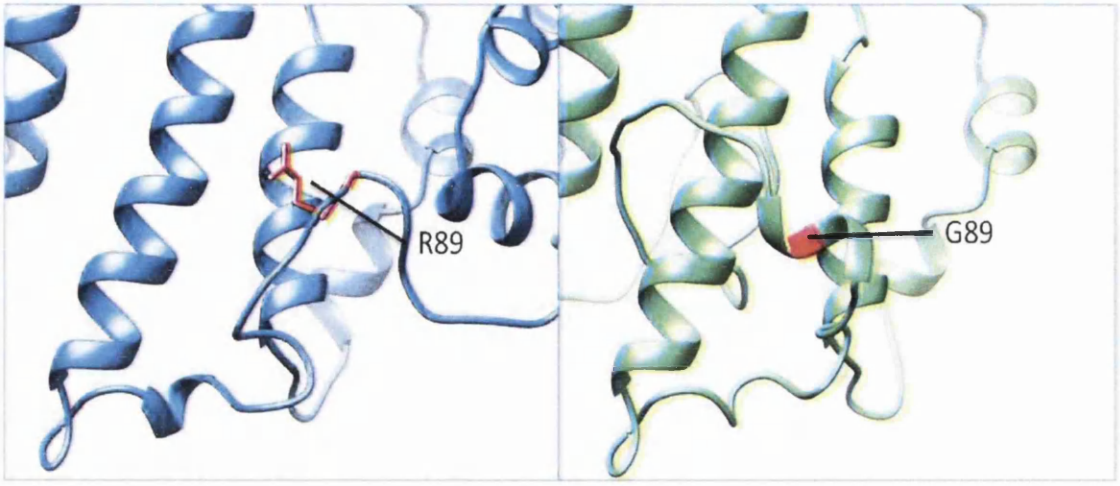

Figure 5.24 3D homology modelling of GAD67 and the variant GAD67$^{p.R89G}$. 3D structural modelling predicts that the positively polar arginine wild-type protrudes toward the centre of the enzyme. In the variant sequence, this protrusion is replaced by the nonpolar amino acid glycine which has no side chain, possibly affecting interaction with other amino acids.

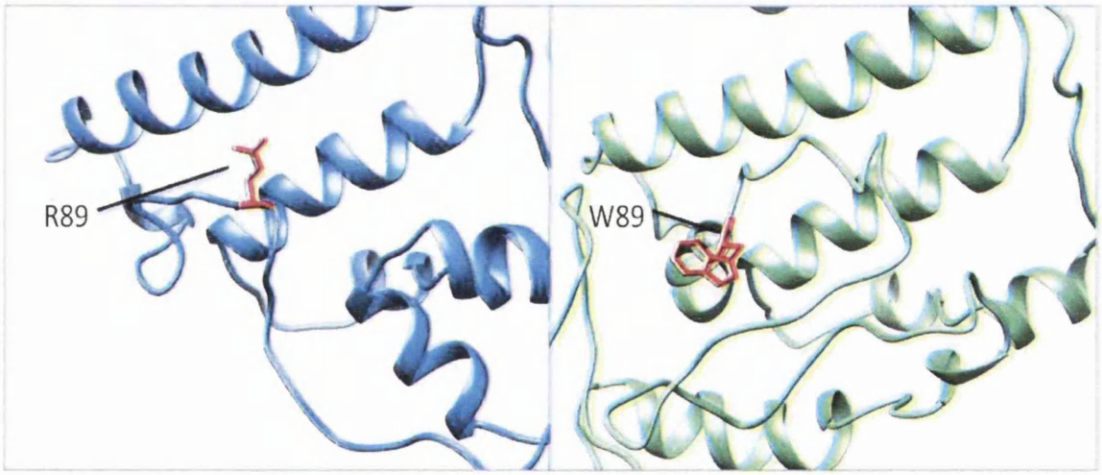

Figure 5.25 Predictive 3D structural modelling of the variant GAD67$^{p.R89W}$ compared to its GAD67 wild-type. The predicted structure of the wild-type protein seems not to largely differ from its corresponding variant protein, however the amino acid side chains show a distinct difference in residue structure, mass, direction and polarity. Inward facing arginine is replaced by the larger nonpolar heterocyclic residue tryptophan which extends away from the enzyme mass.

3D structural modelling of the variant GAD67$^{p.Y127F}$ compared to its GAD67 wild-type protein structure was shown in figure 5.26. Although limited changes to the overall protein were observed, the amino acid change from tyrosine to phenylalanine shows a decrease in mass due to the loss of a hydroxide molecule. Slight changes were also identified in relation to the positioning of the residue side chain as well as a change in polarity from uncharged to nonpolar.

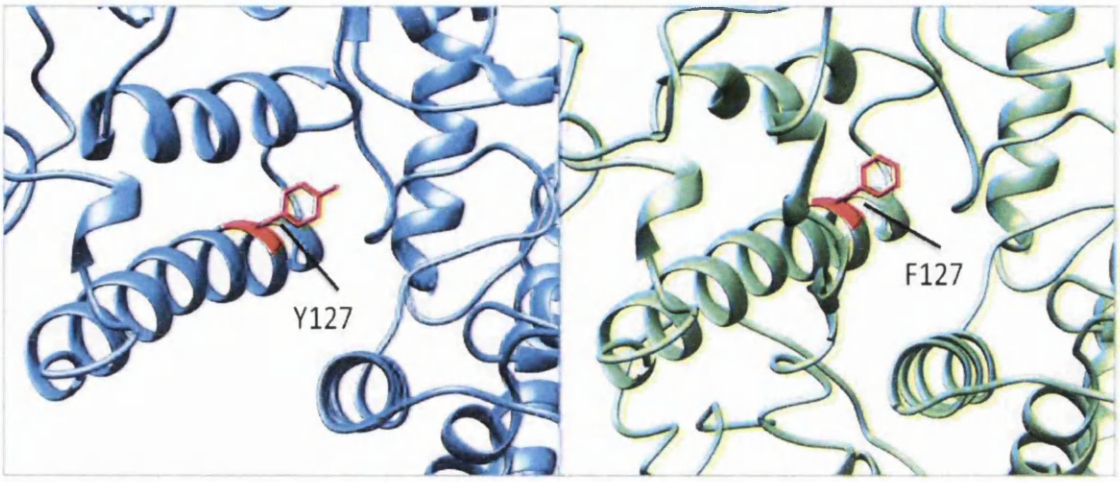

Figure 5.26 Structural 3D homology modelling of the variant GAD67$^{p.Y127F}$ compared to the GAD67 wild-type. The variant sequence compared to wild-type showed slight changes in positioning of the residue side chain and mass as well as a changed in polarity from uncharged to nonpolar.

5.9 Creating Gene-Expression Constructs

To assess the functional effect of each variant, a series of gene constructs were created from sequence validated wild-type constructs for GAT1, GAT3, GAD65, GAD67 as described in Chapter two (Figure 5.27). Following mutagenesis and further sequencing validation, 18 mutation constructs were generated through a miniprep and maxiprep pipeline.

The GABAergic missense variants and wild-type sequences as well as the GAT1 deletion variant p.S594Afs22X, were all sequence validated to ensure no other nucleotide changes had occurred during mutagenesis and cloning steps. The sequences for the identified variants and their corresponding wild-type s for the four genes analysed can be seen in figures 5.28, 5.29, 5.30 and 5.31. Once validated, all the wild-type and mutation constructs were transiently transfected into HEK cells to detect intracellular expression and confirm successful production of their protein.

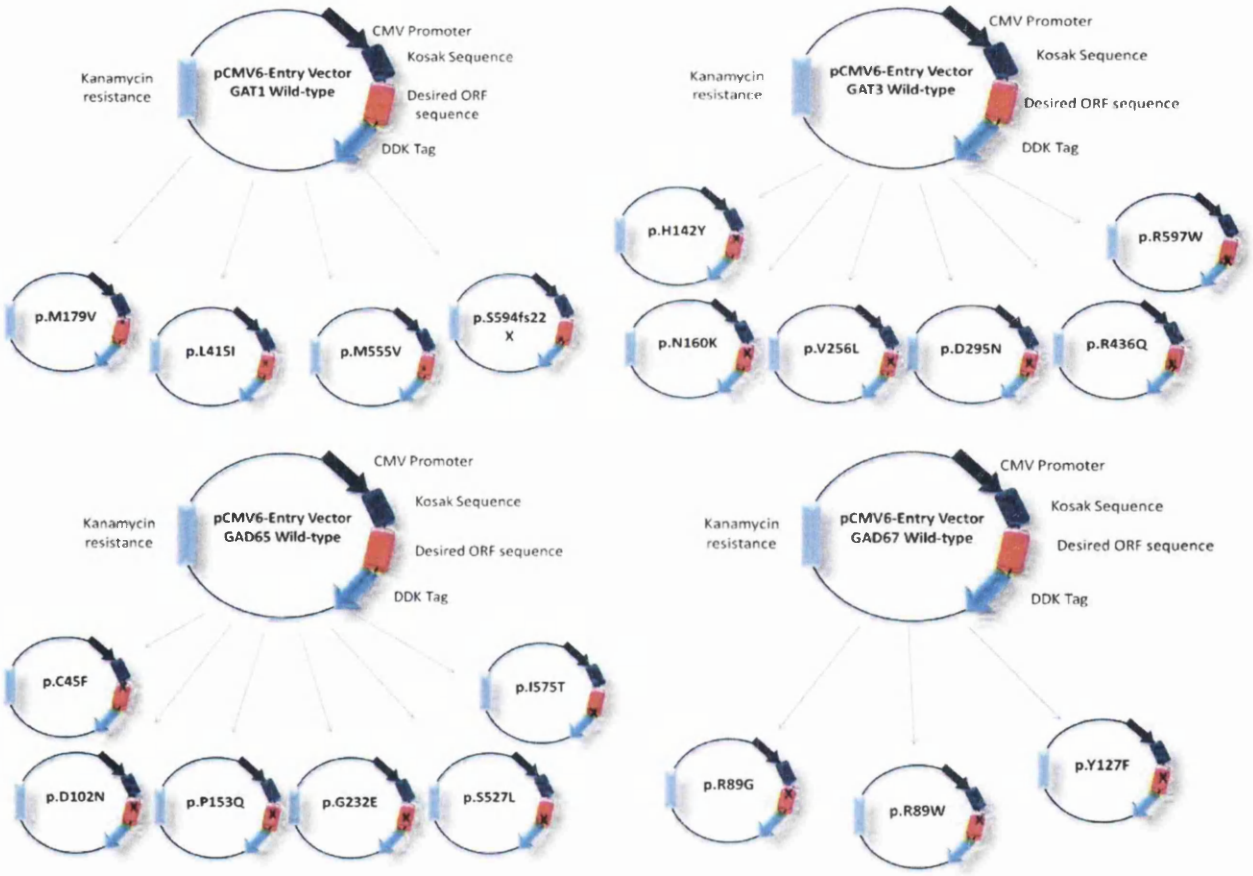

Figure 5.27 Construct generation. An overview of wild-type constructs containing the open reading frames of the GABAergic genes which were then mutated to reflect the variants found in this study.

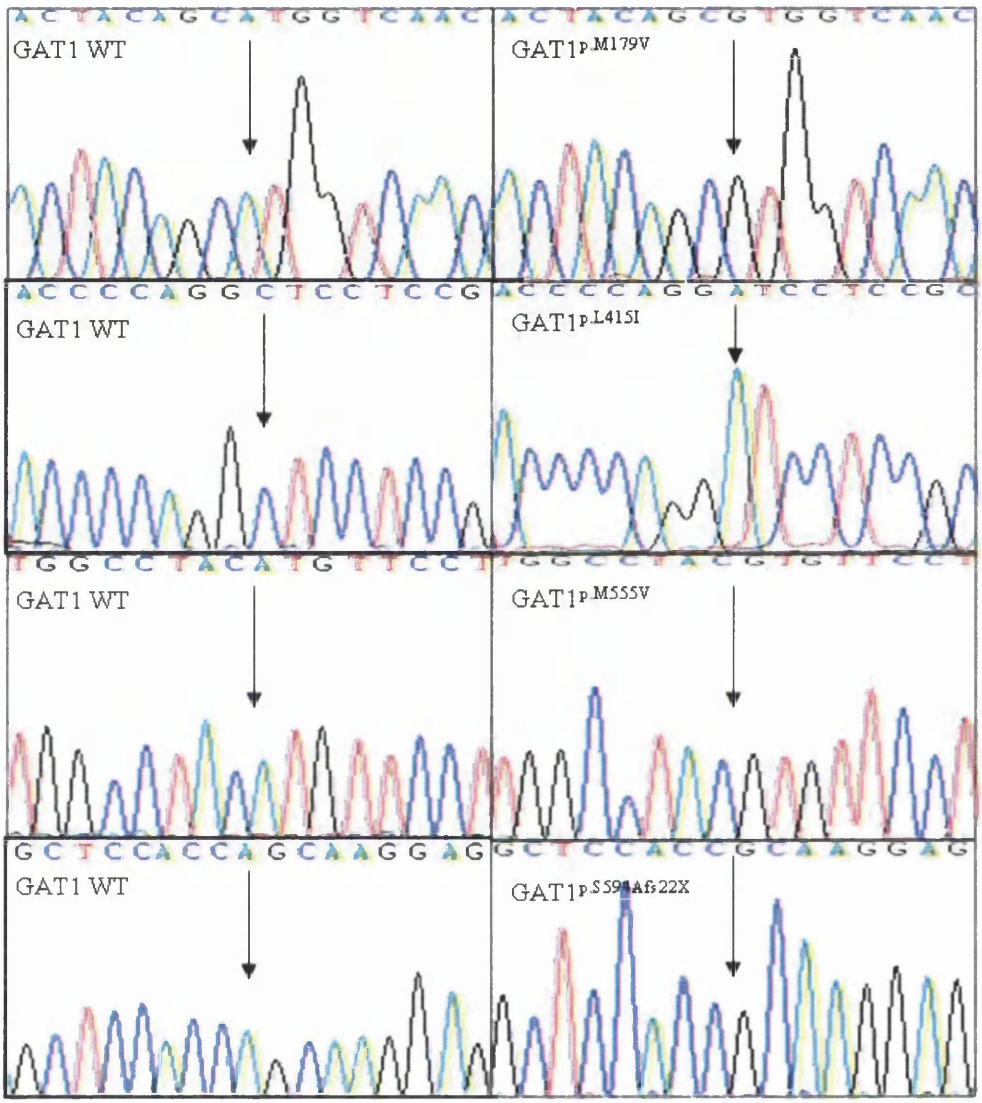

Figure 5.28 GAT1 mutation-construct sequencing results. Mutagenesis steps introduced or removed a nucleotide to create the variant sequence. Transformation into bacteria allowed the amplification of the variant sequence which was purified and sequence validated. The single stranded variant sequence is shown with its corresponding wild-type sequence.

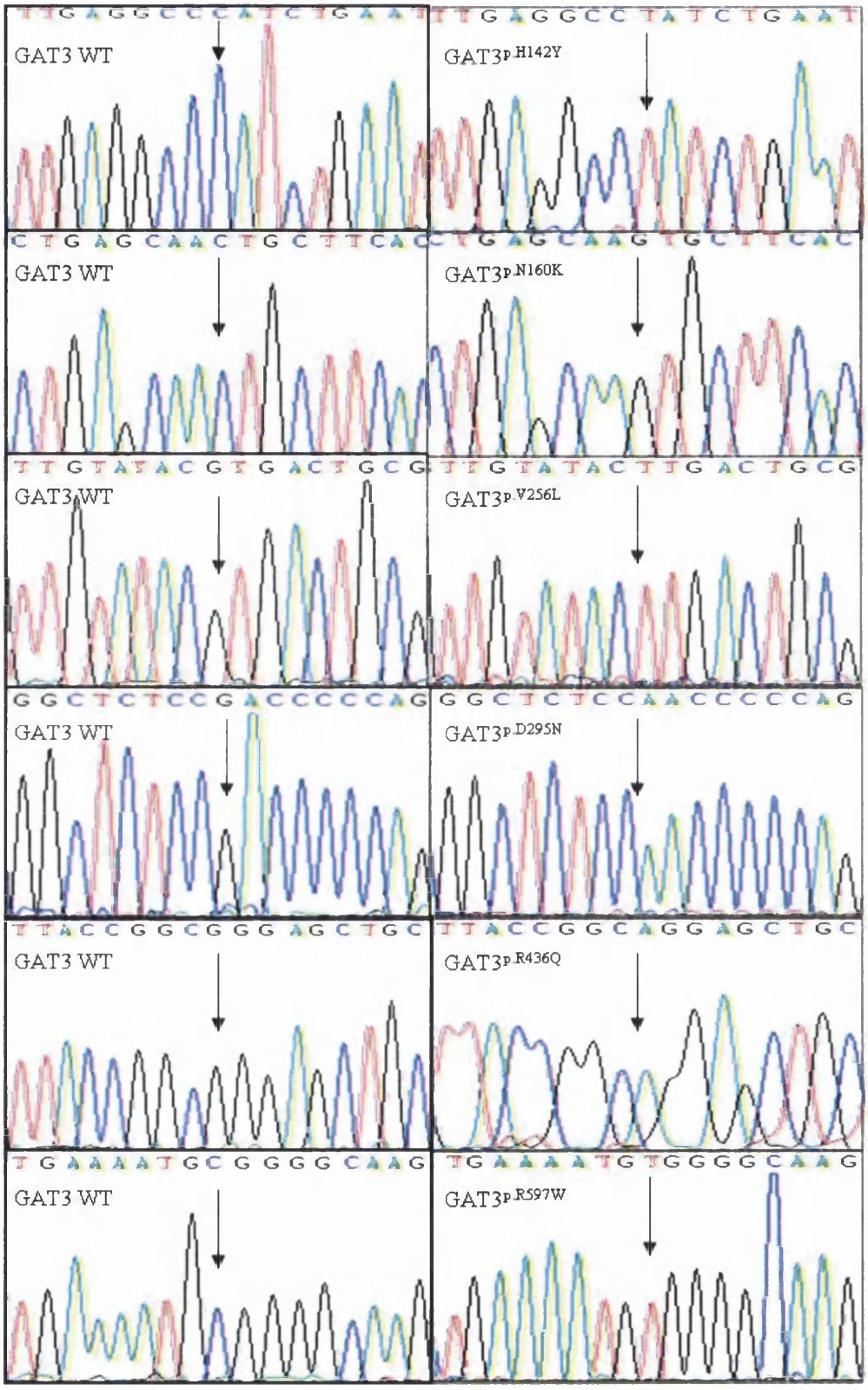

Figure 5.29 GAT3 mutation-construct sequencing results. Mutagenesis and transformation stages as demonstrated in chapter two allowed the introduction of selected variants into the GAT3 wild-type construct sequence. This figure shows the sequencing validation results that demonstrated successful establishment of the nucleotide changes into the sequence and the corresponding wild-type sequences.

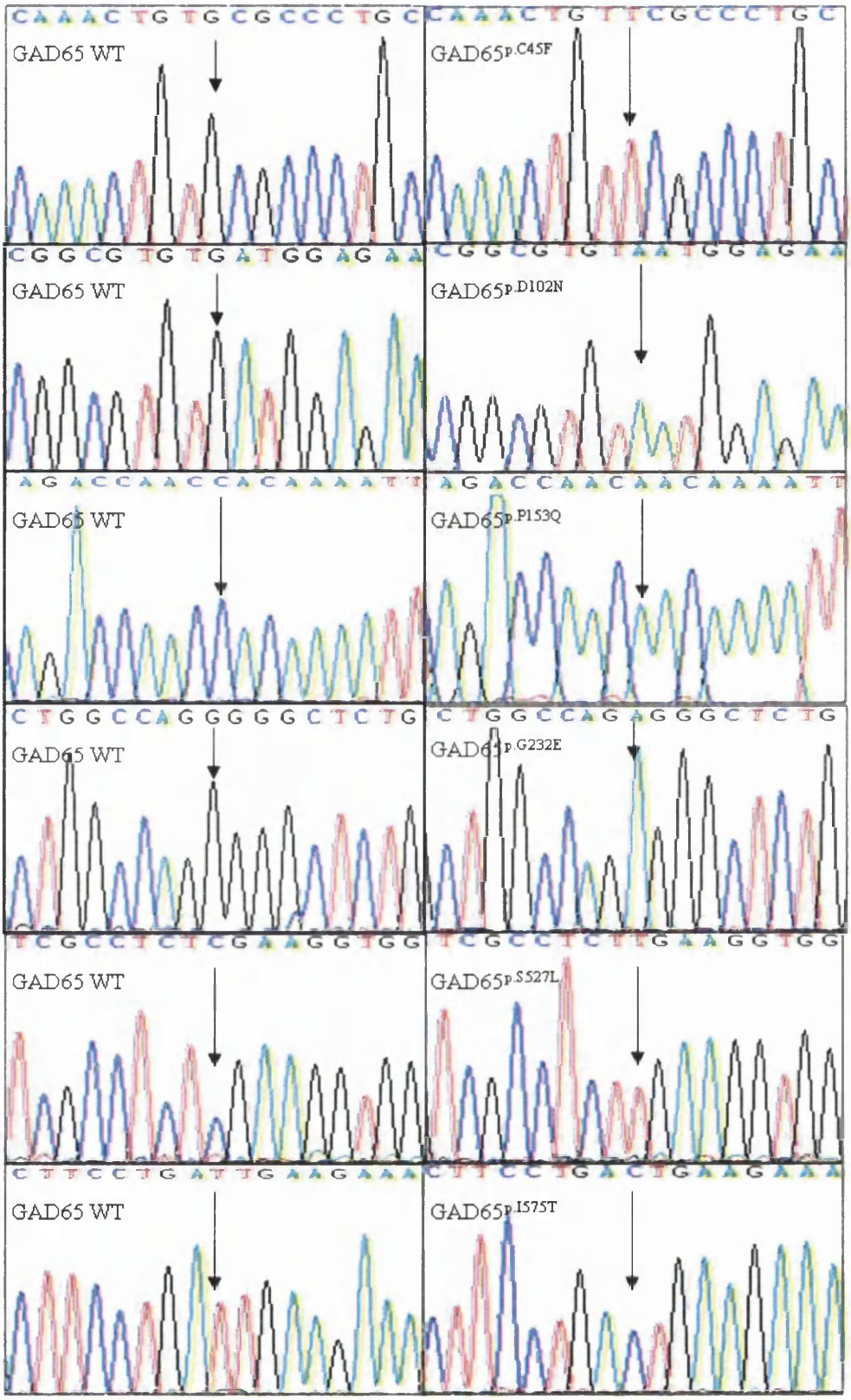

Figure 5.30 GAD65 mutation-construct validation by sequence analysis. GAD65 gene constructs were sequence validated following insertion of desired variants into vectors by mutagenesis and transformation (as described in chapter two). This figure shows the variants sequence and its corresponding wild-type sequence.

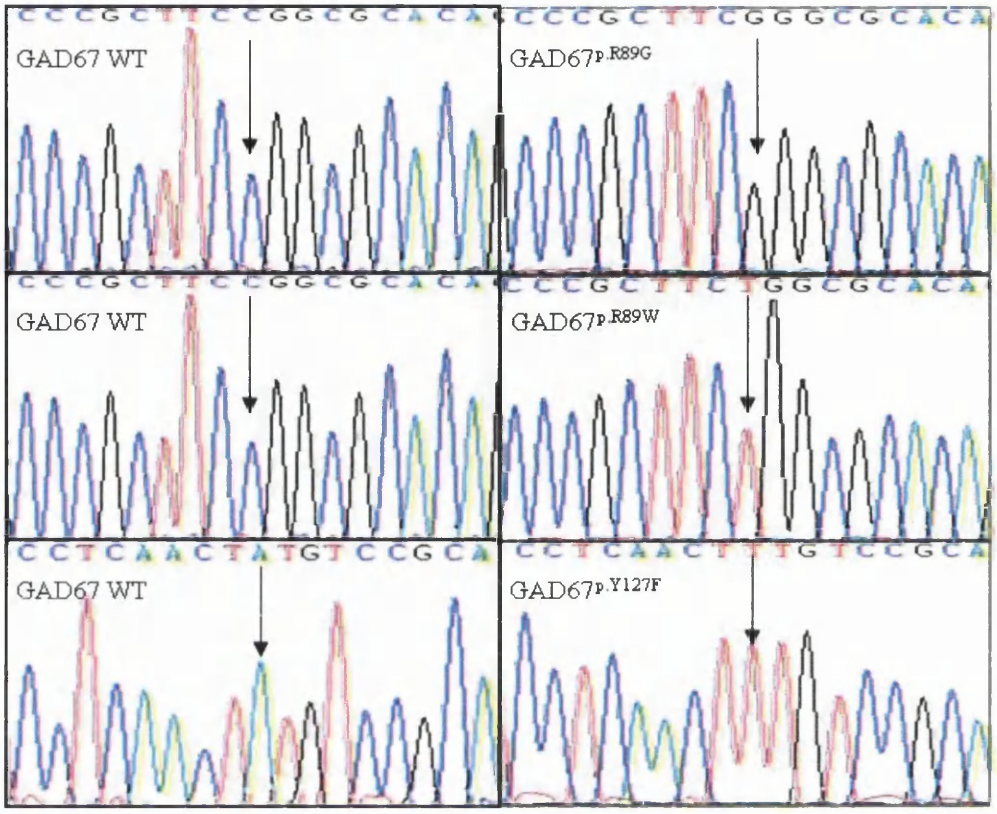

Figure 5.31 GAD67 gene mutation-constructs. Sequencing results of GAD67 variant constructs and their corresponding wild-type s. The variants identified in this study were inserted into vector sequences by mutagenesis before transformation into bacteria for amplification. Sanger sequencing allowed for validation of the variant.

5.6 Variant expression in HEK293 cells.

Mutant expression constructs were created for each missense variant identified in this study (as outlined in chapter two) from their genetic wild-type clones, by site-directed mutagenesis. The DDK tagged wild-type and variant vectors were transfected into cultured HEK293 cells before being fixed with paraformaldehyde and stained with monoclonal mouse anti-DDK primary antibody and anti-mouse 488 secondary antibody. The stained HEK293 cells were imaged using confocal microscopy at x63 magnification and 2x digital zoom. Wild-type constructs for each gene were firstly imaged and the optimal gain level was kept constant for all the gene variants for comparison.

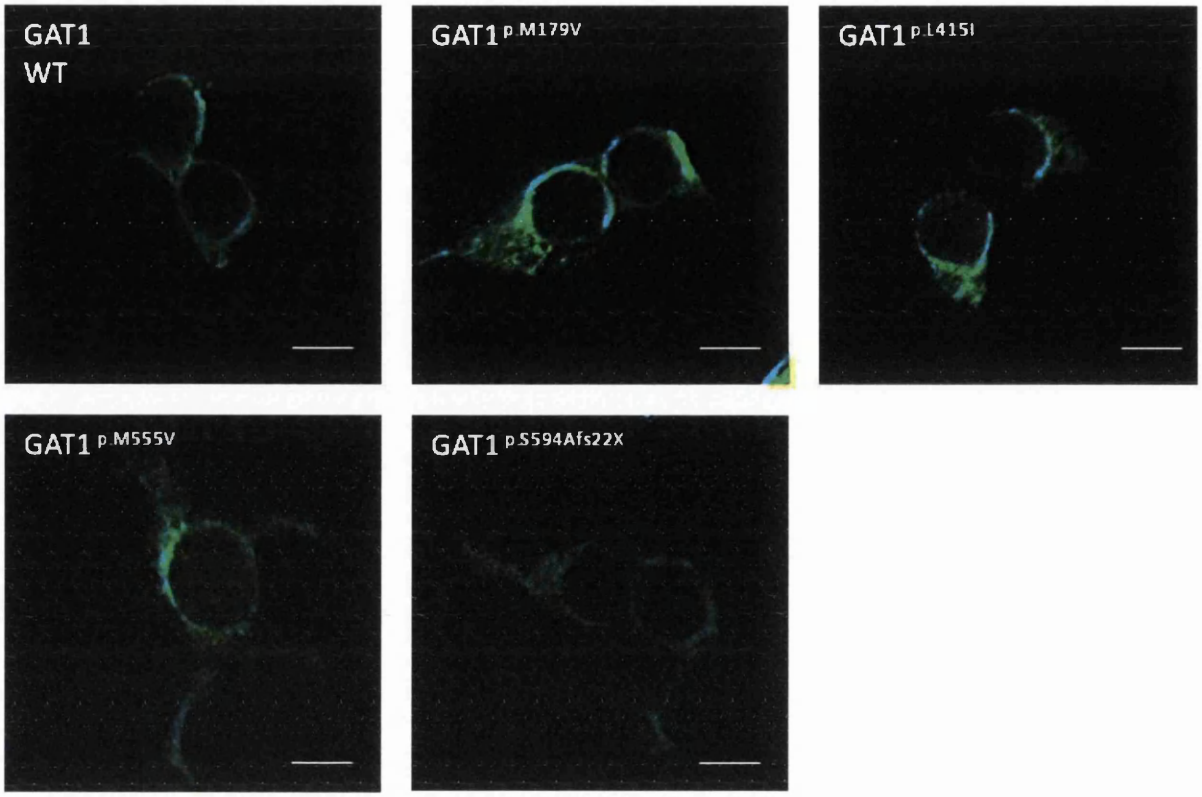

Figure 5.32 GAT1 wild-type and variant expression in HEK293 cells. Cultured HEK293 cells were transfected with C-terminal DDK tagged GAT1 wild-type and variant expression constructs. The expression was visualised using confocal microscopy following fixation and staining. Bar = 10μm.

GAT1 wild-type construct was transfected into HEK293 cells and intracellularly stained. As can be seen from figure 5.32, the GAT1 wild-type protein is expressed intracellularly. This image also demonstrates that the three missense variants ($GAT1^{p.M179V}$, $GAT1^{p.L415I}$ and $GAT1^{p.M555V}$) and the deletion variant ($GAT1^{p.S594Afs22X}$) proteins are also expressed intracellularly. The images show that there is high expression levels surrounding the nucleus and lower expression levels in the extremities of the cells.

The confocal microscopy images of GAT3 wild-type and variants show that the GAT3 protein is expressed intracellularly and the expression level is unaffected by any of the variants that have been inserted. As with GAT1 variants expression seems to be most prominent surrounding the nucleus of the cell and is less concentrated in the extremities (Figure 5.33).

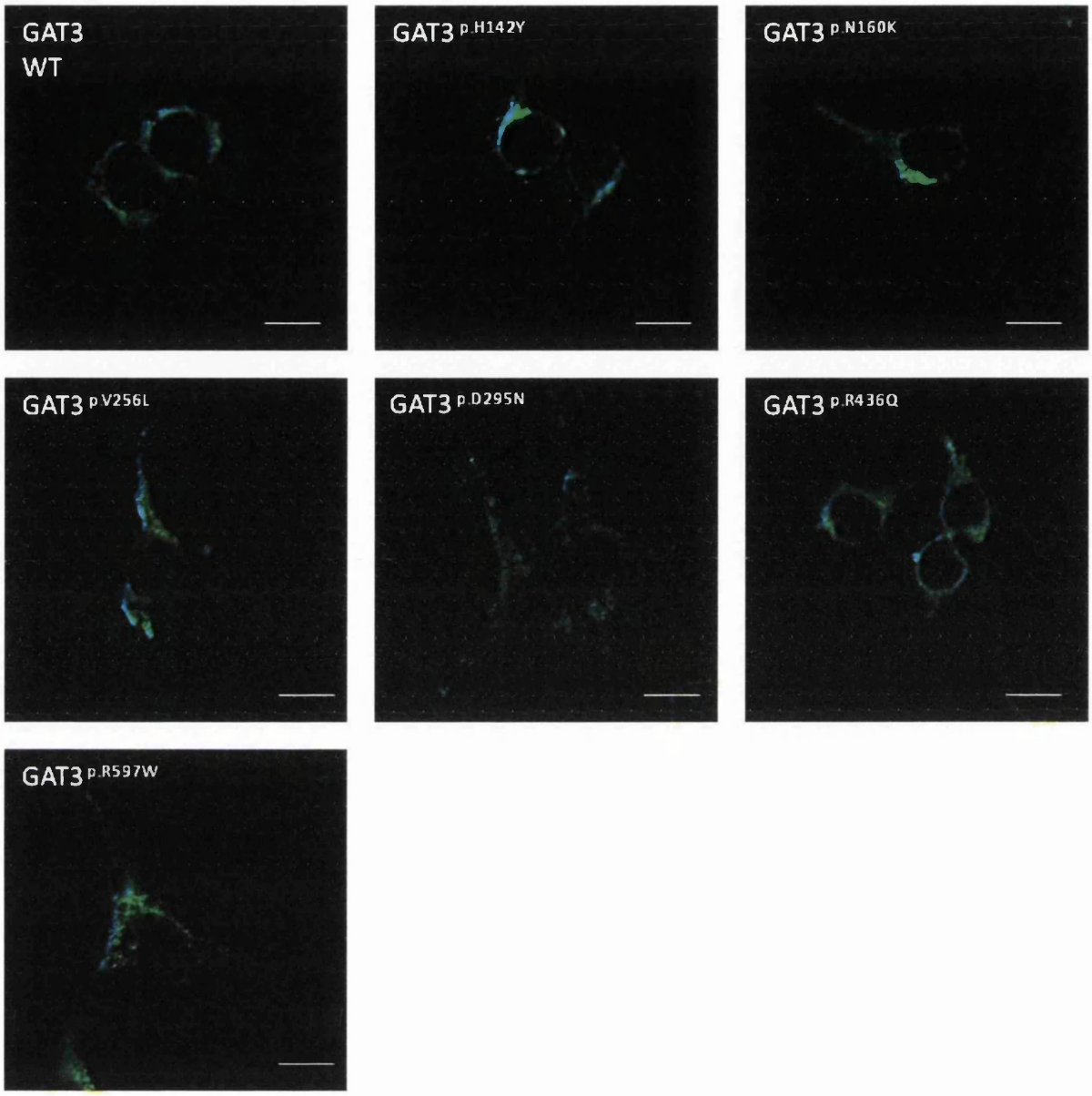

Figure 5.33 GAT3 wild-type and variant expression in HEK293 cells. HEK293 cells were transfected with the GAT3 wild-type and the six GAT3 variants identified in this study (p.H142Y, p.N160K, p.V256L, p.D295N, p.R436Q and p.R597W). The cells were intracellularly stained for the GAT3 protein and expression levels were examined under confocal microscope. GAT3 wild-type and variants were seen to be expressed intracellularly. Bar = 10μm.

To ensure the GAD65 variants identified were expressed intracellularly, GAD65 wild-type as well as the six GAD65 variant constructs (p.C45F, p.D102N, p.P153Q, p.G232E, p.S527L and p.I575T) were transfected into HEK293 cells. Following intracellular staining, the cells containing variant proteins were visualised via confocal microscopy and compared to wild-type. Figure 5.34 shows that all GAD65 variants were expressed and as with the wild-type, a predominant amount of expression occurred perinuclearly whilst some expression was witnessed in the extremities of the cell.

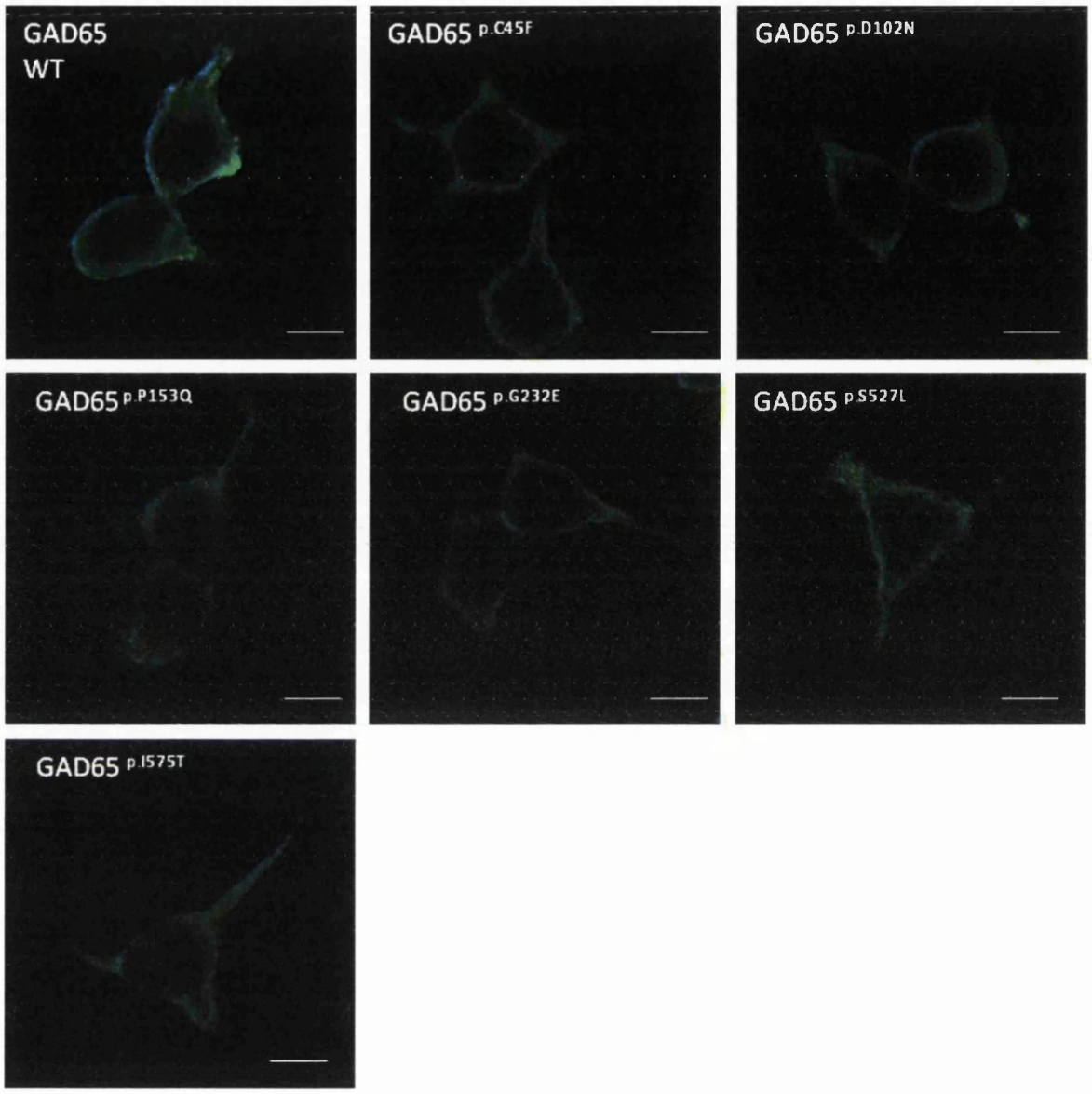

Figure 5.34 GAD65 wild-type and variant expression in HEK293 cells. HEK293 cells were transfected and stained for the GAD65 wild-type protein as well all the six GAD65 variants identified in the study. It can be seen that GAD65 wild-type is expressed throughout the cells predominantly around the nucleus. The variants also express GAD65 and this can be seen surrounding the nucleus and less concentrated in the extremities of the cell. Bar = 10μm.

Images were created for GAD67 wild-type and the GAD67 variants (p.R89G, p.R89W and p.Y127F) in the same way as for the other three genes. Intracellular staining revealed that GAD67 wild-type , $GAD67^{p.R89G}$, $GAD67^{p.R89W}$ and $GAD67^{p.Y127F}$ were expressed intracellularly. As seen with the other genes, the majority of expression occurs surrounding the nucleus whilst some expression can also be observed in the extremities (Figure 5.35).

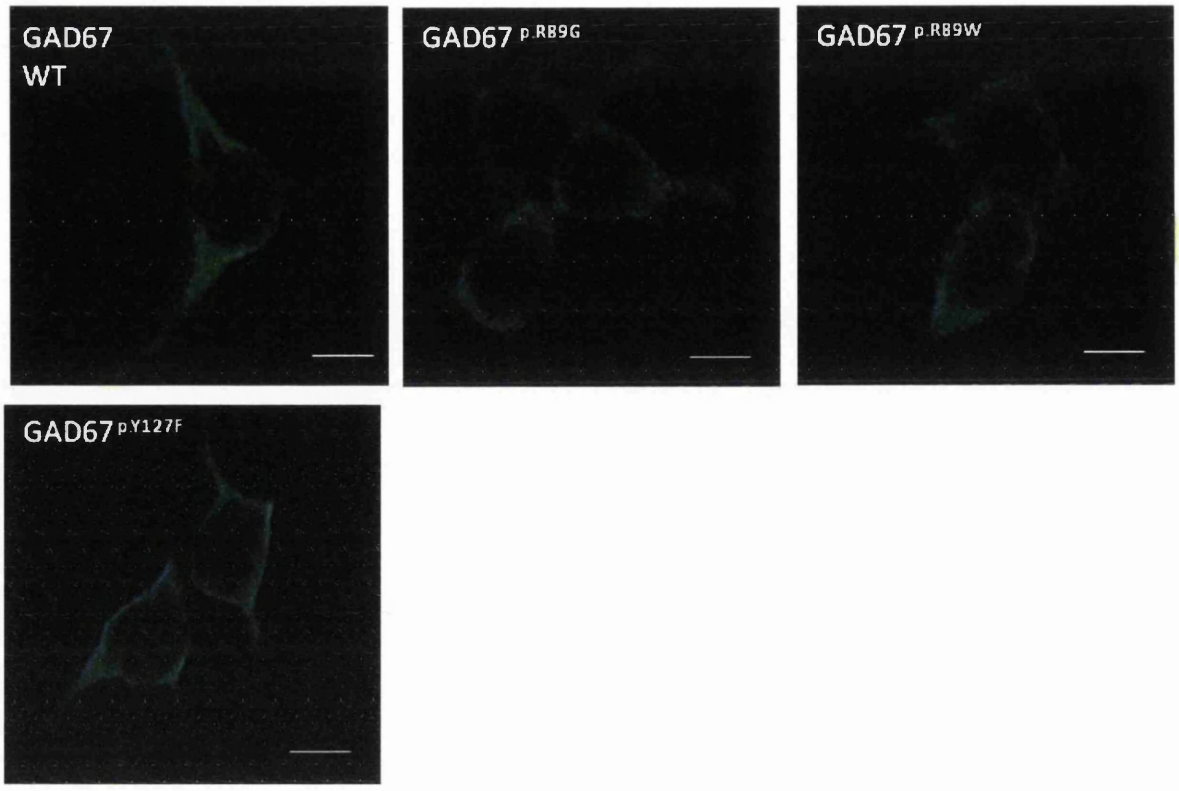

Figure 5.35 GAD67 wild-type and variant expression in HEK293 cells. Following transfection of GAD67 wild-type and variant constructs into HEK293 cells, the cells were stained and imaged via confocal microscopy. The figure demonstrates that GAD67 wild-type is expressed intracellularly as are the variant proteins. Bar = 10μm.

5.7 Utilising genetic constructs

Figures 5.32 to 5.35 demonstrate that the selected proteins are expressed following transfection into HEK293 cells. This information provides a firm platform for the use of the constructs in further analysis, to assess the pathological consequences of the variants identified in the GABA transporters and enzymes.

The GABA transporter constructs could be further examined via their transfection and extracellular staining of cells, to determine the success of transport of the protein. If proteins do reach the cell membrane, electrophysiology analysis could be carried out to determine the efficiency of the protein and determine whether the variant causes a pathological state in this way. Transfection of both GABA transporters and enzymes into cells provides useful information on variant consequence; transfection of constructs into animal models however would also provide a valuable insight into the pathophysiology of variants.

Quantitative enzymatic assays would be a valuable tool for measuring the efficiency of GABAergic enzymes. This assay would determine the activity levels of the enzyme and identify whether the variants cause a decrease in function as predicted. A splicing assay would be an accurate method for determining whether the splice site variant preceding exon three in the GAT1 gene causes changes to splicing. A splice construct would need to be created using an exon trap vector as opposed to the entry vector used for missense variants.

5.8 Summary of protein analysis of GABAergic variants

Exon mapping shows that in all, the variants identified in this study occur in highly-conserved amino acid residues, which occur in crucial domains of the protein. These domains are believed to be involved in the normal function of the protein. *In silico* analysis demonstrated that variants caused changes at a protein level by causing structural changes which in some cases had knock on effects to upcoming amino acids, such as $GAT1^{p.M179V}$, which causes alteration to glycosylation sites of the protein upstream. Variants also cause alteration in side chain size, protrusion, direction and polarity, which could have detrimental effects on protein function. Gene constructs were created for GABAergic variants for immunocytochemisty analysis. Immunocytochemistry results show that the missense variants identified in this study in all four genes were expressed intracellularly.

Chapter Six

Discussion

The GABAergic system has been studied extensively over the last few decades combining genetics, biomarker, molecular animal models, and imaging datasets. No gene variations, however, have been identified in GABA transporters *GAT1* and *GAT3* nor the GABA synthesising enzymes *GAD65* and *GAD67* in relation to epilepsy. Animal models of *GAT1* and *GAD65* show evidence of epileptogenesis and a susceptibility to seizure, which gives reason to believe that variants in these genes and their closely-related genes *GAT3* and *GAD67* are potential targets as valid candidates in human epilepsy (Conti et al., 2004, Asada et al., 1996). This is supported by the importance of GABAergic inhibition in the human brain and clear evidence relating to mediators of regulatory cycles of sleep, consciousness, and neural networks e.g. thalamo-cortical networks.

Given the evidence outlined in Chapter One the screening of these four GABAergic genes in genetic generalised epilepsy patient samples is justified as a start point to test the hypothesis. This chapter will aim to analyse and interpret the outcomes of the previous results as well as to indicate any further work that could be carried out to identify the pathogenic functional consequences of the identified GABAergic variants. Any limitations that were encountered in the study have been highlighted given the revolution in genetics/genomics.

6.1 Variant detection rate in GGE

The genetic screening of *GAT1, GAT3, GAD65* and *GAD67* resulted in the identification of 20 variants, which were identified in 48 of the 707 epilepsy patient samples screened; representing a patient detection rate of 6.8%. Eighteen patients had variants that were identified in GABA transporters representing a detection rate of 2.5%, whilst 30 gene variants were identified in GABAergic enzymes representing a detection rate of 4.24%. All variants identified in this study were found in patients that have a diagnosis of GGE with a high incidence of absence seizures and is the subject of

another clinical PhD. The GABAergic variants were generally not present in control populations (novel) with some having a rare population frequency (rare variant), which were supported by phylogenetic conservation alignments. On-line mutation predictive tools were used to predict damaging consequences of variants using principles of conservation, structure, composition or polarity.

In addition to the *in silico* methods to assess gene-variants, structural modelling was used as another predictive source of pathogenicity evidence and has been integrated into the arguments below. Furthermore, expression mutant constructs were prepared from wild-type GAT1, GAT3 GAD65, and GAD67 clones. The validation of expression in Chapter Five was demonstrated by immunocytochemistry in transiently transfected HEK293 cells and provides the springboard to *in vitro* functional analysis as outlined in Further Work (Section 6.8).

6.2 Putative consequences of GAT1 and GAT3 variants

6.2.1 Variants in pincer formation of transporters

Heterozygous variants GAT1$^{p.L415I}$, GAT3$^{p.V256L}$ and GAT3$^{p.R436Q}$ were identified as part of this thesis, in the pincer like formation of the transporters, which corresponds to transmembrane domains 4, 5, 9 and 10. This region is responsible for protein stability and holding the substrate and ion binding regions in position (Yamashita et al., 2005). Previous studies of other disease-causing SLC6 family transporters show that variants in this region cause decreased transporter activity due to trafficking defects (Hahn and Blakely, 2007, Hahn et al., 2003).

The first disease-associated variant identified in the transporter family *SLC6*, was p.A457P in the Norepinephrine transporter (NET) gene SLC6A2; which was identified by Hahn et al., (2003). This amino acid change caused increased levels of plasma NE due to decreased transporter activity believed to result in elevations in standing-induced heart rate. Multiple cell lines showed that there was a decrease in human NET at the cell membrane compared to wild-type as a result of diminished protein created by p.A457P; which was confirmed by western blot analysis of COS-7 cells. As well as decreased

levels of the variant protein, a dominant negative effect was also exhibited on wild-type transporters (Hahn et al., 2003).

Hahn et al., (2003) identified that the co-transfection of the wild-type protein and p.A457P in COS-7 cells showed a decreased uptake of 60.9% of NE levels compared to when only wild-type was transfected. Western blot analysis showed that there was a 50% decrease in wild-type expression at the cell membrane when co-expressed with the variant protein compared to wild-type only transfection. This suggests that the abnormal trafficking of p.A457P influences the trafficking of human NET wild-type to the plasma membrane (Hahn and Blakely, 2007, Hahn et al., 2003).

Animal models support this theory and show that the heterozygous variant p.A457P causes significant decreases in transport activity in the atria and ventricles of the heart, as well as a 60% decrease in transport levels in the cortex and hippocampus compared to NET wild-type mice (Shirey-Rice et al., 2013). Compared to NET knock-out mice, p.A457P mice maintain high levels of expression of non functioning protein which influences the function of normal transporters; knock-out mice do not express significant changes in NE transport (Shirey-Rice et al., 2013).

It can be hypothesised therefore from previous analysis of NETs, that the variants identified in this thesis, in the pincer like formations of GABA transporters, could cause a decreased uptake of GABA due to trafficking defects which cause a dominant negative effect on wild-type transporters. Decreased GABA uptake into the pre-synapse would result in increased GABA levels in the synaptic cleft.

6.2.2 Variants in the substrate binding domain of transporter

Missense variants GAT1$^{p.M179V}$, GAT3$^{p.H142Y}$ and GAT3$^{p.N160K}$ as well as the GAT1 splice variant IVS3+1 were identified in the substrate binding region (transmembrane domains 3 and 8) of their corresponding transporters (Bismuth et al., 1997, Tamura et al., 1995). Other disease-associated *SLC6* family transporters suggest that variants in this region cause changes in levels of substrate binding, resulting in altered transport levels (Kilic et al., 2003). It has also been identified that glycosylation sites are retained

in this region and alteration to this site can cause trafficking defects, again resulting in changes in membrane transport (Cai et al., 2005) (Hahn et al., 2005).

Variants have been identified in the serotonin transporter SLC6A4 (SERT), which cause psychiatric disorders such as OCD, anorexia nervosa and Asperger's syndrome, due to enhanced transporter activity (Kilic et al., 2003). This enhancement occurred in a study by Kilic et al., (2003) as a result of the variant p.I425V and was identified via western blot analysis. It was demonstrated that this increased activity was due to enhanced binding as a result of up to a 40% increase in maximum binding sites, and along with a large decrease in dissociation constant, a higher binding affinity for the mutant was created compared to wild-type (Kilic et al., 2003).

If this increase in transporter activity causes such effects due to a single point mutation, it gives reason to believe that the variants of similar regions identified in the research carried out for this thesis could have the same effects. This would result in decreased GABA levels in the synaptic cleft and a subsequent reduction in inhibition. This inability to inhibit the excitation of the post-synaptic nerve terminal could result in excessive excitation and ability to seizure.

6.2.3 Variants affecting glycosylation of transporters

Variant GAT1$^{p.M179V}$, as mentioned previously, occurs in the substrate binding domain of the protein. The variant also occurs amongst the three glycosylation sites Asn176, Asn181 and Asn184 (Bismuth et al., 1997). The glycosylation sites are involved in the management of the physicochemical and biological properties of the protein which include protein folding, stability, targeting and ligand binding. The transport activity and surface expression of neurotransmitters is controlled by glycosylation (Bismuth et al., 1997). As demonstrated by figure 6.2, GAT1$^{p.M179V}$ appears to cause significant changes to the glycosylation site positioning, as well as the whole extracellular loop, following the variant amino acid.

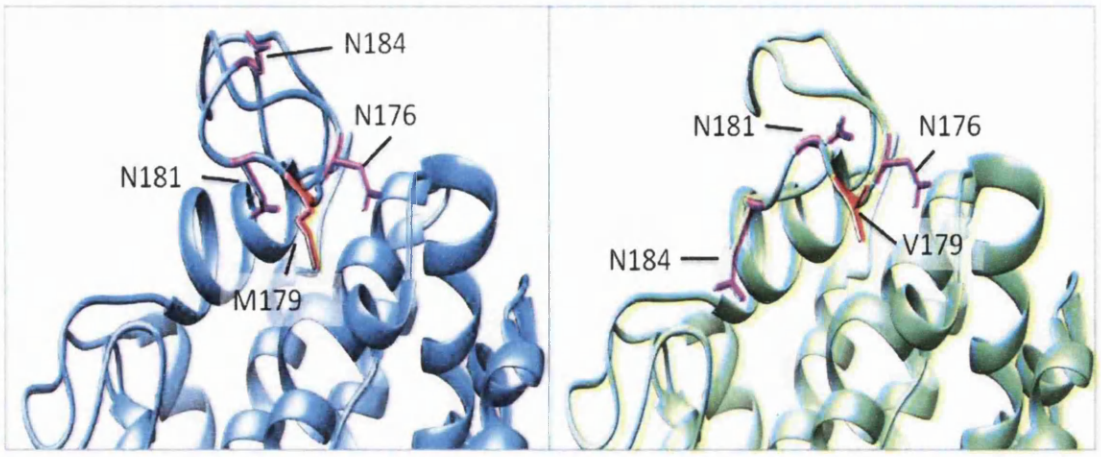

Figure 6.2 3D structure of GAT1$^{p.M179V}$. Chimera analysis created the predicted protein consequences of an amino acid change from methionine to valine at amino acid position 179. The variant has knock on effects that change the shape and overall positioning of glycosylation sites of the protein.

Interruption of glycosylation via genetic variation has been studied by Cai et al., (2005), who identified via GABA uptake assays that GABA uptake in mutant proteins was significantly reduced by *GAT1*. Kinetical analysis of GAT1 wild-type and variant transporter showed that changes to glycosylation sites cause trafficking defects, preventing GAT1 from reaching the cell surface (Cai et al., 2005).

Other variants identified in *SLC6A2*, have been associated with disruption of the glycosylation of the transporter, which has had a knock on effect and interfered with the surface trafficking of the protein (Hahn et al., 2005). Variant p.A369P of extracellular loop six and p.N292T of transmembrane domain five of NET have been identified via sequencing analysis (Hahn et al., 2005). Human NET wild-type and variant constructs were transfected into COS-7 cells to assess the influence of the variants identified on transporter expression, which was measured by immunoblotting. p.A369P transporters were unable to carry out any transport activity of both NE and dopamine (DA), whilst N292T showed a decrease in transport activity. Biotinylation and western blot analysis showed an intense decrease in human NET wild-type at the surface and in total for both variants, suggesting a dominant negative effect by the variants. The NE transporter variants mentioned, cause decreased transporter activity resulting in diseases associated with pathogenic heart rates, such as long QT syndrome (Hahn et al., 2005).

It could therefore be hypothesised that the variant p.M179V identified in *GAT1* as part of this thesis, will cause the protein to have trafficking defects resulting in a lack of

transporters reaching the cell membrane. The level of decreased activity seems to vary amongst amino acid changes so it would be difficult to speculate whether a complete loss of function or reduced levels would be witnessed. However it is likely that p.M179V will cause a decrease in GAT1 wild-type at the cell membrane due to a dominant negative effect, resulting in reduced GABA uptake from the synapse.

6.2.4 Variants in Ion binding region of transporters

$GAT3^{p.D295N}$ resides in the extracellular loop preceding transmembrane domain six which along with transmembrane domain one, forms the ion binding site of the protein (Hansra et al., 2004). The ion binding site along with the substrate binding site (transmembrane domains three and eight) form the central pore of the protein (Bismuth et al., 1997). GAT1 variants in the ion binding domain have been previously identified and have resulted in malfunctioning transporters and therefore a decreased level of GABA uptake was witnessed (Mager et al., 1996).

Mager et al. (1996) demonstrated via concentration and voltage-jump experiments that the variant p.W68L of *GAT1*, which resides in the central ring of the protein, causes a decrease in GABA uptake from the synapse (<5% compared to wild-type). Charge movements show that GAT1 wild-type binds two sodium ions followed by GABA, before releasing GABA intracellularly. Mutant transporter W68L and W68S causes sodium ions to bind tighter and at a faster rate whilst GABA is bound much looser compared to wild-type. As GABA is so poorly bound, the sodium ions remain bound for long periods of time, seized in the transporter resulting in slow release into the cell (Mager et al., 1996).

Although both the variant proteins and wild-type produce charge movements due to conformational changes, the final stage of GABA uptake which is carried out via a currently unknown mechanism is prevented, which would under normal circumstances release GABA into the pre-synaptic cleft. Immunocytochemistry results of the GABA analogue tiagabine binding to GAT1 in HeLa cells, support charge jump results and show that the variant protein W68L was expressed at approximately equal levels to wild-type, however, was functionally faulted (Mager et al., 1996).

It could be hypothesised that GAT3$^{p.D295N}$ could cause alteration in sodium binding, which would lead to the loose binding and lack of GABA uptake from the synapse. Slowed GABA uptake due to variant transporters would result in a build up of GABA in the synapse and decreased GABAergic inhibition.

6.2.5 C-terminal domain of transporters

Deletion variant GAT1$^{p.S594Afs22X}$ was identified in the C-terminal domain of GAT1 of this thesis. The C-terminus is responsible for trafficking, stability and degradation of the protein (de Juan-Sanz et al., 2013). Large alterations in the C-terminal domain sequence, such as the amino acid changes caused by GAT1$^{p.S594Afs22X}$ have been identified to cause disease. Variants of the creatine transporter *SLC6A8* have also been associated with diseases such as X-linked mental retardation (Rosenberg et al., 2004).

Rosenberg et al, (2004) reported by DNA sequence analysis on a panel of 290 unrelated families with X-mental retardation, the insertion Y1378X in *SLC6A8*. This variant affects transmembrane domains 7-12, causes a premature stop codon and changes the length of the C-terminus. It is suggested that this premature stop codon causes unstable or inappropriate folding, resulting in the protein becoming inactive (Rosenberg et al., 2004). GAT1$^{p.S594Afs22X}$ identified in this thesis causes the removal of the stop codon and the addition of 22 amino acids, to the final exon of the protein causing changes to the length of the C-terminal. Comparison with the results from the creatine transporter gives reason to suspect that the additional amino acids will cause changes to the folding of the protein as well as the stability, resulting in the protein becoming inactive (Rosenberg et al., 2004).

GAT1$^{p.M555V}$ and GAT3$^{p.R597W}$ were also identified as part of this thesis in the C-terminal domain. Limited research has been carried out in other membrane transporters, which directly correspond to theses amino acid regions. As these variants are novel in this population it could be predicted from chimera analysis as well other predictive tools that the amino acid changes would have an effect on the protein trafficking, stability and

degradation. This could result in alterations in transporter activity and cause changes in GABA levels in the synaptic cleft.

6.3 Putative consequences of *GAD65* and *GAD67* variants

6.3.1 N-terminal domain of *GAD65* and *GAD67*

$GAD65^{p.C45F}$, $GAD65^{p.D102N}$, $GAD65^{p.P153Q}$, $GAD67^{p.R89G}$, $GAD67^{p.R89W}$ and $GAD67^{p.Y127F}$, identified in this thesis, all occur in their respective N-terminal domains. The N-terminal domain is essential for the dimerisation of two monomers to create a functional protein (Fenalti et al., 2007). Human genetic screening by Lin et al., (2007), identified variant S41Y, in the N–terminal of tryptophan hydroxylase 2 in a highly conserved residue. Recombinant construct analysis demonstrates that there was a decrease in enzymatic activity when the amino acid change was introduced, compared to wild-type. This change in activity was suggested to occur as a result of alterations in regulatory level due to modifications in 3D structure (Lin et al., 2007).

The decrease in active tryptophan hydroxylase causes a reduced level of serotonin production. Abnormally low levels of serotonin synthesis by the enzyme tryptophan hydroxylase, is believed to be associated with ADHD. Sheehan et al., (2005) identified that the removal of the first 156 amino acids of the enzyme caused a decrease in the level of serotonin synthesis correlating to ADHD. It is possible therefore that this region could be equally as crucial in increasing enzymes synthesis of other neurotransmitters such as GAD65 and GAD67. This region corresponds to amino acid residues 185-190 and 199-203 of GAD65 and GAD67 respectively, when aligned (Sheehan et al., 2005). $GAD65^{p.P153Q}$ occurs before this region and could have an effect on the site as a proline change has such significant effects on the protein structure. As proline ordinarily causes a large fold in a protein, the removal of the amino acid would severely alter the shape of the protein, causing knock-on effects structurally downstream (Fu et al., 2003). If this variant causes changes to the structure at amino acid position 185, this could cause a reduction in the level of GABA production from glutamate. Decreased GABA

production could result in diminished inhibition at the post-synaptic nerve terminal causing excessive excitation and seizure.

Proline residues act to slow down the process of folding especially if the proline caps an α-helix. This was witnessed by Fu et al. (2003), using FRET traces to show the refolding of proline mutants in serine hydroxymethyltransferase. GAD65$^{p.P153Q}$ identified in this thesis, also caps an α-helix (as shown in figure 6.3), and the amino acid change from proline to glutamine therefore is predicted to interfere with the rate of folding. This interference could result in insufficient folding and could render the protein inactive (Fu et al., 2003)

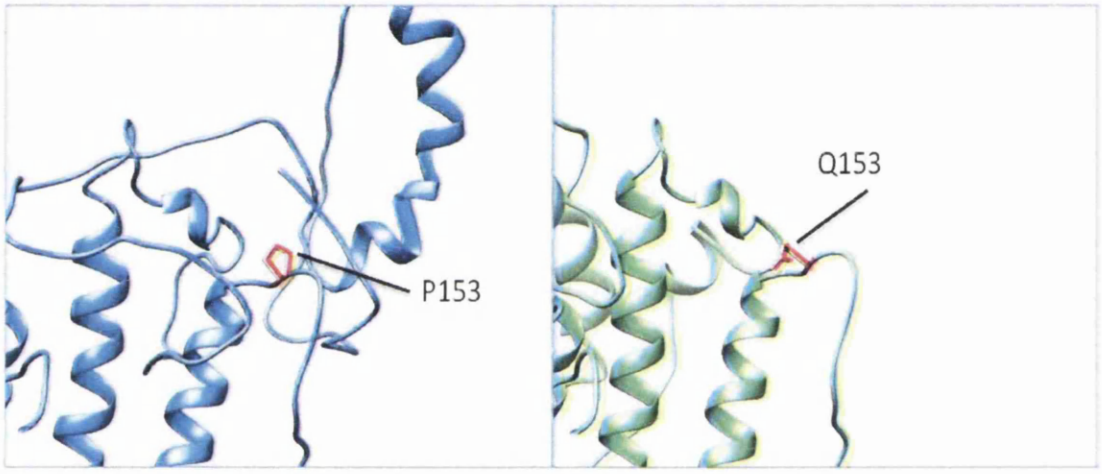

Figure 6.3 3D structure of wild-type and variant GAD65 protein p.P153Q. The 3D structure diagram of GAD65 wild-type shows that the proline residue appears before the α-helix. Clear differences can be seen between the proline side chain which has numerous bends and eventually turns back on itself and the glutamine side chain.

6.3.2 Variants of the C-terminal domain of GABAergic enzymes

This thesis identified variants GAD65$^{p.S527L}$ and GAD65$^{p.I575T}$ in the C-terminal domain of the protein. Fenalti et al., (2007) identified via crystal structure analysis that the highly mobile *GAD65* C-terminal is likely to contribute to the dynamic role of the catalytic loop in enzyme autoinactivation. They also derived that both the sequence of the catalytic loop and the C-terminal, to which it is packed against, is highly crucial for the modulation of the enzyme autoinactivation. The variant Tyr425 of the catalytic loop of *GAD65* was identified to completely eliminate GABA production. Mice models support this and show that variants in the C-terminal domain of neurotransmitter

synthesiser tryptophan hydroxylase can result in a 50-70% reduction of serotonin synthesis compared to wild-type (Posner and Petersen, 1990, Aston-Jones et al., 1999, Fenalti et al., 2007).

Genetic screening of human tryptophan hydroxylase-2 in 300 individuals in a psychosocial group identified the novel SNP, p.R441H (Zhang et al., 2005). This highly conserved variant protein was transfected into pheochromocytoma cells (PC12) and serotonin levels produced were calculated. It was identified that there was an approximately 80% reduction in serotonin levels produced compared to wild-type, demonstrating that the variant causes loss of function (Zhang et al., 2005).

Variants identified in this thesis in the C-terminal domain occur in highly conserved residues. With a current lack of such mouse models for GAD65 and GAD67, it is viable to suggest that the variants could cause a substantial reduction in the level of GABA synthesis. Fenalti et al., (2007) suggest that a single point variant in the C-terminal domain could result in alterations in GABA production. Decreased GABA production could result in decreased GABAergic inhibition at the post-synapse.

6.4 The GABAergic system and absence seizures

The patients with variants identified in this study in *GAT1*, *GAT3*, *GAD65* and *GAD67* had several forms of GGE phenotypes, however all 48 patients had a significant component of absence seizure presentation. Absence seizures are thought to be a genetically determined electro-clinical marker of GGE and are specifically detected by spike and wave electrical activity, primarily in the thalamo-cortical network. In turn, the specific cellular network between the thalamus and the pyramidal cells of the cortex are connected by excitatory (primarily glutamatergic) connections. GABAergic neurons are positioned evenly throughout the cortex and thalamus forming a network of inhibitory influence on excitatory networks and controlling rhythmic oscillations maintaining sleep and consciousness (Figure 6.3).

The impairment, potentially caused by the variants identified in this study, would result in changes in GABA levels and a decrease in the inhibition signal of GABAergic neurons. Excessive GABA levels in the synaptic cleft due to a decreased uptake by GABA transporters cause a pathological state by activating not only $GABA_A$ receptors but also by activating $GABA_B$ receptors, causing slow activating IPSP which would prevent the neuron from creating an action potential, therefore causing a decrease in oscillation frequency (Blumenfeld, 2003). This mechanism could cause the absence seizures experienced by the patients of this study which have variants in the GABA transporters by causing the transporter to become inactive, through an inability to reach the membrane or via a reversal of the transporter activity (Blumenfeld, 2003).

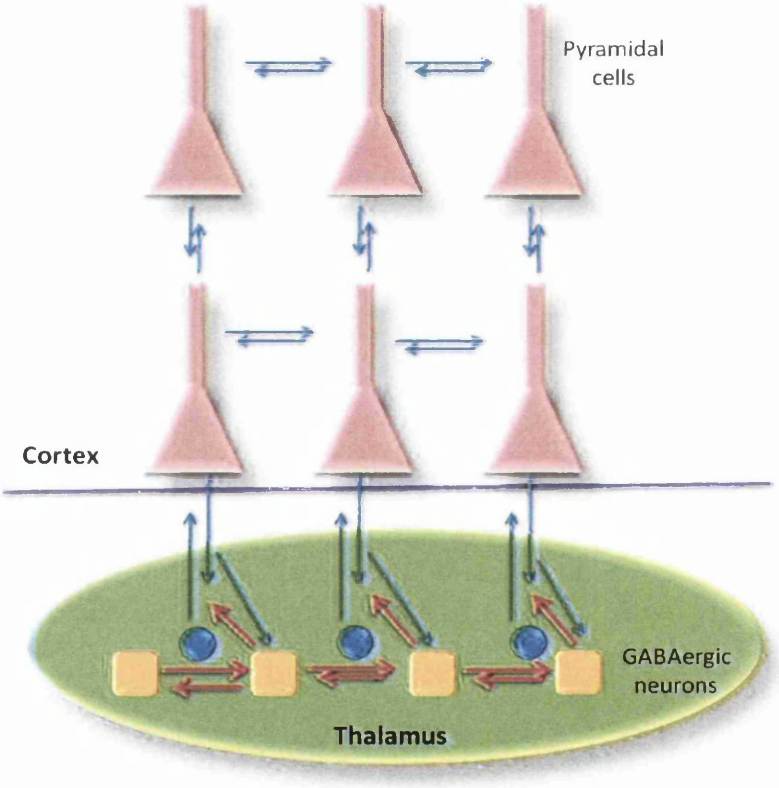

Figure 6.3 Formation of the thalamo-cortical network. Pyramidal cells of the cortex are connected to thalamus by excitatory thalamo-cortical and cortico-thalamic axons. Collaterals from the axons connect with GABAergic neurons and upon excitation, cause GABA release and signal inhibition. Excessive inhibition is reduced by connections between GABAergic neurons. (Adapted from model by Steinlein, 2004).

A decrease in GABA levels in the synapse due to a lack in production by GADs or excessive removal by GABA transporters due to the variants identified in this thesis,

would cause a decrease in inhibitory projections from GABAergic cells to the thalamus. A decrease or elimination of inhibitory projections would not allow intrathalamic oscillations due to a lack of hyperpolarisation of the thalamo-cortical neurons and post-inhibitory rebound action potentials exciting TRN neurons. This decrease in projections causes the absence seizure phenotype whereby the normal synchronous oscillation frequency of approximately 15Hz transforms to a spike wave discharge at approximately 3Hz (Kostopoulos, 2000). We predict that the variants identified in this study cause absence seizures via these mechanisms. For example, GAT1 and GAT3 mutations may result in excess GABA being perpetuated in the synapse leading to over-stimulation of $GABA_A$ and $GABA_B$ receptors, which in turn over-inhibits the balance of bi-directional excitatory tone, leading to cortical deactivation and absence blackouts. Alternatively, the excess GABA may lead to GABA receptor attenuation and under-inhibition of thalamo-cortical networks leading to over-excitation of oscillations and rhythm re-boot phenotypically expressed as cortical deactivation and absence blackouts. If functional analysis proves that GAD65 and GAD67 enzyme activity is compromised then a decreased GABA production is created. Null GABA production would be regarded as a lethal event and explains why this is not observed. A shortage of GABA agonist will result in quantal loss of ligand and under-potentiation of $GABA_A$ receptors and so the lack of inhibition model is more likely here. As with the GABA transporters this may affect the thalamo-cortical network by over-excitation and neuronal re-synchronisation through cortical deactivation, causing a circuit overload.

6.5 GABAergic animal models and absence seizures

Numerous animal models support the genetic link between the GABAergic neurons and absence seizures, including rat models such as GAERS and Wistar Albino Glaxo from Rijswijk (WAG/Rjj) rats. Cope et al, (2009) identified that adult GAERS had elevated GABA levels in the ventral thalamus compared to the non epileptic controls, which is likely to be due to a lack of uptake by GABA transporters.

To test this theory Cope et al, (2009) blocked both GAT1 and GAT3 independently using respective transporter blocking drugs and identified that there was a significant

increase in GABA levels in the thalamus, especially from the blockage of GAT3 which is believed to be most abundant in the thalamus. When both GAT1 and GAT3 were blocked simultaneously, a greater increase in GABA levels in GAERS than non-epileptic animals suggested a compensatory mechanism when only one of the transporters are inhibit; a mechanism wiped out in epileptic strains (Cope et al., 2009). Currently, no GAD animal models of absence seizures are available. GAT animal models, such as those described above, support and strengthen the link between the variants identified in the GGE patient samples of this study and absence seizures. Similar principles can be applied to the GAD variants as they are part of the GABAergic system and can cause the same pathogenic effects.

Animal models of GAERS and WAG/Rjj models show that tiagabine prevents the reuptake of GABA by acting on GABA transporters, enhancing the number and duration of spike wave discharges, which cause an increase in absence seizure (Marescaux et al., 1992) (Coenen et al., 1995). Carbazepine and oxcarbazypine are believed to aggravate absence seizure by their activation on the GABA receptors at a thalamo-cortical level in GAERS and similar animal models. Vigabatrin is a transaminase inhibitor that acts by prevents the breakdown of GABA and its reuptake into the Kreb cycle, therefore causing an increase in whole brain GABA levels. Vigabatrin and tiagabine can aggravate absence seizures or create *de novo* absences (Vrielynck, 2013). Gabapentin acts in a similar way, but causes the reversal of GABA transporters therefore increasing the GABA levels in the synaptic cleft. As described previously, this increase in GABA levels would cause the activation of the $GABA_B$ receptors resulting in slowed IPSP production. These results support the hypothesis that the GABAergic system is involved in the pathology of absence seizures.

It has been identified that up until postnatal day 16 in GAERS, the tonic current in ventrobasal nuclei of the somatosensory thalamus equals that of the non-epileptic control mouse. This changes suddenly between day 16 and 17, with an increase of almost two-fold in the tonic current in the epileptic rat, which remained elevated following seizure onset, until day 30. This data suggests that the enhancement of tonic GABA inhibition during development in GAERS is pathogenic and likely pro-epileptic. This is supported by work carried out by Russo et al (2010), which suggests that early long-term AED treatment that begins before the onset of seizure, which is

approximately two months in WAG/Rjj, can modify the development of absence seizures (Russo et al., 2010). Further studies by Russo et al (2010) suggest that treatment using ethosuximide and levetiracetam from six weeks old reduces the frequency of spike wave discharges witnessed at six months (Russo et al., 2010). Early long-term treatment with zonisamide could cause a reduction in absence seizure generation and synchronisation by altering the development of the pathological state (Russo et al., 2011).

The importance of early detection of absence seizures is emphasised in these studies. This can be achieved by identifying the variants causing the disease, such as those variants identified in this study. Functional analysis of the variants, which we identified, needs to be carried out to determine whether the amino acid changes are pathological. However, predictive 3D modelling, alignment analysis, previous study data and animal models support our hypothesis that the GABAergic variants identified in this study result in changes in GABA levels that, via susceptible neuronal networks, cause absence seizures.

6.6 Conclusion

1. Twenty novel/rare variants have been identified in 48 patient samples in the GABAergic genes *GAT1, GAT3, GAD65 and GAD67* representing a detection rate of 6.8% of the analysed GGE cohort.

2. All 48 patients have a confirmed diagnosis of GGE with a significant component of absence seizure presentation.

3. In GABA transporters, 11 variants were found including one novel splice variant, one deletion variant, two novel missense mutations and seven rare missense variants.

4. In biosynthetic GADs, four novel missense variants and five rare missense mutations were found in GAD65 and GAD67.

5. *In silico* predictive analysis indicates the majority of variants have pathogenic outcomes on protein structure and function and are typically highly conserved in phylogenetic alignment.

6. Structural modelling using the pdb database also provided higher-level prediction of structural changes that would compromise transporter and GAD enzyme activity.

7. Mutation constructs for all missense, splice and deletion variations have been prepared for functional platforms.

8. Immunocytochemistry demonstrates that each variant has intracellular expression, indicating the validation of construct integrity.

9. The core mechanisms of dysfunction remain to be desiphered, although it is suspected that compromised GABA transporter activity and GAD-induced GABA deficiency would produce a GGE phenotype with 3Hz absence features.

10. The evidence for GABAergic pathology in epilepsy is taken from pharmacological studies, animal models, GABA receptor mutations in humans, and knowledge of electrophysiological circuitry in thalamo-cortical networks.

11. Proving the pathogenicity of the GABAergic variants will aid in the early diagnosis of absence seizures and will allow for accurate and timely dispensing of effective medication.

6.7 Limitations of the study

Although every effort was made to identify and solve any issues raised by the study, it was not possible in every case. As a genetic study we took a candidate gene approach, due to the technical limitations at the start of the project (2008). At the time, Lightscanner technology was the fastest way to screen large number of samples in a small laboratory setting. It has only been in the past 2 years that exome sequencing has become affordable and if the project started now it would be likely that 300-400 exomes (or genomes) would have been commissioned. This has resulted in a dataset established around a specific hypothesis with exon and flanking intronic data in targeted genes. Any intronic variants with a regulatory function were therefore missed. Although a limited number of variants have been identified in the intronic regions of genes which have been linked to disease, such as in the ErbB4 gene and schizophrenia (Law et al., 2007), SLC6A3 and ADHD (Greenwood and Kelsoe, 2003), the majority of disease associated mutations identified to date occur in protein coding regions.

Due to costs, not all exons were sequenced for each sample. Instead, all exons for each sample underwent PCR and the lightscanner was used to detect variations in the sample sequence; desired samples would then be selected for sequencing. Although deemed highly-sensitive and every effort was made to select any deviation in melt curve, there is a small chance that a variant was missed by the lightscanner, resulting in the sample not being sequenced for that exon. Also, due to some borderline quality/age issues with some samples it was impossible to get all samples to PCR within normal standards and quality. Many of these samples were third-party cohorts where quality issues were not determined in this laboratory.

Another limitation to the study involved the commercially available unaffected control population samples. Due to the nature of absence seizures, the condition was historically often missed in childhood and patients were not correctly diagnosed but instead categorised as day-dreamers, as having anxiety tics or behavioural problems. If subjects who were overlooked as children then unknowingly become one of the unaffected control samples, this could have implications on our results. This may be one

of the reasons why some variants in the study were identified in the control population and may only be partially informative.

Due to time constraints created by large scale screening and mutation construct creation, we were unable to progress onto various functional studies. However, the project did create the basis for function work, which is now part of a separate study (see section 6.8). One further limitation is the lack of familial samples. This would have helped us understand whether variants were inherited or whether they were *de novo* or mosaic, which would be highly beneficial in assessing the true pathological consequences of each variant.

The immunocytochemistry work carried out in this study was on the HEK293 cell line. This was due to the fact that they have the biochemical capability to carry out the post-translational changes required for this study without interference from endogenous proteins. HEK293 cells do not provide the same level of biochemistry and cell architecture as neuronal preparations, however this methodology has been identified as an invaluable means in faithful reconstruction of numerous neuronal proteins, eliminating the topographical and biochemical complexities of the central nervous system (Thomas and Smart, 2005).

6.8 Further work

This study focused on identifying novel and rare SNPs in epilepsy patient samples. A follow on study would be highly beneficial in determining the functional significance of these variants. For example, extracellular staining of the GABA transporters would be constructive in determining whether the transporters successfully transport to their desired location on the cell membrane. If the transporters traffic to the membrane then the question remains whether they will work effectively or whether they are trafficking mutants that deplete the number of transporters at the cell surface. If they do reach the cell membrane then electrophysiology analysis could be carried out to determine the efficiency of the transporters and to identify whether the variant has a dominant negative or haploinsuffiency effect on the wild-type transporters. Lastly, transporter activity can be assessed by using either a radiolabeled transfection study or a mass

spectrometry approach that can more safely mimic the sensitivity and specificity of the radiolabelled methods.

Some of the mutations will need more specific experimentation. In particular $GAT1^{IVS3+1}$ which is likely to be pathogenic based on the hundreds of genetic disorders that have splice mutations at +1 and +2. A proof of principle splice site assay should be commissioned to show exonic deletion or retention as a direct results of the mutation. GAD65 and GAD67 are not expressed on the cell surface but are intracellular biosynthetic enzymes creating GABA. An appropriate experiment, therefore, is a sensitive and quantitative enzymatic assay which could determine the activity levels of the GAD enzyme by measuring activity metabolites e.g. GABA deficiency or an accumulation of glutamate.

To determine whether the genetic variants identified in the patient samples are inherited or *de novo*, close family members such as parents, grandparent and siblings could be recruited to distinguish whether or not they have the variant. The prevalence of the disease can be determined which would help further aid validation to determine whether the variant identified is pathological and whether it does cause absence seizures. Once the functional consequence of mutations are finalised it would then be possible to source the gene carrier patients and consent them for skin biopsies to create patient specific fibroblast cell-lines which could be used to create pluripotent stem cells to attain genomic context and ex-vivo electrophysiological recordings or transcriptome profiling.

Transgenic animal models would be highly useful in determining the pathogenic effects of the variants as *in vivo* events could be recorded on euthanized brain tissue with no post-mortem delay (as seen in human studies). Live models expressing mutant GAT's and GAD's could be used in seizure termination experiments and profile new and old anti-seizure treatments.

Four genes of the GABAergic system were selected for screening in GGE patient samples. As all the variants identified in the study were present in absence seizure patients, it could be feasible to select other genes from system and screen for these genes in the 707 GGE samples. This could help highlight the GABAergic system

further as a primary cause of absence seizures. Viable options for the candidate gene selection include the genes responsible for GABA breakdown (GABAT) and SSA oxidation (SSADH). Various animal models of GABAT have been identified and demonstrate an increase in synaptic GABA due to reduced GABAT activity (Wu et al., 2001). SSADH knock out models show an extreme increase in GABA levels resulting in absence seizures and eventually tonic-clonic seizures (Akaboshi et al., 2003).

References

1981. Proposal for revised clinical and electroencephalographic classification of epileptic seizures. From the Commission on Classification and Terminology of the International League Against Epilepsy. Epilepsia, 22, 489-501.

1989. Proposal for revised classification of epilepsies and epileptic syndromes. Commission on Classification and Terminology of the International League Against Epilepsy. Epilepsia, 30, 389-99.

AKABOSHI, S., HOGEMA, B. M., NOVELLETTO, A., MALASPINA, P., SALOMONS, G. S., MAROPOULOS, G. D., JAKOBS, C., GROMPE, M. & GIBSON, K. M. 2003. Mutational spectrum of the succinate semialdehyde dehydrogenase (ALDH5A1) gene and functional analysis of 27 novel disease-causing mutations in patients with SSADH deficiency. Hum Mutat, 22, 442-50.

ANGEHAGEN, M., BEN-MENACHEM, E., RONNBACK, L. & HANSSON, E. 2003. Novel mechanisms of action of three antiepileptic drugs, vigabatrin, tiagabine, and topiramate. Neurochem Res, 28, 333-40.

ARCELLI, P., FRASSONI, C., REGONDI, M. C., DE BIASI, S. & SPREAFICO, R. 1997. GABAergic neurons in mammalian thalamus: a marker of thalamic complexity? Brain Res Bull, 42, 27-37.

ASADA, H., KAWAMURA, Y., MARUYAMA, K., KUME, H., DING, R. G., KANBARA, N., KUZUME, H., SANBO, M., YAGI, T. & OBATA, K. 1997. Cleft palate and decreased brain gamma-aminobutyric acid in mice lacking the 67-kDa isoform of glutamic acid decarboxylase. Proceedings of the National Academy of Sciences of the United States of America, 94, 6496-9.

ASADA, H., KAWAMURA, Y., MARUYAMA, K., KUME, H., DING, R., JI, F. Y., KANBARA, N., KUZUME, H., SANBO, M., YAGI, T. & OBATA, K. 1996. Mice lacking the 65 kDa isoform of glutamic acid decarboxylase (GAD65) maintain normal levels of GAD67 and GABA in their brains but are susceptible to seizures. Biochemical and biophysical research communications, 229, 891-5.

ASADI-POOYA, A. A., EMAMI, M. & NIKSERESHT, A. 2012. Early-onset versus typical childhood absence epilepsy; clinical and electrographic characteristics. Seizure, 21, 273-5.

ASTON-JONES, G., RAJKOWSKI, J. & COHEN, J. 1999. Role of locus coeruleus in attention and behavioral flexibility. Biol Psychiatry, 46, 1309-20.

BAI, X., VESTAL, M., BERMAN, R., NEGISHI, M., SPANN, M., VEGA, C., DESALVO, M., NOVOTNY, E. J., CONSTABLE, R. T. & BLUMENFELD, H. 2010. Dynamic time course of typical childhood absence seizures: EEG, behavior, and functional magnetic resonance imaging. J Neurosci, 30, 5884-93.

BAO, J., CHEUNG, W. Y. & WU, J. Y. 1995. Brain L-glutamate decarboxylase. Inhibition by phosphorylation and activation by dephosphorylation. The Journal of biological chemistry, 270, 6464-7.

BATTAGLIOLI, G., LIU, H. & MARTIN, D. L. 2003. Kinetic differences between the isoforms of glutamate decarboxylase: implications for the regulation of GABA synthesis. J Neurochem, 86, 879-87.

BAZHENOV, M., TIMOFEEV, I., STERIADE, M. & SEJNOWSKI, T. J. 1999. Self-sustained rhythmic activity in the thalamic reticular nucleus mediated by depolarizing GABAA receptor potentials. Nat Neurosci, 2, 168-74.

BEAN, B. P. 2007. The action potential in mammalian central neurons. Nat Rev Neurosci, 8, 451-65.

BENNETT, E. R. & KANNER, B. I. 1997. The membrane topology of GAT-1, a (Na+ + Cl-)-coupled gamma-aminobutyric acid transporter from rat brain. The Journal of biological chemistry, 272, 1203-10.

BENNETT, E. R., SU, H. & KANNER, B. I. 2000. Mutation of arginine 44 of GAT-1, a (Na(+) + Cl(-))-coupled gamma-aminobutyric acid transporter from rat brain, impairs net flux but not exchange. The Journal of biological chemistry, 275, 34106-13.

BERG, A. T. & SCHEFFER, I. E. 2011. New concepts in classification of the epilepsies: entering the 21st century. Epilepsia, 52, 1058-62.

BERG, A. T., BERKOVIC, S. F., BRODIE, M. J., BUCHHALTER, J., CROSS, J. H., VAN EMDE BOAS, W., ENGEL, J., FRENCH, J., GLAUSER, T. A., MATHERN, G. W., MOSHE, S. L., NORDLI, D., PLOUIN, P. & SCHEFFER, I. E. 2010. Revised terminology and concepts for organization of seizures and epilepsies: report of the ILAE Commission on Classification and Terminology, 2005-2009. Epilepsia, 51, 676-85.

BERGMAN, J. E., JANSSEN, N., VAN DER SLOOT, A. M., DE WALLE, H. E., SCHOOTS, J., RENDTORFF, N. D., TRANEBJAERG, L., HOEFSLOOT, L. H., VAN RAVENSWAAIJ-ARTS, C. M. & HOFSTRA, R. M. 2012. A novel classification system to predict the pathogenic effects of CHD7 missense variants in CHARGE syndrome. Hum Mutat, 33, 1251-60.

BEYDOUN, A. & D'SOUZA, J. 2012. Treatment of idiopathic generalized epilepsy - a review of the evidence. Expert Opin Pharmacother, 13, 1283-98.

BIRNBOIM, H. C. & DOLY, J. 1979. A rapid alkaline extraction procedure for screening recombinant plasmid DNA. Nucleic Acids Res, 7, 1513-23.

BISMUTH, Y., KAVANAUGH, M. P. & KANNER, B. I. 1997. Tyrosine 140 of the gamma-aminobutyric acid transporter GAT-1 plays a critical role in neurotransmitter recognition. The Journal of biological chemistry, 272, 16096-102.

BLUMENFELD, H. 2003. From molecules to networks: cortical/subcortical interactions in the pathophysiology of idiopathic generalized epilepsy. Epilepsia, 44 Suppl 2, 7-15.

BORDEN, L. A. 1996. GABA transporter heterogeneity: pharmacology and cellular localization. Neurochem Int, 29, 335-56.

BORDEN, L. A., SMITH, K. E., HARTIG, P. R., BRANCHEK, T. A. & WEINSHANK, R. L. 1992. Molecular heterogeneity of the gamma-aminobutyric acid (GABA) transport system. Cloning of two novel high affinity GABA transporters from rat brain. The Journal of biological chemistry, 267, 21098-104.

BOUTIN, P., DINA, C., VASSEUR, F., DUBOIS, S., CORSET, L., SERON, K., BEKRIS, L., CABELLON, J., NEVE, B., VASSEUR-DELANNOY, V., CHIKRI, M., CHARLES, M. A., CLEMENT, K., LERNMARK, A. & FROGUEL, P. 2003. GAD2 on chromosome 10p12 is a candidate gene for human obesity. PLoS biology, 1, E68.

BOWERY, N. G., BETTLER, B., FROESTL, W., GALLAGHER, J. P., MARSHALL, F., RAITERI, M., BONNER, T. I. & ENNA, S. J. 2002. International Union of Pharmacology. XXXIII. Mammalian gamma-aminobutyric acid(B) receptors: structure and function. Pharmacol Rev, 54, 247-64.

BOWSER, D. N., WAGNER, D. A., CZAJKOWSKI, C., CROMER, B. A., PARKER, M. W., WALLACE, R. H., HARKIN, L. A., MULLEY, J. C., MARINI, C., BERKOVIC, S. F., WILLIAMS, D. A., JONES, M. V. & PETROU, S. 2002. Altered kinetics and benzodiazepine sensitivity of a GABAA receptor subunit mutation [gamma 2(R43Q)] found in human epilepsy. Proceedings of the National Academy of Sciences of the United States of America, 99, 15170-5.

BRAMBILLA, P., PEREZ, J., BARALE, F., SCHETTINI, G. & SOARES, J. C. 2003. GABAergic dysfunction in mood disorders. Mol Psychiatry, 8, 721-37, 715.

BU, D. F. & TOBIN, A. J. 1994. The exon-intron organization of the genes (GAD1 and GAD2) encoding two human glutamate decarboxylases (GAD67 and GAD65) suggests that they derive from a common ancestral GAD. Genomics, 21, 222-8.

BU, D. F., ERLANDER, M. G., HITZ, B. C., TILLAKARATNE, N. J., KAUFMAN, D. L., WAGNER-MCPHERSON, C. B., EVANS, G. A. & TOBIN, A. J. 1992. Two human glutamate decarboxylases, 65-kDa GAD and 67-kDa GAD, are each encoded by a single gene. Proceedings of the National Academy of Sciences of the United States of America, 89, 2115-9.

BUDDHALA, C., SUAREZ, M., MODI, J., PRENTICE, H., MA, Z., TAO, R. & WU, J. Y. 2012. Calpain cleavage of brain glutamic acid decarboxylase 65 is pathological and impairs GABA neurotransmission. PloS one, 7, e33002.

BUDDHALA, C., WEI, J. N. & WU, J. Y. 2008. Activity dependent cleavage and protein phosphorylation regulate human glutamate decarboxylase GAD65 activity. Faseb Journal, 22.

BUERLI, T., PELLEGRINO, C., BAER, K., LARDI-STUDLER, B., CHUDOTVOROVA, I., FRITSCHY, J. M., MEDINA, I. & FUHRER, C. 2007. Efficient transfection of DNA or shRNA vectors into neurons using magnetofection. Nat Protoc, 2, 3090-101.

BUHR, A., BIANCHI, M. T., BAUR, R., COURTET, P., PIGNAY, V., BOULENGER, J. P., GALLATI, S., HINKLE, D. J., MACDONALD, R. L. & SIGEL, E. 2002. Functional characterization of the new human GABA(A) receptor mutation beta3(R192H). Hum Genet, 111, 154-60.

CAI, G., SALONIKIDIS, P. S., FEI, J., SCHWARZ, W., SCHULEIN, R., REUTTER, W. & FAN, H. 2005. The role of N-glycosylation in the stability, trafficking and GABA-uptake of GABA-transporter 1. Terminal N-glycans facilitate efficient GABA-uptake activity of the GABA transporter. FEBS J, 272, 1625-38.

CALVO, S. E., TUCKER, E. J., COMPTON, A. G., KIRBY, D. M., CRAWFORD, G., BURTT, N. P., RIVAS, M., GUIDUCCI, C., BRUNO, D. L., GOLDBERGER, O. A., REDMAN, M. C., WILTSHIRE, E., WILSON, C. J., ALTSHULER, D., GABRIEL, S. B., DALY, M. J., THORBURN, D. R. & MOOTHA, V. K. 2010. High-throughput, pooled sequencing identifies mutations in NUBPL and FOXRED1 in human complex I deficiency. Nat Genet, 42, 851-8.

CARNEY, P. W., MASTERTON, R. A., HARVEY, A. S., SCHEFFER, I. E., BERKOVIC, S. F. & JACKSON, G. D. 2010. The core network in absence epilepsy. Differences in cortical and thalamic BOLD response. Neurology, 75, 904-11.

CARVILL, G. L., HEAVIN, S. B., YENDLE, S. C., MCMAHON, J. M., O'ROAK, B. J., COOK, J., KHAN, A., DORSCHNER, M. O., WEAVER, M., CALVERT, S., MALONE, S., WALLACE, G., STANLEY, T., BYE, A. M., BLEASEL, A., HOWELL, K. B., KIVITY, S., MACKAY, M. T., RODRIGUEZ-CASERO, V., WEBSTER, R., KORCZYN, A., AFAWI, Z., ZELNICK, N., LERMAN-SAGIE, T., LEV, D., MOLLER, R. S., GILL, D., ANDRADE, D. M., FREEMAN, J. L., SADLEIR, L. G., SHENDURE, J., BERKOVIC, S. F., SCHEFFER, I. E. & MEFFORD, H. C. 2013. Targeted resequencing in epileptic encephalopathies identifies de novo mutations in CHD2 and SYNGAP1. Nat Genet, 45, 825-30.

CHATTOPADHYAY, M., MATA, M. & FINK, D. J. 2011. Vector-mediated release of GABA attenuates pain-related behaviors and reduces Na(V)1.7 in DRG neurons. European journal of pain (London, England), 15, 913-20.

CHEN, N. H., REITH, M. E. & QUICK, M. W. 2004. Synaptic uptake and beyond: the sodium- and chloride-dependent neurotransmitter transporter family SLC6. Pflugers Arch, 447, 519-31.

CHEN, T. T., KLASSEN, T. L., GOLDMAN, A. M., MARINI, C., GUERRINI, R. & NOEBELS, J. L. 2013. Novel brain expression of ClC-1 chloride channels and enrichment of CLCN1 variants in epilepsy. Neurology, 80, 1078-85.

CHIRGWIN, J. M., PRZYBYLA, A. E., MACDONALD, R. J. & RUTTER, W. J. 1979. Isolation of biologically active ribonucleic acid from sources enriched in ribonuclease. Biochemistry, 18, 5294-9.

CHIU, C. S., BRICKLEY, S., JENSEN, K., SOUTHWELL, A., MCKINNEY, S., CULL-CANDY, S., MODY, I. & LESTER, H. A. 2005. GABA transporter deficiency causes tremor, ataxia, nervousness, and increased GABA-induced tonic conductance in cerebellum. J Neurosci, 25, 3234-45.

CHRISTENSEN, J., KJELDSEN, M. J., ANDERSEN, H., FRIIS, M. L. & SIDENIUS, P. 2005. Gender differences in epilepsy. Epilepsia, 46, 956-60.

CLEMENT, M. J. & WALLACE, S. J. 1988. Juvenile myoclonic epilepsy. Arch Dis Child, 63, 1049-53.

COENEN, A. M., BLEZER, E. H. & VAN LUIJTELAAR, E. L. 1995. Effects of the GABA-uptake inhibitor tiagabine on electroencephalogram, spike-wave discharges and behaviour of rats. Epilepsy Res, 21, 89-94.

CONTI, F., MINELLI, A. & MELONE, M. 2004. GABA transporters in the mammalian cerebral cortex: localization, development and pathological implications. Brain Res Brain Res Rev, 45, 196-212.

COPE, D. W., DI GIOVANNI, G., FYSON, S. J., ORBAN, G., ERRINGTON, A. C., LORINCZ, M. L., GOULD, T. M., CARTER, D. A. & CRUNELLI, V. 2009. Enhanced tonic GABAA inhibition in typical absence epilepsy. Nat Med, 15, 1392-8.

CORDELLI, D. M., GARAVELLI, L., SAVASTA, S., GUERRA, A., PELLICCIARI, A., GIORDANO, L., BONETTI, S., CECCONI, I., WISCHMEIJER, A., SERI, M., ROSATO, S., GELMINI, C., DELLA GIUSTINA, E., FERRARI, A. R., ZANOTTA, N., EPIFANIO, R., GRIONI, D., MALBORA, B., MAMMI, I., MARI, F., BUONI, S., MOSTARDINI, R., GROSSO, S., PANTALEONI, C., DOZ, M., POCH-OLIVE, M. L., RIVIERI, F., SORGE, G., SIMONTE, G., LICATA, F., TARANI, L., TERAZZI, E., MAZZANTI, L., CERRUTI MAINARDI, P., BONI, A., FARAVELLI, F., GRASSO, M., BIANCHI, P., ZOLLINO, M. & FRANZONI, E. 2013. Epilepsy in Mowat-Wilson syndrome: delineation of the electroclinical phenotype. Am J Med Genet A, 161A, 273-84.

COVANIS, A. 2005. Eyelid myoclonia and absence. Adv Neurol, 95, 185-96.

CROMPTON, D. E. & BERKOVIC, S. F. 2009. The borderland of epilepsy: clinical and molecular features of phenomena that mimic epileptic seizures. Lancet Neurol, 8, 370-81.

CRUNELLI, V. & LERESCHE, N. 2002. Childhood absence epilepsy: genes, channels, neurons and networks. Nat Rev Neurosci, 3, 371-82.

CRUNELLI, V., Leresche, N. & Cope, D. 2010. GABAergic gain-of-function in absence seizures. Epilepsia, 51 (Suppl.5):23.

D'ADAMO, M. C., CATACUZZENO, L., DI GIOVANNI, G., FRANCIOLINI, F. & PESSIA, M. 2013. K channelepsy: progress in the neurobiology of potassium channels and epilepsy. Front Cell Neurosci, 7, 134.

DATTA, A. K. 1995. Efficient amplification using 'megaprimer' by asymmetric polymerase chain reaction. Nucleic Acids Res, 23, 4530-1.

DE JUAN-SANZ, J., NUNEZ, E., LOPEZ-CORCUERA, B. & ARAGON, C. 2013. Constitutive endocytosis and turnover of the neuronal glycine transporter GlyT2 is dependent on ubiquitination of a C-terminal lysine cluster. PLoS One, 8, e58863.

DEKEN, S. L., WANG, D. & QUICK, M. W. 2003. Plasma membrane GABA transporters reside on distinct vesicles and undergo rapid regulated recycling. The Journal of neuroscience : the official journal of the Society for Neuroscience, 23, 1563-8.

DELGADO-ESCUETA, A. V. & ENRILE-BACSAL, F. 1984. Juvenile myoclonic epilepsy of Janz. Neurology, 34, 285-94.

DEMARQUE, M., VILLENEUVE, N., MANENT, J. B., BECQ, H., REPRESA, A., BEN-ARI, Y. & ANIKSZTEJN, L. 2004. Glutamate transporters prevent the generation of seizures in the developing rat neocortex. The Journal of neuroscience : the official journal of the Society for Neuroscience, 24, 3289-94.

DENG, H., XIU, X. & SONG, Z. 2013. The Molecular Biology of Genetic-Based Epilepsies. Mol Neurobiol.

DIBBENS, L. M., FENG, H. J., RICHARDS, M. C., HARKIN, L. A., HODGSON, B. L., SCOTT, D., JENKINS, M., PETROU, S., SUTHERLAND, G. R., SCHEFFER, I. E., BERKOVIC, S. F., MACDONALD, R. L. & MULLEY, J. C. 2004. GABRD encoding a protein for extra- or peri-synaptic GABAA receptors is a susceptibility locus for generalized epilepsies. Hum Mol Genet, 13, 1315-9.

DU, J., DUAN, S., WANG, H., CHEN, W., ZHAO, X., ZHANG, A., WANG, L., XUAN, J., YU, L., WU, S., TANG, W., LI, X., LI, H., FENG, G., XING, Q. & HE, L. 2008. Comprehensive analysis of polymorphisms throughout GAD1 gene: a family-based association study in schizophrenia. J Neural Transm, 115, 513-9.

DUTHEY, B., CAUDRON, S., PERROY, J., BETTLER, B., FAGNI, L., PIN, J. P. & PREZEAU, L. 2002. A single subunit (GB2) is required for G-protein activation by the heterodimeric GABA(B) receptor. J Biol Chem, 277, 3236-41.

ENGEL, J., JR. 2001. A proposed diagnostic scheme for people with epileptic seizures and with epilepsy: report of the ILAE Task Force on Classification and Terminology. Epilepsia, 42, 796-803.

ERDO, S. L., ROSDY, B. & SZPORNY, L. 1982. Higher GABA concentrations in fallopian tube than in brain of the rat. J Neurochem, 38, 1174-6.

ESCAYG, A., DE WAARD, M., LEE, D. D., BICHET, D., WOLF, P., MAYER, T., JOHNSTON, J., BALOH, R., SANDER, T. & MEISLER, M. H. 2000. Coding and noncoding variation of the human calcium-channel beta4-subunit gene CACNB4 in patients with idiopathic generalized epilepsy and episodic ataxia. Am J Hum Genet, 66, 1531-9.

EULER, T. & WASSLE, H. 1998. Different contributions of GABAA and GABAC receptors to rod and cone bipolar cells in a rat retinal slice preparation. J Neurophysiol, 79, 1384-95.

FAHN, S., MARSDEN, C. D. & VAN WOERT, M. H. 1986. Definition and classification of myoclonus. Adv Neurol, 43, 1-5.

FARWELL, J. R., DODRILL, C. B. & BATZEL, L. W. 1985. Neuropsychological abilities of children with epilepsy. Epilepsia, 26, 395-400.

FENALTI, G., LAW, R. H., BUCKLE, A. M., LANGENDORF, C., TUCK, K., ROSADO, C. J., FAUX, N. G., MAHMOOD, K., HAMPE, C. S., BANGA, J. P., WILCE, M., SCHMIDBERGER, J., ROSSJOHN, J., EL-KABBANI, O., PIKE, R. N., SMITH, A. I., MACKAY, I. R., ROWLEY, M. J. & WHISSTOCK, J. C. 2007. GABA production by glutamic acid decarboxylase is regulated by a dynamic catalytic loop. Nat Struct Mol Biol, 14, 280-6.

FISHER, R. S., VAN EMDE BOAS, W., BLUME, W., ELGER, C., GENTON, P., LEE, P. & ENGEL, J., JR. 2005. Epileptic seizures and epilepsy: definitions proposed by the International League Against Epilepsy (ILAE) and the International Bureau for Epilepsy (IBE). Epilepsia, 46, 470-2.

FU, T. F., BOJA, E. S., SAFO, M. K. & SCHIRCH, V. 2003. Role of proline residues in the folding of serine hydroxymethyltransferase. J Biol Chem, 278, 31088-94.

GAROFALO, S., CORNACCHIONE, M. & DI COSTANZO, A. 2012. From genetics to genomics of epilepsy. Neurol Res Int, 2012, 876234.

GENTON, P. & GELISSE, P. 2001. Juvenile myoclonic epilepsy. Arch Neurol, 58, 1487-90.

GIBSON, K. M., GUPTA, M., PEARL, P. L., TUCHMAN, M., VEZINA, L. G., SNEAD, O. C., 3RD, SMIT, L. M. & JAKOBS, C. 2003. Significant behavioral disturbances in succinic semialdehyde dehydrogenase (SSADH) deficiency (gamma-hydroxybutyric aciduria). Biol Psychiatry, 54, 763-8.

GLADKEVICH, A., KORF, J., HAKOBYAN, V. P. & MELKONYAN, K. V. 2006. The peripheral GABAergic system as a target in endocrine disorders. Auton Neurosci, 124, 1-8.

GOLDENBERG, M. M. 2010. Overview of drugs used for epilepsy and seizures: etiology, diagnosis, and treatment. P T, 35, 392-415.

GORDON, N. 2004. Succinic semialdehyde dehydrogenase deficiency (SSADH) (4-hydroxybutyric aciduria, gamma-hydroxybutyric aciduria). Eur J Paediatr Neurol, 8, 261-5.

GORLOV, I., GORLOVA, O., SUNYAEV, S., SPITZ, M. & AMOS, C. 2008. Shifting paradigm of association studies: value of rare single nucleotide polymorphisms. AJHG, 82 (1), 100-112.

GRAHAM, F. L., SMILEY, J., RUSSELL, W. C. & NAIRN, R. 1977. Characteristics of a human cell line transformed by DNA from human adenovirus type 5. J Gen Virol, 36, 59-74.

GREENWOOD, T. A. & KELSOE, J. R. 2003. Promoter and intronic variants affect the transcriptional regulation of the human dopamine transporter gene. Genomics, 82, 511-20.

GUASTELLA, J., NELSON, N., NELSON, H., CZYZYK, L., KEYNAN, S., MIEDEL, M. C., DAVIDSON, N., LESTER, H. A. & KANNER, B. I. 1990. Cloning and expression of a rat brain GABA transporter. Science, 249, 1303-6.

GUPTA, M., POLINSKY, M., SENEPHANSIRI, H., SNEAD, O. C., JANSEN, E. E., JAKOBS, C. & GIBSON, K. M. 2004. Seizure evolution and amino acid imbalances in murine succinate semialdehyde dehydrogenase (SSADH) deficiency. Neurobiol Dis, 16, 556-62.

HAHN, M. K. & BLAKELY, R. D. 2007. The functional impact of SLC6 transporter genetic variation. Annu Rev Pharmacol Toxicol, 47, 401-41.

HAHN, M. K., MAZEI-ROBISON, M. S. & BLAKELY, R. D. 2005. Single nucleotide polymorphisms in the human norepinephrine transporter gene affect expression, trafficking, antidepressant interaction, and protein kinase C regulation. Mol Pharmacol, 68, 457-66.

HAHN, M. K., ROBERTSON, D. & BLAKELY, R. D. 2003. A mutation in the human norepinephrine transporter gene (SLC6A2) associated with orthostatic intolerance disrupts surface expression of mutant and wild-type transporters. J Neurosci, 23, 4470-8.

HANSRA, N., ARYA, S. & QUICK, M. W. 2004. Intracellular domains of a rat brain GABA transporter that govern transport. The Journal of neuroscience : the official journal of the Society for Neuroscience, 24, 4082-7.

HAUG, K., WARNSTEDT, M., ALEKOV, A. K., SANDER, T., RAMIREZ, A., POSER, B., MALJEVIC, S., HEBEISEN, S., KUBISCH, C., REBSTOCK, J., HORVATH, S., HALLMANN, K., DULLINGER, J. S., RAU, B., HAVERKAMP, F., BEYENBURG, S., SCHULZ, H., JANZ, D., GIESE, B., MULLER-NEWEN, G., PROPPING, P., ELGER, C. E., FAHLKE, C., LERCHE, H. & HEILS, A. 2003. Mutations in CLCN2 encoding a voltage-gated chloride channel are associated with idiopathic generalized epilepsies. Nat Genet, 33, 527-32.

HELBIG, I., SCHEFFER, I. E., MULLEY, J. C. & BERKOVIC, S. F. 2008. Navigating the channels and beyond: unravelling the genetics of the epilepsies. Lancet Neurol, 7, 231-45.

HESDORFFER, D. C., LOGROSCINO, G., BENN, E. K., KATRI, N., CASCINO, G. & HAUSER, W. A. 2011. Estimating risk for developing epilepsy: a population-based study in Rochester, Minnesota. Neurology, 76, 23-7.

HIGUCHI, R.G. & OCHMAN, H. 1989. Production of single-stranded DNA templates by exonuclease digestion following the polymerase chain reaction. Nucleic Acids Res, 17(14): 5865.

HIRUNSATIT, R., GEORGE, E. D., LIPSKA, B. K., ELWAFI, H. M., SANDER, L., YRIGOLLEN, C. M., GELERNTER, J., GRIGORENKO, E. L., LAPPALAINEN, J., MANE, S., NAIRN, A. C., KLEINMAN, J. E. & SIMEN, A. A. 2009. Twenty-one-base-pair insertion polymorphism creates an enhancer element and potentiates SLC6A1 GABA transporter promoter activity. Pharmacogenet Genomics, 19, 53-65.

HIRUNSATIT, R., ILOMAKI, R., MALISON, R., RASANEN, P., ILOMAKI, E., KRANZLER, H. R., KOSTEN, T., SUGHONDHABIROM, A., THAVICHACHART, N., TANGWONGCHAI, S., LISTMAN, J., MUTIRANGURA, A., GELERNTER, J. & LAPPALAINEN, J. 2007. Sequence variation and linkage disequilibrium in the GABA transporter-1 gene (SLC6A1) in five populations: implications for pharmacogenetic research. BMC Genet, 8, 71.

HOLMES, M. D., BROWN, M. & TUCKER, D. M. 2004. Are "generalized" seizures truly generalized? Evidence of localized mesial frontal and frontopolar discharges in absence. Epilepsia, 45, 1568-79.

HORI, K. & HOSHINO, M. 2012. GABAergic neuron specification in the spinal cord, the cerebellum, and the cochlear nucleus. Neural Plast, 2012, 921732.

HSIEH, D. T., WALKER, J. M. & PEARL, P. L. 2008. Infantile seizures: infants are not just little children. Curr Neurol Neurosci Rep, 8, 139-44.

HUANG, F., SHI, L. J., HENG, H. H., FEI, J. & GUO, L. H. 1995. Assignment of the human GABA transporter gene (GABATHG) locus to chromosome 3p24-p25. Genomics, 29, 302-4.

JACOB, T. C., BOGDANOV, Y. D., MAGNUS, C., SALIBA, R. S., KITTLER, J. T., HAYDON, P. G. & MOSS, S. J. 2005. Gephyrin regulates the cell surface dynamics of synaptic GABAA receptors. J Neurosci, 25, 10469-78.

JAEKEN, J., CASAER, P., DE COCK, P., CORBEEL, L., EECKELS, R., EGGERMONT, E., SCHECHTER, P. J. & BRUCHER, J. M. 1984. Gamma-aminobutyric acid-transaminase deficiency: a newly recognized inborn error of neurotransmitter metabolism. Neuropediatrics, 15, 165-9.

JALLON, P., LOISEAU, P. & LOISEAU, J. 2001. Newly diagnosed unprovoked epileptic seizures: presentation at diagnosis in CAROLE study. Coordination Active du Reseau Observatoire Longitudinal de l' Epilepsie. Epilepsia, 42, 464-75.

JEAVONS, P. M. 1977. Nosological problems of myoclonic epilepsies in childhood and adolescence. Dev Med Child Neurol, 19, 3-8.

JENTSCH, T. J. 2000. Neuronal KCNQ potassium channels: physiology and role in disease. Nat Rev Neurosci, 1, 21-30.

JIN, X. T., PARE, J. F. & SMITH, Y. 2011. Differential localization and function of GABA transporters, GAT-1 and GAT-3, in the rat globus pallidus. Eur J Neurosci, 33, 1504-18.

JONES, N. C., O'BRIEN, T. J. & POWELL, K. L. 2011. Morphometric changes and molecular mechanisms in rat models of idiopathic generalized epilepsy with absence seizures. Neurosci Lett, 497, 185-93.

JOSHI, C. N. & PATRICK, J. 2007. Eyelid myoclonia with absences: routine EEG is sufficient to make a diagnosis. Seizure, 16, 254-60.

KADO, C. I. & LIU, S. T. 1981. Rapid procedure for detection and isolation of large and small plasmids. J Bacteriol, 145, 1365-73.

KANAANI, J., EL-HUSSEINI AEL, D., AGUILERA-MORENO, A., DIACOVO, J. M., BREDT, D. S. & BAEKKESKOV, S. 2002. A combination of three distinct trafficking signals mediates axonal targeting and presynaptic clustering of GAD65. J Cell Biol, 158, 1229-38.

KANAANI, J., KOLIBACHUK, J., MARTINEZ, H. & BAEKKESKOV, S. 2010. Two distinct mechanisms target GAD67 to vesicular pathways and presynaptic clusters. J Cell Biol, 190, 911-25.

KANAANI, J., LISSIN, D., KASH, S. F. & BAEKKESKOV, S. 1999. The hydrophilic isoform of glutamate decarboxylase, GAD67, is targeted to membranes and nerve terminals independent of dimerization with the hydrophobic membrane-anchored isoform, GAD65. The Journal of biological chemistry, 274, 37200-9.

KANAANI, J., PATTERSON, G., SCHAUFELE, F., LIPPINCOTT-SCHWARTZ, J. & BAEKKESKOV, S. 2008. A palmitoylation cycle dynamically regulates partitioning of the GABA-synthesizing enzyme GAD65 between ER-Golgi and post-Golgi membranes. J Cell Sci, 121, 437-49.

KELLEY, L. A. & STERNBERG, M. J. 2009. Protein structure prediction on the Web: a case study using the Phyre server. Nat Protoc, 4, 363-71.

KHOSRAVANI, H., ALTIER, C., SIMMS, B., HAMMING, K. S., SNUTCH, T. P., MEZEYOVA, J., MCRORY, J. E. & ZAMPONI, G. W. 2004. Gating effects of mutations in the Cav3.2 T-type calcium channel associated with childhood absence epilepsy. J Biol Chem, 279, 9681-4.

KILIC, F., MURPHY, D. L. & RUDNICK, G. 2003. A human serotonin transporter mutation causes constitutive activation of transport activity. Mol Pharmacol, 64(2), 440-446.

KIM, D. U., KIM, M. K., CHO, Y. W., KIM, Y. S., KIM, W. J., LEE, M. G., KIM, S. E., NAM, T. S., CHO, K. H., KIM, Y. O. & LEE, M. C. 2011. Association of a synonymous GAT3 polymorphism with antiepileptic drug pharmacoresistance. J Hum Genet, 56, 640-6.

KIM, U., SANCHEZ-VIVES, M. V. & MCCORMICK, D. A. 1997. Functional dynamics of GABAergic inhibition in the thalamus. Science, 278, 130-4.

KIM, Y. G., LEE, S., KWON, O. S., PARK, S. Y., LEE, S. J., PARK, B. J. & KIM, K. J. 2009. Redox-switch modulation of human SSADH by dynamic catalytic loop. EMBO J, 28, 959-68.

KINS, S., BETZ, H. & KIRSCH, J. 2000. Collybistin, a newly identified brain-specific GEF, induces submembrane clustering of gephyrin. Nat Neurosci, 3, 22-9.

KOSTOPOULOS, G. K. 2000. Spike-and-wave discharges of absence seizures as a transformation of sleep spindles: the continuing development of a hypothesis. Clin Neurophysiol, 111 Suppl 2, S27-38.

KRALIC, J. E., KORPI, E. R., O'BUCKLEY, T. K., HOMANICS, G. E. & MORROW, A. L. 2002. Molecular and pharmacological characterization of GABA(A) receptor alpha1 subunit knockout mice. J Pharmacol Exp Ther, 302, 1037-45.

KUMAR, P., HENIKOFF, S. & NG, P. C. 2009. Predicting the effects of coding non-synonymous variants on protein function using the SIFT algorithm. Nat Protoc, 4, 1073-81.

LAM, D. M., FEI, J., ZHANG, X. Y., TAM, A. C., ZHU, L. H., HUANG, F., KING, S. C. & GUO, L. H. 1993. Molecular cloning and structure of the human (GABATHG) GABA transporter gene. Brain Res Mol Brain Res, 19, 227-32.

LANCE, J. W. 1963. Sporadic and familial varieties of tonic seizures. J Neurol Neurosurg Psychiatry, 26, 51-9.

LAW, A. J., KLEINMAN, J. E., WEINBERGER, D. R. & WEICKERT, C. S. 2007. Disease-associated intronic variants in the ErbB4 gene are related to altered ErbB4 splice-variant expression in the brain in schizophrenia. Hum Mol Genet, 16, 129-41.

LEE, C., KIM, S. M., JUNG, Y. J., IM, C. H., KIM, D. W. & JUNG, K. Y. 2014. Causal influence of epileptic network during spike-and-wave discharge in juvenile myoclonic epilepsy. Epilepsy Res, 108, 257-66.

LEMKE, J. R., RIESCH, E., SCHEURENBRAND, T., SCHUBACH, M., WILHELM, C., STEINER, I., HANSEN, J., COURAGE, C., GALLATI, S., BURKI, S., STROZZI, S., SIMONETTI, B. G., GRUNT, S., STEINLIN, M., ALBER, M., WOLFF, M., KLOPSTOCK, T., PROTT, E. C., LORENZ, R., SPAICH, C., RONA, S., LAKSHMINARASIMHAN, M., KROLL, J., DORN, T., KRAMER, G., SYNOFZIK, M., BECKER, F., WEBER, Y. G., LERCHE, H., BOHM, D. & BISKUP, S. 2012. Targeted next generation sequencing as a diagnostic tool in epileptic disorders. Epilepsia, 53, 1387-98.

LEPPIK, I. E. 2003. Classification of the myoclonic epilepsies. Epilepsia, 44 Suppl 11, 2-6.

LIN, Y. M., CHAO, S. C., CHEN, T. M., LAI, T. J., CHEN, J. S. & SUN, H. S. 2007. Association of functional polymorphisms of the human tryptophan hydroxylase 2 gene with risk for bipolar disorder in Han Chinese. Arch Gen Psychiatry, 64, 1015-24.

LUSCHER, B., FUCHS, T. & KILPATRICK, C. L. 2011. GABAA receptor trafficking-mediated plasticity of inhibitory synapses. Neuron, 70, 385-409.

LYNEX, C. N., CARR, I. M., LEEK, J. P., ACHUTHAN, R., MITCHELL, S., MAHER, E. R., WOODS, C. G., BONTHON, D. T. & MARKHAM, A. F. 2004. Homozygosity for a missense mutation in the 67 kDa isoform of glutamate decarboxylase in a family with autosomal recessive spastic cerebral palsy: parallels with Stiff-Person Syndrome and other movement disorders. BMC Neurol, 4, 20.

MACDONALD, R. L. 2001. GABAA Receptor Defects Can Cause Epilepsy. Epilepsy Curr, 1, 74.

MADSEN, K. K., WHITE, H. S. & SCHOUSBOE, A. 2010. Neuronal and non-neuronal GABA transporters as targets for antiepileptic drugs. Pharmacol Ther, 125, 394-401.

MAGER, S., KLEINBERGER-DORON, N., KESHET, G. I., DAVIDSON, N., KANNER, B. I. & LESTER, H. A. 1996. Ion binding and permeation at the GABA transporter GAT1. J Neurosci, 16, 5405-14.

MALCANGIO, M. & BOWERY, N. G. 1996. GABA and its receptors in the spinal cord. Trends Pharmacol Sci, 17, 457-62.

MAO, X., GUO, F., YU, J., MIN, D., WANG, Z., XIE, N., CHEN, T., SHAW, C. & CAI, J. 2010. Up-regulation of GABA transporters and GABA(A) receptor alpha1 subunit in tremor rat hippocampus. Neurosci Lett, 486, 150-5.

MARESCAUX, C., VERGNES, M. & DEPAULIS, A. 1992. Genetic absence epilepsy in rats from Strasbourg--a review. J Neural Transm Suppl, 35, 37-69.

MARKO, A. M. & BUTLER, G. C. 1951. The isolation of sodium desoxyribonucleate with sodium dodecyl sulfate. The Journal of biological chemistry, 190, 165-76.

MARKS, D. A., KIM, J., SPENCER, D. D. & SPENCER, S. S. 1992. Characteristics of intractable seizures following meningitis and encephalitis. Neurology, 42, 1513-8.

MARTINEZ-MAZA, R., POYATOS, I., LOPEZ-CORCUERA, B., E, N. U., GIMENEZ, C., ZAFRA, F. & ARAGON, C. 2001. The role of N-glycosylation in transport to the plasma membrane and sorting of the neuronal glycine transporter GLYT2. J Biol Chem, 276, 2168-73.

MCGEE, T. L. SEVEDAHMADI, B. J., SWEENEY, M. O., DRYIA, T. P. & BERSON, E. L. 2010. Novel mutations in the long isoform of the USH2A gene in patients with Usher syndrome type II or non-syndromic retinitis pigmentosa. J Med Genet 47(7), 499-506.

MEDINA-KAUWE, L. K., TOBIN, A. J., DE MEIRLEIR, L., JAEKEN, J., JAKOBS, C., NYHAN, W. L. & GIBSON, K. M. 1999. 4-Aminobutyrate aminotransferase (GABA-transaminase) deficiency. J Inherit Metab Dis, 22, 414-27.

MELDRUM, B. & HORTON, R. 1978. Blockade of epileptic responses in the photosensitive baboon, Papio papio, by two irreversible inhibitors of GABA-transaminase, gamma-acetylenic GABA (4-amino-hex-5-ynoic acid) and gamma-vinyl GABA (4-amino-hex-5-enoic acid). Psychopharmacology, 59, 47-50.

MERWICK, A., O'BRIEN, M. & DELANTY, N. 2012. Complex single gene disorders and epilepsy. Epilepsia, 53 Suppl 4, 81-91.

MILLER, L. P., WALTERS, J. R. & MARTIN, D. L. 1977. Post-mortem changes implicate adenine nucleotides and pyridoxal-5' -phosphate in regulation of brain glutamate decarboxylase. Nature, 266, 847-8.

MINELLI, A., DEBIASI, S., BRECHA, N. C., ZUCCARELLO, L. V. & CONTI, F. 1996. GAT-3, a high-affinity GABA plasma membrane transporter, is localized to astrocytic processes, and it is not confined to the vicinity of GABAergic synapses in the cerebral cortex. The Journal of neuroscience : the official journal of the Society for Neuroscience, 16, 6255-64.

MULLEY, J. C., SCHEFFER, I. E., PETROU, S., DIBBENS, L. M., BERKOVIC, S. F. & HARKIN, L. A. 2005. SCN1A mutations and epilepsy. Hum Mutat, 25, 535-42.

MYKHAYLYK, O., ANTEQUERA, Y. S., VLASKOU, D. & PLANK, C. 2007. Generation of magnetic nonviral gene transfer agents and magnetofection in vitro. Nat Protoc, 2, 2391-411.

NAGGA, K., BOGDANOVIC, N. & MARCUSSON, J. 1999. GABA transporters (GAT-1) in Alzheimer's disease. J Neural Transm, 106, 1141-9.

NAMCHUK, M., LINDSAY, L., TURCK, C. W., KANAANI, J. & BAEKKESKOV, S. 1997. Phosphorylation of serine residues 3, 6, 10, and 13 distinguishes membrane anchored from soluble glutamic acid decarboxylase 65 and is restricted to glutamic acid decarboxylase 65alpha. The Journal of biological chemistry, 272, 1548-57.

NG, P. C. & HENIKOFF, S. 2001. Predicting deleterious amino acid substitutions. Genome Res, 11, 863-74.

NICOLSON, A. & MARSON, A. G. 2010. When the first antiepileptic drug fails in a patient with juvenile myoclonic epilepsy. Pract Neurol, 10, 208-18.

NOEBELS, J. L. 2003. The biology of epilepsy genes. Annu Rev Neurosci, 26, 599-625.

OLSEN, R. W. & SIEGHART, W. 2009. GABA A receptors: subtypes provide diversity of function and pharmacology. Neuropharmacology, 56, 141-8.

O'SULLIVAN, G. A., KNEUSSEL, M., ELAZAR, Z. & BETZ, H. 2005. GABARAP is not essential for GABA receptor targeting to the synapse. Eur J Neurosci, 22, 2644-8.

PAL, D. K., DURNER, M., KLOTZ, I., DICKER, E., SHINNAR, S., RESOR, S., COHEN, J., HARDEN, C., MOSHE, S. L., BALLABAN-GILL, K., BROMFIELD, E. B. & GREENBERG, D. A. 2006. Complex inheritance and parent-of-origin effect in juvenile myoclonic epilepsy. Brain Dev, 28, 92-8.

PANAYIOTOPOULOS, C. P. 1999. Typical absence seizures and their treatment. Arch Dis Child, 81, 351-5.

PATEL, A. B., DE GRAAF, R. A., MARTIN, D. L., BATTAGLIOLI, G. & BEHAR, K. L. 2006. Evidence that GAD65 mediates increased GABA synthesis during intense neuronal activity in vivo. J Neurochem, 97, 385-96.

PAZZAGLIA, P., D'ALESSANDRO, R., AMBROSETTO, G. & LUGARESI, E. 1985. Drop attacks: an ominous change in the evolution of partial epilepsy. Neurology, 35, 1725-30.

PEARL, P. L., GIBSON, K. M., CORTEZ, M. A., WU, Y., CARTER SNEAD, O., 3RD, KNERR, I., FORESTER, K., PETTIFORD, J. M., JAKOBS, C. & THEODORE, W. H. 2009. Succinic semialdehyde dehydrogenase deficiency: lessons from mice and men. J Inherit Metab Dis, 32, 343-52.

PERUCCA, E., FRENCH, J. & BIALER, M. 2007. Development of new antiepileptic drugs: challenges, incentives, and recent advances. Lancet Neurol, 6, 793-804.

PETTERSEN, E., GODDARD, T., HUANG, C., COUCH, G., GREENBLATT, D., MENG, E. & FERNIN, T. 2004. UCSF Chimera- A visualisation system for exploratory research and analysis. Comput Chem 25: 1605–1612.

PIRTTIMAKI, T., PARRI, H. R. & CRUNELLI, V. 2013. Astrocytic GABA transporter GAT-1 dysfunction in experimental absence seizures. J Physiol, 591, 823-33.

PORTER, T. G. & MARTIN, D. L. 1984. Evidence for feedback regulation of glutamate decarboxylase by gamma-aminobutyric acid. J Neurochem, 43, 1464-7.

POSNER, M. I. & PETERSEN, S. E. 1990. The attention system of the human brain. Annu Rev Neurosci, 13, 25-42.

PURCELL, GAITATZIZ, SANDER, MAJEED. Epilepsy Prevalence and prescribing patters in England and Wales, Office of National Statistics, Autumn 2002.

RAMENSKY, V., BORK, P. & SUNYAEV, S. 2002. Human non-synonymous SNPs: server and survey. Nucleic Acids Res, 30, 3894-900.

REES, M. I., HARVEY, K., PEARCE, B. R., CHUNG, S. K., DUGUID, I. C., THOMAS, P., BEATTY, S., GRAHAM, G. E., ARMSTRONG, L., SHIANG, R., ABBOTT, K. J., ZUBERI, S. M., STEPHENSON, J. B., OWEN, M. J., TIJSSEN, M. A., VAN DEN MAAGDENBERG, A. M., SMART, T. G., SUPPLISSON, S. & HARVEY, R. J. 2006. Mutations in the gene encoding GlyT2 (SLC6A5) define a presynaptic component of human startle disease. Nat Genet, 38, 801-6.

RIMMER, E. M. & RICHENS, A. 1984. Double-blind study of gamma-vinyl GABA in patients with refractory epilepsy. Lancet, 1, 189-90.

ROSENBERG, E. H., ALMEIDA, L. S., KLEEFSTRA, T., DEGRAUW, R. S., YNTEMA, H. G., BAHI, N., MORAINE, C., ROPERS, H. H., FRYNS, J. P., DEGRAUW, T. J., JAKOBS, C. & SALOMONS, G. S. 2004. High prevalence of SLC6A8 deficiency in X-linked mental retardation. Am J Hum Genet, 75, 97-105.

ROSSIGNOL, E. 2011. Genetics and function of neocortical GABAergic interneurons in neurodevelopmental disorders. Neural Plast, 2011, 649325.

ROSSO, O. A., BLANCO, S. & RABINOWICZ, A. 2003. Wavelet analysis of generalized tonic-clonic epileptic seizures. Signal Processing, 83, 1275-1289.

RUDOMIN, P. & SCHMIDT, R. F. 1999. Presynaptic inhibition in the vertebrate spinal cord revisited. Exp Brain Res, 129, 1-37.

RUSSO, E., CITRARO, R., SCICCHITANO, F., DE FAZIO, S., DI PAOLA, E. D., CONSTANTI, A. & DE SARRO, G. 2010. Comparison of the antiepileptogenic effects of an early long-term treatment with ethosuximide or levetiracetam in a genetic animal model of absence epilepsy. Epilepsia, 51, 1560-9.

RUSSO, E., CITRARO, R., SCICCHITANO, F., DE FAZIO, S., PERROTTA, I., DI PAOLA, E. D., CONSTANTI, A. & DE SARRO, G. 2011. Effects of early long-term treatment with antiepileptic drugs on development of seizures and depressive-like behavior in a rat genetic absence epilepsy model. Epilepsia, 52, 1341-50.

SAHARA, S., YANAGAWA, Y., O'LEARY, D. D. & STEVENS, C. F. 2012. The fraction of cortical GABAergic neurons is constant from near the start of cortical neurogenesis to adulthood. The Journal of neuroscience : the official journal of the Society for Neuroscience, 32, 4755-61.

SANDERS, S. J., MURTHA, M. T., GUPTA, A. R., MURDOCH, J. D., RAUBESON, M. J., WILLSEY, A. J., ERCAN-SENCICEK, A. G., DILULLO, N. M., PARIKSHAK, N. N., STEIN, J. L., WALKER, M. F., OBER, G. T., TERAN, N. A., SONG, Y., EL-FISHAWY, P., MURTHA, R. C., CHOI, M., OVERTON, J. D., BJORNSON, R. D., CARRIERO, N. J., MEYER, K. A., BILGUVAR, K., MANE, S. M., SESTAN, N., LIFTON, R. P., GUNEL, M., ROEDER, K., GESCHWIND, D. H., DEVLIN, B. & STATE, M. W. 2012. De novo mutations revealed by whole-exome sequencing are strongly associated with autism. Nature, 485, 237-41.

SCHEFFER, I. E. & BERKOVIC, S. F. 2003. The genetics of human epilepsy. Trends Pharmacol Sci, 24, 428-33.

SCHOUSBOE, A., WESTERGAARD, N., SONNEWALD, U., PETERSEN, S. B., HUANG, R., PENG, L. & HERTZ, L. 1993. Glutamate and glutamine metabolism and compartmentation in astrocytes. Dev Neurosci, 15, 359-66.

SCHULER, V., LUSCHER, C., BLANCHET, C., KLIX, N., SANSIG, G., KLEBS, K., SCHMUTZ, M., HEID, J., GENTRY, C., URBAN, L., FOX, A., SPOOREN, W., JATON, A. L., VIGOURET, J., POZZA, M., KELLY, P. H., MOSBACHER, J., FROESTL, W., KASLIN, E., KORN, R., BISCHOFF, S., KAUPMANN, K., VAN DER PUTTEN, H. & BETTLER, B. 2001. Epilepsy, hyperalgesia, impaired memory, and loss of pre- and postsynaptic GABA(B) responses in mice lacking GABA(B(1)). Neuron, 31, 47-58.

SEMYANOV, A., WALKER, M. C., KULLMANN, D. M. & SILVER, R. A. 2004. Tonically active GABA A receptors: modulating gain and maintaining the tone. Trends Neurosci, 27, 262-9.

SHEEHAN, K., LOWE, N., KIRLEY, A., MULLINS, C., FITZGERALD, M., GILL, M. & HAWI, Z. 2005. Tryptophan hydroxylase 2 (TPH2) gene variants associated with ADHD. Mol Psychiatry, 10, 944-9.

SHEKHAR, A., HINGTGEN, J. N. & DIMICCO, J. A. 1990. GABA receptors in the posterior hypothalamus regulate experimental anxiety in rats. Brain Res, 512, 81-8.

SHERIF, F. M. & AHMED, S. S. 1995. Basic aspects of GABA-transaminase in neuropsychiatric disorders. Clin Biochem, 28, 145-54.

SHIREY-RICE, J. K., KLAR, R., FENTRESS, H. M., REDMON, S. N., SABB, T. R., KRUEGER, J. J., WALLACE, N. M., APPALSAMY, M., FINNEY, C., LONCE, S., DIEDRICH, A. & HAHN, M. K. 2013. Norepinephrine transporter variant A457P knock-in mice display key features of human postural orthostatic tachycardia syndrome. Dis Model Mech, 6, 1001-11.

SHORVON, S. D. 2009. Epilepsy, Oxford ; New York, Oxford University Press.

SLAGHT, S. N. J., LERESCHE, N., DENIAU, J. M., CRUNELLI, V. & CHARPIER, S. P. 2002. Activity of thalamic reticular neurons during spontaneous genetically determined spike and wave discharges. Journal of Neuroscience, 22, 2323-2334.

STEINLEIN, O. K. 2004. Genetic mechanisms that underlie epilepsy. Nat Rev Neurosci, 5, 400-8.

STERIADE, M. & DESCHENES, M. 1984. The thalamus as a neuronal oscillator. Brain Res, 320, 1-63.

STOKES, T., SHAW EJ., JUAREZ, GARCIA, A., CAMOSSO, STEFANOVIC, J., Baker, R. Clinical Guidelines and Evidence Review for the Epilepsies: diagnosis and management in adults and children in primary and secondary care London: Royal College of General Practitioners, 2004.

STRAUB, R. E., LIPSKA, B. K., EGAN, M. F., GOLDBERG, T. E., CALLICOTT, J. H., MAYHEW, M. B., VAKKALANKA, R. K., KOLACHANA, B. S., KLEINMAN, J. E. & WEINBERGER, D. R. 2007. Allelic variation in GAD1 (GAD67) is associated with schizophrenia and influences cortical function and gene expression. Mol Psychiatry, 12, 854-69.

STROH, A., ADELSBERGER, H., GROH, A., RUHLMANN, C., FISCHER, S., SCHIERLOH, A., DEISSEROTH, K. & KONNERTH, A. 2013. Making waves: initiation and propagation of corticothalamic Ca2+ waves in vivo. Neuron, 77, 1136-50.

STUART, G., SPRUSTON, N., SAKMANN, B. & HAUSSER, M. 1997. Action potential initiation and backpropagation in neurons of the mammalian CNS. Trends Neurosci, 20, 125-31.

SULLIVAN, J. E. & DLUGOS, D. J. 2004. Idiopathic Generalized Epilepsy. Curr Treat Options Neurol, 6, 231-242.

SULS, A., MULLEN, S. A., WEBER, Y. G., VERHAERT, K., CEULEMANS, B., GUERRINI, R., WUTTKE, T. V., SALVO-VARGAS, A., DEPREZ, L., CLAES, L. R., JORDANOVA, A., BERKOVIC, S. F., LERCHE, H., DE JONGHE, P. & SCHEFFER, I. E. 2009. Early-onset absence epilepsy caused by mutations in the glucose transporter GLUT1. Ann Neurol, 66, 415-9.

TAMURA, S., NELSON, H., TAMURA, A. & NELSON, N. 1995. Short external loops as potential substrate binding site of gamma-aminobutyric acid transporters. The Journal of biological chemistry, 270, 28712-5.

TANAKA, M., OLSEN, R. W., MEDINA, M. T., SCHWARTZ, E., ALONSO, M. E., DURON, R. M., CASTRO-ORTEGA, R., MARTINEZ-JUAREZ, I. E., PASCUAL-CASTROVIEJO, I., MACHADO-SALAS, J., SILVA, R., BAILEY, J. N., BAI, D., OCHOA, A., JARA-PRADO, A., PINEDA, G., MACDONALD, R. L. & DELGADO-ESCUETA, A. V. 2008. Hyperglycosylation and reduced GABA currents of mutated GABRB3 polypeptide in remitting childhood absence epilepsy. Am J Hum Genet, 82, 1249-61.

TANIGUCHI, H., OKADA, Y., SHIMADA, C. & BABA, S. 1977. GABA in pancreatic islets. Arch Histol Jpn, 40 Suppl, 87-97.

TASAN, R. O., BUKOVAC, A., PETERSCHMITT, Y. N., SARTORI, S. B., LANDGRAF, R., SINGEWALD, N. & SPERK, G. 2011. Altered GABA transmission in a mouse model of increased trait anxiety. Neuroscience, 183, 71-80.

THOMAS, P. & SMART, T. G. 2005. HEK293 cell line: a vehicle for the expression of recombinant proteins. J Pharmacol Toxicol Methods, 51, 187-200.

THOMAS, R. H., CHUNG, S. K., HAMANDI, K., REES, M. I. & KERR, M. P. 2013. Translation of genetic findings to clinical practice in juvenile myoclonic epilepsy. Epilepsy Behav, 26, 241-6.

TREIMAN, D. M. 2001. GABAergic mechanisms in epilepsy. Epilepsia, 42 Suppl 3, 8-12.

TRINKA, E., BAUMGARTNER, S., UNTERBERGER, I., UNTERRAINER, J., LUEF, G., HABERLANDT, E. & BAUER, G. 2004. Long-term prognosis for childhood and juvenile absence epilepsy. J Neurol, 251, 1235-41.

USHIMARU, M., UETA, Y. & KAWAGUCHI, Y. 2012. Differentiated participation of thalamo-cortical subnetworks in slow/spindle waves and desynchronization. J Neurosci, 32, 1730-46.

UTTAM, A. K., JOSHI, R., DWIVEDI, R., PRASAD, K., PADMA, M. V., BHATIA, R., SINGH, M. B. & TRIPATHI, M. 2013. Applicability of the new ILAE classification for epilepsies (2010) in persons with epilepsy at a tertiary care center in India. Epilepsia, 54, 751-6.

VELAZQUEZ, J. L., HUO, J. Z., DOMINGUEZ, L. G., LESHCHENKO, Y. & SNEAD, O. C., 3RD 2007. Typical versus atypical absence seizures: network mechanisms of the spread of paroxysms. Epilepsia, 48, 1585-93.

VELISEK, L., SHANG, E., VELISKOVA, J., CHACHUA, T., MACCHIARULO, S., MAGLAKELIDZE, G., WOLGEMUTH, D. J. & GREENBERG, D. A. 2011. GABAergic neuron deficit as an idiopathic generalized epilepsy mechanism: the role of BRD2 haploinsufficiency in juvenile myoclonic epilepsy. PloS one, 6, e23656.

VRIELYNCK, P. 2013. Current and emerging treatments for absence seizures in young patients. Neuropsychiatr Dis Treat, 9, 963-75.

WALKER, M. C. 2002. The mechanism of action of tiagabine. Reviews in Contemporary Pharmacotherapy, 12, 213-223.

WALLACE, R. H., MARINI, C., PETROU, S., HARKIN, L. A., BOWSER, D. N., PANCHAL, R. G., WILLIAMS, D. A., SUTHERLAND, G. R., MULLEY, J. C., SCHEFFER, I. E. & BERKOVIC, S. F. 2001. Mutant GABA(A) receptor gamma2-subunit in childhood absence epilepsy and febrile seizures. Nat Genet, 28, 49-52.

WOERMANN, F. G., SISODIYA, S. M., FREE, S. L. & DUNCAN, J. S. 1998. Quantitative MRI in patients with idiopathic generalized epilepsy. Evidence of widespread cerebral structural changes. Brain, 121 (Pt 9), 1661-7.

WOLF, P. & INOUE, Y. 1984. Therapeutic response of absence seizures in patients of an epilepsy clinic for adolescents and adults. J Neurol, 231, 225-9.

WONG, C. G., BOTTIGLIERI, T. & SNEAD, O. C., 3RD 2003. GABA, gamma-hydroxybutyric acid, and neurological disease. Ann Neurol, 54 Suppl 6, S3-12.

WU, Y., WANG, W. & RICHERSON, G. B. 2001. GABA transaminase inhibition induces spontaneous and enhances depolarization-evoked GABA efflux via reversal of the GABA transporter. J Neurosci, 21, 2630-9.

YAMASHITA, A., SINGH, S. K., KAWATE, T., JIN, Y. & GOUAUX, E. 2005. Crystal structure of a bacterial homologue of Na+/Cl--dependent neurotransmitter transporters. Nature, 437, 215-23.

YAMAUCHI, A., UCHIDA, S., KWON, H. M., PRESTON, A. S., ROBEY, R. B., GARCIA-PEREZ, A., BURG, M. B. & HANDLER, J. S. 1992. Cloning of a Na(+)- and Cl(-)-dependent betaine transporter that is regulated by hypertonicity. The Journal of biological chemistry, 267, 649-52.

YANG, P., CAI, G., CAI, Y., FEI, J. & LIU, G. 2013. Gamma aminobutyric acid transporter subtype 1 gene knockout mice: a new model for attention deficit/hyperactivity disorder. Acta Biochim Biophys Sin (Shanghai).

YU, N., CAO, Y., MAGER, S. & LESTER, H. A. 1998. Topological localization of cysteine 74 in the GABA transporter, GAT1, and its importance in ion binding and permeation. FEBS Lett, 426, 174-8.

ZARRELLI, M. M., BEGHI, E., ROCCA, W. A. & HAUSER, W. A. 1999. Incidence of epileptic syndromes in Rochester, Minnesota: 1980-1984. Epilepsia, 40, 1708-14.

ZHANG, X., GAINETDINOV, R. R., BEAULIEU, J. M., SOTNIKOVA, T. D., BURCH, L. H., WILLIAMS, R. B., SCHWARTZ, D. A., KRISHNAN, K. R. & CARON, M. G. 2005. Loss-of-function mutation in tryptophan hydroxylase-2 identified in unipolar major depression. Neuron, 45, 11-6.

ZHANG, Z., LIAO, W., WANG, Z., XU, Q., YANG, F., MANTINI, D., JIAO, Q., TIAN, L., LIU, Y. & LU, G. 2014. Epileptic discharges specifically affect intrinsic connectivity networks during absence seizures. J Neurol Sci, 336, 138-45.

ZINK, M., VOLLMAYR, B., GEBICKE-HAERTER, P. J. & HENN, F. A. 2009. Reduced expression of GABA transporter GAT3 in helpless rats, an animal model of depression. Neurochem Res, 34, 1584-93.